The Investigation of the Absolute Intensities of Emission of Characteristic Kα Radiation from Thick Targets

by

V. MITCHNIK (M.Sc)

A Thesis

presented for the Degree of

Doctor of Philosophy

in the

Physics Department

University of Adelaide

AUGUST 1961

CONTENTS

Section 3.

Section 4.

Section 5.

This thesis contains no material previously submitted for a Degree in any University, either by the Candidate or by any other person, except when due reference is made.

W. MITCHNIK.

PREFACE

The subject matter for the Ph.D. Thesis represents the work carried out at the Physics Department, University of Adelaide, under the supervision of Dr. S.G. Tomlin while the Author was employed as a full time Demonstrator.

An expression for N_ϕ, the number of Kα quants emitted from a thick target per unit solid angle per electron at an angle of emission ϕ to the target surface was obtained for the case when the incident electron beam was (a) parallel, (b) inclined to the target normal. These theoretical derivations take into account the diffusion of the incident beam of electrons in the target. Experimentally, the values of N_ϕ for Copper and Silver targets were determined for angles of emission ϕ ranging from 1° - 50° and for varying accelerating voltages of the incident electron beam. Experiments were also carried out on the energy distibution of secondary electrons emitted from a Copper target.

The ratio of Kα to white radiation from a Copper target was found for an accelerating voltage of 30 kilovolts of the incident electron beam and for angles of emission $\phi = 6^\circ$, 15° and 30°.

The X ray tube was constructed in the Physics Workshop by Mr. A. Bowers. I am grateful to Mr. Bowers for his cooperation and skill in the construction of the X ray tube.

My thanks are due also to Mr. R. Roper for his advice in building a Pulse Height Discriminator.

In particular, I wish to acknowledge the supervision, guidance and encouragement given to me by Dr. S.G. Tomlin.

INTRODUCTION

As early as 1920 Duane and Stenstrom measured the relative ionisation currents produced by the K series of Tungsten. Other relative intensity measurements in the K series were made by Zacek and Siegbahn (1923), Allison and Armstrong (1925) and Woo (1926). In 1929 Meyer, by a photographic photometric method measured the relative intensities of the K series from $_{23}$Vanadium to $_{49}$Indium. The values given by him are the relative intensities at the surface of the target. Later in 1923 Williams made measurements on the K series from $_{24}$Chromium to $_{52}$Tellurium using the ionisation chamber method.

In 1933 Webster *et al* investigated the manner in which the intensity of the Kα lines of Silver vary with the energy of the electron bombardment which causes their emission, but again all intensities were in arbitrary units. Worthington and Tomlin in 1956 made a single determination of the absolute intensity of Copper Kα radiation. Their result showed that when electrons accelerated at 30 kilovolts strike a Copper target, the number of Copper Kα quanta emitted per unit solid angle, per electron, at an angle of emission of 2° to the target surface was 5×10^{-4}, while their theoretical development predicted 10×10^{-4} quanta. They attributed their result to experimental error.

1·1 THEORETICAL.

The condition for the production of a line in the characteristic X ray spectrum is that an electron be removed from an inner shell of one of the atoms of the radiator. For our purpose, we will consider that this effect may be accomplished in the target of an X ray tube by:

(a) the collision of an electron with an atom of the target,

(b) ionisation by internal absorption of the X radiation in the target.

In general the intensity of characteristic X ray emission will be a function of the angle ϕ between the direction of emission and the target surface, the atomic number Z of the target material, and the acceleration potential V of the incident electrons.

1·11

Consider a target of atomic number Z, bombarded by electrons accelerated by a potential V_0. The number of Kα quanta emitted in a direction making an angle ϕ with the surface of the target will be calculated.

For a layer of material of thickness dx at a distance

x below the surface of the target (Fig. 1) let the number of K shell ionisations produced per electron be δn. If each ionisation results in the emission of one quantum of radiation, the number of quanta radiated into the solid angle $\delta\omega$ in the direction making an angle ϕ with the surface of the target is $\frac{\delta\omega}{4\pi}\delta n$.

This radiation however must traverse a length of path equal to $x\,\mathrm{Cosec}\,\phi$ in emerging out of the target. If ρ is the density of the target material, and μ is the mass absorption coefficient, then the quanta emitted at an angle ϕ with the target surface have their intensity diminished by a factor

$$\exp(-\mu\rho x\,\mathrm{Cosec}\,\phi)$$

Hence if we call $\delta\nu_\phi$ the number of quanta produced between a layer of target between x and x + dx and emerging in the solid angle $\delta\omega$, then

$$\delta V_\phi = \frac{\delta\omega}{4\pi}\delta n\,\exp(-\mu\rho x\,\mathrm{Cosec}\,\phi)$$

The electrons will have a certain depth x_k in the target at which their energy is reduced to that of the K shell excitation energy. Thus the total number of quanta emerging per electron is

SUMMARY

An expression for the number of Kα quanta emitted from thick targets per unit solid angle per electron for varying angles of emission to the target surface and varying accelerating voltages of the primary electron beam was derived, taking into account electron scattering. This derivation included the case when the incident electron beam was (a) parallel, (b) inclined to the target normal. Measurements of absolute intensity were made on thick targets of Copper and Silver using different types of detectors in conjunction with a pair of balanced filters and a crystal monochromator. Rediffusion from targets of Copper and Silver for varying accelerating voltages of the primary electron beam was investigated. The ratio of characteristic Kα to white radiation from a Copper target was determined as well as the efficiency of the white radiation.

FIG 1.

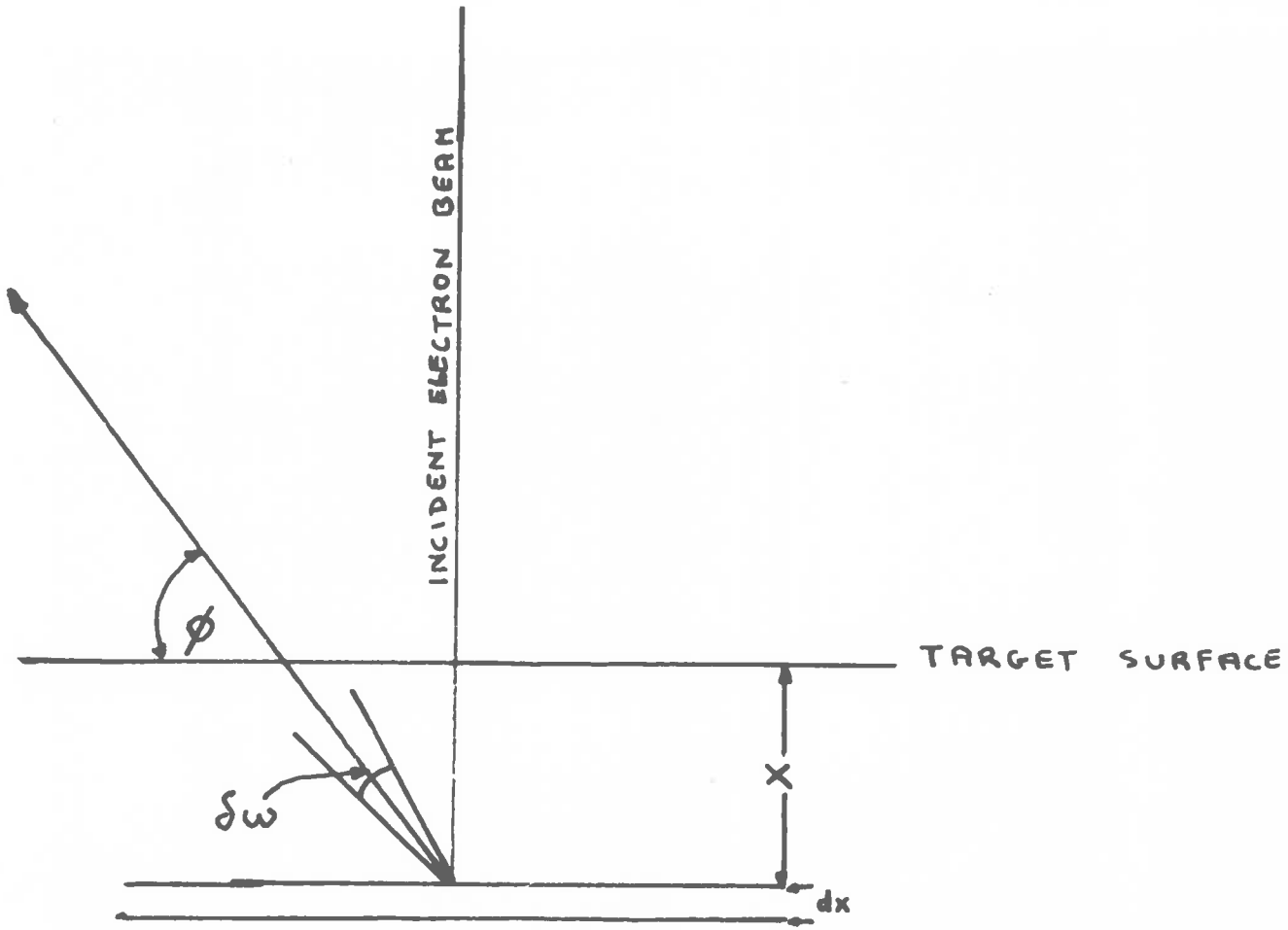

$$V_\phi = \frac{\delta\omega}{4\pi}\int_0^{x_k} \exp(-\mu\rho x \operatorname{Cosec}\phi)\frac{\partial n}{\partial x}dx = \frac{\delta\omega}{4\pi}N_\phi$$

where $N_\phi = \int_0^{x_k} \exp(-\mu\rho x \operatorname{Cosec}\phi)\frac{\partial n}{\partial x}dx$; a result first obtained by Worthington and Tomlin (1956). Here $\frac{\partial n}{\partial x} = NQ$ where N is the number of atoms per unit volume in the target, and is equal to $\frac{\rho N_A}{A}$,

ρ is density of the target,

N_A is Avogadro's number,

A is the atomic weight of the target material, and

Q is the total cross section for K shell ionisations.

1·12

That the relation $\frac{\partial n}{\partial x} = NQ$ is correct can be seen from the following considerations. A layer of material of thickness dx cm, containing N atoms/cm^3 will represent N dx scattering centres per square cm to normally incident electrons. If the cross section of each scattering centre is Q cm^2, then the scattering centres comprise the fraction

QN dx of the total area of the foil.

Thus if I_0 electrons are incident normally on the layer of thickness dx, I electrons will be scattered in the direction

represented by the particular value of the cross section Q being used. The fraction so scattered is simply

$$\partial n = \frac{I}{I_0} = QN\,dx$$

$$\text{or } \frac{\partial n}{\partial x} = QN$$

1·2

Upon closer consideration, however, it is seen that the emission of characteristic X radiation is complicated by the following secondary effects.

(a) Indirect production of characteristic radiation by the photo-electric absorption of the continuous radiation.

(b) Fluorescence Yield.

(c) Electron rediffusion.

(d) Ratio of the number of Kα quanta to the total number of K quanta produced.

These effects introduce a factor k into the expression for the number of Kα quanta produced per electron, per unit solid angle, emerging at an angle ϕ to the surface of the target, viz.

$$N_\phi = k \int_0^{x_k} \exp(-\mu\rho x \operatorname{Cosec} \phi) \frac{\partial n}{\partial x} dx$$

1·21 (a) Indirect production of characteristic radiation by the photo-electric absorption of the continuous radiation.

The ratio P of the probability of exciting the K shell of Copper by direct cathode ray impact to the probability of exciting the same shell by fluorescence in a thick target has been determined by Stoddard (1934). Stoddard's measurements extended over a range of voltages from 2 to 17·4 times the K shell excitation voltage V_k. In principle the method consists of covering the target with a foil of adjacent atomic number. The foil used was of sufficient thickness to stop all the incident electrons from reaching the target, thus ensuring that all characteristic radiation from the target is excited by fluorescence.

If I = intensity of Copper Kα lines from Copper target

d = fraction of I excited directly

i = fraction of I excited by fluorescence.

Then by definition $P = \frac{d}{i}$

Also $P + 1 = \frac{I}{i}$

and the Kα line intensity produced directly is a fraction $\frac{P}{P+1}$ of the total. Calling V the accelerating voltage of the incident electrons and V_k the K shell excitation voltage, Stoddard obtained the following results.

$U = V/V_k$	2	4	6	8	12	14·7	17·4
P/P_{+1}	0·869	0·870	0·872	0·873	0·875	0·877	0·878

This ratio is seen to be very nearly constant over a wide range of accelerating voltages, and for purposes of calculation it will be assumed that not more than 13 percent of the characteristic radiation in Copper is indirectly produced.

1·22 (b) Fluorescence Yield.

When a target is irradiated with a beam of X rays, let us assume that there are K shell photo-electrons ejected from N_k atoms per second. In the steady state N_k atoms per second are returning to the normal configuration and, in order to replace the vacancy in the K shell, electrons must drop in from the L, M, N shells etc. with the constant emission of K quanta. Of these N_k atoms, N_1 will emit the $K\alpha_1$ line, N_2 will emit the $K\alpha_2$ line etc. If one defines the fluorescence yield for the K level as

$$\omega_k = \frac{N_1 + N_2 + N_3 + \ldots}{N_k}$$

it would at first seem that ω_k must necessarily be equal to unity, and yet the earliest experiments on the yield of fluorescence radiation indicated that ω_k is distinctly less

than unity. When a K shell electron is ejected from an atom, the vacancy may be filled by one of the L shell electrons, but it is not necessary that one quantum of K radiation actually leave the atom. Instead, the quantum of K radiation may be converted into the energy necessary for the ejection of an L shell electron plus the energy of the electron produced. Or, it is possible that the Kα quantum may eject an electron from the M levels, leaving the L levels undisturbed. The first observations were made by Auger (1923) who found that, by passing X rays of sufficient short wavelength in a Wilson cloud chamber filled with Argon, tracks of photoelectrons ejected from the K shell of Argon were accompanied by shorter tracks occurring at the origin of the photoelectron track. His studies showed that the photoelectron track and the short track (Auger electron) arise at the same point, but whereas the length of the Auger electron track is independent of the wavelength of the incident X rays, the length of the photoelectron track increases with decrease of wavelength. Later, Compton (1929), Balderston (1926), Martin (1927) and Haas (1933) extended the method to non gaseous elements. For Copper, the fluorescence yield ω_K is 0·42.

1·23 (c) Electron rediffusion.

When a beam of electrons is allowed to fall on a metal surface, some of the electrons are scattered elastically or inelastically and may have their directions deflected through angles greater than 90°, in which case they will appear to be reflected. If such electrons have been scattered elastically, they will emerge from the surface with an energy practically equal to that of the incident electrons while if they have suffered inelastic scattering they will emerge with energies less than that of the primary electrons. It is found however, that another group of electrons emerges from the metal. These electrons possess low energies and these energies are practically independent of the energy of the electrons incident on the target. The electrons in this group are actually ejected from the metal as a result of the bombardment of the incident electrons. Fig. 2 illustrates a typical energy distribution curve obtained by Rudberg (1944) for electrons emerging from a target of Gold as a result of bombardment by primary electrons of 150 ev energy. Of the three regions considered, A consists of the electrons which have undergone large angle scattering and appear as reflected electrons. They are the elastically scattered ones. The low energy group B represents true secondary

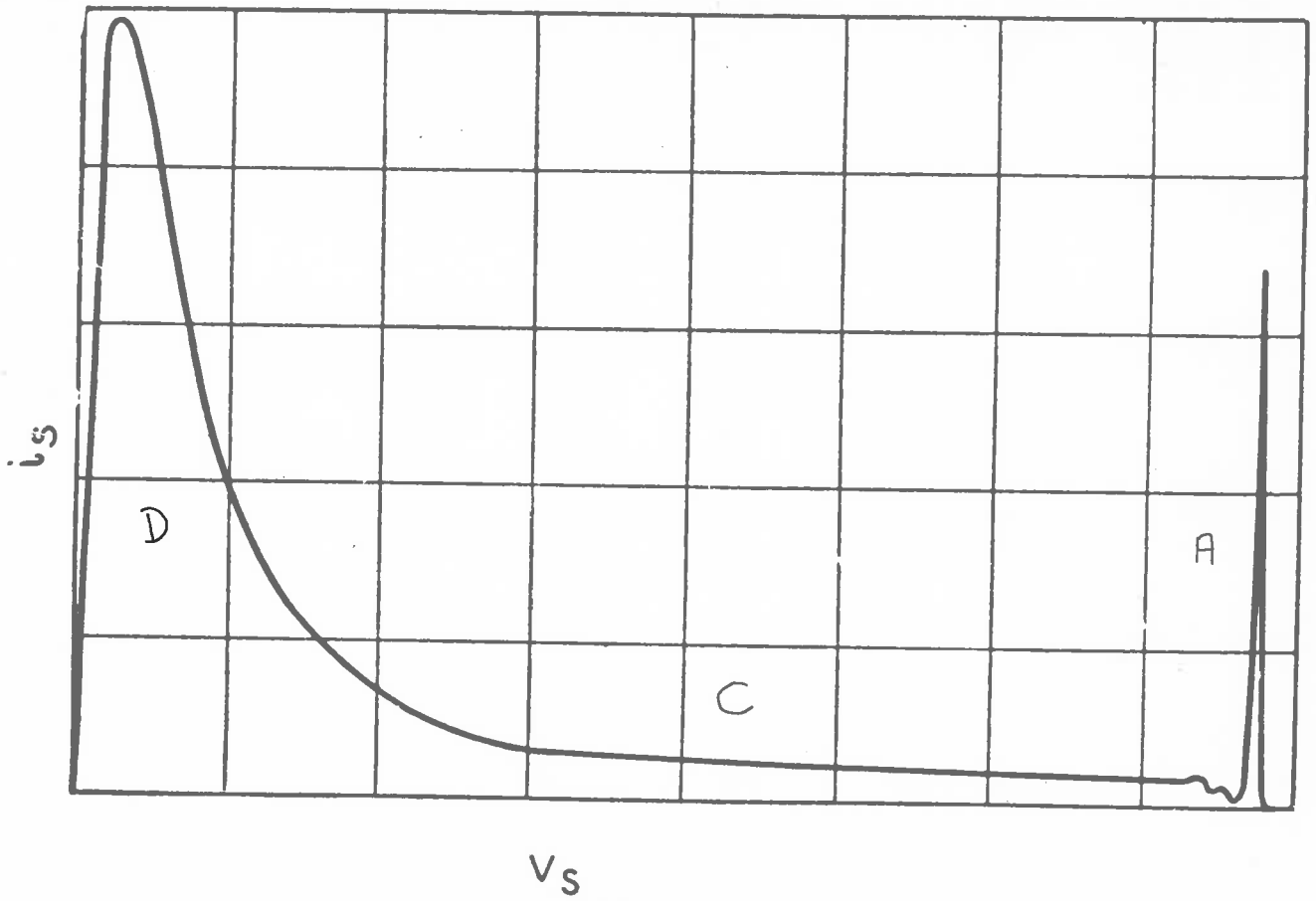

Secondary electron velocity distribution from gold.

FIG 2

emission of electrons from the metal. The intermediate group C represent those electrons that are reflected to the surface only after having passed through a layer of the target material. The electrons of this group are called the rediffused electrons. In particular it should be noted that there is no borderline distinction between the rediffused and the true secondaries. In a thick target the effect of rediffusion is to diminish the intensity of X rays emitted, since the electrons that have suffered rediffusion are removed from the target before they have made their full quota of impacts. Experiments were carried out by the author to determine the number of electrons emerging from a Copper target with an energy loss of 8·9 kilovolts, the K shell excitation energy of Copper, with an incident beam of 20 kilovolt electrons. These experiments are described in Section 5.

1·24 (d) Ratio of the number of Kα quants to the total number of K quants produced.

The ratio of the number of Kα quants to the total number of K quants produced may be estimated from the experiments of Meyer (1929) and Williams (1933). For Copper, with Z = 29, they find that the ratio of the intensities is:

$$\frac{K\alpha_2}{K\alpha_1} = 0{\cdot}46 \; ; \qquad \frac{K\beta_1}{K\alpha_1} = 0{\cdot}158 \; ; \qquad \frac{K\beta_2}{K\alpha_1} = 0{\cdot}0019$$

$$\therefore \; \frac{K\alpha_2 + K\alpha_1}{K\alpha_1} = 1{\cdot}460 \; ; \; \frac{K\beta_1 + K\beta_2}{K\alpha_1} = 0{\cdot}160$$

$$\text{and } \frac{K\alpha_2 + K\alpha_1}{K\beta_1 + K\beta_2} = \frac{1{\cdot}46}{0{\cdot}160}$$

$$\therefore \; \frac{K\alpha \text{ Quanta}}{\text{Total K quanta}} = 0{\cdot}88$$

1·31

From Section 1·11 we have that the total number of quanta emerging per electron is given by

$$V_\phi = \frac{\delta\omega}{4\pi}\int_0^{x_k} \exp(-\mu\rho x \operatorname{Cosec}\phi)\frac{\partial n}{\partial x}\,dx$$

To determine x_k, the depth of penetration in the target at which the incident electrons have their energy reduced to that of the K shell excitation, we need to know an expression for electron stopping power. Bethe (1930), basing his arguments upon Born's approximate collision theory, obtained the expression

$$-\frac{\partial T}{\partial x} = \frac{N.4\pi e^4 Z}{mc^2\beta^2}\left\{\ln\left(\frac{mc^2\beta^2}{J(1-\beta^2)}\right) - \beta^2\right\}$$

Where J is the mean excitation energy of the target volume,

N the number of atoms per unit volume,

Z the atomic number of the target,

e the electronic charge,

T the electronic kinetic energy at depth x below the target surface,

β the ratio of the velocity of an electron to that of light.

According to Wilson (1930) the mean excitation energy of the

target atoms may be taken as 18.4×10^{-12} Z erg.

It has been assumed in connection with the above formula for stopping power that the speeds of the incident electrons are large compared to the speeds of the atomic electrons. Since in the experiments carried out the incident electron energy never exceed 70 kilovolts the non relativistic expression for stopping power was used.

$$-\frac{\partial T}{\partial x} = \frac{2\pi e^4 ZN}{T} \ln\left(\frac{2T}{J}\right)$$

Calling To the kinetic energy of the electrons incident on the target, then the kinetic energy T of the electrons at a distance x below the surface of the target is

$$x = \int_{To}^{T} \frac{\partial x}{\partial T} dT$$

$$= \frac{J^2}{8\pi e^4 NZ} \left| Ei\left(2 \ln \frac{2To}{J}\right) - Ei\left(2 \ln \frac{2T}{J}\right) \right|$$

where Ei(x) is the exponential integral.

To test the validity of this formula, Worthington and Tomlin (1956) calculated the range R of the electrons in the target. They pointed out however, that if the range of integration is extended from To to zero, then x becomes the range R which is clearly not valid since

$$\lim_{T \to 0} \quad Ei\left(2 \ln \frac{2T}{J}\right) \longrightarrow \infty$$

These authors fixed the upper limit of integration by choosing the value of T for which

$$Ei\left(2 \ln \frac{2T}{J}\right) = 0$$

This gave $T = 0{\cdot}6J$, and the electrons could then be considered to be effectively at the end of their range which is then given by

$$R = \frac{J^2}{8\pi e^4 NZ} Ei\left(2 \ln \frac{2To}{J}\right)$$

Using this formula, Worthington and Tomlin calculated the ranges of electrons in Aluminium and Copper, and compared their results with the experimental data of Schonland (1925). As a further check, they used the formula to calculate the ranges of electrons in a photographic emulsion as was done by Zajac and Ross (1949). These results which are shown in Fig. 3 show that the formula for electron stopping power can be used for energy ranges up to 70 kilovolts, beyond which relativistic effects appear.

FIG 3

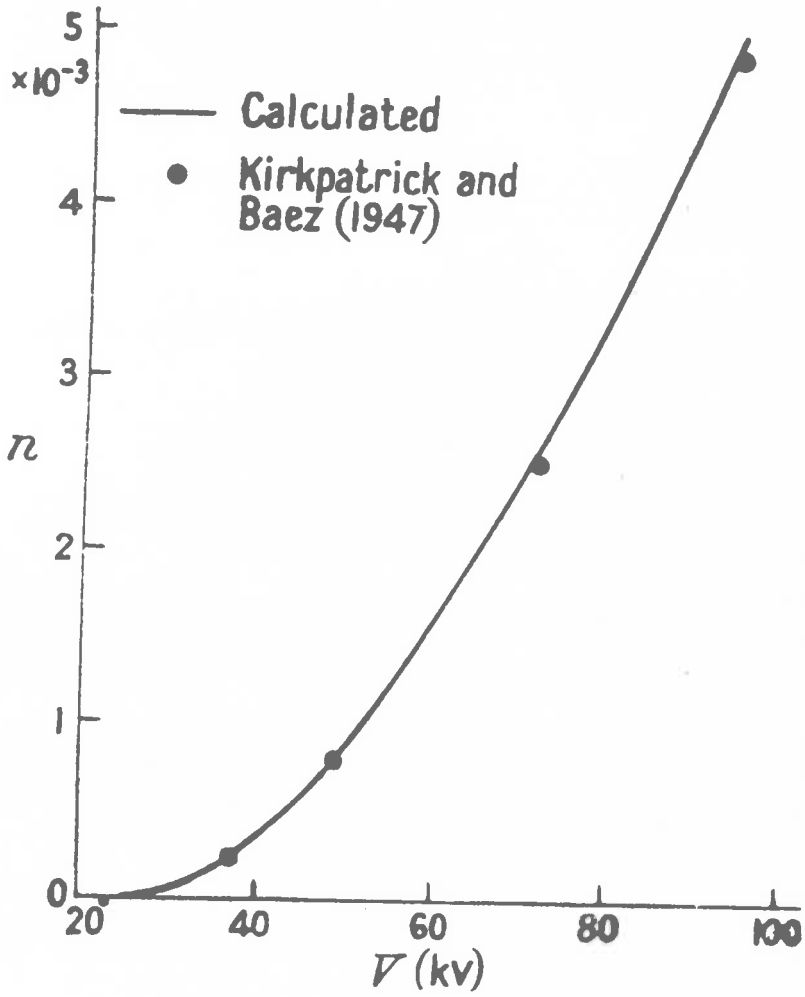

K-shell ionizations per electron n as a function of voltage for a silver target.

1·32

It has already been shown in Section 1·12 that

$$\frac{\delta n}{\delta x} = NQ$$

For K shell ionisation, Bethe's (1930) non-relativistic formula for total ionisation cross section can be written as

$$Q = \frac{2\pi e^4}{T|E|} b \ln \frac{4T}{B}$$

where T is the kinetic energy of the incident electron,

E the ionisation energy of the K shell,

e the electronic charge.

b and B are constants which Mott and Massey (1949) conclude, after careful weighing of the experimental results available, should be 0·35 and 1·65 E respectively for K shell ionisation. If the electron energy is expressed in the form

$$U = \frac{V}{V_k}$$

where V is the electron accelerating voltage,

V_k the K shell excitation potential,

the formula for total ionisation cross section can then be written in the form

$$QV_k^2 = 0{\cdot}7\ re^2 \cdot \frac{1}{U} \ln \frac{4U}{1{\cdot}65}$$

The product QV_k^2 is seen to be independent of Z, the atomic number, and is the same function of U for all atoms. Worthington and Tomlin (1956) extended the above theory to include smaller values of U. They chose

$$B = \left(1{\cdot}65 + 2{\cdot}35 \exp(1-U)\right)E$$

This value of B satisfies the condition that Q must be zero for U = 1, while for large values of U,

B = 1·65 E as suggested by Mott and Massey.

Fig. 4 compares the calculated values of QV_k^2 as obtained by Worthington and Tomlin with the experimental points for Silver and Nickel as given by Kirkpatrick and Baez (1947) and Peckman et al (1947) respectively. The function QV_k^2 rises sharply from zero at U = 1 to a maximum at about U = 2·5, and then falls off as U is further increased. The experimental values however reach their maximum at a higher value of U, and then fall off less rapidly than the theory suggests. In calculating integrals of the type shown in Section 1·31, the experimental values for Nickel were used assuming that these would be close to the figures for Copper.

FIG 4

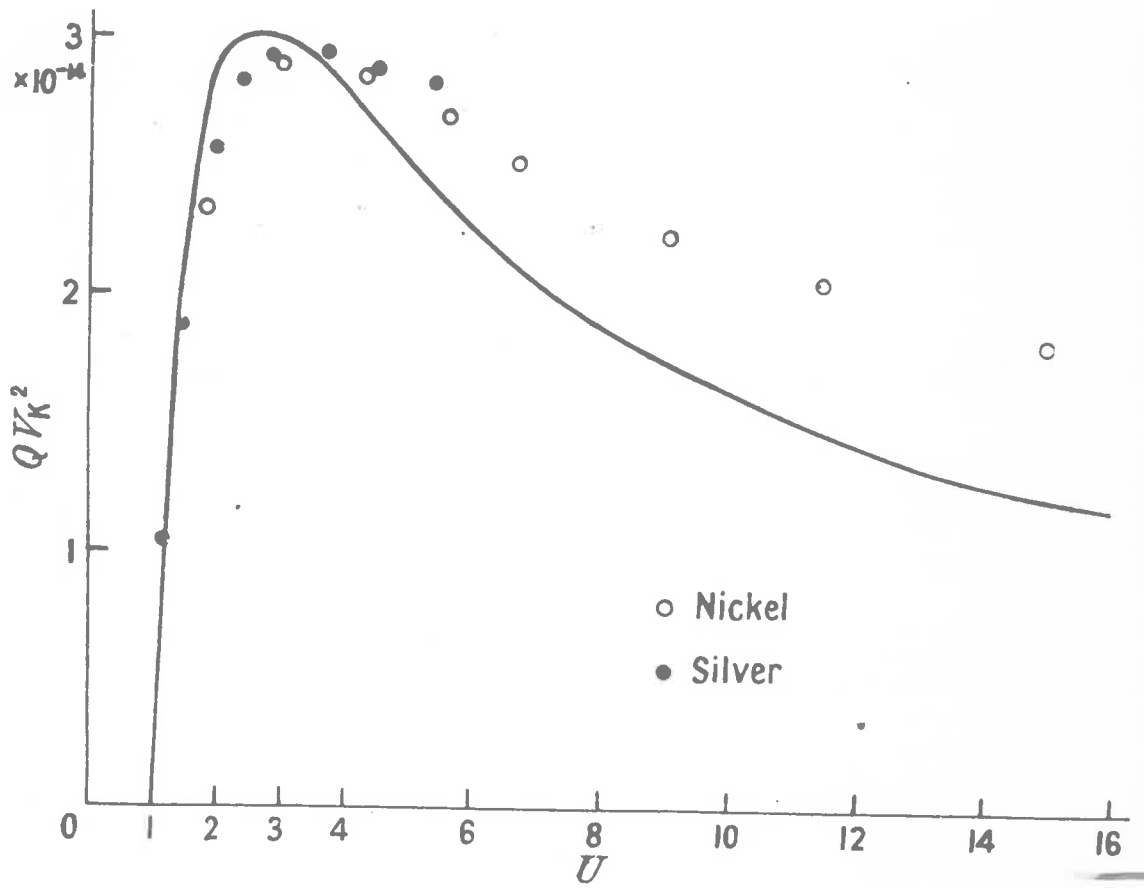

Comparison of the modified formula for the total cross section Q with the experimental values for nickel and silver.

1·33

The evaluation of the integral in the equation

$$N_{\phi} = k \int_{0}^{x_k} \exp(-\mu\rho x \operatorname{Cosec} \phi) \frac{\partial n}{\partial x} dx$$

was done numerically, and Fig. 5 shows N_{ϕ} plotted against accelerating voltage for different angles of emission with respect to the target surface.

FIG 5

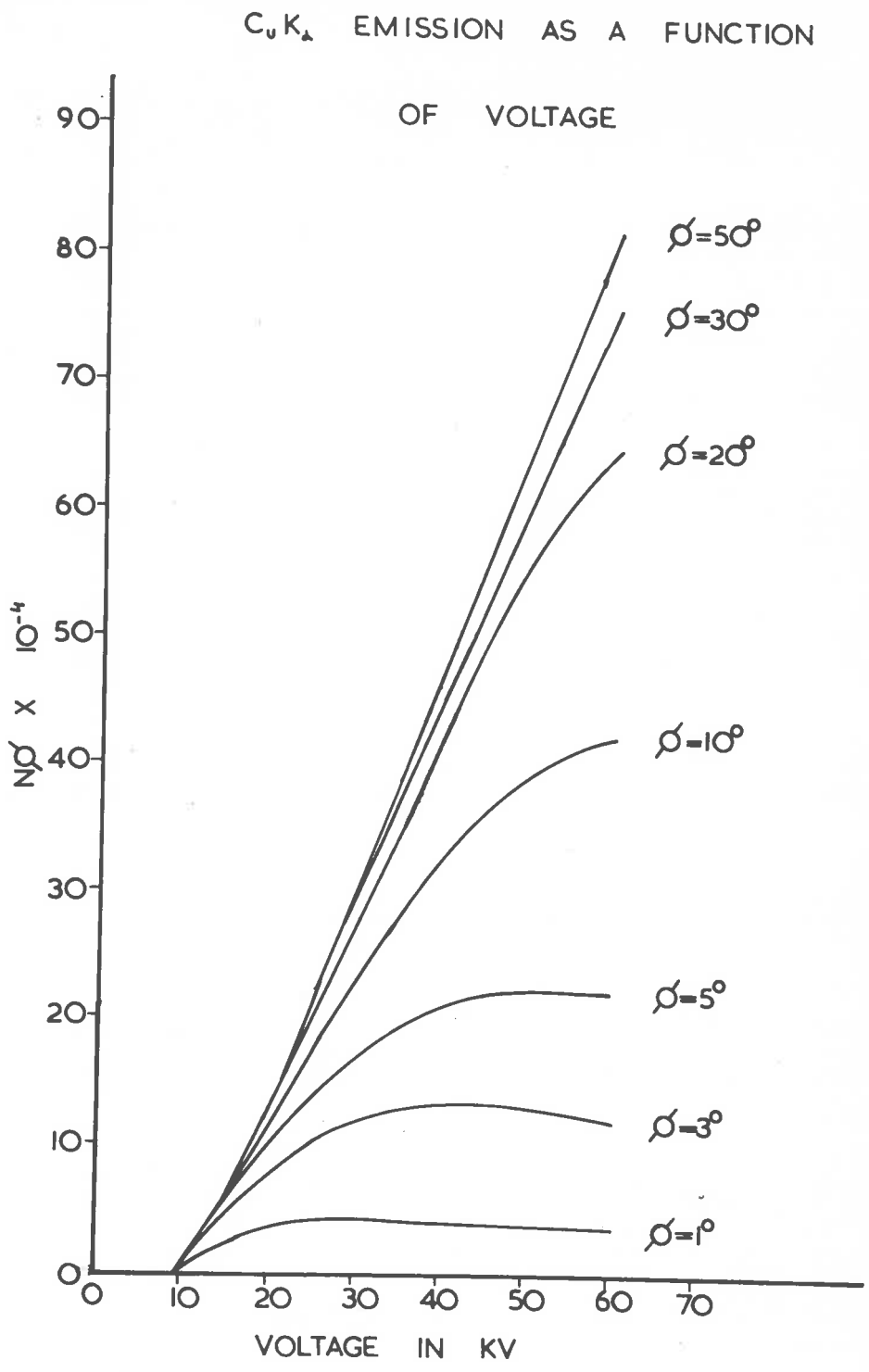
$C_u K_\alpha$ EMISSION AS A FUNCTION OF VOLTAGE
$NO \times 10^{-4}$
VOLTAGE IN KV
0
10
20
30
40
50
60
70
80
90
$\phi=50°$
$\phi=30°$
$\phi=20°$
$\phi=10°$
$\phi=5°$
$\phi=3°$
$\phi=1°$

1·4

The previous derivation of the expression for N_ϕ, the number of Kα quanta produced per electron per unit solid angle $\delta\omega$ emerging at an angle ϕ to the surface of the target, assumed that the normal to the target was parallel to the incident beam of electrons. It was decided to investigate the change arising in N_ϕ when the normal to the target was inclined to the incident electron beam. Let θ be the angle that the normal makes with the incident beam. From Fig. 6 if one considers a layer of material of thickness dx at a distance x below the surface of the target, the Kα radiation emerging at an angle ϕ with respect to the surface of the target must have travelled a distance y in the target material. We have that

$$\frac{y}{\text{Cos } \theta} = \frac{x}{\text{Sin } \phi}$$

$$\therefore \quad y = x \text{Cos } \theta \text{ Cosec } \phi$$

If ρ is the density of the target material

μ is the mass absorption coefficient

then the Kα quanta emerging at the target surface have their intensity diminished by a factor

$$\exp(-\mu\rho x \text{Cos } \theta \text{ Cosec } \phi)$$

FIG 6

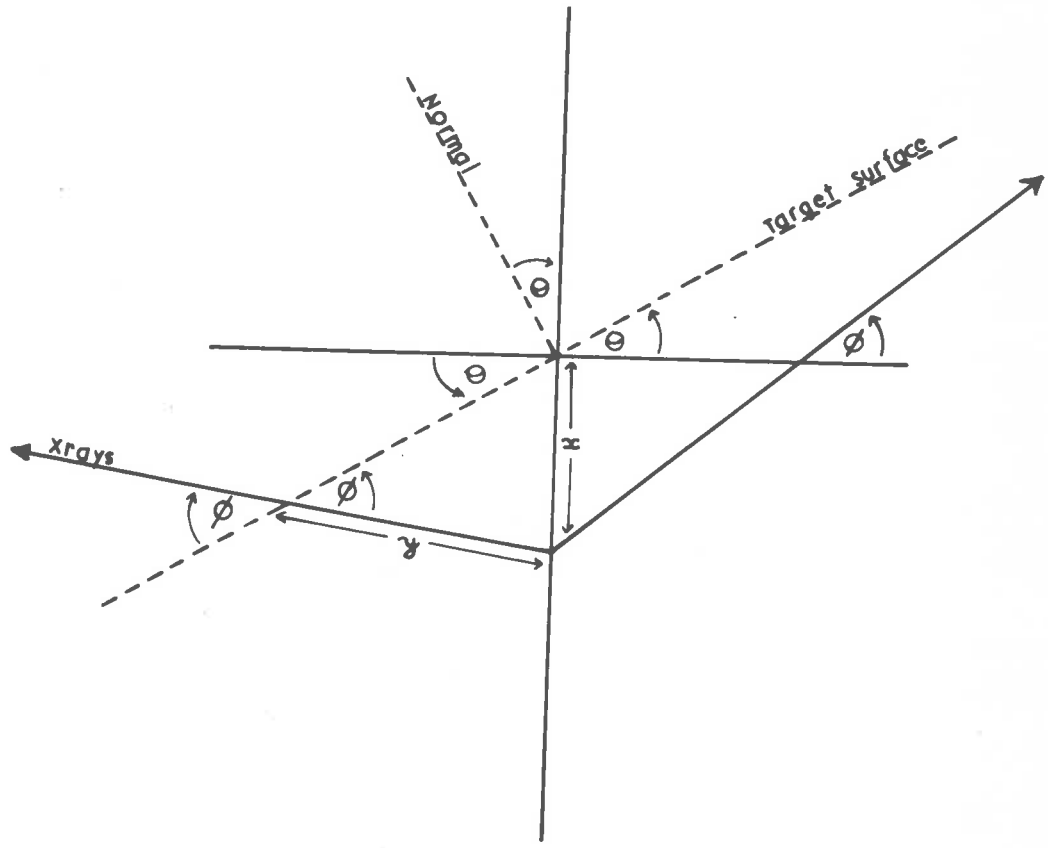

Proceeding as in Section 1·11 we now have

$$N_\phi = k \int_0^{x_t} \exp(-\mu\rho x \operatorname{Cosec}\phi \operatorname{Cos}\theta) \frac{\partial n}{\partial x} dx$$

This expression for N_ϕ predicts that the intensity of Kα radiation should increase the greater the angle θ that the normal to the target makes with the incident electron beam. Consider the term $\exp(-\mu\rho x \operatorname{Cosec}\phi \operatorname{Cos}\theta)$. The value of this expression is very little altered for values of θ within the range $0 < \theta \leq 10^\circ$. Practically the increase should be detectable for values of θ equal to or greater than 20°. The above integral was evaluated for values of φ ranging from 1° - 60° and for corresponding values of θ from 20° - 60°. Graphs of these calculations are shown in Figs. 7-12 for values of θ equal to 20° and 40° with $\theta = 0^\circ$ as a comparison. From these graphs it is seen that for angles of emission φ equal to 40° and 50° the increase in Copper Kα emission is only of the order of a few per cent even when θ, the angle between the normal to the target and the incident beam, is equal to 40°. Furthermore this increase is apparent for values of the accelerating voltage larger than 40 kilovolts. As the angle of emission φ is reduced the increase in Copper Kα emission for $\theta = 40^\circ$ becomes much more significant. It can be noticed that for $\phi = 1^\circ$, 3°, 5° and 10° and for $\theta = 20^\circ$ and 40° the curves for N_ϕ show a

FIG 7

EMISSION OF CuK$_\alpha$ RADIATION WHEN NORMAL TO TARGET IS INCLINED TO INCIDENT BEAM

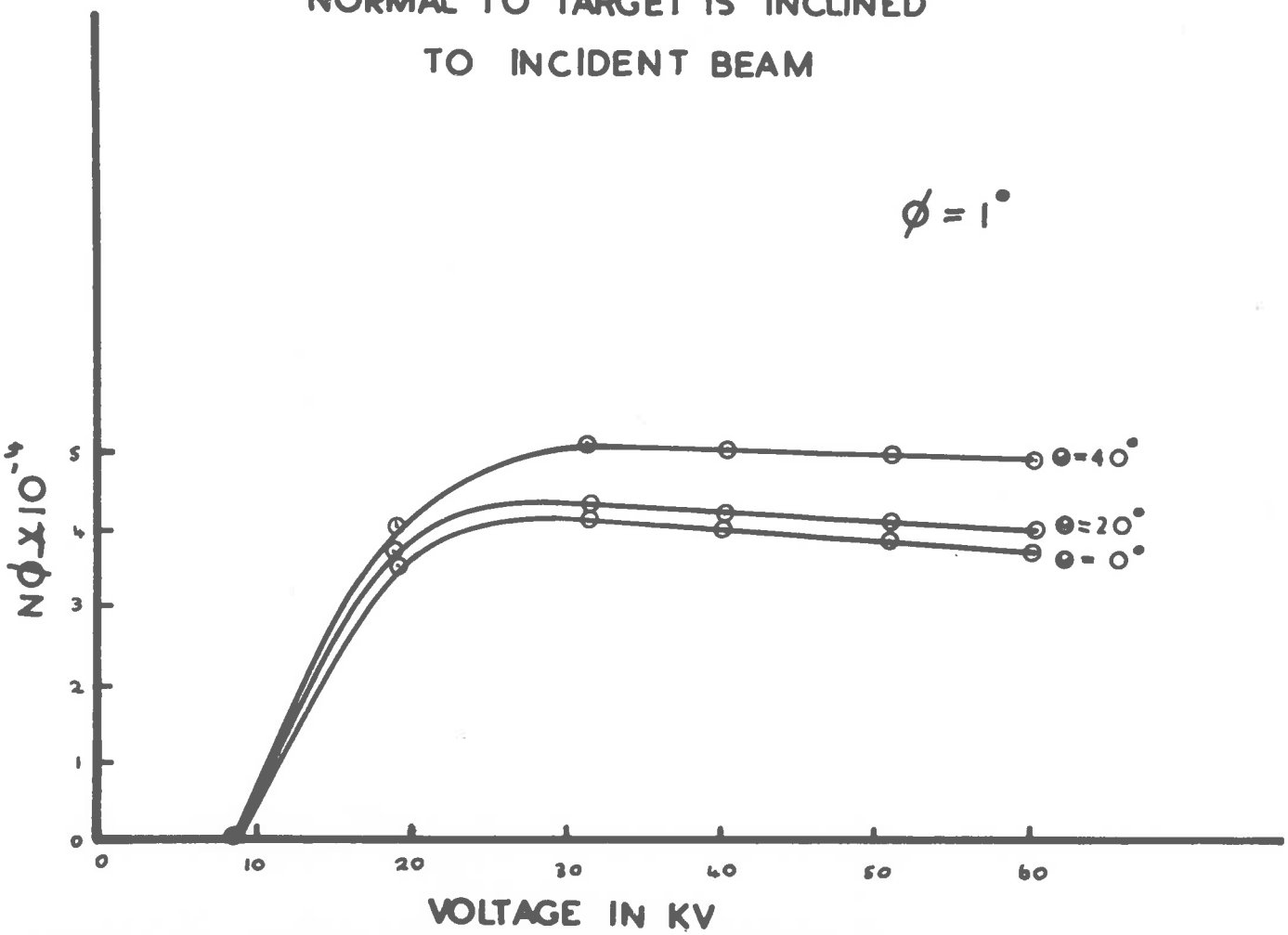

FIG 8

EMISSION OF CuK_{α} RADIATION WHEN NORMAL TO TARGET IS INCLINED TO INCIDENT ELECTRON BEAM

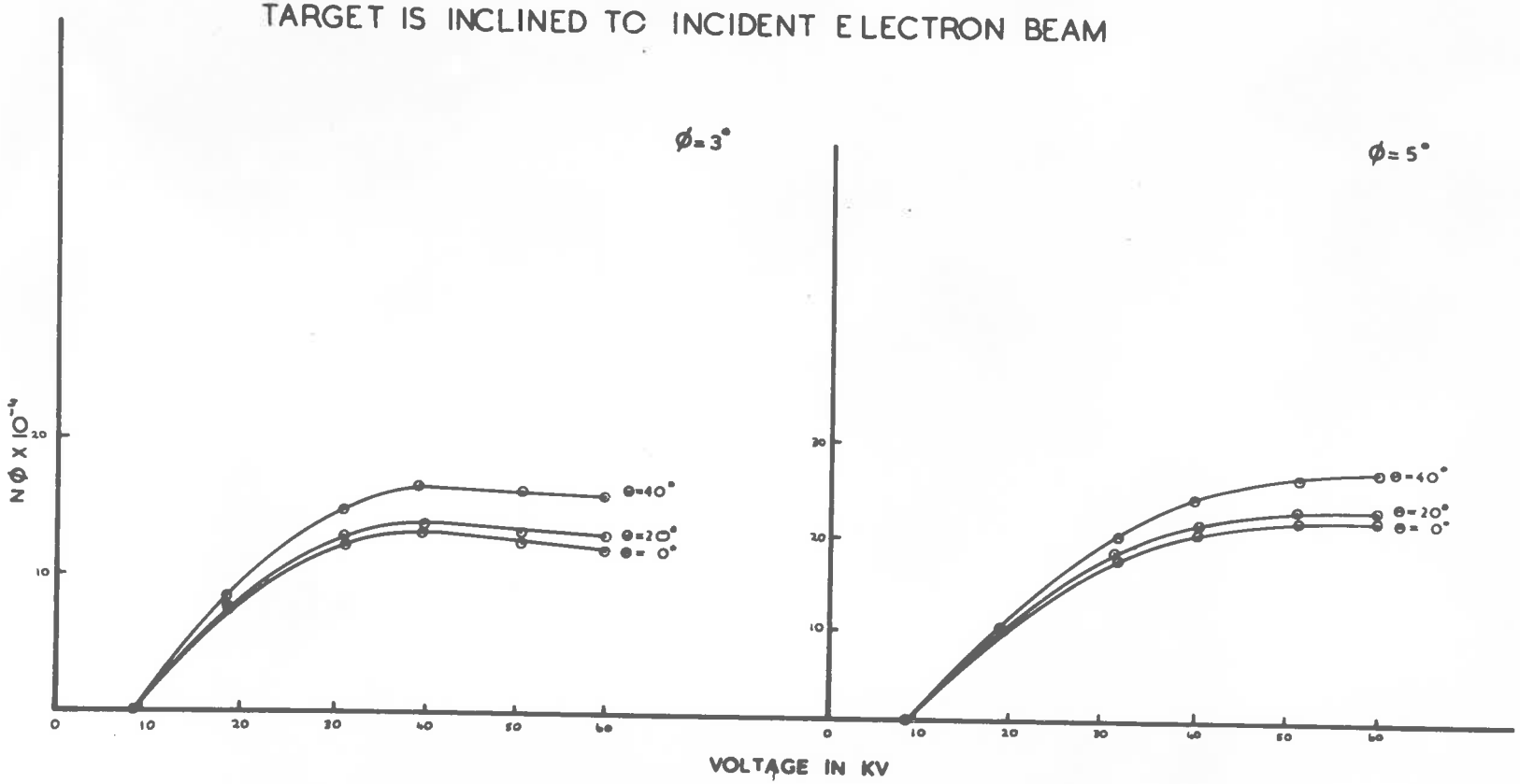

FIG 9

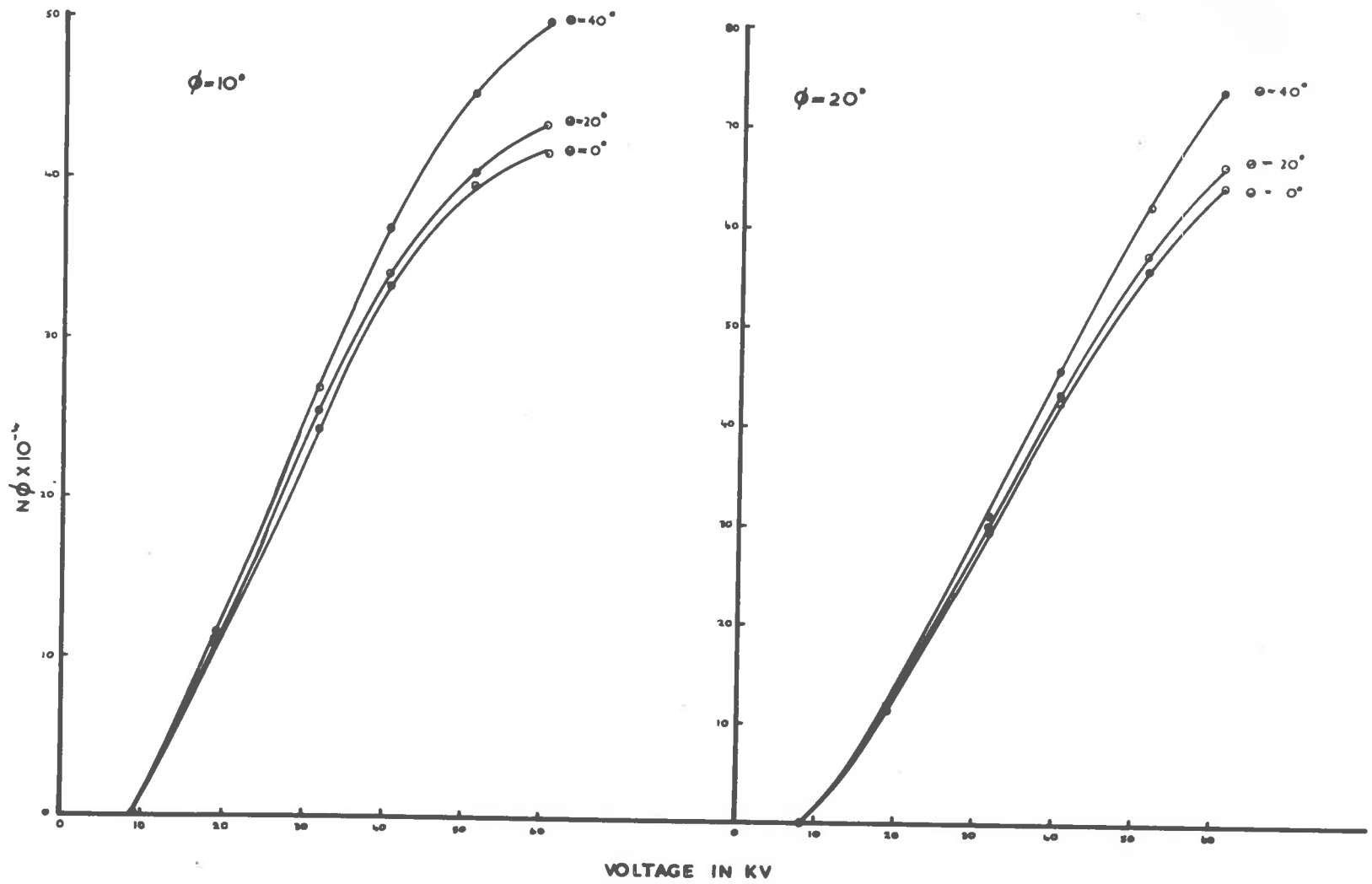

ϕ=30°

FIG 10

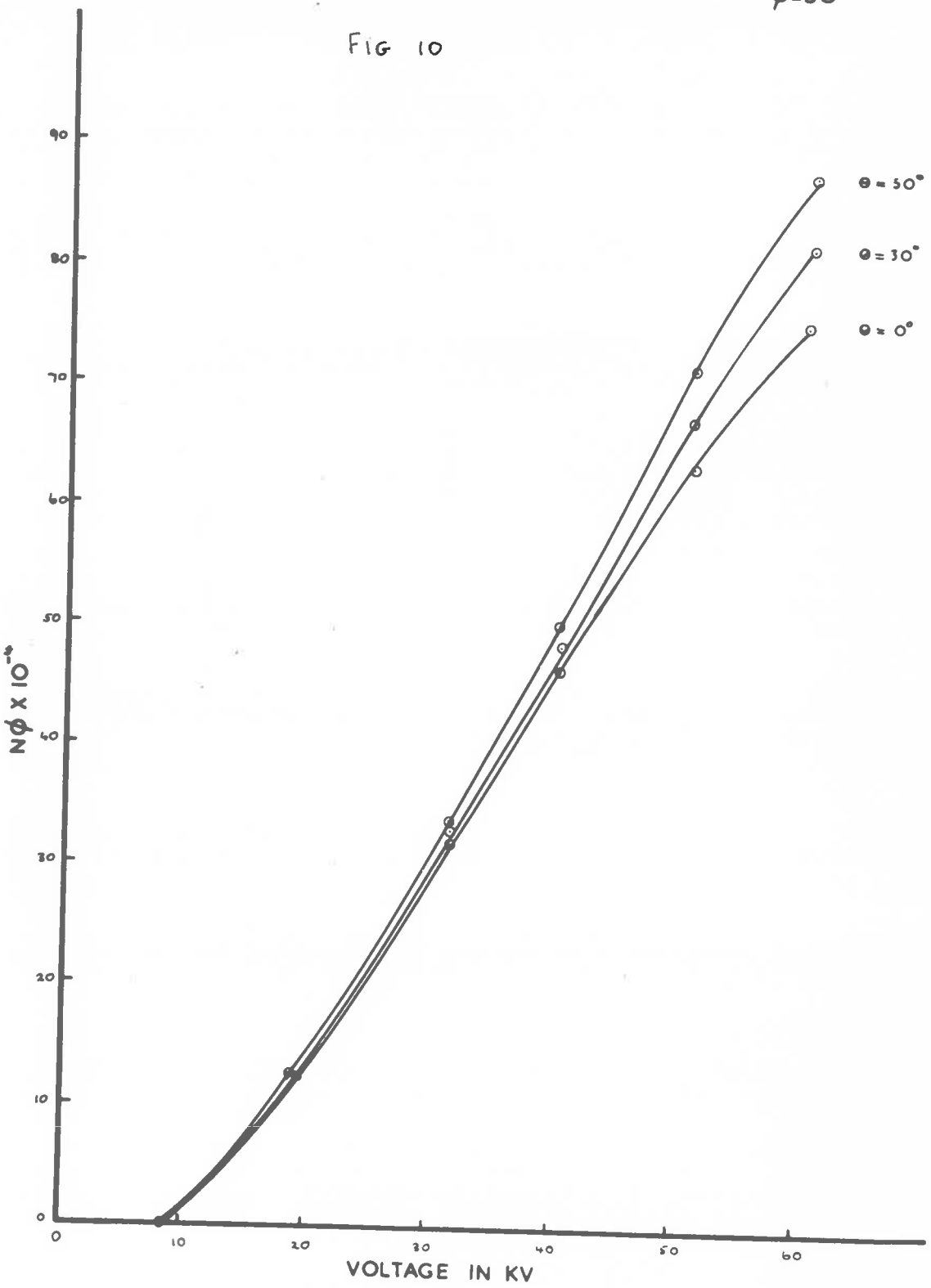

FIG 11

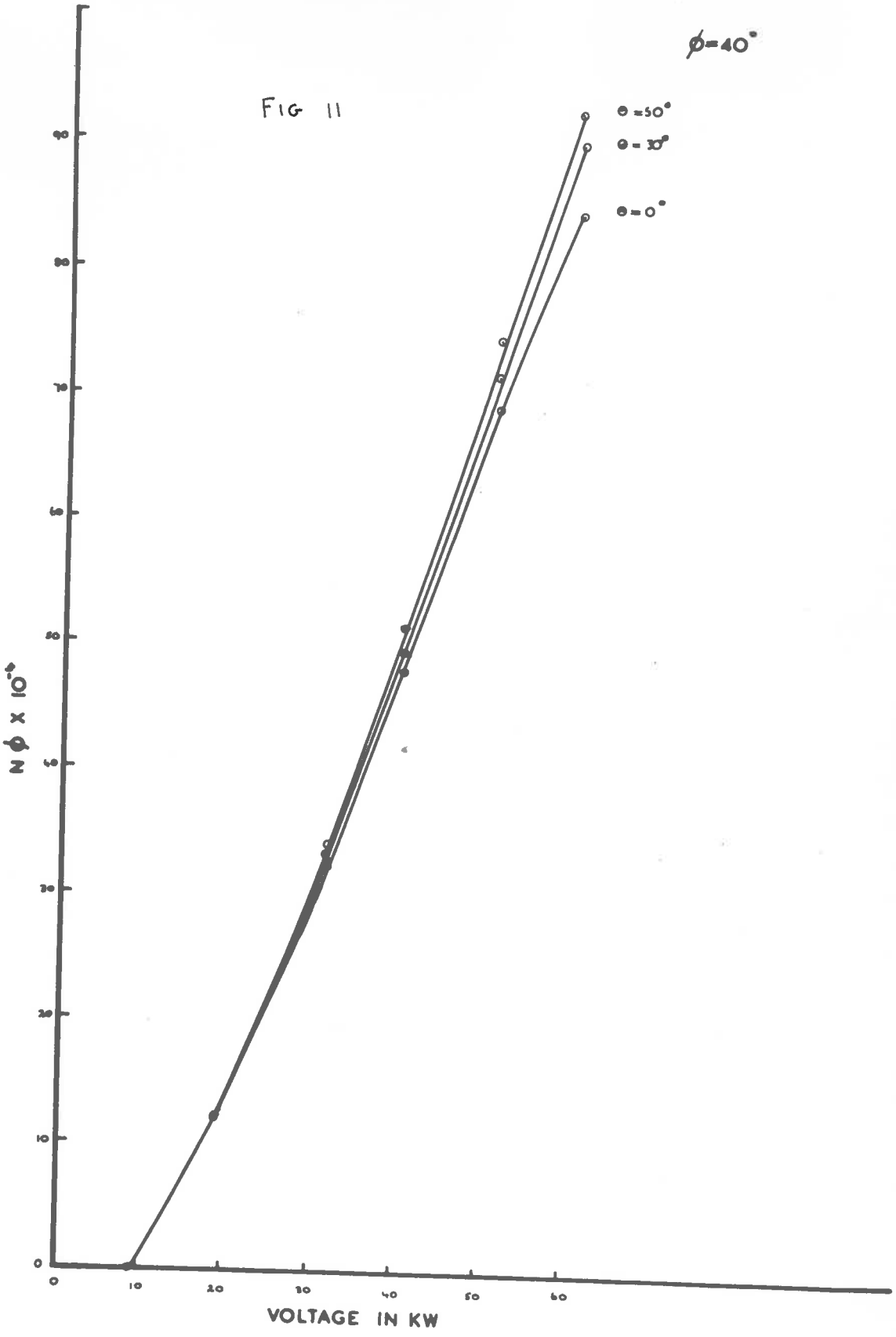

FIG 12

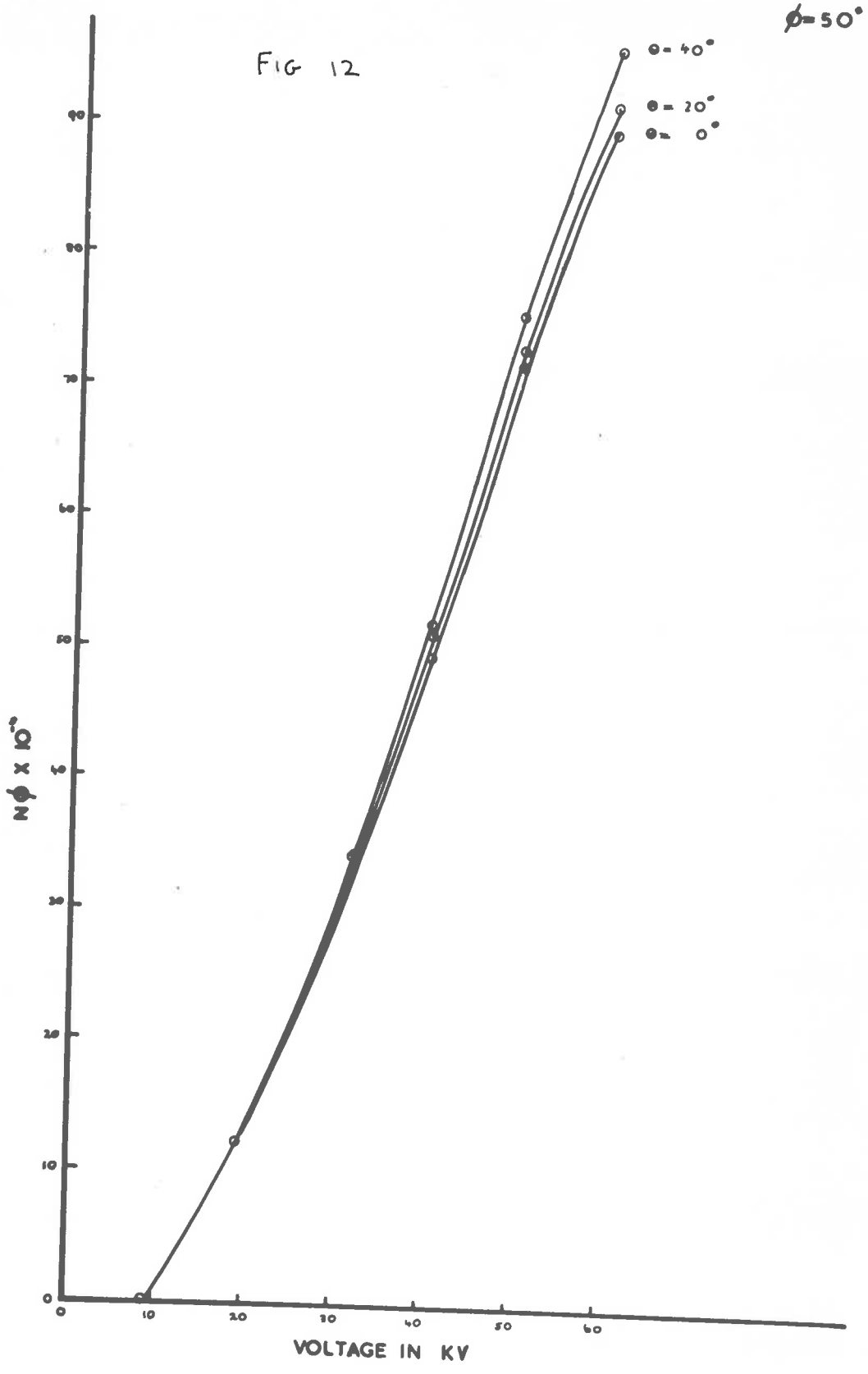

similar trend to those calculated at $\theta = 0^\circ$. Thus for ϕ equal to 1° the curves reach their maximum at an accelerating voltage of 30 kilovolts. However for $\phi = 1^\circ$ and $\theta = 40^\circ$, the decrease in emission occurring at voltages larger than 30 kilovolts is less pronounced than at θ equal to 0°. At $\phi = 5^\circ$, whereas the emission has reached a maximum at $\theta = 0^\circ$ for an accelerating voltage equal to 50 kilovolts, the curve for $\theta = 40^\circ$ is still increasing at that voltage. At $\phi = 10^\circ$, 20° and 30° and for values of the accelerating voltage larger than 40 kilovolts, it can be seen that the emission for $\theta = 20^\circ$ and 40° is increasing at a faster rate than for $\theta = 0^\circ$.

1·41

The theory as outlined in Section 1·11 is not quite valid, the discrepancy arising through the assumption that the electrons follow straight line paths through the target, undeviated from the direction of incidence. Since electron scattering within the metal must occur this factor will be considered in some detail and a suitable correction applied.

1·42

When electrons pass through even a very thin layer of matter, they are normally influenced by a number of atoms. However, deflections through a considerable angle may on the average be imparted to electrons in transit by a single atom only. When this is the case, single scattering is said to take place. For a thick target which is the case under consideration, every electron undergoes many deflections and, if each angular deflection is regarded as quite independent of the preceding ones, the total deflections produced by repeated scattering in a layer of matter have a distribution given by Gauss' error curve.

$$I(\theta) = \frac{1}{\sqrt{2\pi}\,\Delta}\exp(\theta^2/2\Delta^2)$$

Δ being the root mean square (r.m.s.) or standard deviation. The value of Δ is obtained by adding up statistically the deflections received in successive thin layers of thickness 'd' of the specimen, 'd' being made so small that application of single scattering theory is valid. From these considerations Bothe (1927) developed the formula

$$\Delta = \frac{800}{V}\left(\frac{V + 511}{V + 1022}\right) Z \left(\frac{\rho x}{A}\right)^{\frac{1}{2}}$$

Where V is the energy of incident electrons in kilovolts,

Z the atomic number of the target material,

ρ the density of target,

A the atomic weight of the target material.

1·43

Consider electrons that are deflected through an angle θ, after having traversed a distance x below the surface of the target. From Fig. 13 it is seen that

$$y = x \operatorname{Cos} \theta$$

$$Z = y \operatorname{Cosec} \phi$$

$$\text{and hence } Z = x \operatorname{Cos} \theta \operatorname{Cosec} \phi$$

Provided that Δ, the standard deviation, is small, the number of $K\alpha$ quanta emitted per electron at an angle ϕ with

FIG 13

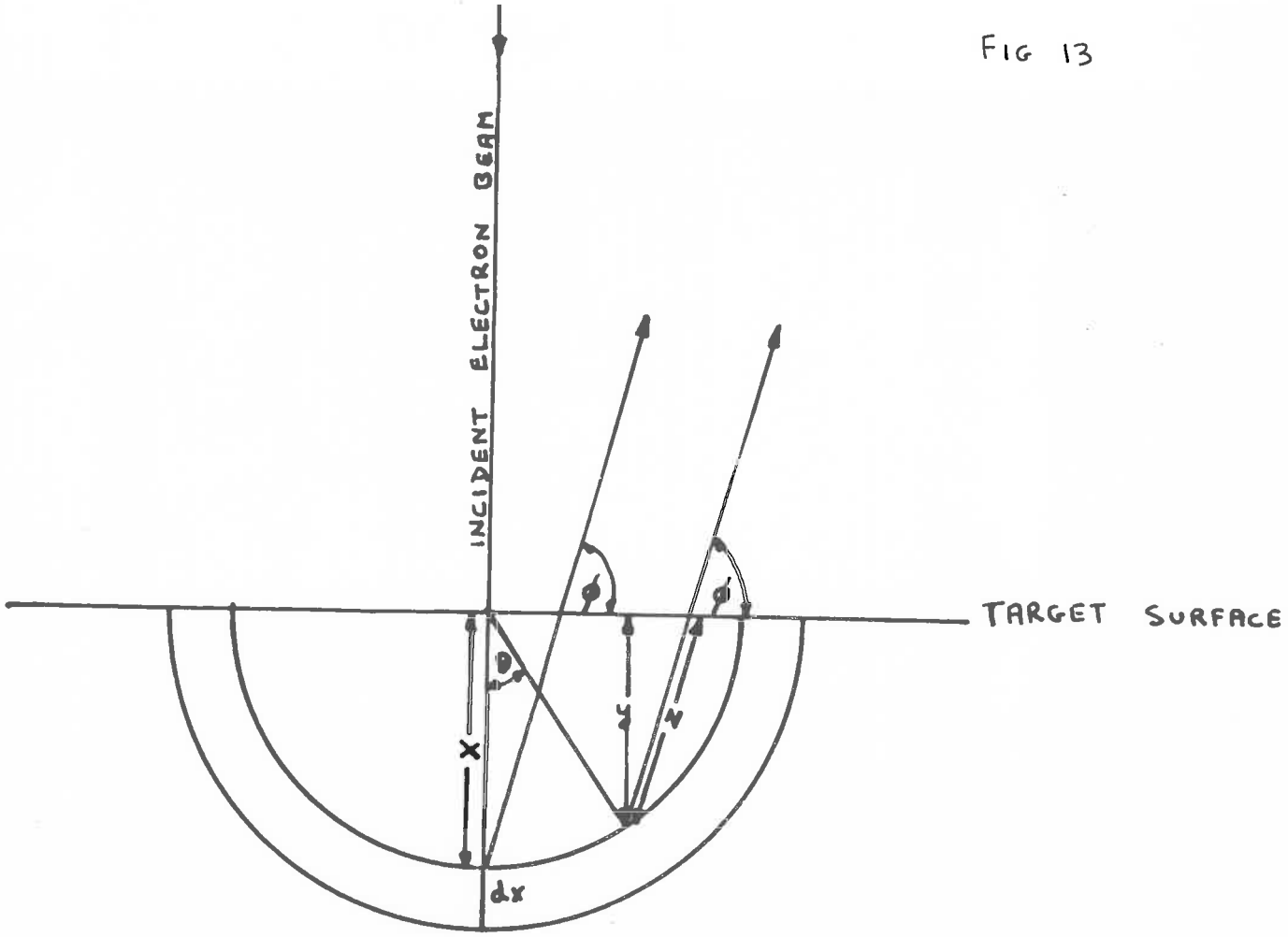

the target surface is given by

$$v_\phi = \frac{\delta\omega}{4\pi}\cdot\frac{1}{\sqrt{2\pi}.\Delta}\int_{-\infty}^{\infty}\int_{0}^{x_k}\exp(-\theta^2/2\Delta^2)\exp(-\mu\rho x\,\mathrm{Cosec}\phi\,\mathrm{Cos}\theta)\frac{\partial n}{\partial x}dx\,d\theta \qquad ..(1)$$

The limits of integration $-\infty$ to $+\infty$ for the angle integral is clearly permissible when the diffusion of electrons in the target is weak.

1·44

As a first step in solving the integral in 1·43 one can write

$$\mathrm{Cos}\,\theta = 1 - \frac{\theta^2}{2}$$

Substituting this value of Cos θ in (1), Section 1·43, we have

$$v_\phi = \frac{\delta\omega}{4\pi}\cdot\frac{1}{\sqrt{2\pi}.\Delta}\int_{0}^{x_k}\int_{-\infty}^{\infty}\exp\left(-\mu\rho x(1-\theta^2/2)\mathrm{Cosec}\phi\right)\exp(-\theta^2/2\Delta^2)d\theta\frac{\partial n}{\partial x}dx \qquad ..(1)$$

$$= \frac{\delta\omega}{4\pi}\cdot\frac{1}{\sqrt{2\pi}.\Delta}\int_{0}^{x_k}\exp(-\mu\rho x\,\mathrm{Cosec}\phi)\frac{\partial n}{\partial x}dx\int_{-\infty}^{\infty}\exp\left(-\theta^2/2(1/\Delta^2-\mu\rho x\,\mathrm{Cosec}\phi\right)d\theta \qquad ..(2)$$

but

$$\int_{-\infty}^{\infty} \exp\left(-\theta^2/2(1/\Delta^2-\mu\rho x \operatorname{Cosec}\phi)\right)d\theta = \frac{\sqrt{2\pi}}{\sqrt{1/\Delta^2-\mu\rho x \operatorname{Cosec}\phi}}$$

and hence

$$\nu_\phi = \frac{\delta\omega}{4\pi}\int_0^{x_k} \frac{\exp(-\mu\rho x \operatorname{Cosec}\phi)}{\sqrt{1-\mu\rho x\Delta^2 \operatorname{Cosec}\phi}}\cdot\frac{\partial n}{\partial x}dx \qquad ..(3)$$

This integral can be evaluated numerically. If the restriction of a small standard deviation Δ is removed, then clearly the expression for ν_ϕ in equation (3) is not valid. The problem of evaluating an expression for ν_ϕ without enforcing any restrictions is considered in the next section.

1.52

The expression for ν_ϕ is

$$\nu_\phi = \frac{\delta\omega}{4\pi}\cdot\frac{1}{\sqrt{2\pi}}\cdot\frac{1}{\Delta}\int_0^{x_k}\int_{-\pi/2}^{\pi/2} \exp(-\theta^2/2\Delta^2)\exp(-\mu\rho x \cos\theta \operatorname{Cosec}\phi)\frac{\partial n}{\partial x}dx\,d\theta$$

If we consider for the present the angle integral, one can write

$$\int_{-\pi/2}^{\pi/2} \exp(-\theta^2/2\Delta^2)\exp(-\mu\rho x \cos\theta \operatorname{Cosec}\phi)d\theta$$

$$= \int_{-\pi/2}^{\pi/2} \exp(-a\theta^2 - b\cos\theta)d\theta \qquad ..(1)$$

where $a = 1/2\Delta^2$

$b = \mu\rho \times \mathrm{Cosec}\,\phi$

Also

$$\exp(b\cos\theta) = \exp\left(b\left(1 - \frac{\theta^2}{2!} + \frac{\theta^4}{4!} - \frac{\theta^6}{6!} + \cdots + \frac{\theta^n}{n!}\right)\right)$$

$$= \exp(b).\exp\left(-\frac{b\theta^2}{2!}\right).\exp\left(\frac{b\theta^4}{4!}\right).\exp\left(-\frac{b\theta^6}{6!}\right).....$$

$$= \exp(b)\left\{\left(1-\frac{b\theta^2}{2!}+\frac{b^2\theta^4}{2!(2!)^2}-\frac{b^3\theta^6}{3!(2!)^3}+....\right)\left(1+\frac{b\theta^4}{4!}+\frac{b^2\theta^8}{2!(4!)^2}+....\right)\right.$$

$$\left.\left(1-\frac{b\theta^6}{6!}+\frac{b^2\theta^{12}}{2!(6!)^2}-.....\right)(.....)\right\}$$

Multiplying out the terms in the brackets we can write

$$\exp(-b\cos\theta) = \exp(-b)\left\{1 + \frac{b\theta^2}{2!} + (3b^2-b)\theta^4/4! - (-15b^3+15b^2-b)\theta^6/6!\right.$$

$$+(105b^4-210b^3+63b^2-b)\theta^8/8!$$

$$-(-945b^5+3150b^4-2205b^3+256b^2+b)\theta^{10}/10!$$

$$\left.+(10395b^6-51975b^5+65835b^4-15345b^3+561b^2-b)\theta^{12}/12!\right.$$

$$\left.+.....\right\}$$

The angle integral (1) in Section 1·45 can now be written

$$\int_{-\pi/2}^{\pi/2} \exp(-b\,\mathrm{Cos}\,\theta - a\theta^2)d\theta = 2\int_{0}^{\pi/2} \exp(-b\,\mathrm{Cos}\,\theta - a\theta^2)d\theta$$

$$= 2\int_{0}^{\pi/2} \exp(-a\theta^2)\exp(-b)\left\{1+f_1(b)\theta^2+f_2(b)\theta^4+f_3(b)\theta^6\ldots\right\}d\theta\ldots(2)$$

where $f_1(b) = b/2!$

$f_2(b) = (3b^2-b)/4!$

$f_3(b) = (15b^3-15b^2+b)/6!$

.

.

. etc.

From equation (2) the integral can be modified by writing

$$\int_{0}^{\pi/2} \exp(-a\theta^2).\theta^2\,d\theta = -\frac{d}{da}\int_{0}^{\pi/2} \exp(-a\theta^2)\,d\theta$$

$$\int_{0}^{\pi/2} \exp(-a\theta^2).\theta^4\,d\theta = -\frac{d}{da}\int_{0}^{\pi/2} \exp(-a\theta^2).\theta^2 d\theta$$

$$= \frac{d^2}{da^2}\int_{0}^{\pi/2} \exp(-a\theta^2)d\theta$$

$$\int_{0}^{\pi/2} \exp(-a\theta^2).\theta^6 d\theta = -\frac{d^3}{da^3}\int_{0}^{\pi/2} \exp(-a\theta^2)d\theta$$

.

.

.

.

$$\int_{0}^{\pi/2} \exp(-a\theta^2).\theta^{2n} = (-1)^n\,\frac{d^n}{da^n}\int_{0}^{\pi/2} \exp(-a\theta^2)d\theta$$

We can now write

$$\int_{-\pi/2}^{\pi/2} \exp(-a\theta^2 - b\cos\theta)\,d\theta = 2\int_0^{\pi/2} \exp(-a\theta^2 - b\cos\theta)\,d\theta$$

$$= 2\exp(-b)\left\{\int_0^{\pi/2} \exp(-a\theta^2)d\theta - f_1(b)\frac{d}{da}\int_0^{\pi/2} \exp(-a\theta^2)d\theta\right.$$

$$+ f_2(b)\frac{d^2}{da^2}\int_0^{\pi/2} \exp(-a\theta^2)d\theta \quad f_3(b)\frac{d^3}{da^3}\int_0^{\pi/2} \exp(-a\theta^2)d\theta$$

$$\left. + \ldots\ldots\ldots\ldots\ldots\ldots\ldots\right\}$$

Also

$$\int_0^{\pi/2} \exp(-a\theta^2)d\theta = \left(\frac{\pi}{2} - \frac{a\pi^3}{3x2^3} + \frac{a^2\pi^5}{5x2!x2^5} - \frac{a^3\pi^7}{7x3!x2^7} + \ldots\ldots\ldots\ldots\right.$$

$$\left. + \frac{(-1)^n a^n \pi^{2n+1}}{(2n+1)(n!)2^n}\right)$$

$$= \phi(a)$$

$$\int_0^{\pi/2} \exp(-a\theta^2).\theta^2 d\theta = -\frac{d}{da}\int_0^{\pi/2} \exp(-a\theta^2)d\theta$$

$$= \left(\frac{\pi^3}{3x2^3} - \frac{a\pi^5}{5x2^5} + \frac{a^2\pi^7}{7x2!x2^7} + \ldots\ldots\right)$$

$$= \phi_1(a)$$

.

.

.

$$\int_0^{\pi/2} \exp(-a\theta^2).\theta^n d\theta = \frac{\pi^{n+1}}{(n+1)2^{n+1}} - \frac{a\pi^{n+3}}{(n+3)2^{n+3}} + \frac{a^2\pi^{n+5}}{(n+5)x2!x2^{n+5}} + \cdots$$

$$= \psi_{n-1}$$

$$\therefore \int_{-\pi/2}^{\pi/2} \exp(-a\theta^2 - b\cos\theta\, d\theta)$$

$$= 2\exp(-b)\left\{\psi(a) - \psi_1(a)f_1(b) + \psi_2(a)f_2(b) - \ldots + \psi_{n-1}(a)f_{n-1}(b)\ldots\right\}$$

where $f_1(b)$, $f_2(b)$ etc.

and $\psi_1(a)$, $\psi_2(a)$ etc.

are defined as shown previously.

The number of quanta emerging per electron is therefore

$$\nu_\phi = \frac{\delta\omega}{4\pi}\cdot\frac{1}{\sqrt{2\pi}}\cdot\frac{1}{\delta}\int_0^{x_k} 2\exp(-b)\left(\psi(a) - \psi_1(a)f_1(b) + \psi_2(a)f_2(b)\ldots\right)\frac{\partial n}{\partial x}dx$$

The above integral can now be evaluated numerically, and results are shown in the appendix. These show the values of N_ϕ obtained for different accelerating voltages, and different angles of emission with respect to the target surface.

1·46

The graphs of Copper Kα emission against accelerating voltage are plotted in Fig. 14 - 20 for values of ϕ equal to 1°, 3°, 5°, 10°, 20°, 30°, 40° and 50° and for a range of accelerating voltages up to 60 kilovolts. For comparison there is plotted the emission at corresponding angles ϕ when the incident electron beam is assumed to follow a straight line path in the target undeviated from the direction of incidence, i.e. when diffusion in the target is not accounted for. It is at once evident from these curves that the value of Copper Kα emission increases when diffusion in the target is taken into account. This is to be expected since the loss from self absorption in the target is diminished, and particularly so for angles of emission $\phi \leq 5^{\circ}$. At a sufficiently high voltage, whatever the angle of emission, a maximum in the graph for emission is to be expected since the greater the acceleration of the incident electron beam, the more the X ray quanta are produced at greater depths below the target surface and the greater the loss from self absorption in the target. For angles of emission ϕ equal to 30°, 40° and 50° and for accelerating voltages below 30 kilovolts, there is very little difference in the values of N_{ϕ} when corrected and when not corrected for diffusion.

$\phi = 1^\circ$

FIG 14

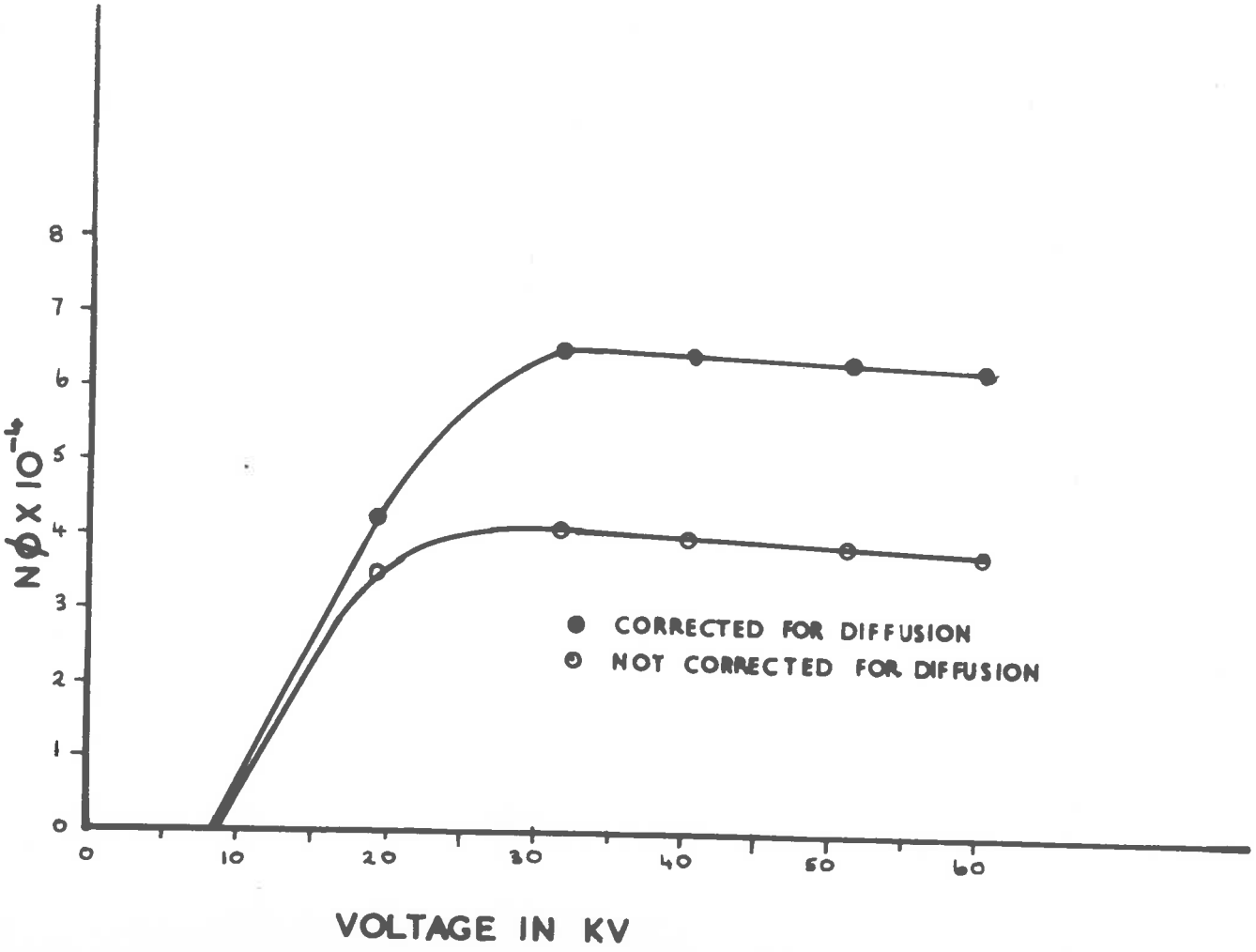

FIG 15

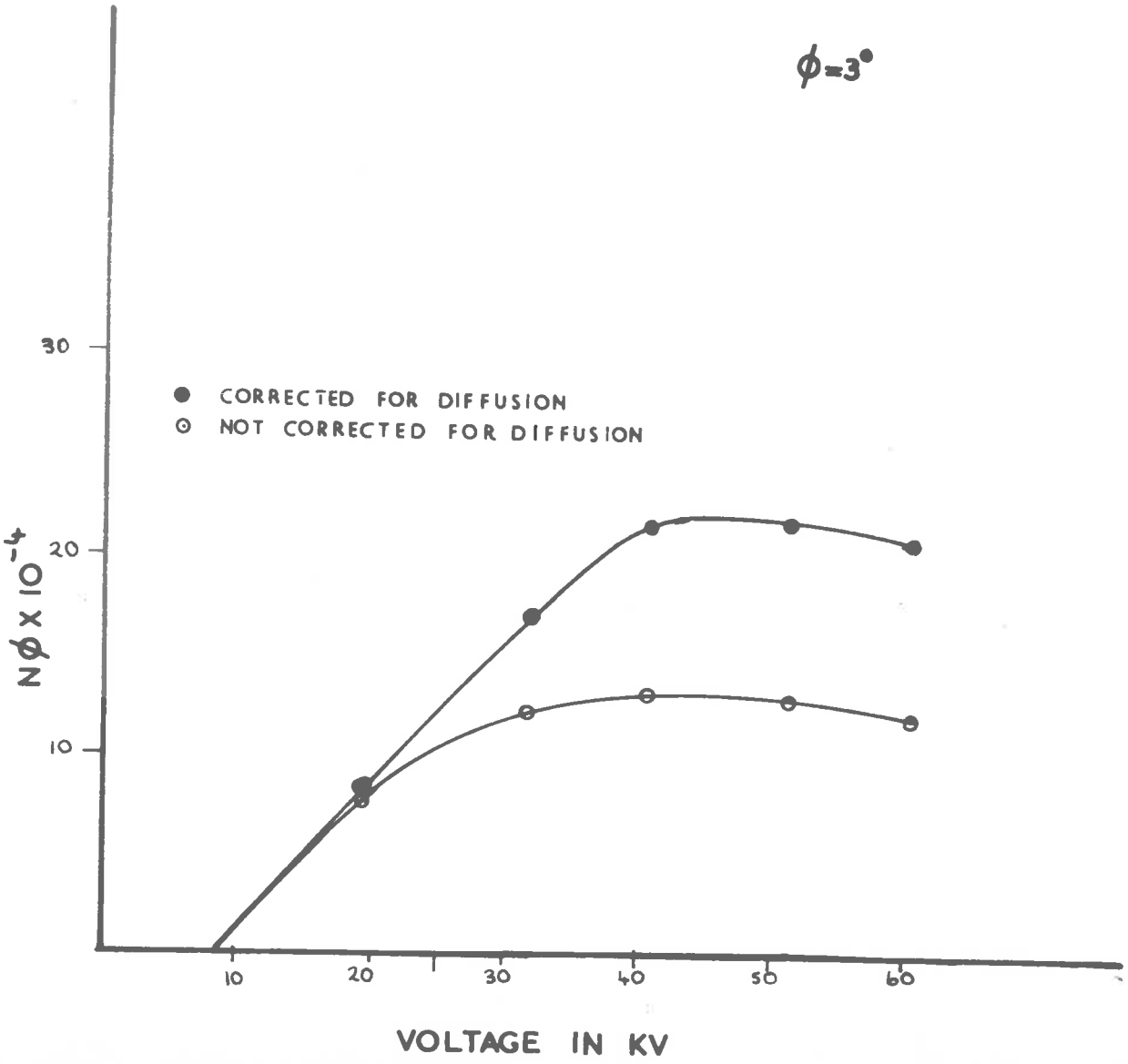
$\phi=3^\circ$
30
20
10
$N\phi \times 10^{-4}$
CORRECTED FOR DIFFUSION
NOT CORRECTED FOR DIFFUSION
10
20
30
40
50
60
VOLTAGE IN KV

FIG 16

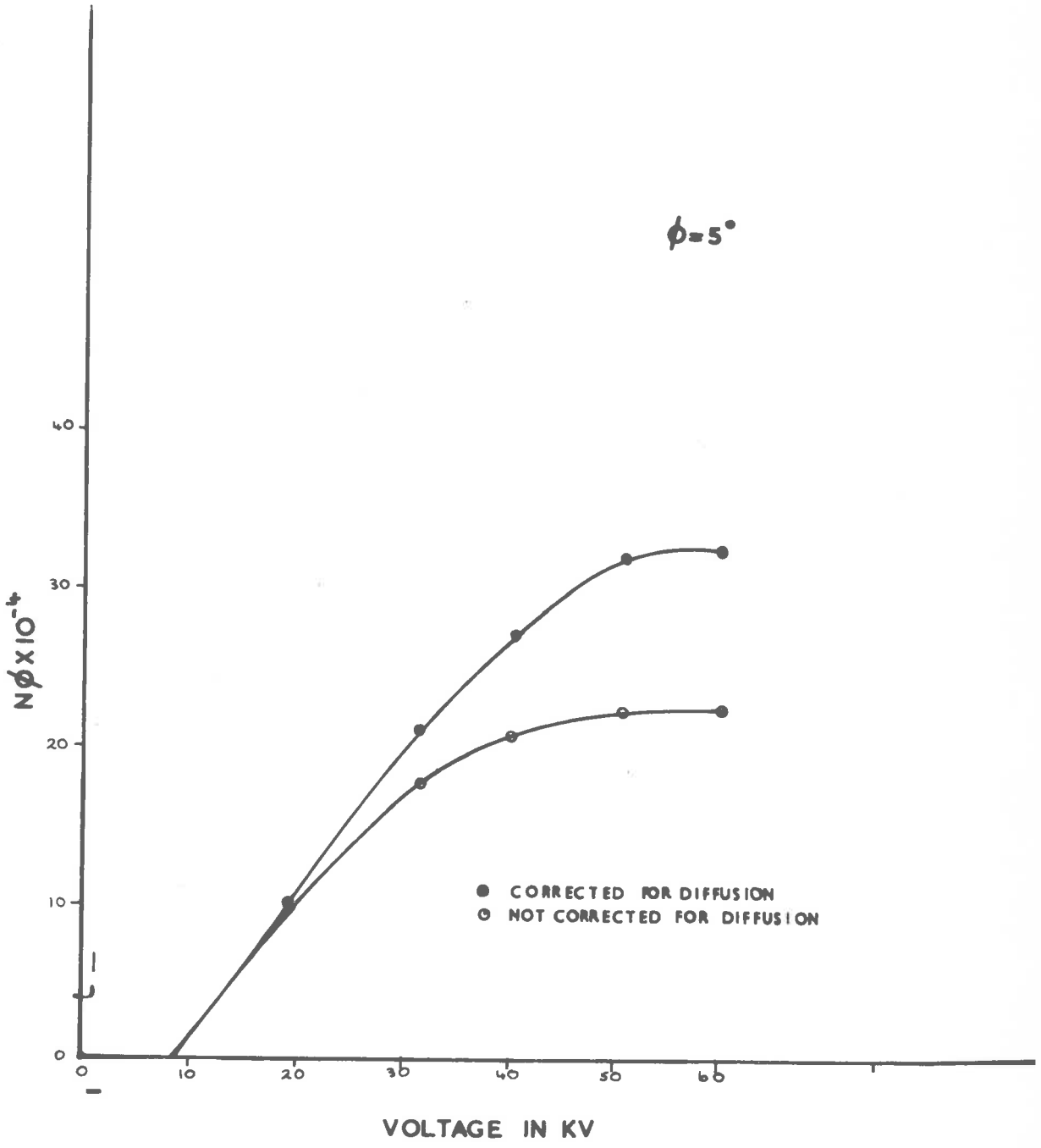
φ=5°
40
30
20
10
0
NφX10⁻⁴
0
10
20
30
40
50
60
● CORRECTED FOR DIFFUSION
⊙ NOT CORRECTED FOR DIFFUSION
VOLTAGE IN KV

FIG 17

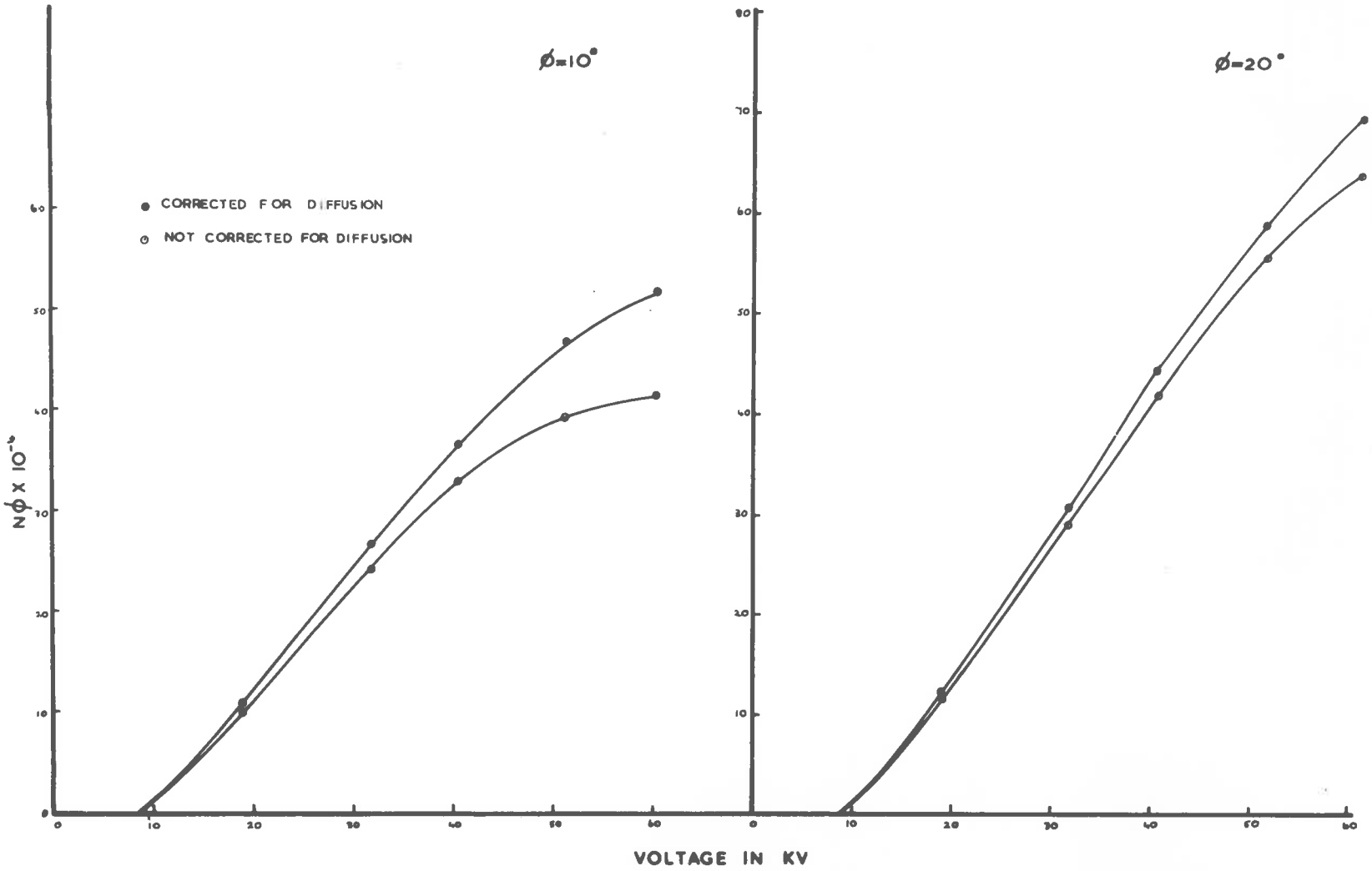
ϕ=10°
ϕ=20°
● CORRECTED FOR DIFFUSION
⊙ NOT CORRECTED FOR DIFFUSION
Nϕ X 10⁻⁶
VOLTAGE IN KV

FIG 18

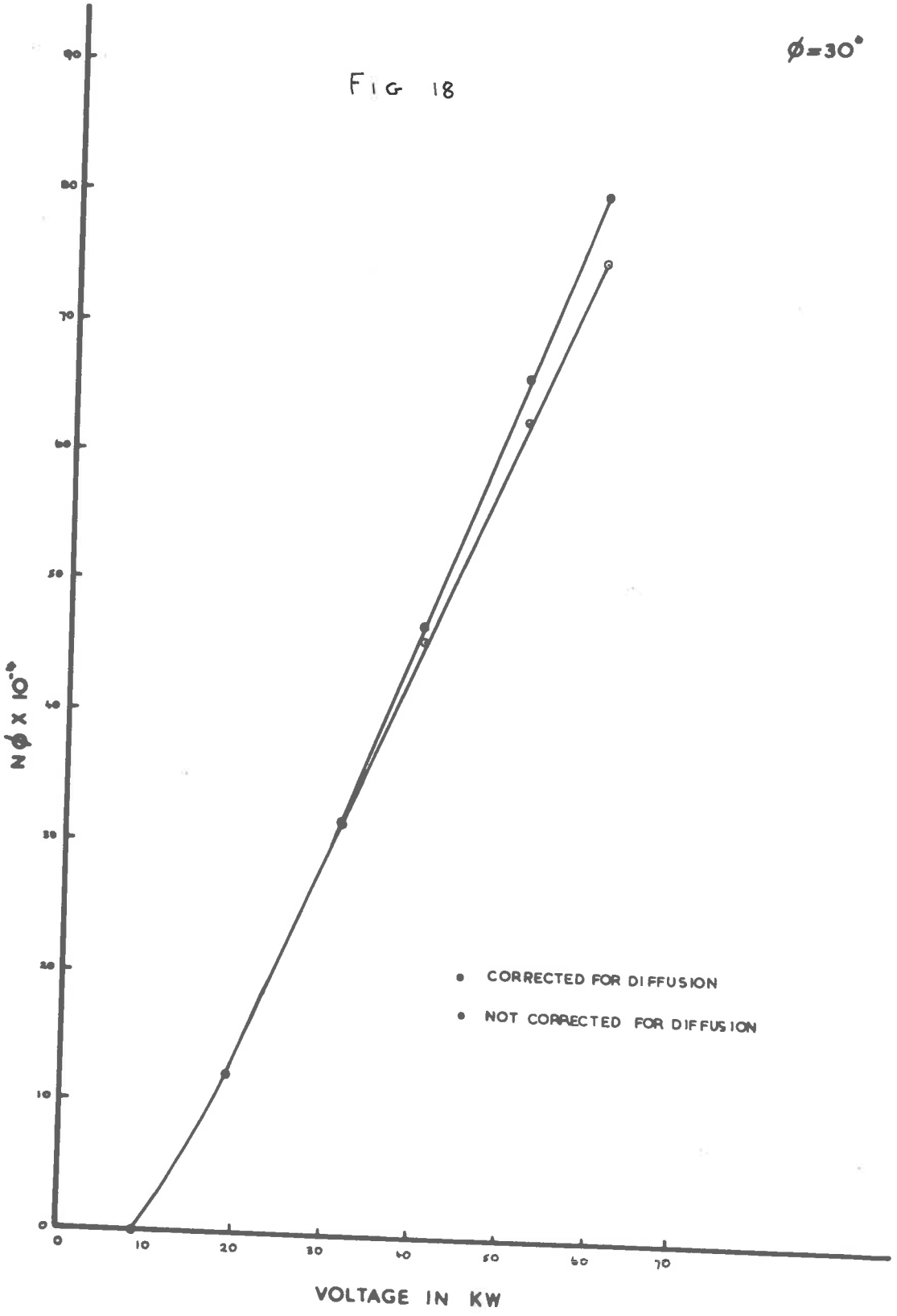
ϕ=30°
$N\phi \times 10^{-6}$
VOLTAGE IN KW
0
10
20
30
40
50
60
70
80
90
• CORRECTED FOR DIFFUSION
• NOT CORRECTED FOR DIFFUSION

FIG 19

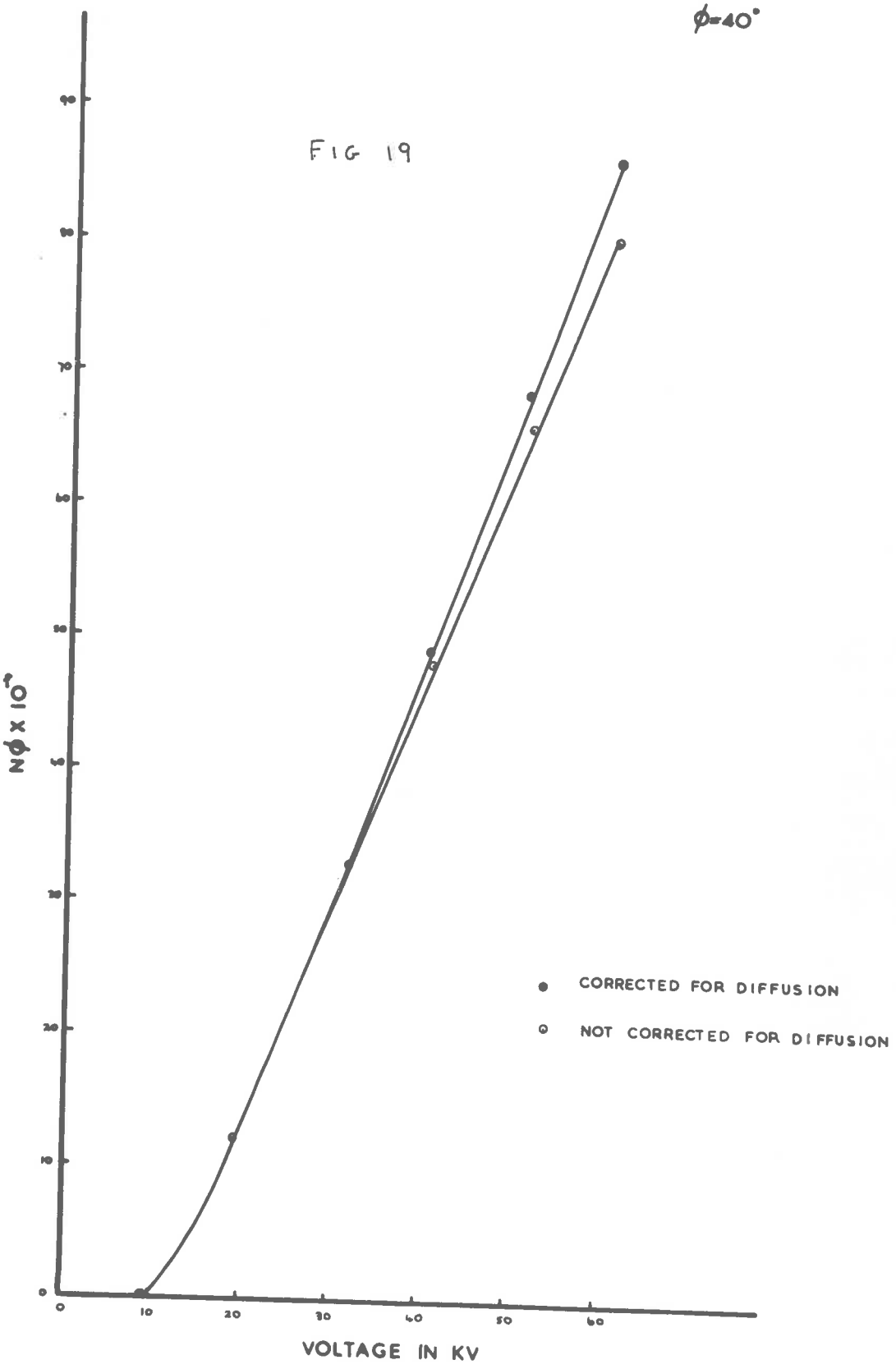
φ=40°
Nφ x 10⁻⁶
0
10
20
30
40
50
60
VOLTAGE IN KV
CORRECTED FOR DIFFUSION
NOT CORRECTED FOR DIFFUSION

FIG 20

$\phi = 50°$

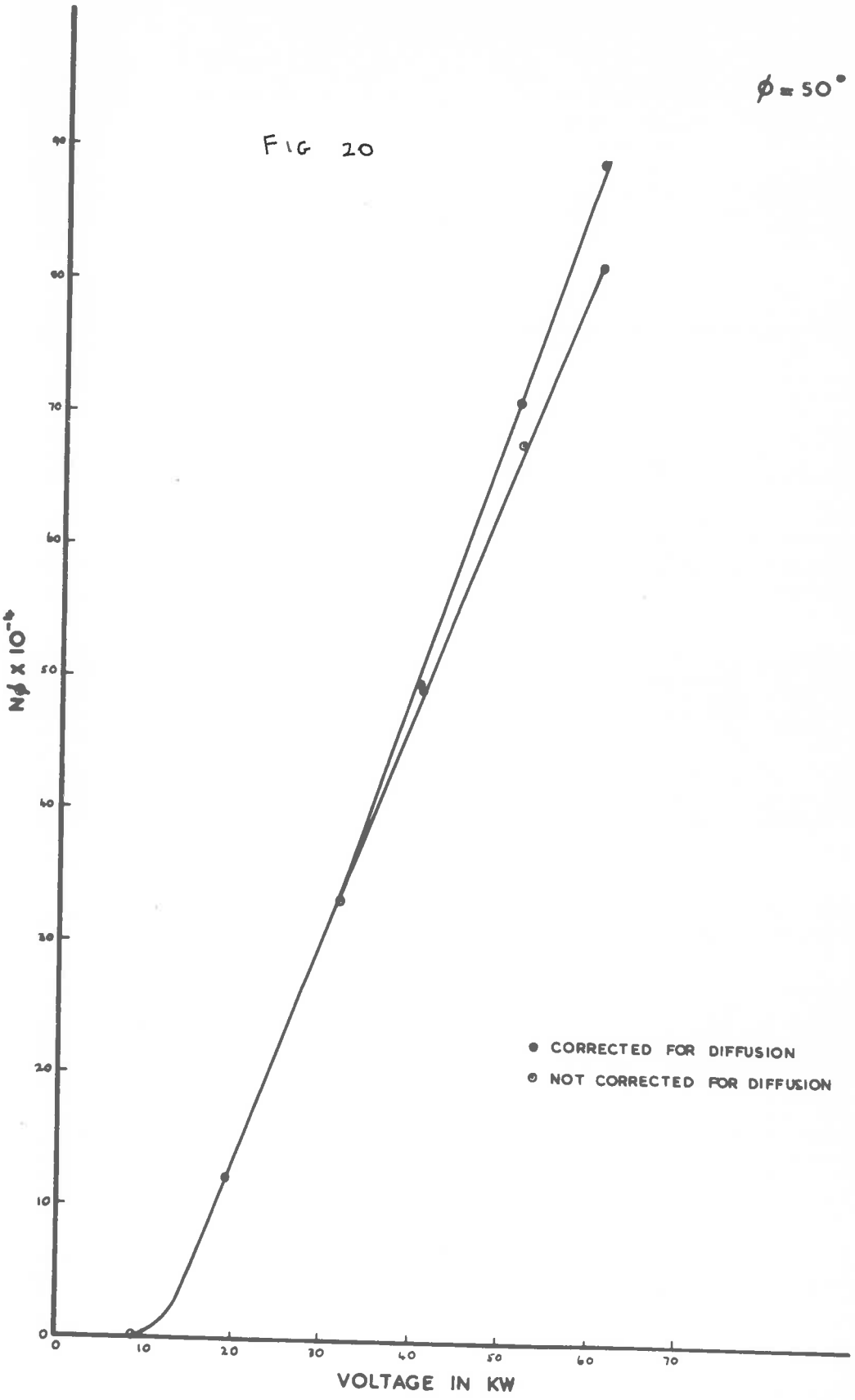
Nϕ X 10⁻⁴
0
10
20
30
40
50
60
70
VOLTAGE IN KW
● CORRECTED FOR DIFFUSION
⊙ NOT CORRECTED FOR DIFFUSION

For accelerating voltages greater than 30 kilovolts there is an appreciable difference in the emission which becomes larger especially as the angle of emission ϕ becomes smaller.

1•2

Assuming diffusion in the target, an expression for the intensity of Kα radiation is obtained when the normal to the target makes an angle α with the incident electron beam. From Fig. 21 it is seen that

$$\frac{r}{\sin\left(90-(\alpha+\theta)\right)} = \frac{x}{\sin\phi}$$

$$\text{and } \therefore \quad r = x\,\mathrm{Cosec}\,\phi\,\cos(\alpha+\theta)$$

which reduces to $x\,\mathrm{Cosec}\,\phi\cos\theta$, when $\alpha = 0$, i.e. when the normal to the target and the incident electron beam are parallel. The quanta emitted at an angle ϕ with the target surface have their intensity diminished by a factor

$$\exp(-\mu\rho x\,\mathrm{Cosec}\,\phi\cos(\alpha+\theta))$$

where μ and ρ are defined as before, and the angles ϕ, α and θ are shown in Fig. 21. Proceeding as before, the expression for the intensity of emission per electron is

$$\nu_{\phi}^{\alpha} = \frac{\delta\omega}{4\pi}\cdot\frac{1}{\sqrt{2\pi}}\cdot\frac{1}{\Delta}\int_0^{x_k}\int_{-\pi/2}^{\pi/2}\exp(-\theta^2/2\Delta^2)\exp\left(-\mu\rho x\,\mathrm{Cosec}\phi\cos(\theta+\alpha)\right)\frac{\partial n}{\partial x}dx\,d\theta$$

FIG 21

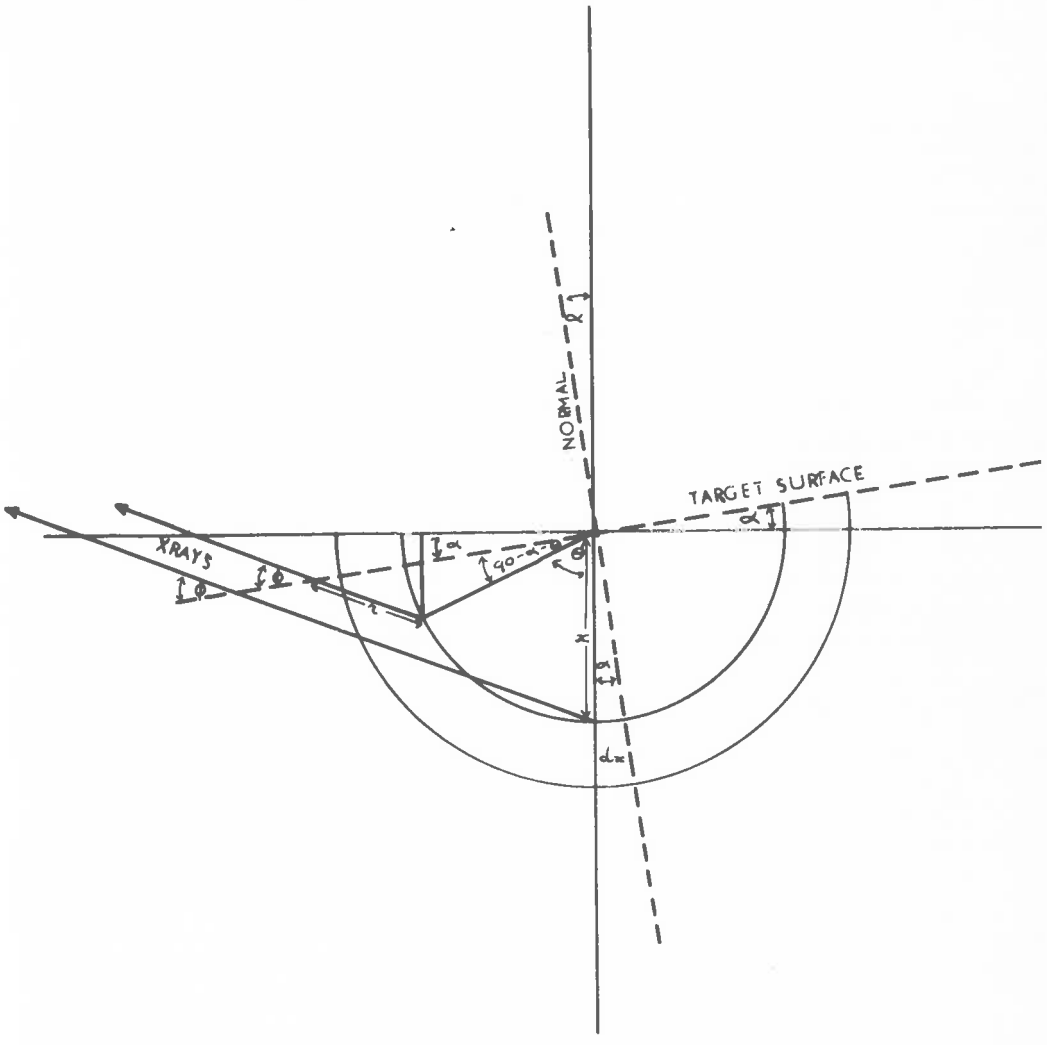

$$= \frac{\delta\omega}{4\pi}\cdot\frac{1}{\sqrt{2\pi}}\cdot\frac{1}{\Delta}\int_0^{x_2}\int_{-\pi/2}^{\pi/2} \exp\Big(-a\theta^2 - b\,\mathrm{Cos}(\theta+\alpha)\Big)\frac{\delta n}{\delta x}\,dx\,d\theta \qquad ..(1)$$

$$\text{where } a = \frac{1}{2\Delta^2}$$

$$b = \mu\rho \times \mathrm{Cosec}\,\phi$$

By comparison with Section 1·45 where the expression for $\exp(\pm b\,\mathrm{Cos}\,\theta)$ was obtained, we can here write

$$\exp\Big(-b\,\mathrm{Cos}(\theta+\alpha)\Big) = \exp(-b)\Big\{1 + f_1(b)(\theta+\alpha)^2 + f_2(b)(\theta+\alpha)^4 + f_3(b)(\theta+\alpha)^6 + \ldots + f_n(b)(\theta+\alpha)^n + ..\Big\} \qquad ..(2)$$

where $f_1(b)$, $f_2(b)$ .... etc. are as defined in Section 1·45.

Considering the angle integral in (1), we can write after making use of (2)

$$\int_{-\pi/2}^{\pi/2} \exp\Big(-a\theta^2 - b\,\mathrm{Cos}(\theta+\alpha)\Big)d\theta$$

$$= \exp(-b)\int_{-\pi/2}^{\pi/2} \exp(-a\theta^2)\Big\{1 + f_1(b)(\theta+\alpha)^2 + f_2(b)(\theta+\alpha)^4 + f_3(b)(\theta+\alpha)^6 + \ldots + f_n(b)(\theta+\alpha)^{2n} \ \ldots\Big\}$$

$$= \exp(-b)\Big\{ \int_{-\pi/2}^{\pi/2} \exp(-a\theta^2)d\theta \quad f_1(b)\int_{-\pi/2}^{\pi/2} \exp(-a\theta^2)(\theta^2+2\theta\alpha+\alpha^2)d\theta$$

$$+ f_2(b)\int_{-\pi/2}^{\pi/2} \exp(-a\theta^2)(\theta^4 + 4\theta^3\alpha + 6\theta^2\alpha^2 + 4\theta\alpha^3 + \alpha^4)\,d\theta$$

$$+ f_3(b)\int_{-\pi/2}^{\pi/2} \exp(-a\theta^2)(\theta^6+6\theta^5\alpha+15\theta^4\alpha^2+20\theta^3\alpha^3+15\theta^2\alpha^4+6\theta\alpha^5+\alpha^6)d\theta$$

$$+ \cdots\cdots + \cdots\cdots + \text{etc.} \Big\}$$

In each of the above integrands, it is readily seen that any odd powers of θ multiplying the factor $\exp(-a\theta^2)$ will cause that term to vanish. Thus

$$\int_{-\pi/2}^{\pi/2} \exp\Big(-a\theta^2 - b\cos(\theta+\alpha)\Big)d\theta$$

$$= \exp(-b)\Big\{ \int_{-\pi/2}^{\pi/2} \exp(-a\theta^2)d\theta + f_1(b)\int_{-\pi/2}^{\pi/2} \exp(-a\theta^2)(\theta^2+\alpha^2)d\theta$$

$$+ f_2(b)\int_{-\pi/2}^{\pi/2} \exp(-a\theta^2)(\theta^4 + 6\theta^2\alpha^2 + \alpha^4)d\theta$$

$$+ f_3(b)\int_{-\pi/2}^{\pi/2} \exp(-a\theta^2)(\theta^6 + 15\theta^4\alpha^2 + 15\theta^2\alpha^4 + \alpha^6)d\theta$$

$$+ \cdots\cdots + \text{etc.} \Big\}$$

$$\therefore \int_{-\pi/2}^{\pi/2} \exp\left(-a\theta^2 - b\,\mathrm{Cos}(\theta+\alpha)\right)d\theta$$

$$= 2\exp(-b)\Big\{\psi(a) + f_1(b)\left(\psi_1(a) + \alpha^2\psi(a)\right)$$

$$+ f_2(b)\left(\psi_2(a) + 6\alpha^2\psi_1(a) + \alpha^4\psi(a)\right)$$

$$+ f_3(b)\left(\psi_3(a) + 15\alpha^2\psi_2(a) + 15\alpha^4\psi_1(a) + \alpha^6\psi(a)\right)$$

$$+ \ldots\ldots + \text{etc.}\Big\} = G(p)$$

where $f_1(b)$, $f_2(b)$ ... etc.

and $\psi(a)$, $\psi_1(b)$, $\psi_2(b)$ ... etc.

are as defined previously in Section 1·45.

We can now write for ν_ϕ, the intensity of Kα radiation per electron at an angle ϕ with the target surface

$$\nu_\phi = \frac{\delta\omega}{4\pi}\cdot\frac{1}{\sqrt{2\pi}}\cdot\frac{1}{\Delta}\int_0^{x_k} 2\exp(-b)\,G(p)\,\frac{\partial n}{\partial x}\,dx$$

The evaluation of this integral has been carried out numerically, and results are given in the appendix for the following values of the parameters

α: 20°, 30°, 40° and 50°

ϕ: 1°, 3°, 5°, 10°, 20°, 30°, 40° and 50°

V: 20 - 60 kilovolts

These results are shown plotted in Figures 22 - 28 where the emission N_ϕ is plotted as a function of accelerating voltage for values of $\phi = 1^\circ$, 3°, 5°, 10°, 20°, 30°, 40° and 50° and for values of $\alpha = 30^\circ$. For comparison there is plotted the emission N_ϕ at corresponding angles of ϕ and θ when the incident electron beam is assumed to follow a straight line path in the target. For angles of emission $\phi = 30^\circ$, 40° and 50° and when the normal to the target is inclined at 30° to the incident electron beam it can be seen from these graphs that there is very little difference between the values of emission N_ϕ calculated from either of the two formulae

$$N_\phi = \frac{1}{\sqrt{2\pi}} \cdot \frac{k}{\Delta} \int_0^{x_k} 2 \exp(-b)\, G(p) \frac{\partial n}{\partial x} dx \qquad ..(1)$$

and

$$N_\phi = k \int_0^{x_k} \exp(-\mu\rho x \operatorname{Cosec} \phi \operatorname{Cos} \theta) \frac{\partial n}{\partial x} dx \qquad ..(2)$$

when the accelerating voltage is less than 40 kilovolts. For higher accelerating voltages and for the same angles of

FIG 22

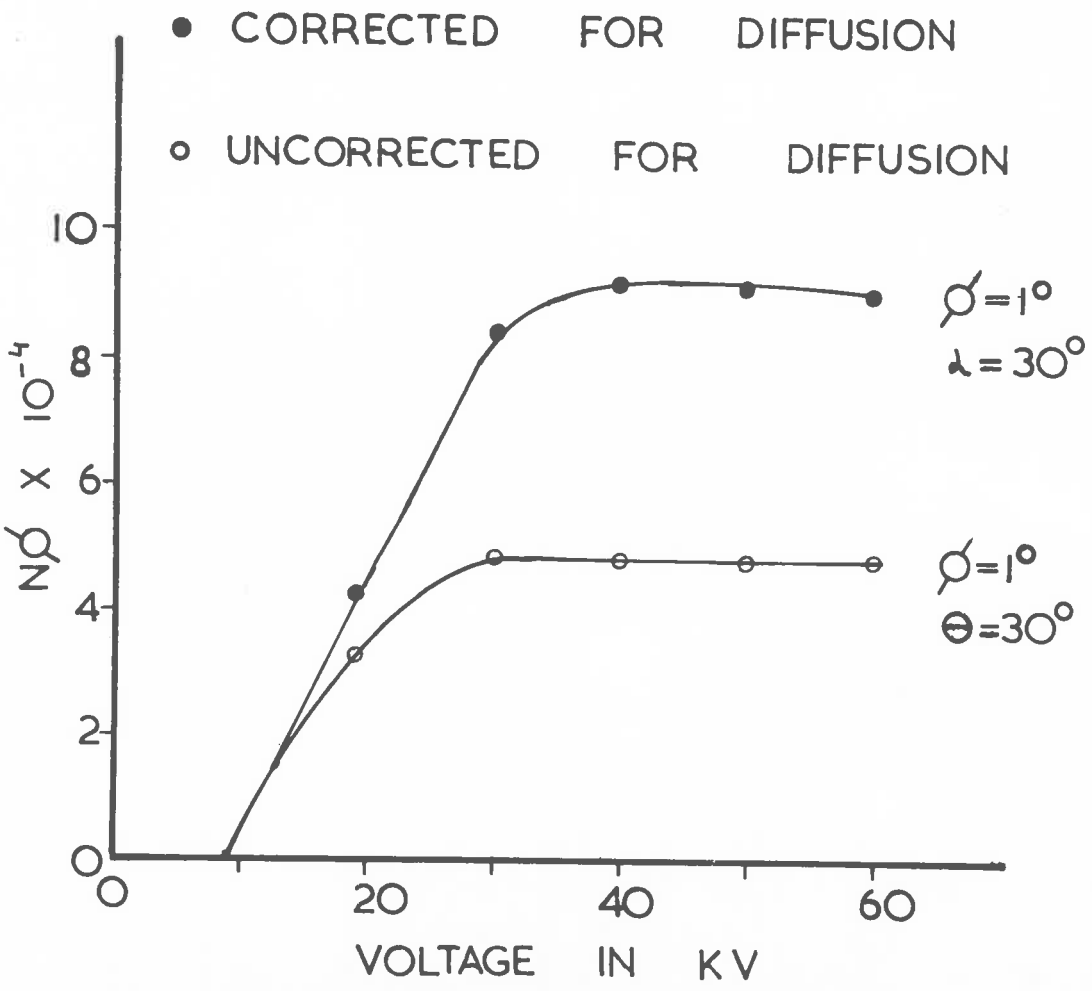
CORRECTED FOR DIFFUSION
UNCORRECTED FOR DIFFUSION
10
8
6
4
2
0
$N\sigma \times 10^{-4}$
0
20
40
60
VOLTAGE IN KV
$\sigma = 1°$
$\lambda = 30°$
$\sigma = 1°$
$\Theta = 30°$

FIG 23

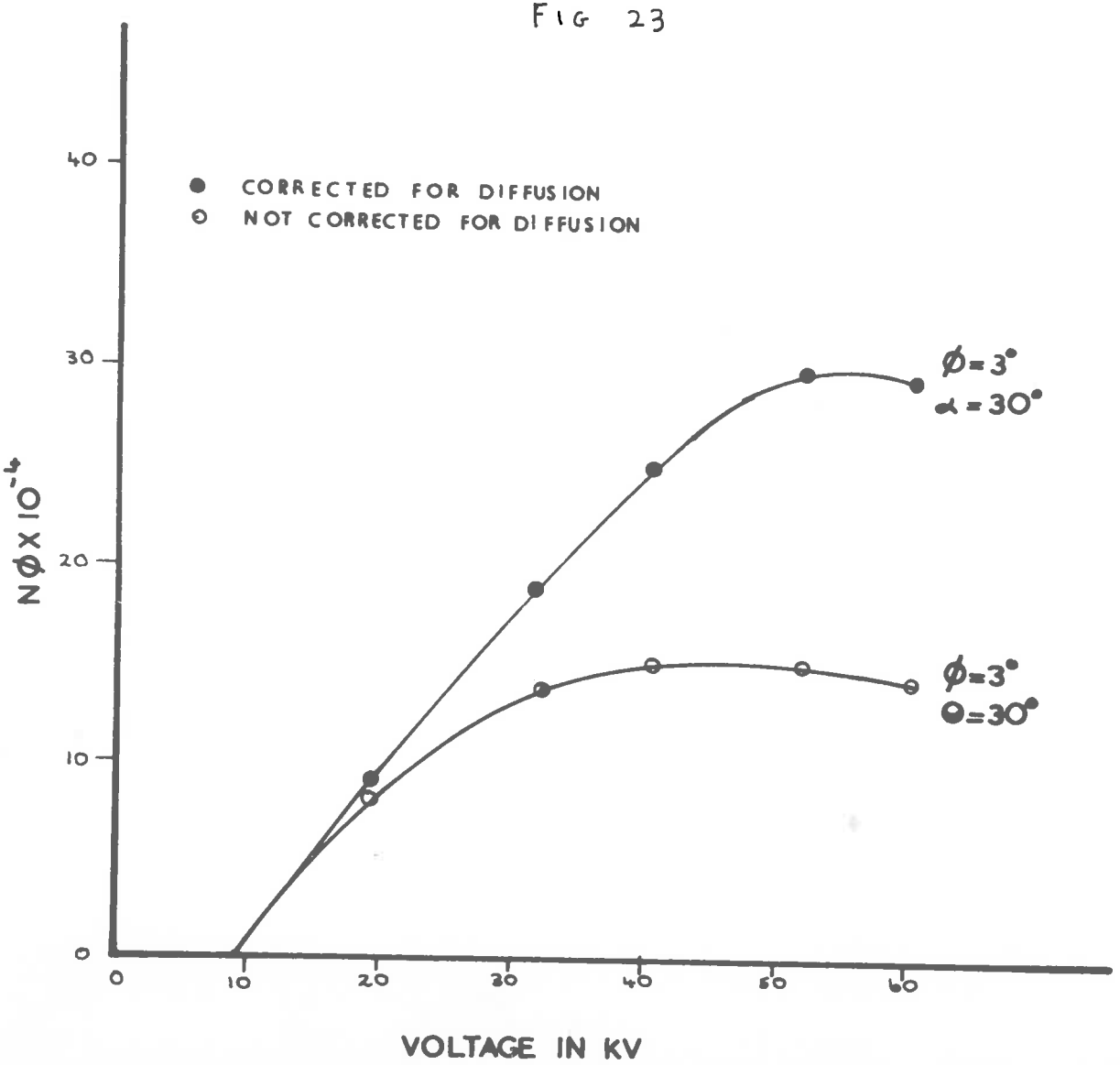
CORRECTED FOR DIFFUSION
NOT CORRECTED FOR DIFFUSION
Nϕ X 10⁻⁴
40
30
20
10
0
0
10
20
30
40
50
60
ϕ=3°
α=30°
ϕ=3°
θ=30°
VOLTAGE IN KV

FIG 24

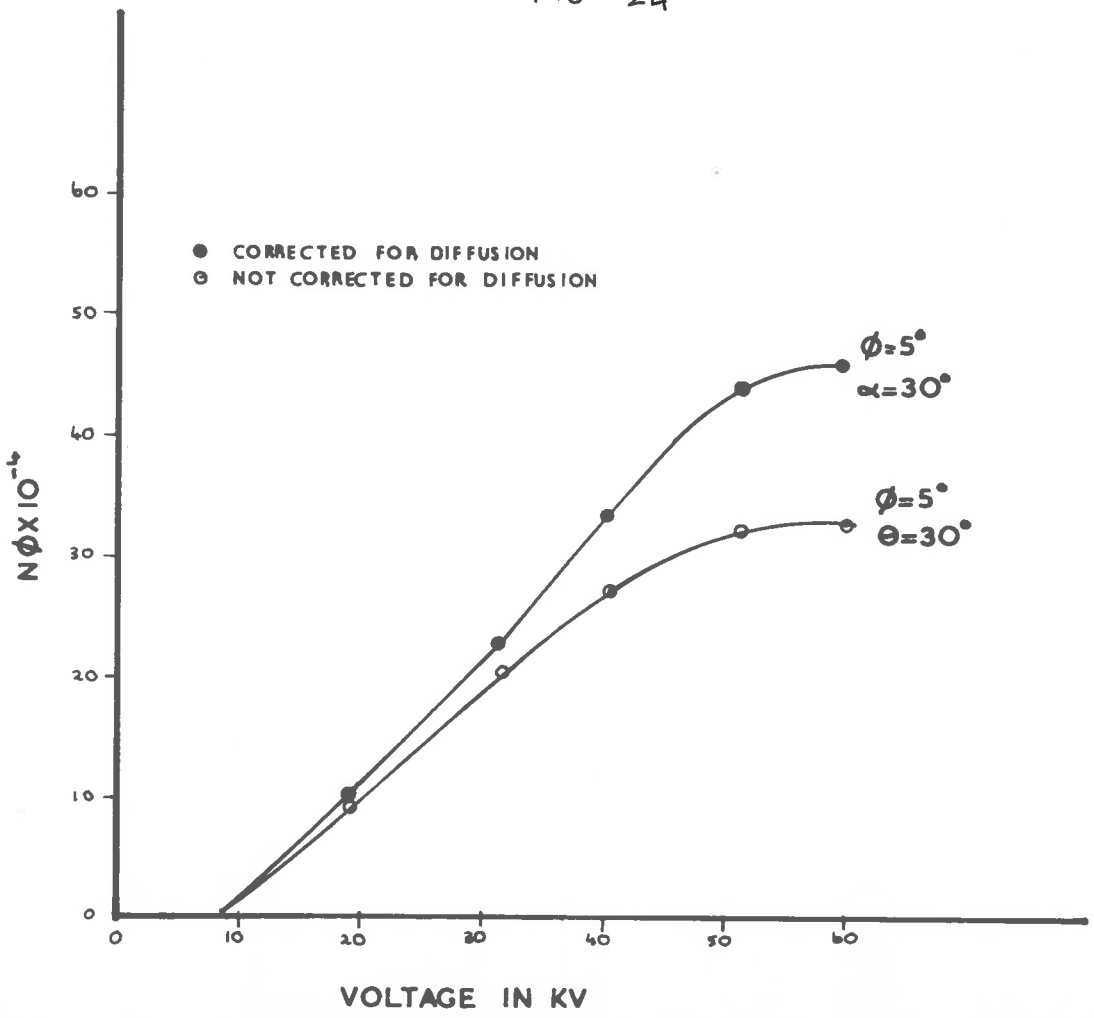
CORRECTED FOR DIFFUSION
NOT CORRECTED FOR DIFFUSION
Ø=5°
α=30°
Ø=5°
Θ=30°
NØX10⁻⁴
0
10
20
30
40
50
60
VOLTAGE IN KV

FIG 25

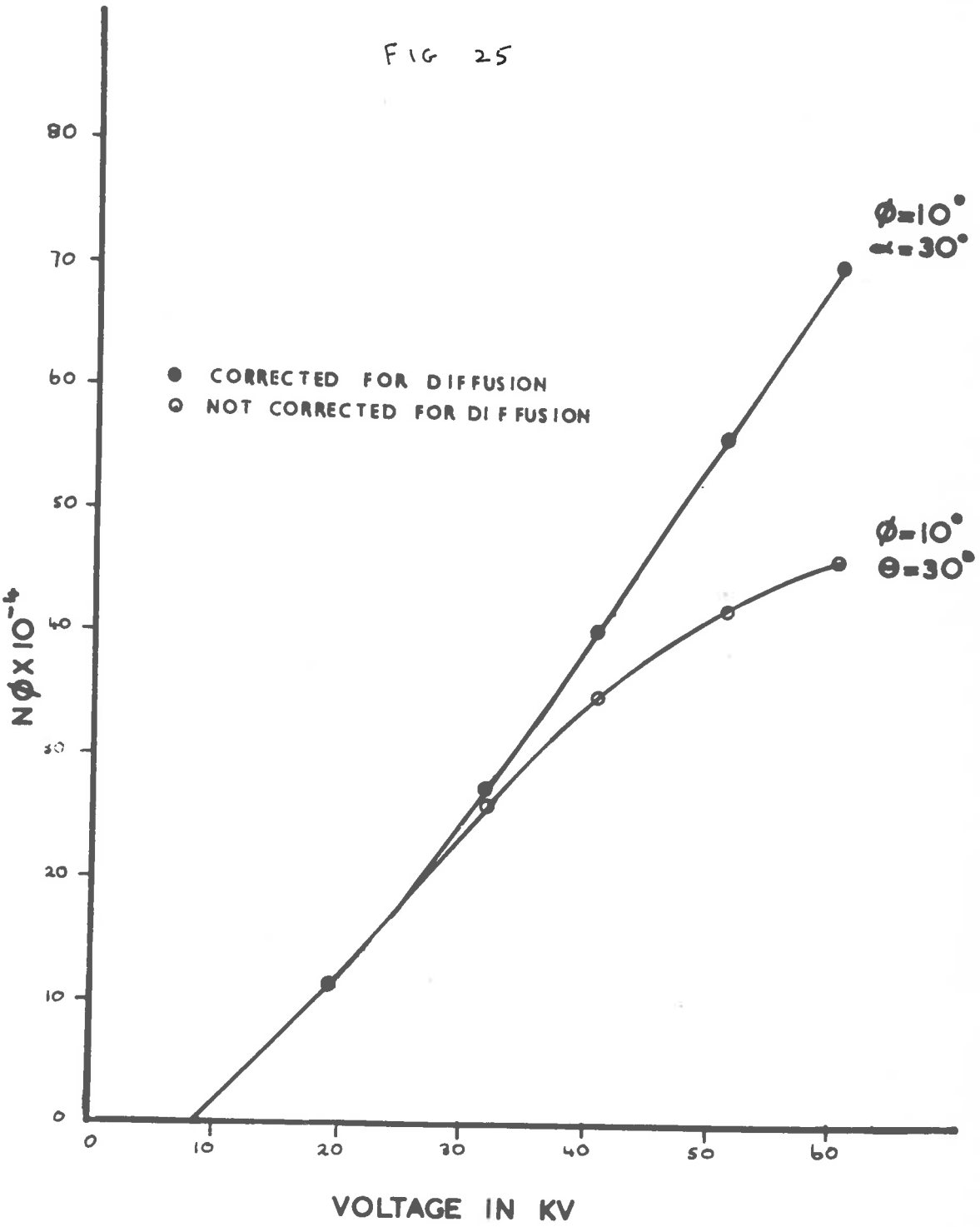
80
70
60
50
40
30
20
10
0
0
10
20
30
40
50
60
Nφ X 10⁻⁴
VOLTAGE IN KV
● CORRECTED FOR DIFFUSION
○ NOT CORRECTED FOR DIFFUSION
φ=10°
α=30°
φ=10°
θ=30°

FIG 26

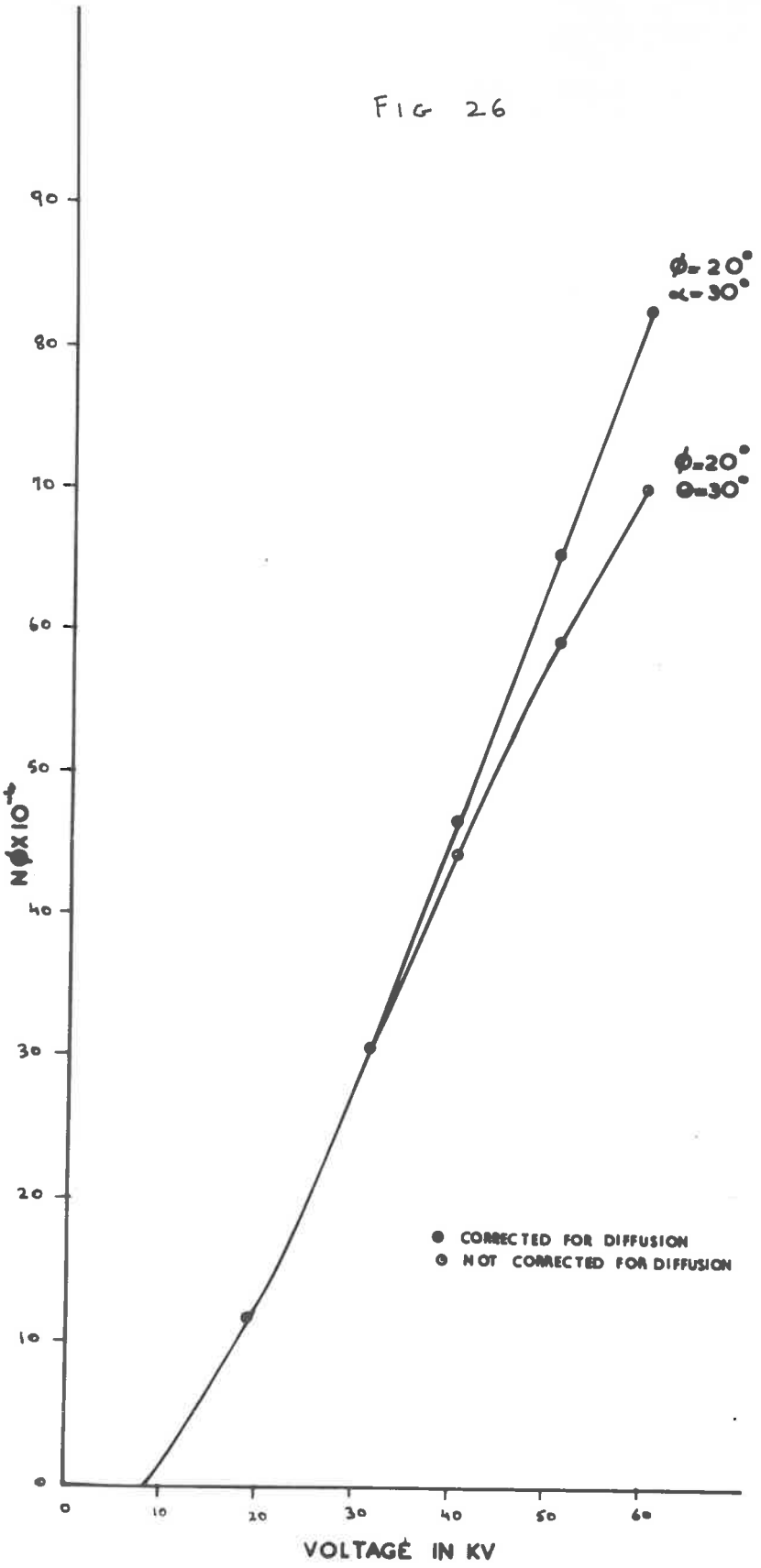
90
80
70
60
50
40
30
20
10
0
Nϕ X 10⁴
ϕ= 20°
α= 30°
ϕ=20°
θ=30°
● CORRECTED FOR DIFFUSION
⊙ NOT CORRECTED FOR DIFFUSION
0
10
20
30
40
50
60
VOLTAGE IN KV

FIG 27

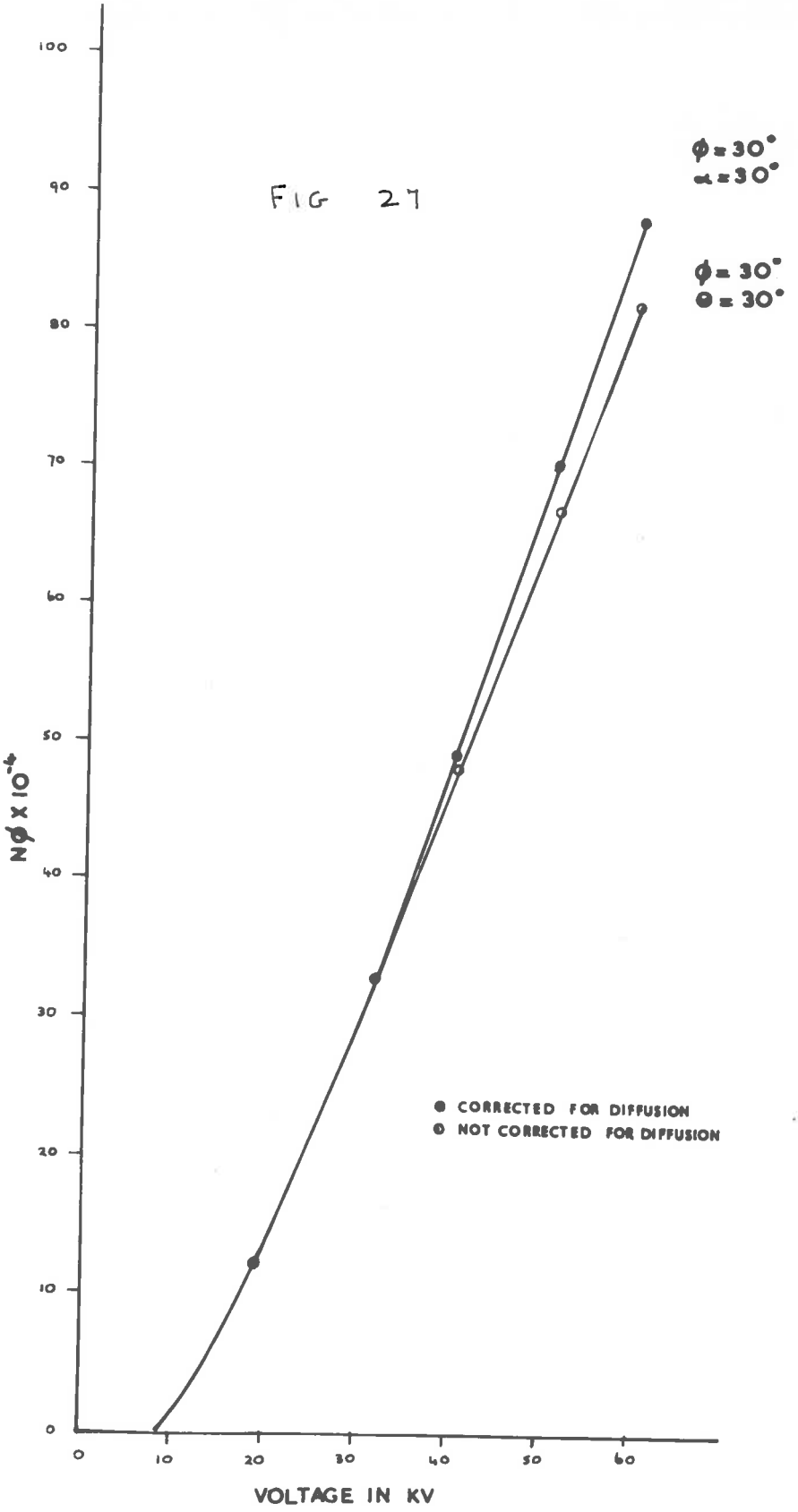
φ = 30°
α = 30°
φ = 30°
θ = 30°
Nφ X 10⁻⁴
VOLTAGE IN KV
● CORRECTED FOR DIFFUSION
○ NOT CORRECTED FOR DIFFUSION
0
10
20
30
40
50
60
70
80
90
100

FIG 28

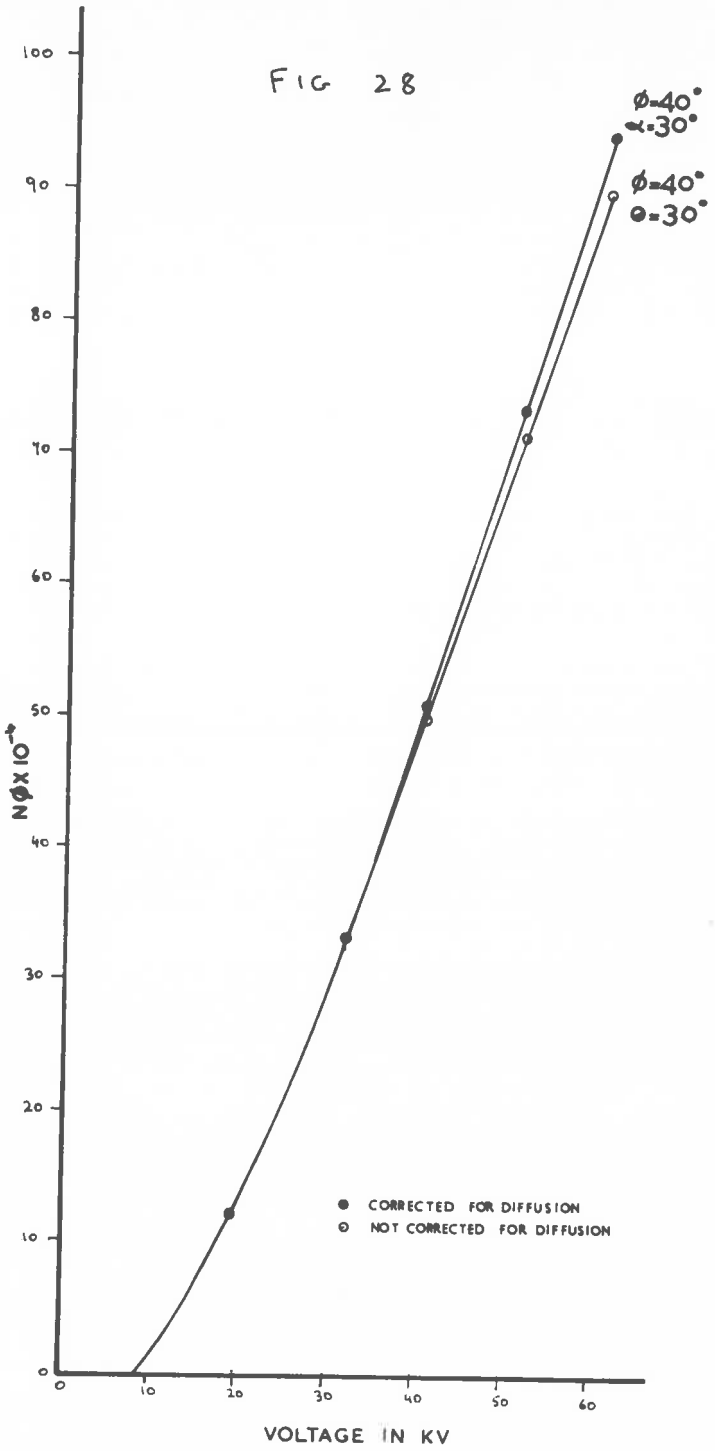
Ø=40°
α=30°
Ø=40°
Θ=30°
100
90
80
70
60
50
40
30
20
10
0
N Ø X 10⁻⁴
0
10
20
30
40
50
60
VOLTAGE IN KV
● CORRECTED FOR DIFFUSION
⊙ NOT CORRECTED FOR DIFFUSION

Fig 28(a)

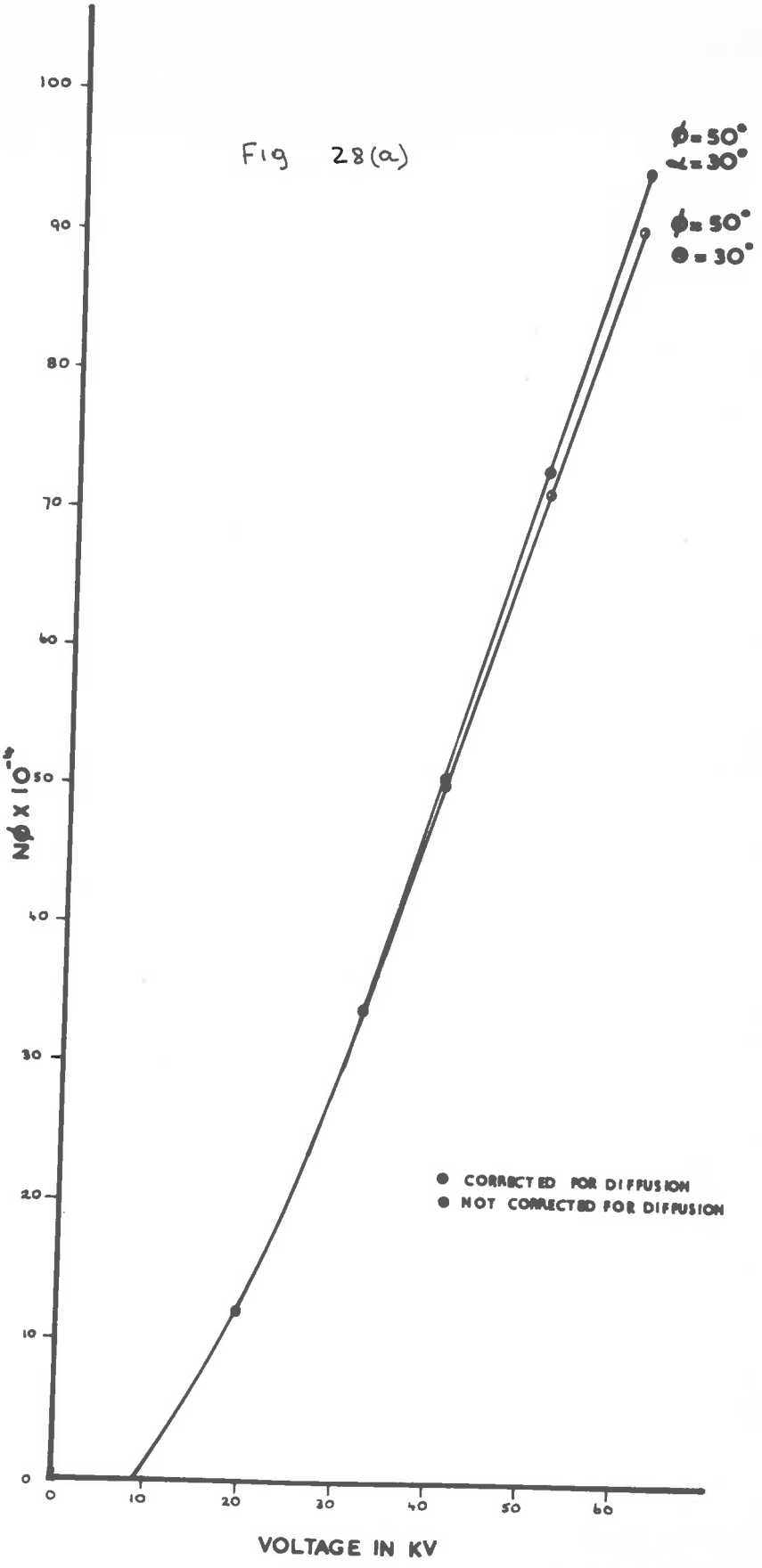
100
90
80
70
60
50
40
30
20
10
0
Nφ X 10⁻⁹
0
10
20
30
40
50
60
VOLTAGE IN KV
φ = 50°
α = 30°
φ = 50°
● = 30°
● CORRECTED FOR DIFFUSION
● NOT CORRECTED FOR DIFFUSION

emission ϕ, the value of the emission N_ϕ calculated from either (1) or (2) do not differ by more than 10 per cent.

However the effect of diffusion of the incident electron beam in the target becomes apparent especially for small angles of emission and large accelerating voltages. Thus for $\phi = 5^\circ$, the value of the emission N_ϕ at 60 kilovolts calculated from (1) above is 30 per cent larger than that calculated from (2) where the beam of electrons is assumed to follow a straight line path in the target. At $\phi = 1^\circ$ and for an accelerating voltage greater than 40 kilovolts the ratio of the calculated value of the emission N_ϕ from the above two formulae is almost 2:1.

EXPERIMENTAL PROBLEM FOR THE ISOLATION OF COPPER Kα RADIATION.

2·1

Before the measurements of the absolute intensities of Copper Kα radiation were begun a considerable amount of effort was devoted to determining the most efficient means of seperating the Copper Kα quanta from the heterogenous radiation emitted from a Copper target of an X ray tube. This can be achieved by two methods:

(a) by using non dispersive methods,

(b) by means of a crystal monochromator.

Since the latter method is complicated it was first decided to investigate the non dispersive methods available to select the desired wavelength from the X ray continuum.

Fig. 29(a) is a typical spectrum obtained from an X ray tube with a Copper target (W. Parrish and T. Kohler 1956). The tube was operated at 40 kilovolts peak voltage with full wave rectification the analysing crystal being Silicon ((111) plane). Besides the continuous spectrum there is the Copper Kβ radiation of wavelength 1·39 Å and of intensity approximately 12 per cent that of the Copper Kα radiation. Curve (b) of Fig. 29 shows the effect of placing a Nickel filter of 0·02 cm. thickness in front of

FIG 29

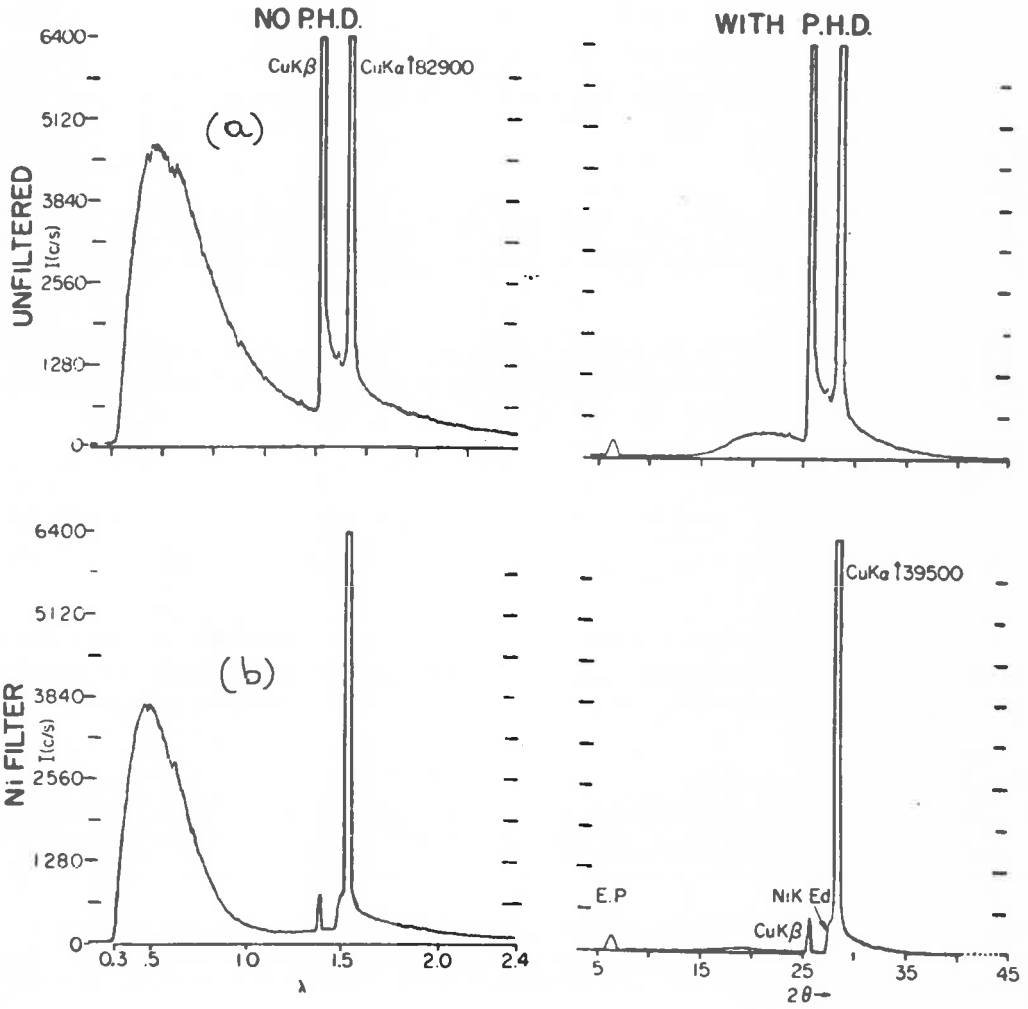
NO P.H.D.
WITH P.H.D.
UNFILTERED
I(c/s)
6400
5120
3840
2560
1280
0
(a)
CuKβ
CuKα ↑82900
Ni FILTER
(b)
CuKα ↑39500
E.P
NiK Ed
CuKβ
0.3
.5
1.0
1.5
2.0
2.4
λ
5
15
25
35
45
2θ

the window of the X ray tube. In particular it can be noticed that although the intensity of the continuous spectrum is still appreciable, the Kβ radiation has its intensity reduced to a negligible amount of its value without the Nickel filter.

To eliminate both the Kβ and the continuous radiation, a pair of differential or balanced filters are used. These filters have their thicknesses so adjusted that the transmitted spectrum is the same for all wavelengths except those lying within a narrow band between their K absorption limits. This band will be referred to as the 'pass band'. The filters are allowed to intercept alternately the heterogenous radiation from the X ray window, and the intensities recorded with a suitable detector. The difference in intensities is then due to the unbalanced band between the absorption limits. In practice a perfect match is not possible, and consequently some of the differential intensity arises from X rays outside the K absorption limits. Although thicker foils may be chosen to increase the contrast, this would result in a sacrifice of total intensity. Furthermore, statistical considerations become important when selecting the parameters for the differential filter. Thus if N_A photons are recorded through foil A and N_B through foil B, the differential intensity is $N_A - N_B$. If the foils were perfectly matched,

this differential intensity would correspond to photons in the pass band region exclusively. The expected relative error (E.R.E.) in the differential intensity is given by

$$E.R.E. = \frac{(N_A + N_B)^{\frac{1}{2}}}{N_A - N_B}$$

Obviously there exists a thickness of foil A and a matching thickness for foil B, such that the expected relative error given above is a minimum. The actual calculation of this optimum thickness depends on the spectral distribution of the intensity in the incident beam and on the forms of the absorption coefficient curves of the two metals A and B. The absorption coefficient curves of the two metals can be drawn from available data in the literature (Compton and Allison), but the form of the incident spectrum must be obtained experimentally. If this is not possible, then as shown in Section 2·10 any error in the differential filters due to imperfect balance may be corrected for by the method of Pulse Height Discrimination.

2.3

Crystal Monochromator.

The desired radiation could also effectively be separated by the use of a crystal monochromator.

In principle this method makes use of the Bragg equation

$$n\lambda = 2d \sin\theta$$

where λ is the wavelength,

n the order of diffraction,

θ the Bragg Angle

and d the interplanar spacing.

Knowing the d spacing and the wavelength to be selected the crystal is set at the Bragg Angle θ to diffract the desired radiation, and a suitable detector placed at an angle 2θ to receive the diffracted beam.

If this method were chosen one must consider the choice of analysing crystal which is governed by the following considerations. The analysing crystal must be large and of good quality and must be stable in air. It should have a high intensity of reflection and must have a suitable d spacing since, theoretically at least, the maximum wavelength that can be diffracted from a crystal is equal to the 2d

spacing. A further requirement refers to the higher order 'reflections' since the second order 'reflection' of radiation with wavelength $\frac{\lambda}{2}$ and the third order of wavelength $\frac{\lambda}{3}$ will occur at the same angle 2θ as the first order. Thus the multiplicity of the crystal must be weak. Also since the reflectivity of a crystal depends on the wavelength one factor still remains undertermined and that is the reflection coefficient of the crystal. It might appear that the intensity of reflection from a crystal face might be obtained by setting the crystal to the position of maximum reflection and determining with a suitable detector the intensity then reflected. If now the detector were set to receive the direct beam, the ratio of the intensities of the reflected and direct beams would apparently give the correct measure of the reflecting power of the crystal.

Closer examination of the problem shows however that this is not strictly correct. The above holds true only for the specular reflection of light, but is not true for X rays. A crystal is seldom perfect, and if it is rotated uniformly through the position of maximum reflection, different portions of the crystal are successively brought into the position of maximum reflection. Thus when the crystal is reflecting the greatest amount of X rays, only a part of the crystal is in fact contributing, and in order to give every portion of the

crystal a chance to contribute, the crystal must be rotated through the whole reflecting position. Hence one must distinguish between peak intensities and total integrated intensities.

Furthermore in order to determine either the peak intensity or the total integrated intensity of a crystal for Copper Kα radiation, necessitates that the X radiation falling on the crystal be monochromatic. This in turn necessitates the use of a double crystal monochromator. Since the X ray tube with which the Author carried out the intensity measurements had a beam current of a few microamperes, and since the X ray beam after two crystal reflections would have had an extremely small intensity, making detection difficult if not impossible, (the loss of intensity is certainly very much greater than when using non dispersive methods), it was therefore decided to use the non dispersive methods available to separate the Copper Kα radiation from the X ray continuum and later when a Hilger Microfocus X ray tube was made available to the Author use was made of a crystal monochromator to compare the results with those of the balanced filters. This part of the work and the description of the double crystal monochromator are given in Section 6.

2·4

For Copper Kα radiation the filters used were Nickel and Iron. (Cobalt was not available). The Author was kindly given the use of part of the X ray equipment of the C.S.I.R.O., by Dr. K. Norrish of the Division of Soils laboratory at the University, for the determination of the appropriate filter thickness. The target used was Zirconium, since the Zirconium Kα radiation has a wavelength of 0·78 Å which is approximately equal to the peak intensity of the white radiation from a Copper target.

The detector used was a Scintillation Counter in conjunction with a Pulse Height Discriminator. With the Discriminator set for 90 per cent transmission of Zirconium Kα radiation, it was found that the same counting rate was obtained for a Nickel filter of $2{\cdot}28 \times 10^{-3}$ cm. and an Iron filter of $2{\cdot}84 \times 10^{-3}$ cm.

2·41

The ideal method for the determination of the efficiency of a pair of balanced filters is to record the spectrum from the target of an X ray tube by means of a crystal monochromator, Scintillation Counter and pen recorder.

For the case of a Copper target if the spectrum is recorded once with the Nickel filter interposed between the X ray tube window and the crystal monochromator and once with the Iron filter then, (after correcting for crystal reflectivity, absorption in the window of the X ray tube, absorption in the detector window, etc.) the difference in area outside the pass band is a measure of the efficiency of the filters. Unfortunately the above equipment was not available to the Author. Use was made however, of the spectral intensity curve from a Copper target obtained by Arndt and Riley (1952). These Authors used an almost new Copper X ray tube operated at 30 kilovolts d.c. and corrected for the following factors.

(a) Reflectivity of the crystal analyser,

(b) Air absorption between X ray tube window and detector,

(c) Efficiency of the detector.

The mass absorption coefficients of Nickel and Iron as a function of wavelength were obtained from the literature and their transmission as applied to the spectral distribution curve of Arndt and Riley plotted as a function of wavelength. The difference in transmission of the Nickel and Iron filters is shown plotted in Fig. 30 from which one can conclude that the efficiency of the balanced filters is better than 99 per cent.

FIG 30

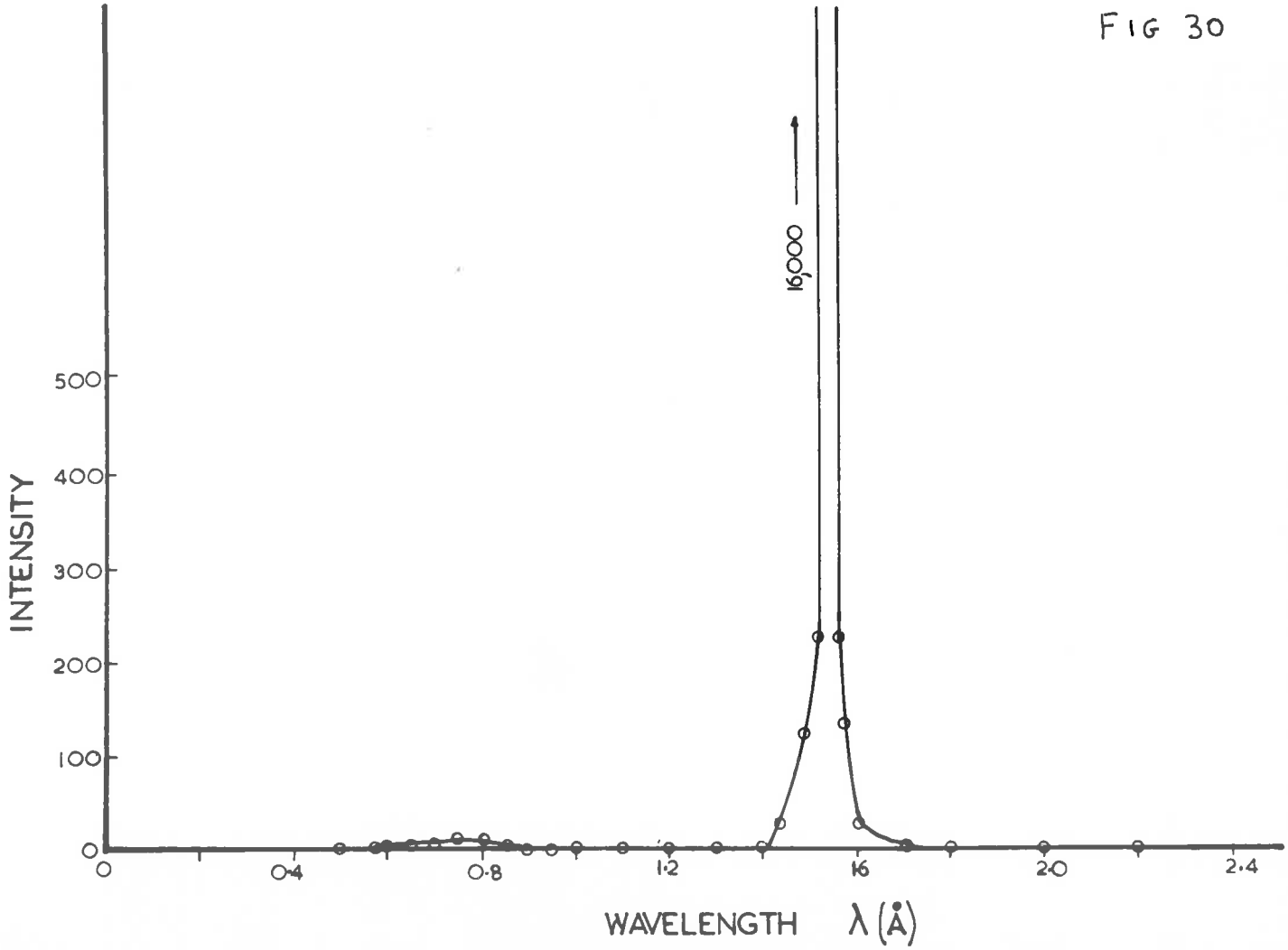
16,000
500
400
300
200
100
0
INTENSITY
0
0·4
0·8
1·2
1·6
2·0
2·4
WAVELENGTH λ (Å)

2·5
Choice of Detector.

For the detection of X radiation 4 types of detectors are available. These are the Ionization Chamber, Geiger Counter, Proportional Counter and Scintillation Counter.

2·51
Ionization Chamber.

Certainly the oldest method used in the measurement of intensities was by means of an ionization chamber. The Author seriously considered using this detector but was forced to reject the idea from the following considerations. The electric current in an ionization chamber depends on the plate collector voltage as shown in Fig. 31. In region I, the current is approximately proportional to the voltage, obeying Ohm's law. In this range the drift velocities of the charge carriers are so small that an appreciable recombination takes place. As the voltage between the plates is increased, the current reaches a saturation value proportional to the radiation. This is the saturation region II. In this region the recombination of ions and electrons is negligible and they are all collected by the

FIG 31

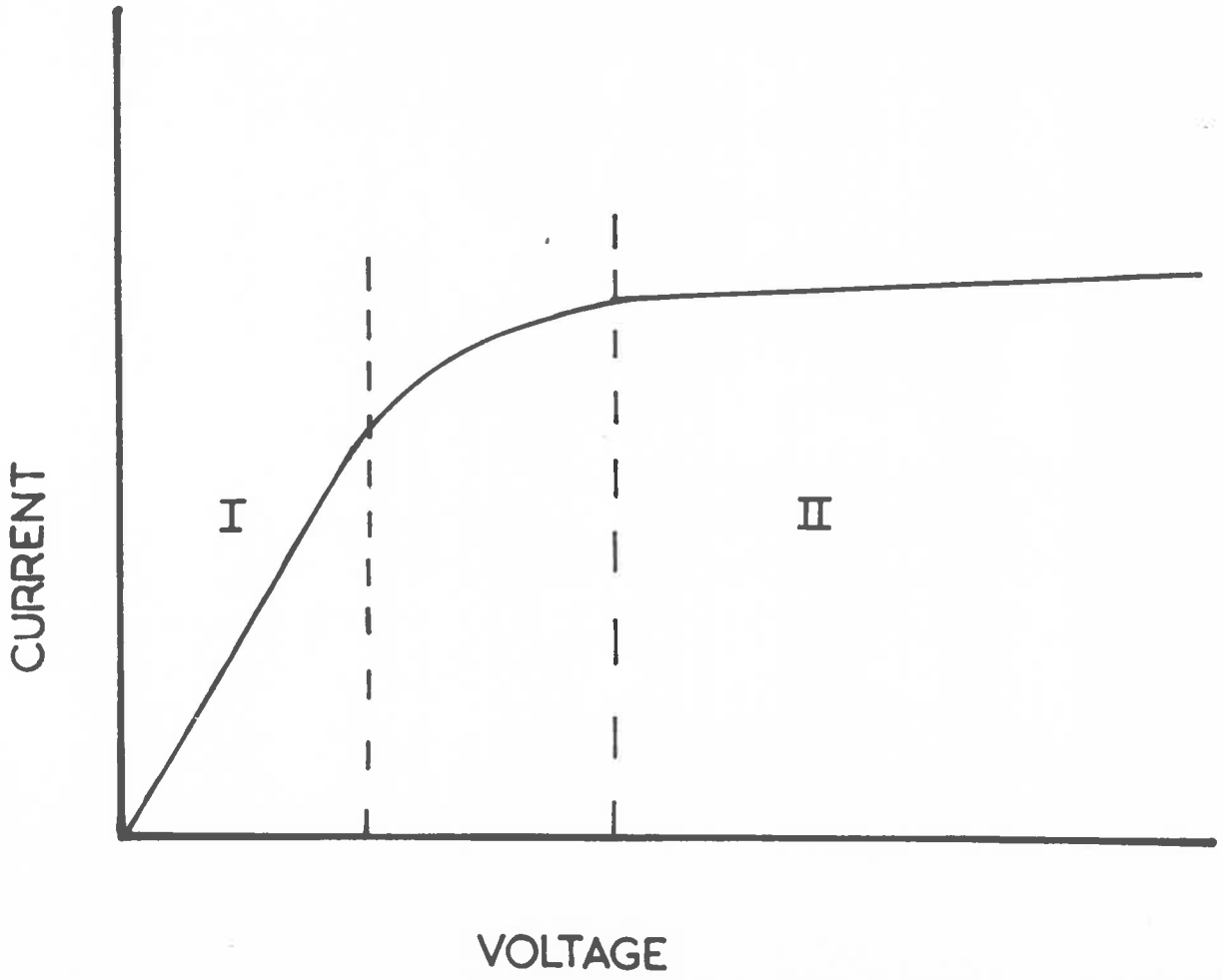

electrodes. For the saturation range, if diffusion be neglected, the collector current can be written.

$$i = e \int_V n_0 \, dV = e N_0$$

where n_0, the ionisation, is the number of ion pairs produced in an element dV of the volume of the chamber per second. For a monochromatic beam of wavelength λ and energy flux $I(\lambda)$ the number of ion pairs N_0 produced per second in the sensitive volume of the chamber is proportional to $I(\lambda)$ multiplied by a factor $Ga(\lambda)$ which embodies the absorption characteristics of the gas and is a function of λ. We can therefore write that

$$i(\lambda) = Ga(\lambda) I(\lambda)$$

Also, the energy absorbed in the sensitive volume of the ion chamber of length L is

$$I(\lambda)\left(1 - \exp(-\mu_g(\lambda)L)\right)$$

where μ_g is the linear absorption coefficient of the gas in the chamber.

A fraction y of this energy will be used effectively for ionization work, equal to eU_i for one ion, where U_i is the ionization potential and e is the charge of an electron. Thus the total number N_0 of ion pairs produced per second in the sensitive volume is

$$N_0 = \frac{y}{eU_i}\left(1 - \exp(-\mu_g(\lambda)L)\right)I(\lambda)$$

and therefore

$$Ga(\lambda) = \frac{y}{U_i}\left(1 - \exp(-\mu_g(\lambda)L)\right)I(\lambda)$$

The ratio U_i/y depends on the gas and to some extent on the construction of the chamber. For air, the value recommended is 34 ev. (Report of the International Commission on Radiological Units and Measurements (ICRU), 1956).

For an ionization chamber with an active length of 50 cms, with air at atmospheric pressure, the absorption of Copper Ka radiation would be about 64 per cent. From the theoretical curves of Copper Ka emission, one can estimate that for small angles of emission (1^0 - 5^0) and for voltages of the order of 20 kilovolts with a beam current of 10^{-6} amperes, the number of Copper Ka quanta emitted would be about 1000/sec. Since for air at atmospheric pressure each

ion pair requires the expenditure of 34 ev, and taking the ionization potential of Copper Kα as 8·93 kilovolts, then the number of electrons produced per second in the ion chamber is $1{\cdot}2 \times 10^{5}$, which is equivalent to a current of approximately 2×10^{-14} ampere. With the differential filter method which depends on allowing the filters to intercept alternately the radiation from the X ray window, this value of current would be smaller owing to absorption by the filters. Even if the active length of the ion chamber were doubled, and a heavier gas at greater than atmospheric pressure were used, quite apart from the inconvenience of using such a detector, the value of the current would certainly not be increased by a factor of more than 3. Furthermore the system would have to incorporate an electrometer valve amplifier and associated circuitary both of which are liable to drift and pick up. It was therefore decided to consider the other detectors in common use in the hope that they would be more adaptable to intensity measurements.

2·6
Quantum Counting Efficiency and 'Dead Volume' of a Counter.

One of the main requirements demanded of a detector is that it have a high Quantum Counting Efficiency. Assuming for the moment that every absorbed quantum is 'counted' then the Quantum Counting Efficiency is defined as the percentage of incident monochromatic X ray quanta that produce detectable electrical impulses. It is calculated as the product of the gas or scintillation crystal absorption and the detector window transmission.

At present, the three most commonly used detectors are the Geiger Counter, Proportional Counter and Scintillation Counter. Gas Counters like the Geiger and Proportional Counters are either of the end window type or the side window type. In the case of the end window counters however, if their efficiency were calculated from the absorption in the gas of the counter using published values of the absorption coefficients, an incorrect result would be obtained. This is because in end window counters not only is the field not uniform along the length of the anode wire but the window and high tension side of the counter are at a small distance from the ends of the anode wire, with the result that there is a dead volume of gas near the ends.

2·7
Geiger Counter.

Measurements were carried out to determine the sensitivity of an end window Geiger Counter along its length. A collimated beam of γ rays from a Co^{60} source placed at a distance of 3 ft from the counter was used, the beam being incident at right angles to the axis of the Geiger Counter. The Counter stand had a wooden base with two brass struts supporting two horizontal rails on which was mounted a rectangular brass plate. (Fig. 32). The brass plate which could slide on the rails, supported an upright rod at whose end was soldered a slit collar which could clamp on to the counter. This rod had a clamping device in the form of a knurled nut activating a collar which enabled vertical adjustments to be made.

In front of the counter stand was a 1/4" Lead shield screen with a slit 1 cm. long and 1 mm. wide enabling the whole of the central wire of the counter to be irradiated. Starting with one end of the counter parallel to the slit, the Geiger Counter was moved equal distances of 0·2 inches along the rails and the counts recorded. A plot of counting rate against counter length is shown in Fig. 33. If the field surrounding the whole length of anode wire were uniform

FIG 32

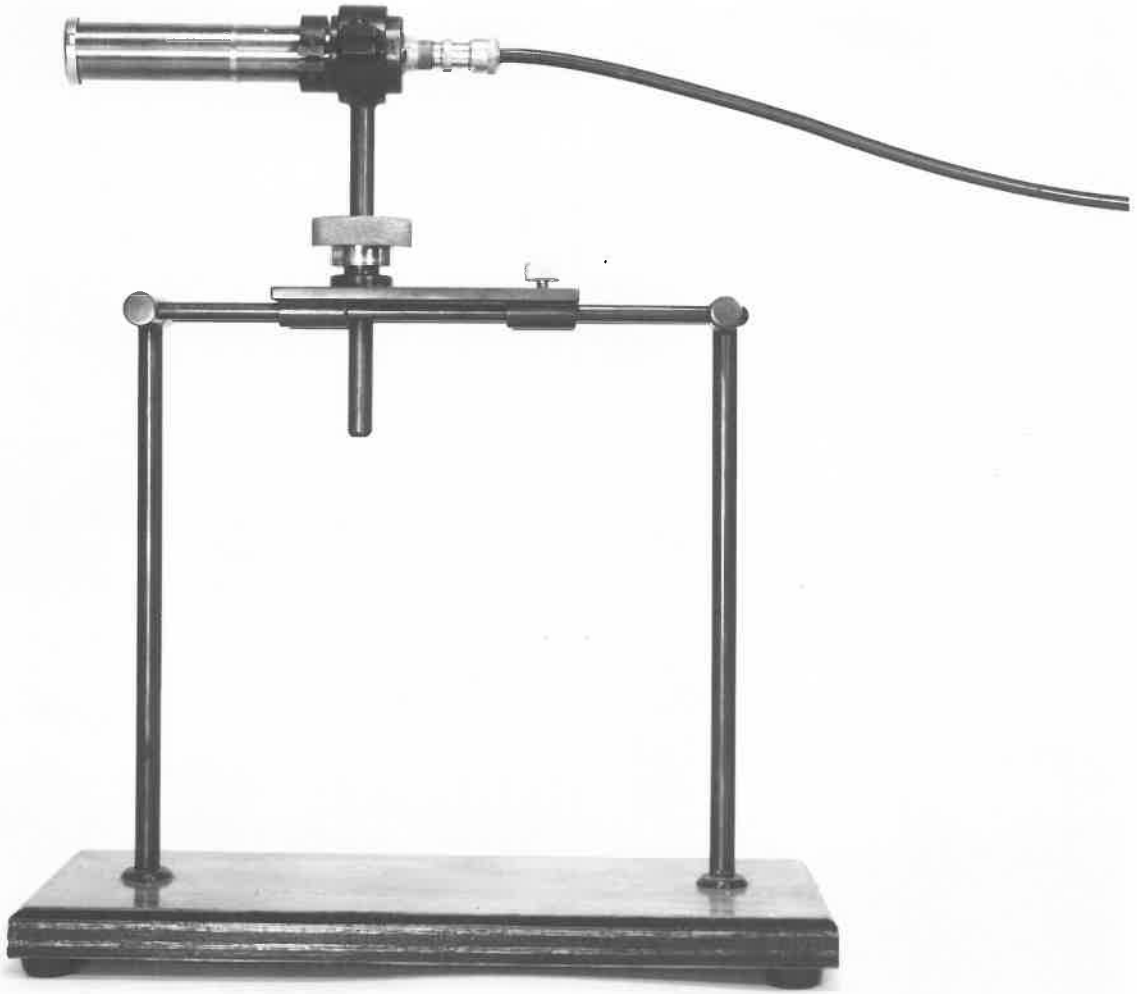

FIG 33

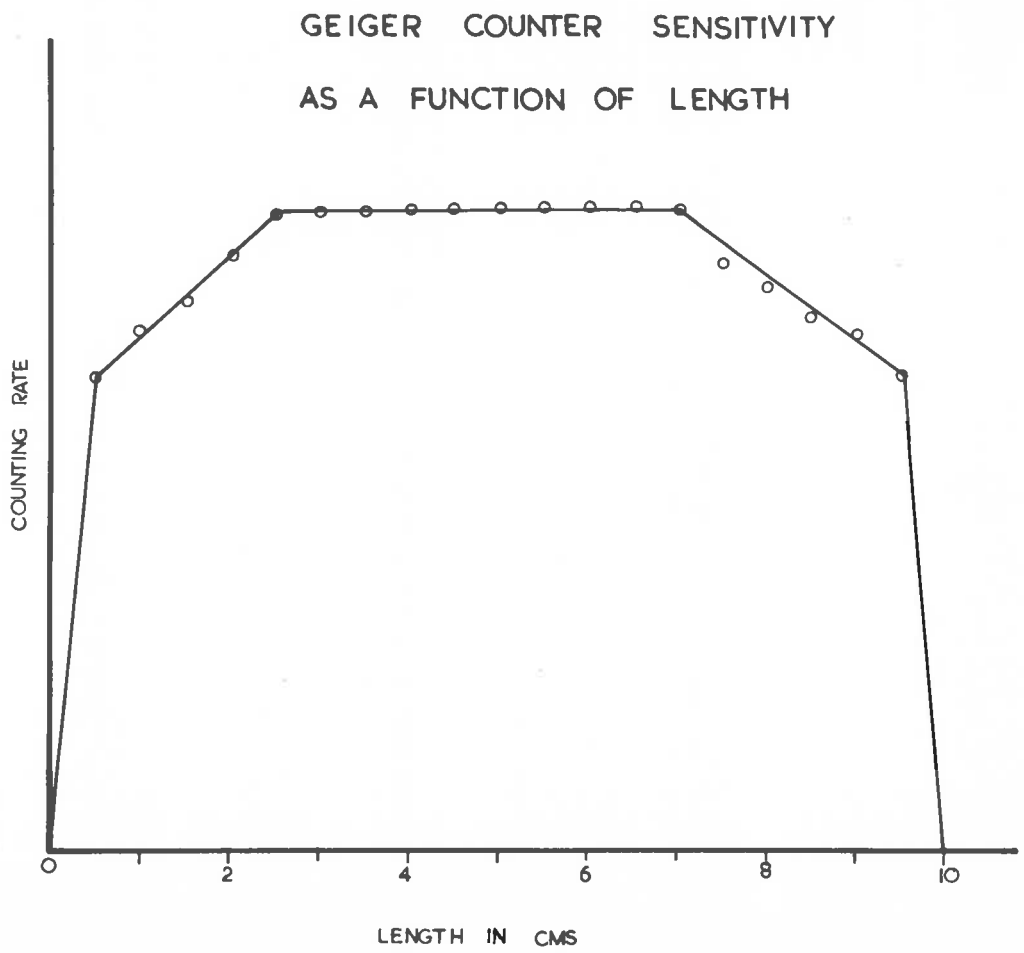
GEIGER COUNTER SENSITIVITY
AS A FUNCTION OF LENGTH
COUNTING RATE
0
2
4
6
8
10
LENGTH IN CMS

and there was no 'dead volume' of gas, then a plot of counting rate against counter length would result in a straight line of zero slope. In practice this is not the case. These measurements also show how essential it is to reduce the dead volume of the counter to a minimum by arranging the window to be as close as possible to the anode wire. Since the effect of a non-uniform field and dead volume is to reduce the actual length of a counter gas, suitable corrections must be made when this type of counter is used for absolute intensity measurements.

2·71

Correction for the 'Dead Volume' of an End Window Geiger Counter.

Consider X radiation falling on an end window Geiger Counter. If for the moment one neglects the absorption in the window of the counter, and letting μ be the linear absorption coefficient of the counter gas for a particular wavelength, then if the counter is considered to be an ideal one, that is, the absorption of the X radiation is uniform along its length and every quantum absorbed gives rise to a 'count', a plot of counting rate against counter length would give rise to a line of zero slope as shown in

Fig. 34(a).

In travelling a distance x in the counter gas the quanta absorbed are proportional to

$$1 - \exp(-\mu x)$$

while in travelling a distance $x + \Delta x$ the quanta absorbed are proportional to

$$1 - \exp\Big(-\mu(x + \Delta x)\Big)$$

Hence the number absorbed in a distance Δx is proportional to

$$\exp(-\mu x) - \exp\Big(-\mu(x + \Delta x)\Big)$$

or in the limit as Δx becomes small

$$\exp(-\mu x) - \left|\exp(-\mu x) + \left(\frac{\partial}{\partial x}\exp(-\mu x)\right)dx + \ldots\right|$$

$$= \mu \exp(-\mu x)\, dx$$

Consider now Fig. 34(b). This is an assumed plot of counting rate against counter length when the counter does not record

FIG 34

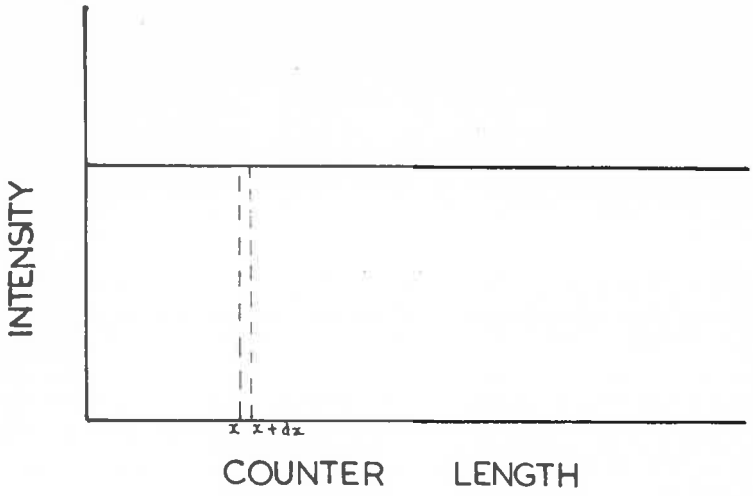
INTENSITY
x x+dx
COUNTER LENGTH

(a)

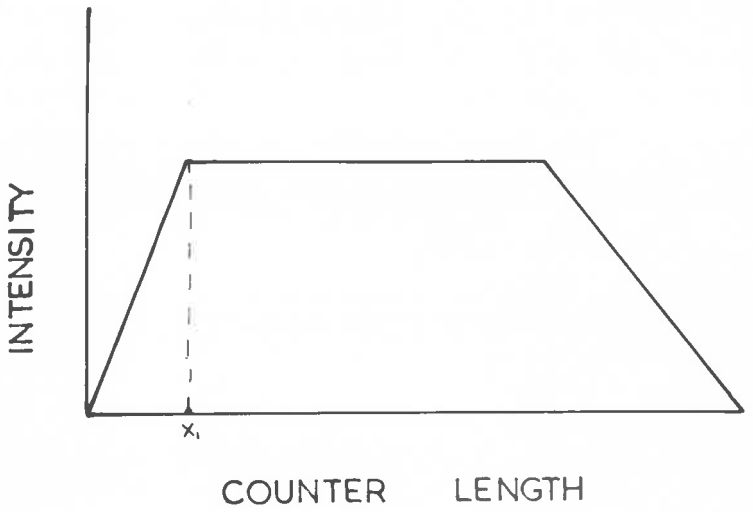
INTENSITY
X_1
COUNTER LENGTH

(b)

uniformly along its length owing to the effects of the 'dead volume' in the counter. The probability that quanta be counted before X_1 is proportional to

$$\int_0^{X_1} P(x)\mu \exp(-\mu x)\,dx \qquad \text{where } P(x) = \frac{x}{X_1} \text{ for } 0 < x \leq X_1$$

therefore

$$\frac{\text{No. of counts that would have been recorded by an ideal counter}}{\text{No. of counts actually recorded}} = \frac{\int_0^L \mu \exp(-\mu x)dx}{\int_0^L P(x)\mu \exp(-\mu x)dx}$$

For the experimental curve obtained in Fig. 33, these theoretical considerations show that the actual number of counts recorded by the Geiger Counter in absolute intensity measurements must be increased by 12 per cent.

2·72

Linearity of the Detector.

For a Geiger Counter, if successively increasing thicknesses of absorbers each having the same stopping power

are placed in front of the window, then for monochromatic X rays the intensity of radiation falling on the counter is given by

$$\frac{I}{I_0} = \exp(-\mu\rho x)$$

(neglecting for the moment the absorption due to the counter window) where

I_0 is the intensity of monochromatic radiation falling on the absorber.

ρ the density of absorber,

μ the mass absorption coefficient of the absorber for the particular monochromatic radiation,

x the thickness of absorber,

I the intensity falling on the counter window.

If the detector system were perfect, then a graph of intensity I plotted on a logarithmic scale against absorber thickness x should result in a straight line. For a Geiger Counter, the departure from linearity occurs for counting rates of about 100 per sec. The reason for this non-linearity is that every counter has a certain

'dead time' during which quanta that arrive at the detector are not counted.

2·73

Dead Time.

The correction for the loss of counting rate of a detector due to its dead time can be estimated in the following way. Let τ be the dead time of the detector. When quanta arrive at the detector at a mean rate of N_0 per sec., some will arrive too closely together in time to be counted separately. Suppose that N quanta per sec. are recorded. The detector is then effectively unable to operate for $N\tau$ sec. per sec., during which time $N_0N\tau$ quanta arrive and are not recorded. Thus we have

$$N = N_0 - N_0N\tau$$

$$\therefore N_0 = \frac{N}{1 - N\tau}$$

and the actual number of quanta falling on the detector can be determined from the recorded rate.

2·74

Fluctuations.

Closely associated with counting rates is the problem of statistical fluctuations arising in the counting rate from a source of constant intensity.

If the average counting rate recorded from a constant source is r counts per second, then the number of counts obtained is any interval of time t will not be exactly equal to rt, but will be subject to fluctuations governed by the laws of Probability.

The probability P(n) of measuring a number of counts in the time t is given by

$$P(n) = \frac{(rt)^n \exp(-rt)}{n!}$$

While the average number of counts recorded in a time t is

$$\bar{n} = rt$$

The average of the square of the deviation is

$$\sigma^2 = \sum_{n=0}^{\infty} (n-\bar{n})^2 P(n) = rt = \bar{n}$$

The standard deviation is thus equal to the square root of the average number of counts, while the relative standard deviation is

$$\rho = \frac{1}{\sqrt{n}}$$

In an experiment where the total number of counts is 100, the relative standard deviation is 10 per cent. To get an accuracy of 1 per cent the total number of counts must be 10,000.

It is essential however to realise that for absolute measurements of intensities, there is the effect of the background rate of counting. Thus if n is the average number of counts from a source in time t, and B is the background count for the same time, the relative standard deviation is

$$\frac{(n + 2B)^{\frac{1}{2}}}{n}$$

2·75

Probe Unit and Multiple Discharges.

In using the Geiger Counter for intensity measurements,

not only is its dead time difficult to determine, but it may not even be consistent. It is therefore desirable to utilise a known dead time interval in order to allow for this correction. This was achieved by using a Probe Unit in conjunction with the Geiger Counter. The Probe Unit reduced the potential applied to the central wire of the Geiger Counter by 200 volts for a known period following each registered pulse. The Probe Unit's Quenching time (which should be larger than the dead time of the Geiger Counter) could be set at 200, 300, 400 or 500 μ secs with a 5 per cent accuracy.

A further cause of error when using this type of counter is that of multiple discharges. These discharges result from emission by the Cathode of secondary electrons due to positive ion bombardment. This bombardment results from a drift across the tube of the ion sheath and therefore always occurs later than the initial discharge. The reduction of the counter voltage prevents such secondary electrons from reaching the anode and therefore reduces this form of error.

It should also be noted that for a Geiger Counter the gas amplification produces a pulse of 1 - 10 volts and this is independent of the wavelength of the X radiation incident on the counter window.

2·76

The errors due to dead volume are offset in counters having a side window. The absorption of X radiation now takes place in a region of uniform field distribution, and the Quantum Counting Efficiency as a function of gas absorption can now be calculated. Because of the shorter path length of the radiation in side window counters, a heavy gas such as Xenon is used rather than Argon or Krypton for end window counters. Counters with two side windows are also in use, the second window being placed opposite the entrance window. This is to allow the unabsorbed portion of the beam to escape without causing fluorescence from the counter tube wall.

THE PROPORTIONAL COUNTER.

2·8

Gas Amplification.

The gas amplification in the case of the Proportional Counter results in distinctive properties of this counter. The pulses produced by a Proportional Counter are about 10^3 - 10^4 times smaller than for a Geiger Counter, and therefore a linear amplifier with a high gain must be used in conjunction with the Proportional Counter to bring the level of the pulses sufficiently high for them to operate a counting circuit.

A notable feature of this counter is that the pulses it produces are proportional to the wavelength of the absorbed quanta. This proportionality enables the elimination of unwanted radiation by the method of Pulse Height Discrimination which discriminates against both low amplitude and high amplitude pulses and is described in Sec. 2·10.

2·81

Spectral Response Curve.

When the Quantum Counting Efficiency is plotted as

function of the wavelength the resulting curve is called the Spectral Response Curve. For a Xenon filled Proportional Counter, the spectral response curve is certainly not uniform but attains its maximum at about 1·7 Å. The efficiency of this counter can certainly be improved by using higher gas pressures provided these do not become excessive since besides demanding a thicker window, the operating voltage of the counter rises rapidly.

2·82

Dead Time.

Unlike the Geiger Counter, the Proportional Counter has a dead time of about 2×10^{-7} secs and hence can handle pulses at a rate of 10,000 per sec.

THE SCINTILLATION COUNTER.

2·9

Like the Proportional Counter, the Scintillation Counter with NaI Tℓ crystal has a dead time of 2×10^{-7} secs which virtually eliminates the non-linearity problem. The pulses produced by a Scintillation Counter are about 10^4 times smaller than those produced by a Geiger Counter and hence this counter must be used in conjunction with a linear amplifier. Furthermore the pulses produced by a Scintillation Counter are proportional to the wavelength of the absorbed quanta and thus the methods of Pulse Height Discrimination are also applicable.

The outstanding feature of the Scintillation Counter is its very high Quantum Counting Efficiency, and its almost uniform spectral response curve in the wavelength region from 0·5 to 2·5 Å. The decrease in Quantum Counting Efficiency for shorter wavelengths is due to the fact that the high frequency photons are not absorbed by the thin NaI Tℓ crystal, while at large wavelengths the decrease in Quantum Counting Efficiency is caused by the increasing absorption of the counter window.

2·10

Escape Peak.

In Proportional and Scintillation Counters, a pulse amplitude distribution curve for monochromatic radiation will show an additional peak on the low energy side of the main peak. This secondary peak which may under certain circumstances be of the same order of magnitude or even larger than the primary peak is known as the escape peak. It results from the fact that the gas in the Proportional Counter and crystal in the Scintillation Counter are also subject to fluorescence radiation. When the radiation which is being detected by the counter strikes the gas molecules or the crystal in the counter, it can give rise to X radiation characteristic of the gas or crystal itself. As a result, a number of quanta giving rise to ionization no longer have the full value of the energy corresponding to the monochromatic radiation incident on the detector, but instead have an energy corresponding to the energy of the incident radiation less the energy required to excite the K radiation of the counter gas or crystal.

Thus if E_i is the energy of the original quanta

E_f the energy of fluorescence radiation,

a fraction of the original quanta result in pulses with

amplitude proportional to $E_i - E_f$.

For the Geiger Counter, which is not used with any electronic energy discrimination, the existence of the escape peak presents no problem since the pulses in the escape peak are counted together with those in the main peak as if they had been in the main peak. However when Proportional and Scintillation Counters are used with Pulse Height Discrimination to discriminate against any unwanted radiation, a sizeable fraction of the radiation which it is desired to measure can be lost if the escape peak is large.

There are two ways of overcoming this problem. The first is to use two channels of Pulse Amplitude Discrimination one for the main peak and one for the escape peak. This method however entails the use of very complex electronics.

The other method is to use a particular detector gas such that for the problem at hand the escape peak does not contain a significant number of counts. Thus for Copper Ka the Xenon proportional counter has a Ka radiation that is not excited below 34 kilovolts. As long as the wavelengths of radiation to be measured are greater than the wavelength corresponding to this energy, the Ka line of Xenon cannot be excited, and the only escape peak occurring in the Proportional Counter is due to the Xenon L lines which are very weak.

2·11

Pulse Height Discrimination (P.H.D.).

The output pulse of either a Proportional Counter or a Scintillation Counter being proportional to the energy of the incident radiation are fed through a linear amplifier (output pulse proportional to the input pulse) to a Pulse Height Discriminator.

In using a Pulse Height Discriminator, a base line and window width are selected to bracket a desired range of pulse heights in which all the pulses exceed the voltage of the base line, and none exceed the voltage of the base line plus the window width. Fig. 35(c) and (d) (obtained by W.Parrish and T.Kohler 1956) shows the effect of Pulse Height Discrimination on the spectrum of a Copper target X ray tube with and without the addition of a Nickel filter. In (d) not only is the white radiation almost completely eliminated, but the intensity of the $K\beta$ radiation is negligible. (The small bump at about 0·35 Å is due to the escape peak phenomenon).

It must be noticed however that in practice there occurs a loss of not more than 10 per cent of the intensity of the desired radiation. The reason for this loss of intensity can be appreciated from the fact that quants of a single

FIG 35

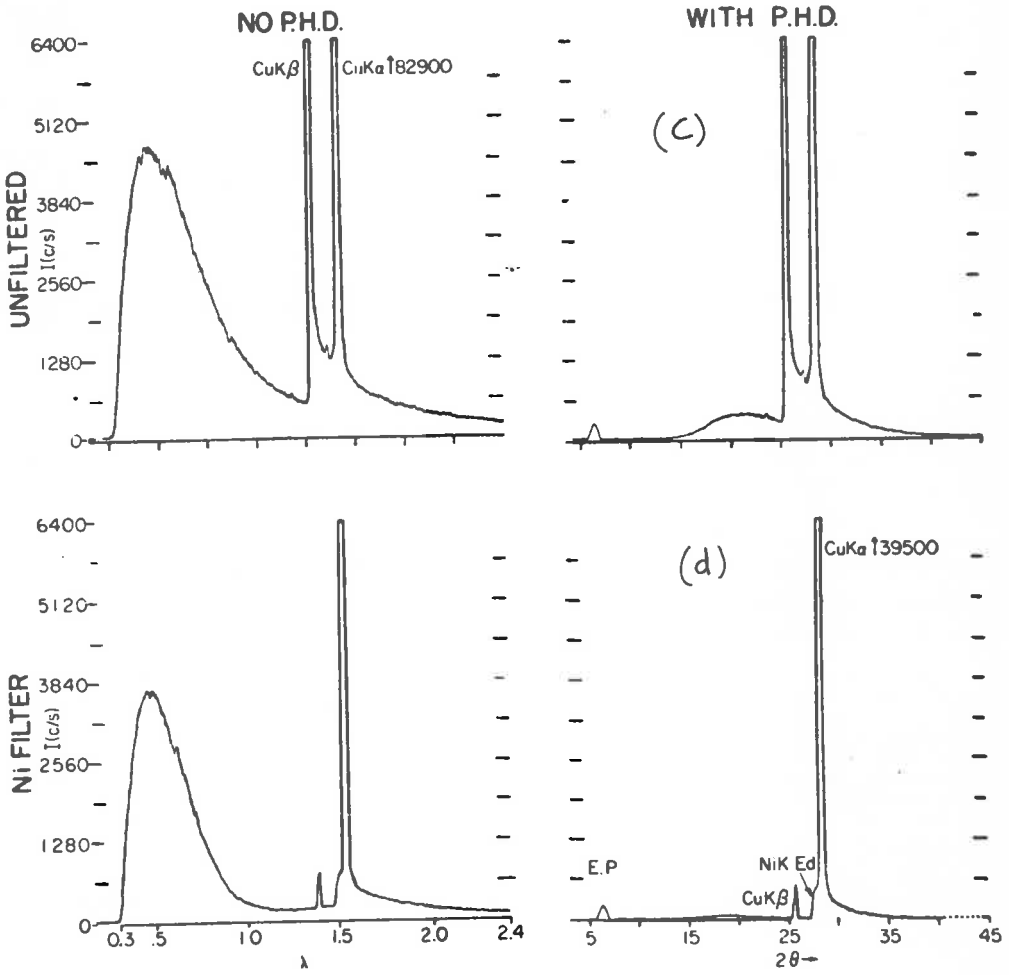
NO P.H.D.
WITH P.H.D.
UNFILTERED
I(c/s)
6400
5120
3840
2560
1280
0
CuKβ
CuKα ↑82900
(C)
Ni FILTER
I(c/s)
6400
5120
3840
2560
1280
0
0.3
.5
1.0
1.5
2.0
2.4
λ
(d)
CuKα ↑39500
E.P
NiK Ed
CuKβ
5
15
25
35
45
2θ

energy produce pulses of different amplitude varying around an average value. This value corresponds to the true quantum energy. It is this variation that limits the power of the detector to separate quanta of closely spaced wavelengths and is due to the statistics of the ionisation in the case of the Proportional Counter and excitation in the case of the Scintillation Counter, and the amplification processes involved. The separating power or energy resolution which cannot of course be increased by narrowing the window width of the Pulse Height Discriminator (this would merely result in more intensity losses of the desired radiation) is measured by the ratio W/A, where W is the width at half peak height of the pulse amplitude distribution curve, and A is the average pulse amplitude. Fig. 36 shows a pulse amplitude distribution curve also called a 'differential curve' in which the counting rate is plotted against voltage amplitude. It is seen to centre about the most frequent values of the amplitude. This curve was obtained by using an Urea oxalate crystal mounted on a goniometer to obtain a monochromatic beam of Copper Kα radiation from the Copper target of a Philips X ray tube operated at 20 kilovolts r.m.s. The base line of the discriminator was set at 60 volts and the window width at $\frac{1}{8}$ volt. Keeping the window width at $\frac{1}{2}$ volt the base line

FIG 36

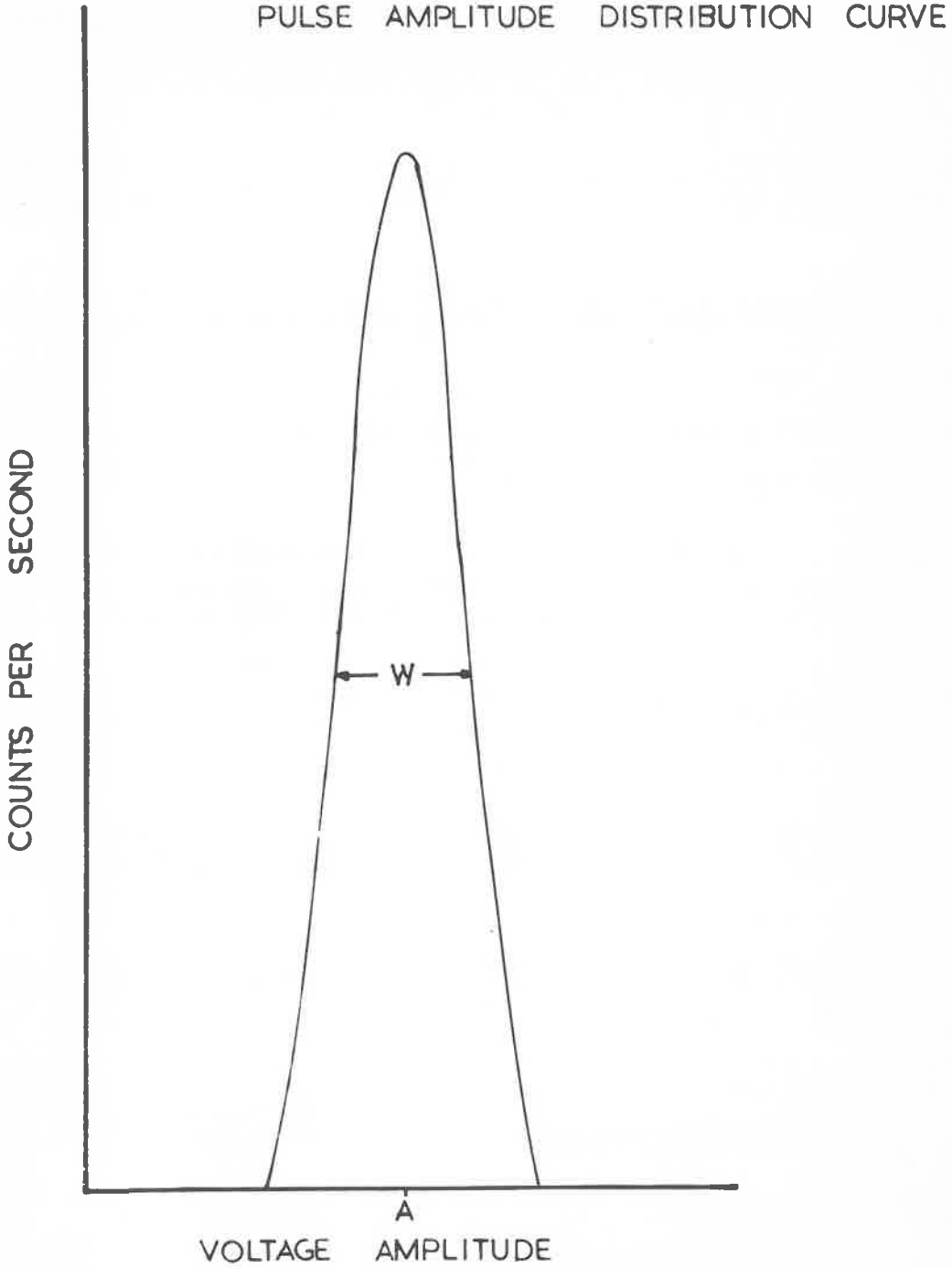
PULSE AMPLITUDE DISTRIBUTION CURVE
COUNTS PER SECOND
W
A
VOLTAGE AMPLITUDE

was then lowered in steps of 1 volt, and the number of counts in 100 seconds was obtained.

2·12
Integral Curve.

In measuring the intensity of the Copper Kα radiation it is important to realise that one must not use arbitrary settings of amplifier gain and detector voltage, accepting the value of A whenever it may occur and adjusting the base line voltage and window settings accordingly.

One method of setting the value of A, the average pulse amplitude, is by the use of the 'integral curve'. This curve is obtained by opening the window of the Pulse Height Discriminator to its maximum and scanning the base line voltage from 80 volts downwards.

As the base line becomes progressively lower, more and more pulses are accepted until a plateau will result at the lower baseline, (the plateau measures the maximum possible counting rate) since all pulses are now accepted. If the base line voltage is further decreased, the result will be a sharp increase in the curve as noise pulses are accepted. If this increase occurs before reaching a plateau then there is not enough gain in the system to bring the X ray

pulses above the noise pulses.

Figs. 37(a) and (b) show integral curves obtained using an Urea Oxalate crystal. Curve (a) was obtained with an Amplifier gain of 110 d.b. with 1200 volts applied to the photomultiplier. Clearly no plateau is reached.

Fig. (b) was obtained by using an Amplifier gain of 110 d.b. and a photomultiplier voltage of 1400 volts. In this case it is seen that the noise pulses become apparent only after the plateau is reached.

It is apparent that for absolute intensity measurements the setting of the discriminator base line and upper window width must not fall on the steep portion of the curve, since this will magnify the effect of any slight drifts in window and base line voltages, in addition to resulting in a loss of a large percentage of the counting rate.

FIG 37 (a)

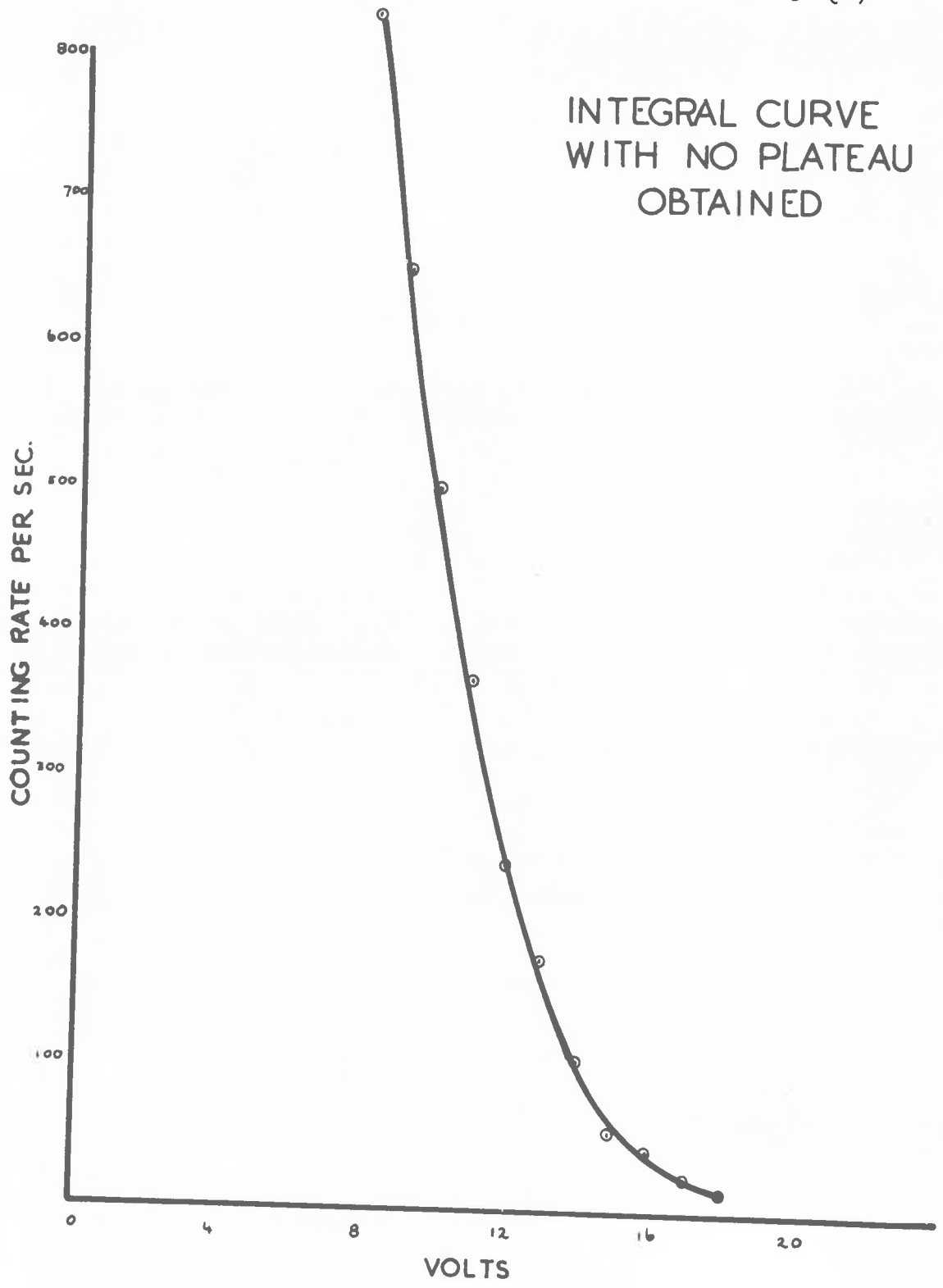
INTEGRAL CURVE
WITH NO PLATEAU
OBTAINED
COUNTING RATE PER SEC.
800
700
600
500
400
300
200
100
0
4
8
12
16
20
VOLTS

Fig 37 (b)

INTEGRATING CURVE
SHOWING PLATEAU

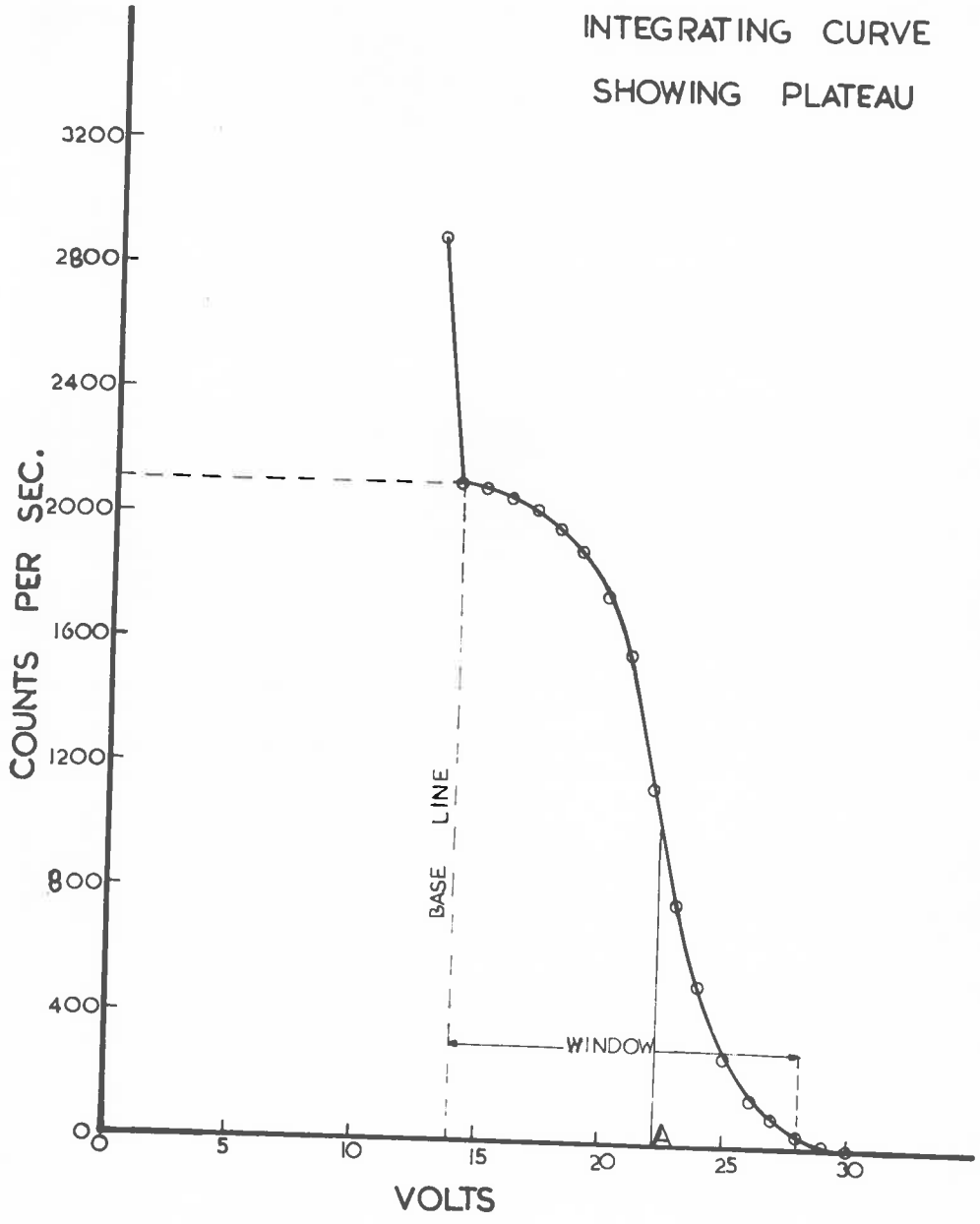

2·13 Conclusion.

The Geiger Counter as a detector although simple to use has two serious limitations; (a) its long dead time which limits the maximum counting rate that can be measured, (b) its efficiency varies along its length.

Proportional and Scintillation Counters are nearly as simple to use as a Geiger Counter. They have two important advantages over the Geiger Counter.

1. Their resolving times of the order of less than 1 μ second virtually eliminate the non-linearity problem.
2. Pulse Amplitudes proportional to the energy of the X ray quanta are produced, making it possible to employ simple electronic Pulse Height Discrimination methods to obtain very good Peak/Background ratios with little loss of intensity.

Lastly, it should be noted that although the Proportional Counter has an energy resolution about 2·5 times better than the Scintillation Counter, neither of these counters has sufficient energy resolution to separate the Kβ from the Kα radiation without strongly

reducing the efficiency for the Kα. A β filter is therefore always desirable.

The Author used a Scintillation Counter for the measurements of the absolute intensity of Copper Kα emission when the normal to the target was, (a) parallel (b) inclined to the incident electron beam. Later a Proportional Counter and a Geiger Counter were used as a check on the results obtained with a Scintillation Counter.

ELECTRONIC CIRCUITS USED IN CONJUNCTION WITH PROPORTIONAL AND SCINTILLATION COUNTERS.

2·14

When using either a Proportional or Scintillation Counter, the pulses from these counters are of the order of a millivolt, and must be amplified before they can be fed into the input of the Scaler. The equipment used in conjunction with these two counters comprised a Main Amplifier and a high frequency Head Amplifier. The maximum overall voltage gain was 10^6 (120 d.b.) with an overall stability of better than 0·1 per cent for mains voltage variation of up to ± 10 per cent. The Head Amplifier accepted pulses of either polarity, with means provided to enable inputs of the correct polarity (negative) to be applied to the main amplifier.

The main Amplifier (ECKO N 56813) was an A.C. coupled pulse Amplifier of high gain stability and with a wide frequency response. The gain was variable from 200 times (46 d.b.) to 20,000 (86 d.b.) in 2 d.b. steps.

To obtain optimum signal to noise ratio equal differentiation and integration time constants were used. These were variable between 0·08 μ secs - 250 μ secs and 0·09 μ secs - 8 μ secs respectively.

2·15

Scaler.

The Scaler (ECKO N 530.D) was a six decade Scaler and timer which could be used to time either a predetermined count, or to count for a predetermined time. Preceding the counting circuits and incorporated in the Scaler was a Pulse Height Discriminator which permitted pulses with an amplitude exceeding a predetermined level to be counted. This acceptance level was between 5 - 50 volts. The Scaler had an input resolution time of 5 μ secs, with an input sensitivity of not less than 5 volts positive either to the direct input or to the probe unit. For the case of the Geiger Counter the input sensitivity was 0·2 volts negative.

In practice corrections for the dead time for both the Proportional and Scintillation Counters were governed by the input resolution time of the Scaler.

2·16

Single Channel Pulse Height Discriminator.

As a preliminary to building a Pulse Height Discriminator it was decided to build a "Schmidt discriminator"

since the Pulse Height Discriminator consists of two Schmidt discriminators fed into an anti-coincidence circuit.

A desirable feature of a discriminator circuit is that the output signal is independent of the amount by which the input pulse exceeds the discriminator bias.

This is achieved in the Schmidt circuit Fig. 38, which consists of a two tube directly coupled, common cathode circuit. The control grid of the left tube is biased below cut off by the desired discriminator bias. This tube is non-conducting and the right hand tube is conducting. When a pulse arrives that has an amplitude sufficiently large to drive the left tube to conduction, a switching action occurs, with conduction shifting from the right tube to the left. This switching action continues until the input falls below the appropriate level.

2·17

The circuit used in the window type Discriminator (Electronics 1952), incorporated two Schmidt discriminators and an anti-coincidence network (Fig. 39). A pulse above the base line will trigger the base line discriminator. If it is also above the window level, the window width discriminator is also triggered. When this is the case, the

FIG 38

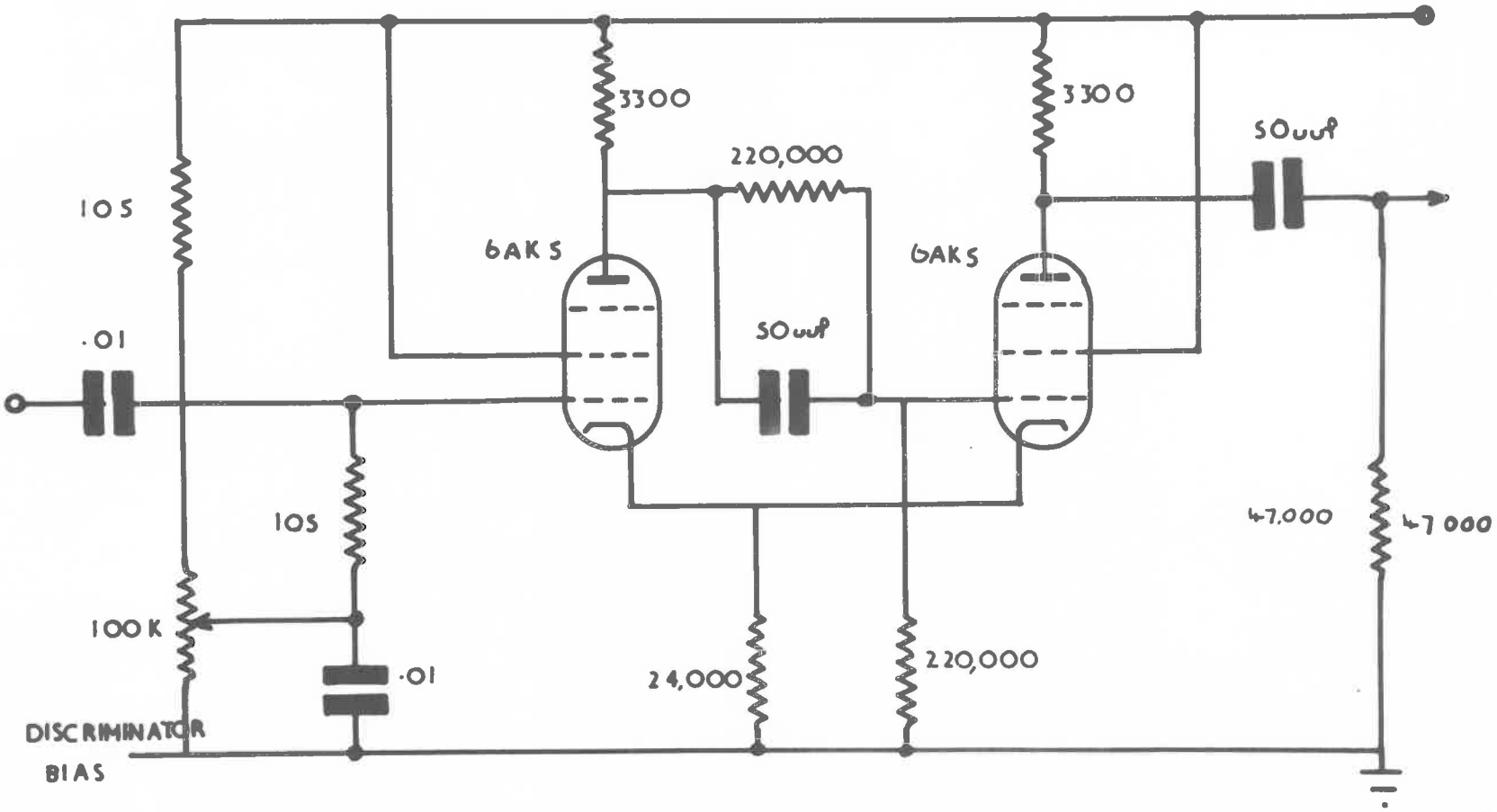

THE SCHMIDT CIRCUIT

FIG 39

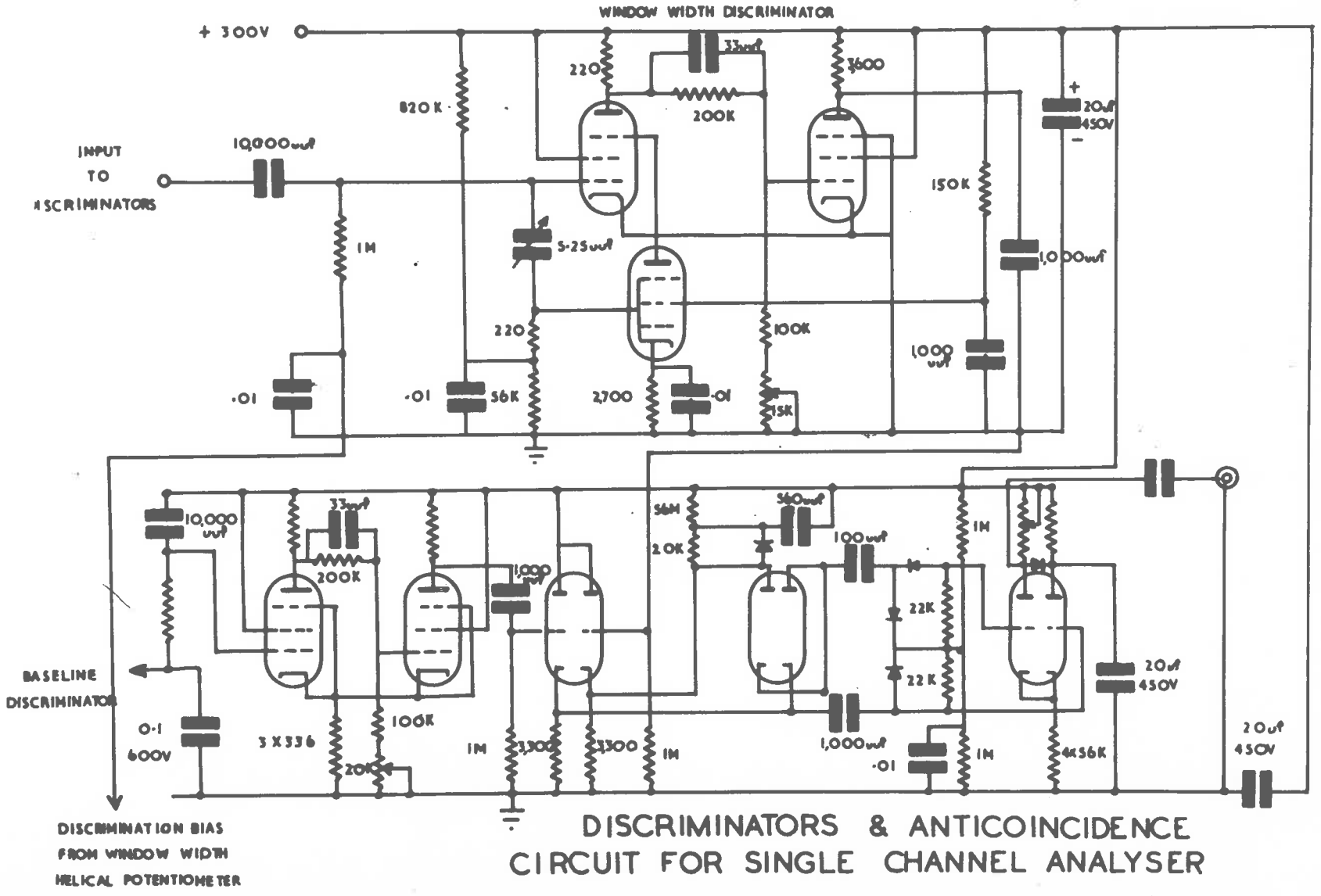

DISCRIMINATORS & ANTICOINCIDENCE CIRCUIT FOR SINGLE CHANNEL ANALYSER

output from the two discriminators are fed via separate cathode followers to an R.C. diode network, which acts as a memory cell and anti-coincidence circuit. These pulses cancel, and no output pulse is generated.

If the base line discriminator alone triggers (the pulse height lies in the selected window) then an output pulse appears at the plate of the output tube. This pulse is independent in width of the input pulse to the discriminator.

The base line and window width are determined by the bias on each of the discriminator circuits. These can be raised or lowered by two helical potentiometers (Fig. 40). Owing to hysteresis of the Schmidt circuit it is impractical to trigger the unit with pulses less than 5 volts in height. The power supply used in conjunction with the discriminator is shown in Fig. 41.

2·18

For ascertaining the upper limit to the counting rate of the amplifier-discriminator scaler system, the circuit shown in Fig. 42 was used in conjunction with an audio signal generator covering the range from 15 c.p.s. to 50 K.C. The first 12 AT 7 squares the output waveform from the generator, and this is subsequently differentiated and

FIG 40

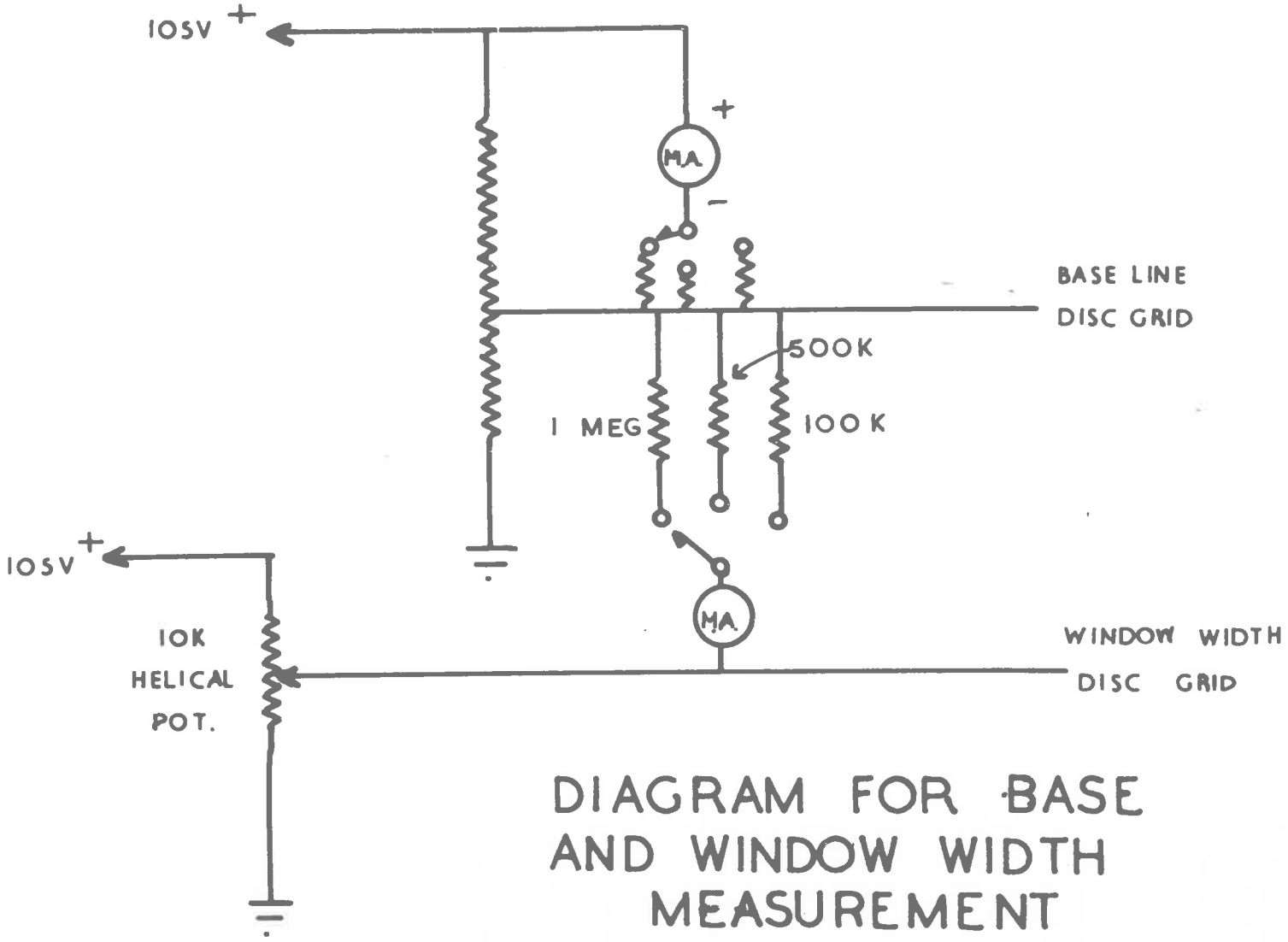

DIAGRAM FOR BASE AND WINDOW WIDTH MEASUREMENT

FIG 41

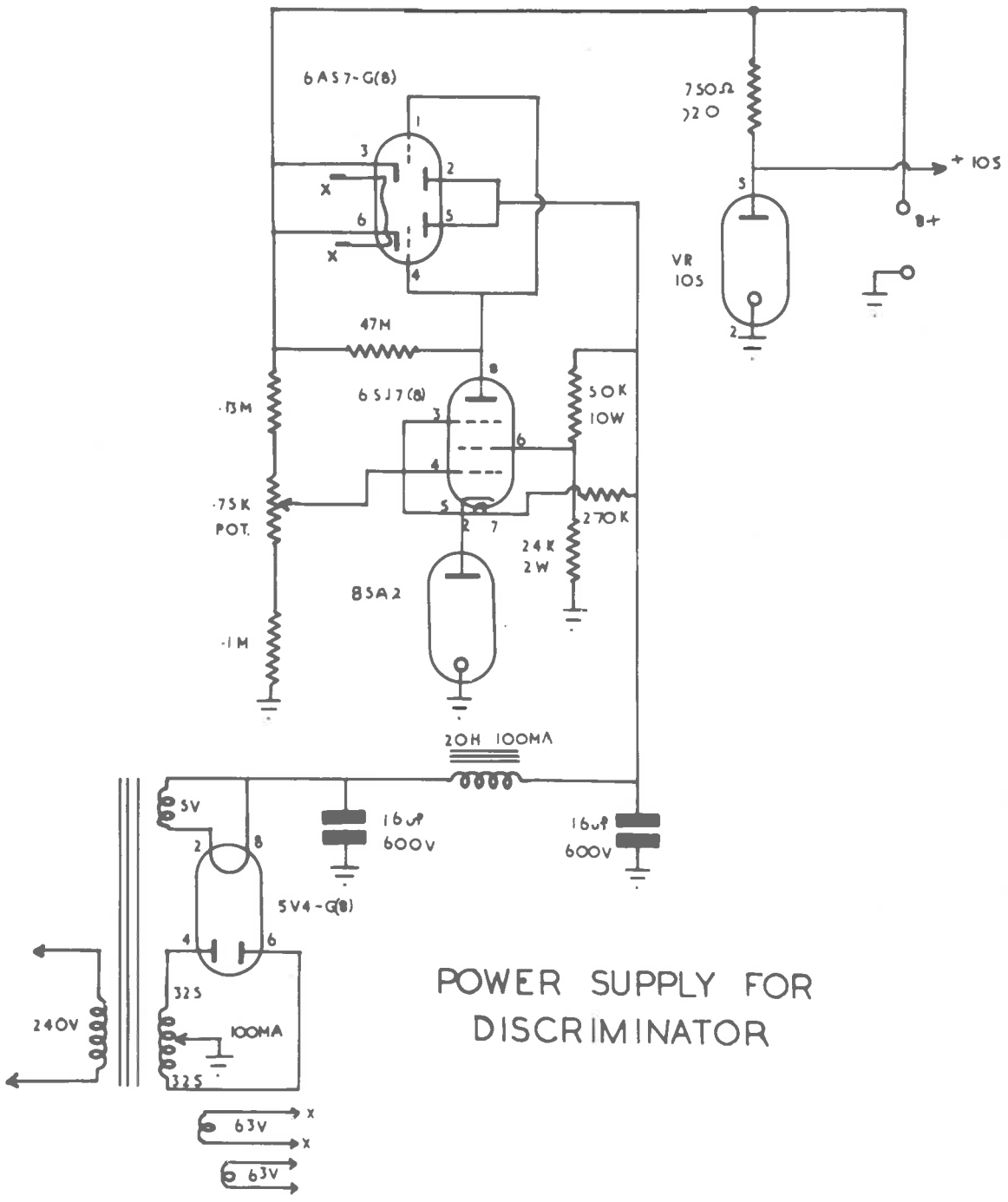

POWER SUPPLY FOR DISCRIMINATOR

FIG 42

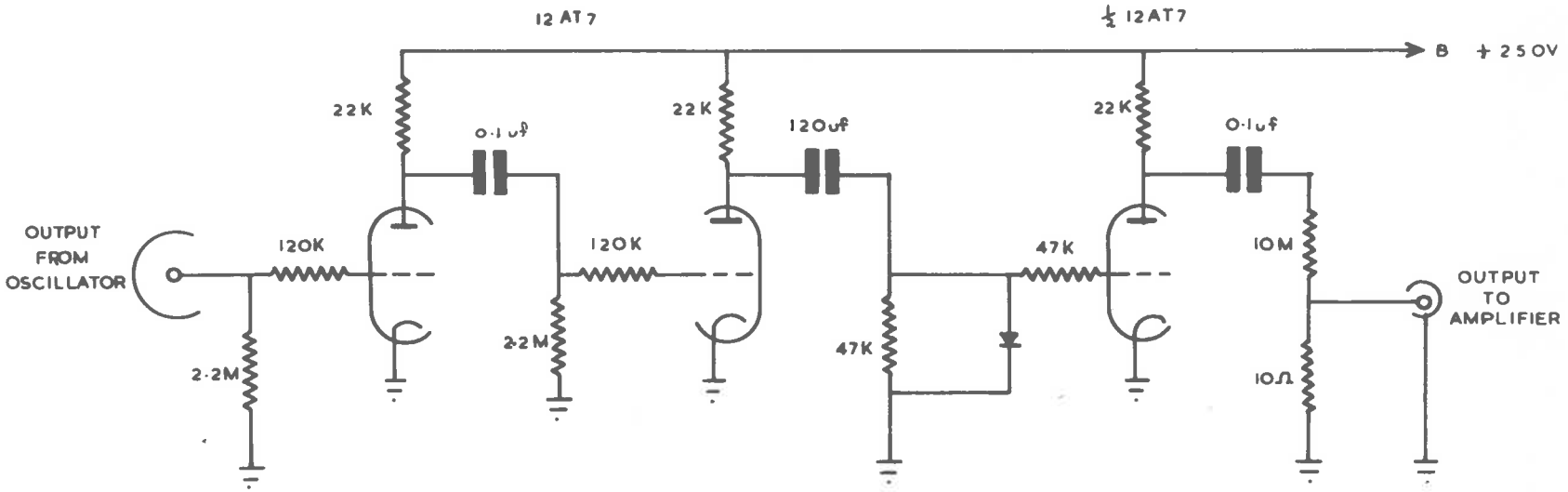
12 AT 7
½ 12AT7
B + 250V
22K
0·1 uf
22K
120uf
22K
0·1uf
OUTPUT FROM OSCILLATOR
120K
120K
47K
10M
OUTPUT TO AMPLIFIER
2·2M
2·2M
47K
10Ω

amplified by the other ½ 12 AT 7.

Because of the 0A 81 in the grid circuit of this tube, one positive pulse per cycle is produced at the output.

The 10 M, 10 Ω voltage divider produces an output voltage of the order of 100 μv; the width of the output pulse, determined by the differentiating network, was measured at 0·1 to 2 μv over the range of oscillator frequencies used. This is shorter than the 5 μ sec. pulse generated by the Schmidt triggers in the discriminator which is the limiting factor in resolution.

With the circuit constants shown in Fig. 42 there was 100 per cent correlation between oscillator frequency and scaler counts up to 10 KC per second. Above this frequency, output from the differentiating network fell off, and the signal from the test unit became lost in the amplifier noise. However increasing the value of the 10 Ω to compensate for this, extended the range of correlation. Since counting rates greater than 6,000 per second were never encountered throughout the course of the experiments, no attempt was made to establish the absolute value of the upper limit.

Note that the proceedure used here does not determine the limit of resolution for incoherent pulses. Examination

of amplifier output on a Solartron cathode ray oscilloscope revealed that for best signal to noise ratio, the amplifier differentiation and integration constants were set to give an output pulse 4 micro-secs in width on output from the photo-multiplier.

The discriminator was found to handle pulses of this width up to a repetition frequency of 200 KC. This determination was made using a variable width pulse generator with a fixed output of 40 V, applied to the discriminator and scaler only.

APPARATUS.

3·1

High Tension Supply.

The power supply shown in Fig. 43 consisted of a 50 kilovolt transformer whose primary circuit is fed by a variac and whose secondary feeds a Cockroft Walton doubler. Because of the small currents involved (the beam current of the X ray tube was ~ 10^{-6} ampere) selenium rectifiers were used, and since their inverse peak voltage rating was given as 13 kilovolts, it was found necessary to use eight rectifiers in series in each arm.

Adequate smoothing, above that inherent in the voltage doubler circuit is provided by the 2 megohms, 0·03 microfarad R.C. filter. The output voltage was measured by means of a micro ammeter having 100 μA full scale deflection, the multiplier for which consisted of one hundred (100) 10 megohms resistances in series. The absolute value of resistance and stability of this chain was determined by passing various currents through sections of the multiplier chain. See Appendix.

Electron emission and beam current control were effected by means of a 6 volt accumulator. To the top of the 0·03

FIG 43

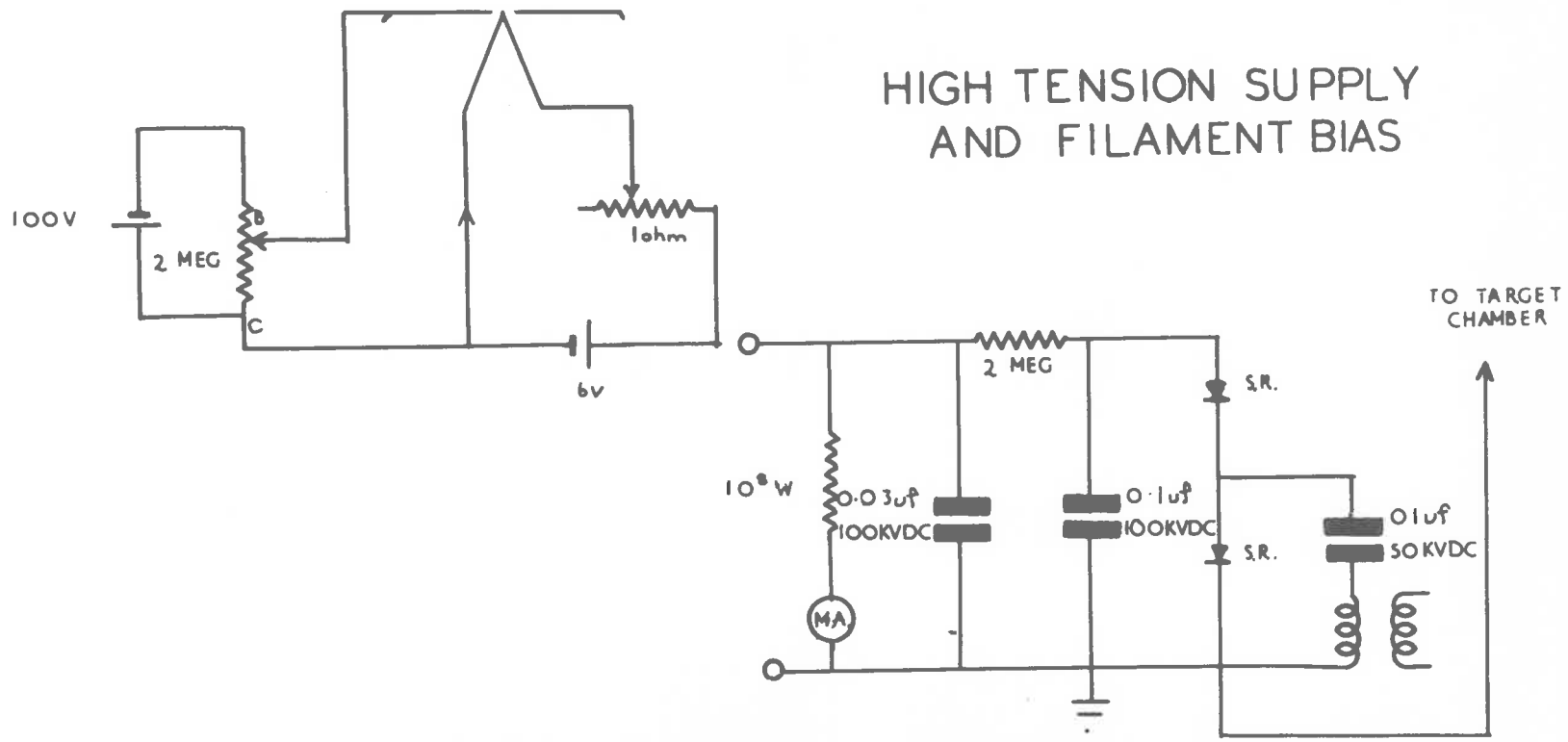
HIGH TENSION SUPPLY
AND FILAMENT BIAS
100V
2 MEG
B
C
1ohm
6v
TO TARGET
CHAMBER
2 MEG
S.R.
10⁸ W
0·03uf
100KVDC
0·1uf
100KVDC
S.R.
01uf
50KVDC
MA

microfarad condensor was bolted an Aluminium chamber which had a removable lid (Fig. 44). This chamber contained the 6 volt accumulator supplying the filament heating current and associated filament voltage control rheostat, and a bias battery and potentiometer controlling the beam current. Insulated rods connected to these controls enabled adjustments to be made from outside the wire safety cage built around the entire high tension supply. If the door of the cage were opened, a contact connecting the variac to the primary of the transformer was broken.

3·12
Pumping System.

The pumping system consisted of a mechanical pump (Speedivac ISC 50) together with an oil diffusion pump (Edwards F 20). Two vacuum taps were included so that the diffusion pump could be bypassed. Water vapor was prevented from entering the mechanical pump by the use of a Phosphorous Pentoxide (P_2O_5) trap.

All parts of the X ray tube assembly were separately tested for vacuum leaks with a hydrogen mass spectrometer leak detector on an auxiliary vacuum system.

FIG 44

The pressure was measured by an ionisation gauge which was constructed from an 807 Power tube. A brass ring having a circular groove in which was a neoprene ring fitted a 2" diameter glass sleeve with a B 19 adapter, the latter fitting a similar brass adapter in the vacuum line of the X ray tube.

To the brass ring were soft soldered four Kovar seals on which plate, grid and filament of the 807 Power tube were supported. When this ionisation gauge was calibrated, its sensitivity was found to be 70 microampere per milliampere at 5×10^{-5} cm. Hg. The ionisation gauge was also used as a discharge tube by using a spark coil as the source of high voltage connected to the plate of the ionization gauge.

3·13

Baffle and Cut-off Valve.

A mild steel tube, 1/8" wall thickness and 3½" O.D. was arc welded to two flanges made of mild steel, 1/4" thick. The top flange was machined to take a 4" diameter neoprene ring and had five suitably spaced holes for bolting on to the main vacuum system. The lower flange was machined to take a $2\frac{1}{4}$" O.D. neoprene ring and was bolted on to the oil

diffusion pump. For exact positioning and operating, the baffle was suspended from a cam lever which raised and lowered the valve vertically (Fig. 45), the operating rod being sealed with an O ring. The external operating wheel was arranged to have a spring loaded "open position". Internally the pressure on the valve in the "closed position" was maintained by a coiled spring.

3·2

Porcelain Insulator and Electron Gun.

The insulator consisted of a glazed porcelain tube, 1 foot in length, 3" in external diameter and 2" in internal diameter. The insulator was sealed to two steel flanges by araldite. This involved considerable difficulty and was finally accomplished by first raising the temperature of the porcelain insulator to 140°C, wiping with a stick of Araldite over the joints and leaving it to cure for a period of eight hours in an oven. By this process vacuum tight joints were obtained.

One of the steel flanges machined to accommodate an O ring and seven clamping holes was bolted on to the X ray tube. The other steel flange was also machined to accommodate an O ring and was threaded for a clamping ring. This ring

FIG 45

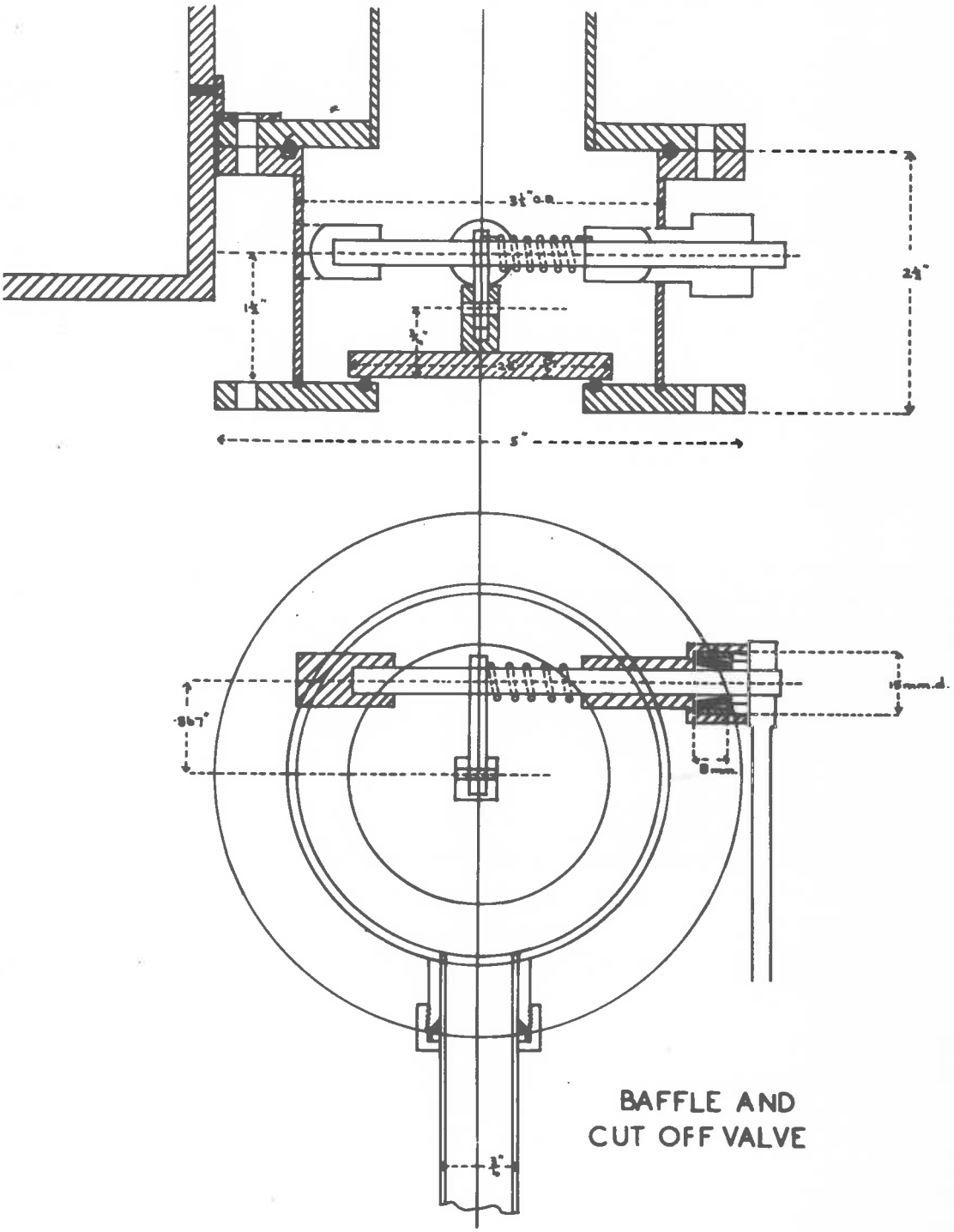

BAFFLE AND
CUT OFF VALVE

was designed to clamp a 1/4" thick Nickel plated brass plate on which were soft soldered two Kovar seals. Two stainless steel clips were silver soldered to the inside contacts of the Kovar seals, and accommodated the contact pins of the filament which was housed in a sointered glass insulator (Fig. 46). This insulator rested in a machined brass holder the latter being centred by means of three equally spaced adjusting screws. In particular, these screws could be adjusted through holes in the Whenelt cylinder, enabling the point of the filament to be correctly centred with respect to the 2mm. diameter hole in the Whenelt cylinder.

The filament assembly which was surrounded by a highly polished brass cylinder to prevent discharge could be withdrawn from the porcelain insulator, the filament changed and the assembly replaced in position all in a matter of minutes.

To the outer contacts of the Kovar Seals was a plug with a sleeve that fitted into the clamping ring. The two filament leads passed through a flexible metal pipe one end of which was attached to the plug, the other end being clamped to a hole in the Aluminium chamber.

FIG 46

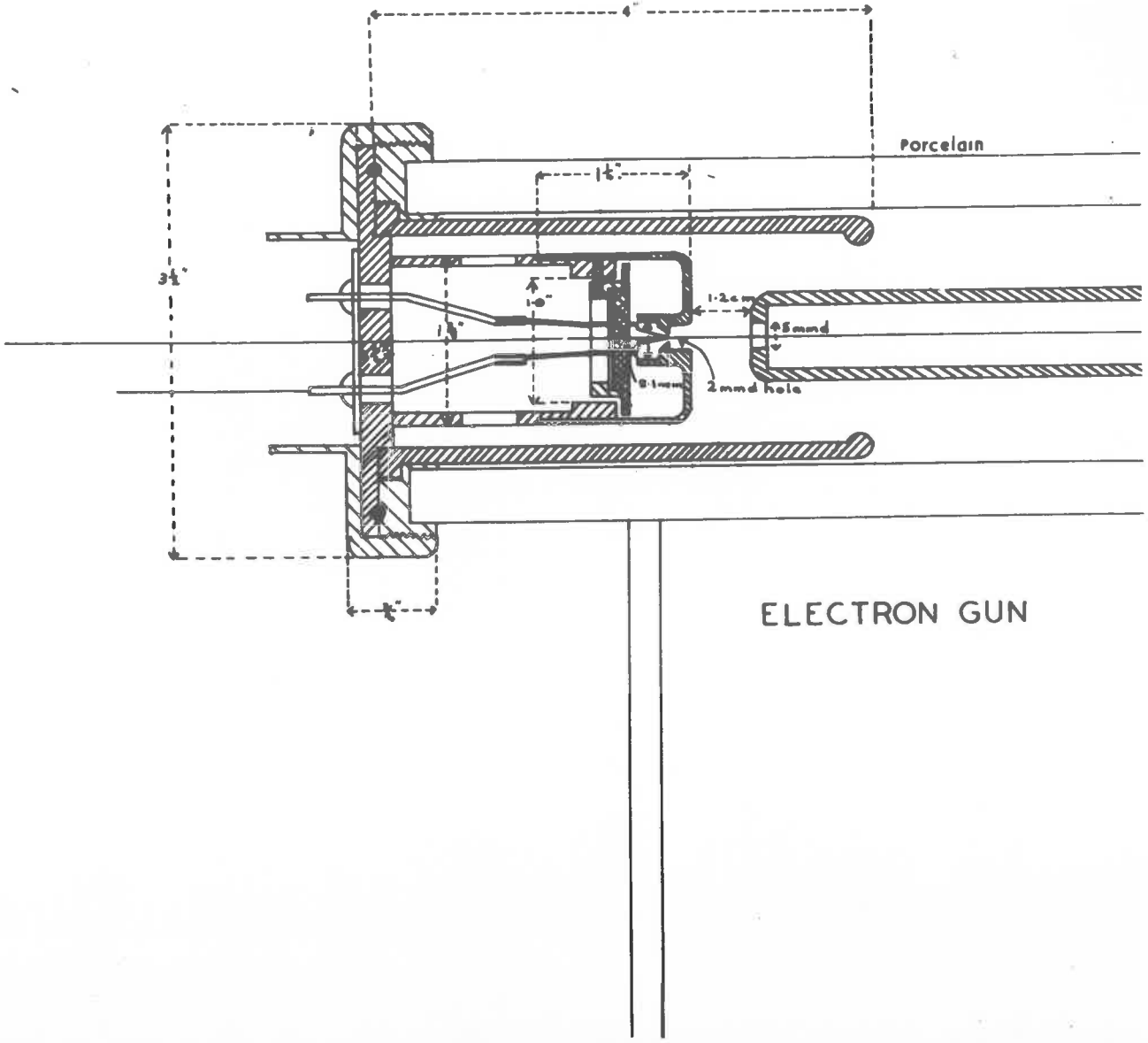

3.22

Magnetic Lens.

A magnetic lens is formed by an iron encased coil with a suitable non-magnetic gap. Pole pieces of a highly permeable material can be attached to the casing to restrict the effective gap to a very small region surrounding the electron beam. The purpose of the pole pieces and the casing is to increase the intensity of the magnetic field on the axis and to concentrate it on a small portion of the axis of the lens thus permitting the attainment of short focal lengths. For low values of ampere turns nI, the focal length of a magnetic lens is very nearly equal to that of the field formed by a single circular loop of wire carrying a current of nI amperes and having a diameter equal to d_p, the pole piece diameter (Zworykin 1945). Since the axial field of a loop of radius $a = \frac{d}{2}$ is

$$H_Z = \frac{2\pi nI\, a^2}{10(z^2 + a^2)^{3/2}}$$

and for magnetic lenses of small focal length f we have (Zworykin 1945)

$$\frac{1}{f} = \frac{0{\cdot}022}{V}\int_{-\infty}^{\infty} H^2 dz$$ Where V is the accelerating voltage of the electron beam.

Then, provided f >> a, the focal length of an iron encased lens is

$$f = \frac{48{\cdot}4\, d_p V}{n^2 I^2} \cdot k \quad \text{where } k = \frac{d}{d_p} \text{ is the 'form factor'}$$

For focussing the electron beam on the target, a magnetic lens shown in Fig. 48 was used. The lens consisted of an iron core with a brass pole gap of $\frac{1}{2}$" length, the distance of the brass gaps being 22 mms. The current to the magnetic lens which was wound with 1000 turns of Copper 20 S.W.G. wire was supplied by means of a two volt accumulator in series with an ammeter and a variable rheostat. For fine adjustment the rheostat was varied by means of a gear drive. Three screws at each end were used to position the lens on the beam current tube. The magnetic lens was 'calibrated' by finding the lens current to be used with different accelerating voltages, which would give focal spots of the order of 1 mm. diameter. A graph of lens current against accelerating voltages is shown in fig. 49, the two curves

FIG 48

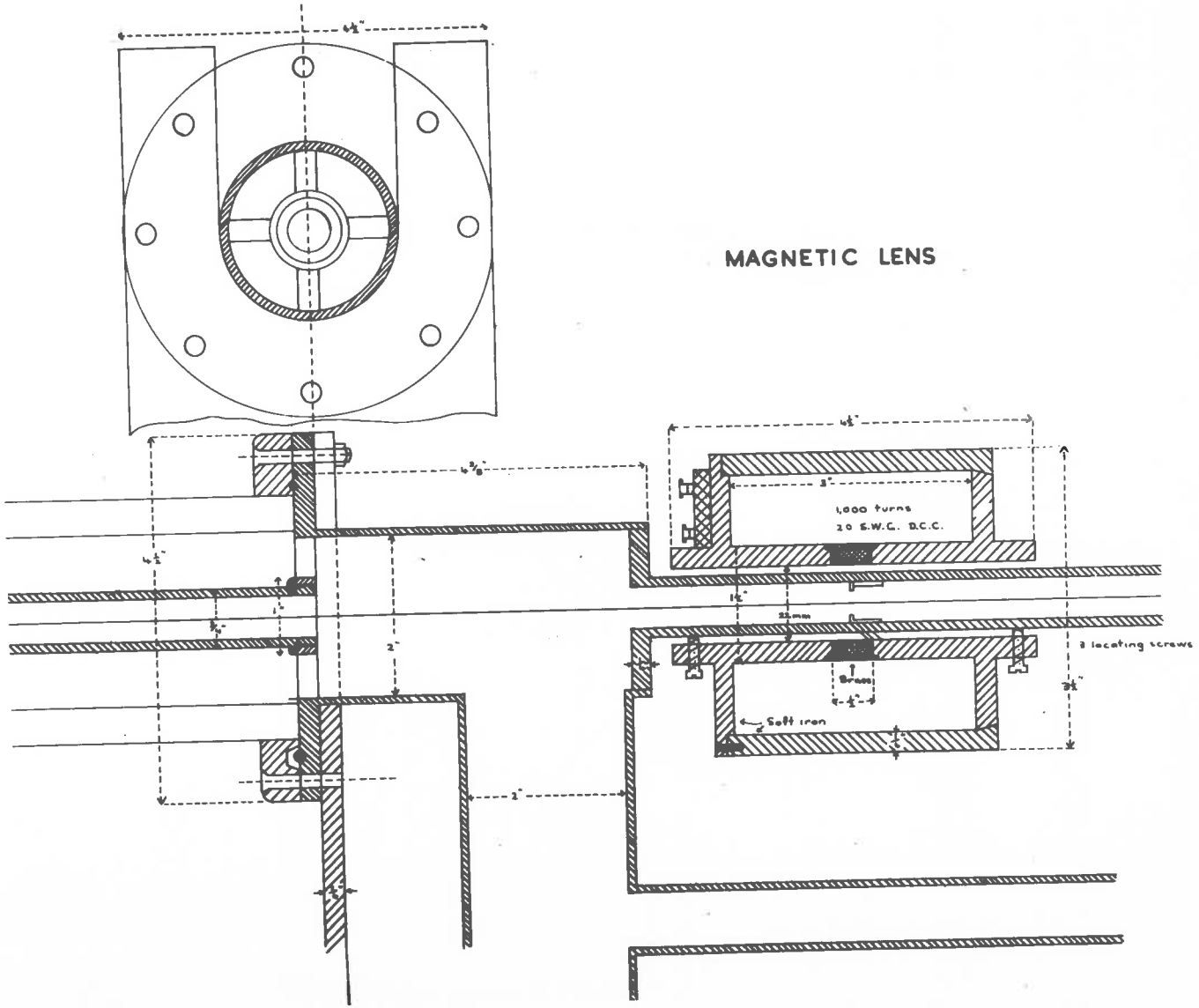
MAGNETIC LENS
1,000 turns
20 S.W.G. D.C.C.
3 locating screws
Soft iron

being obtained with the magnetic lens at each end of the beam current tube. Fig. 49(a) is with the magnetic lens close to the target chamber while Fig. 49(b) is with the magnetic lens at the other end of the beam current tube.

3·23

Target Chamber.

The target chamber is shown in Fig. 50. The casing consists of a bronze cylindrical casting 3/8" thick with an 8" outer diameter. The casting was machined and a semi-circular slot 2 mm. wide cut on the curved portion of the cylindrical casting, such that its length was 0·4 of the circumference of the chamber. The slot was covered by an Aluminium strip 1 inch wide and $2·74 \times 10^{-3}$ cm. thick and was sealed to the external surface of the chamber by W_{100} vacuum wax (Fig. 51). A Lead glass window 4 mm. thick and $\frac{1}{8}$" diameter was sealed by means of W_{100} wax into a hole cut in the end of the target chamber such that the axis of the electron beam, the centre of the 2 mm. slit and the centre

FIG 49

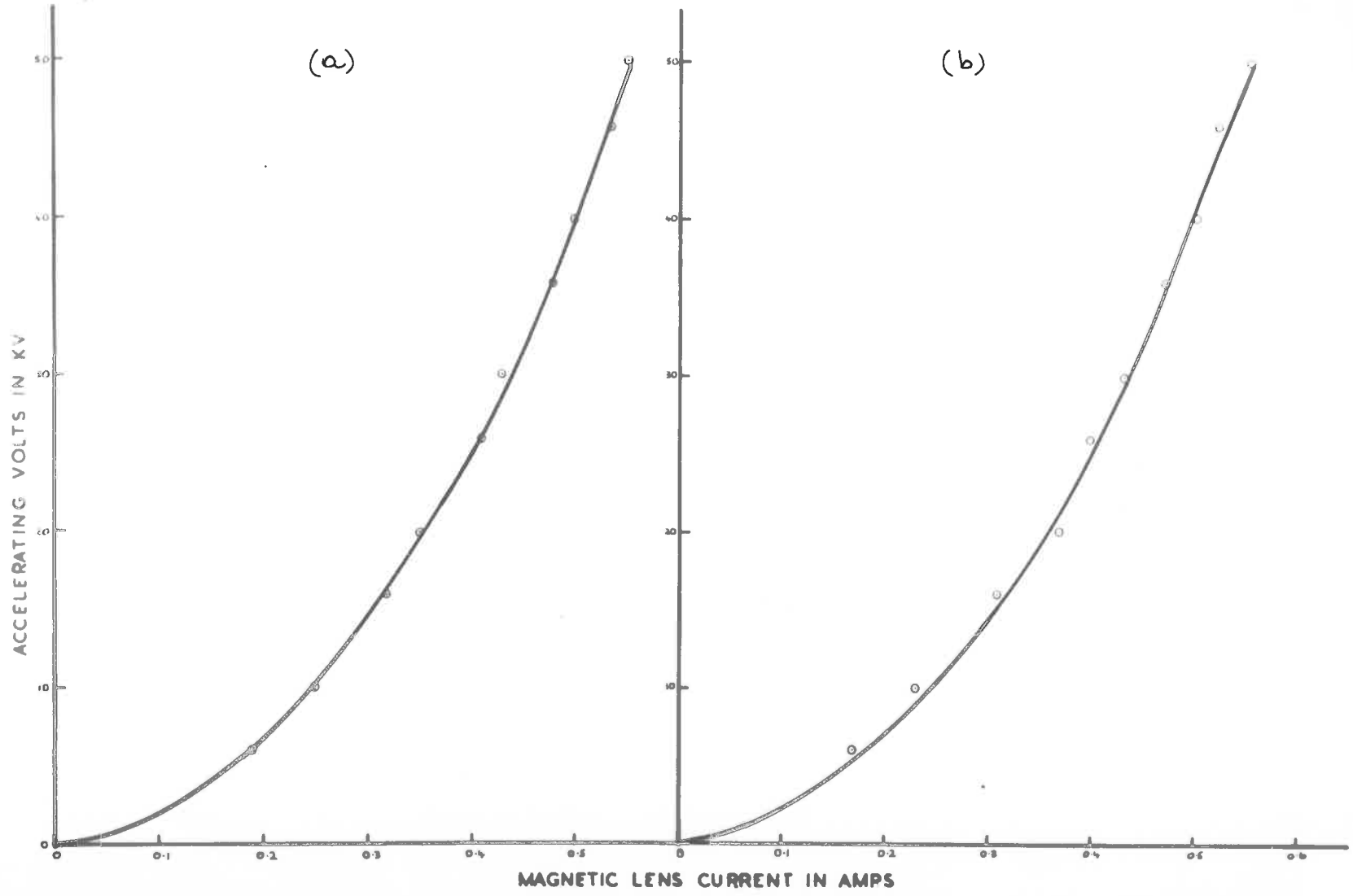
(a)
(b)
ACCELERATING VOLTS IN KV
0
10
20
30
40
50
0
0·1
0·2
0·3
0·4
0·5
0·6
MAGNETIC LENS CURRENT IN AMPS

FIG 50

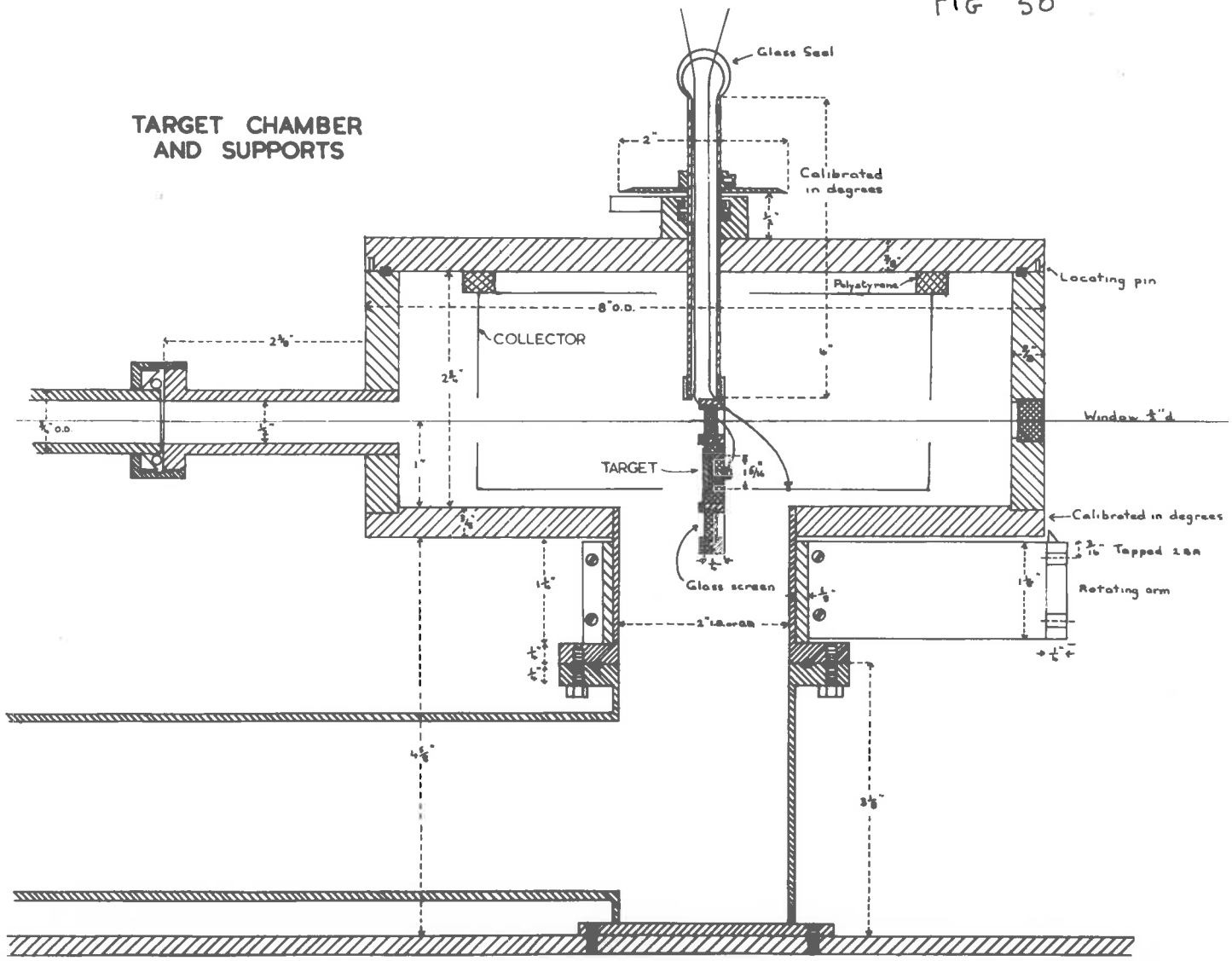
TARGET CHAMBER
AND SUPPORTS
Glass Seal
2"
Calibrated
in degrees
Locating pin
Polystyrene
8" O.D.
COLLECTOR
6"
Window ¼" d.
TARGET
Calibrated in degrees
Tapped 2 ea
Glass screen
Rotating arm
2" I.D. ea

FIG 51

of the $\frac{1}{2}$" diameter hole were all coplanar.

The top of the chamber was machined to accommodate a neoprene ring and four locating pins, the latter being fitted to correspond with holes in the lid of the target chamber. In the centre of the lid was a cast boss which was bored and machined for two neoprene rings. A nickel plated copper tube passing through the cast boss supported the mountings of the target and fluorescent screen.

Electrical connections to the target and collector were made by two tungsten to glass seals through the glass tubing which was joined to the upper end of the copper tube by means of a Housekeeper seal. The internal connections to the target and collector were copper wires insulated by ceramic spacers.

The copper tube was screwed on to a Nickel plated brass rectangular plate which carried the fluorescent screen and target, the latter being insulated from the plate by means of a machined micalex insulator. The fluorescent screen was made from a mixture of Zinc Sulphide and Sodium Silicate (Water Glass).

The collector was a brass cylinder in which a semicircular slot 4 mm. wide was cut to allow the X radiation to reach the Aluminium window of the target

chamber without being absorbed.

Two 3/4" diameter holes drilled at opposite ends of the collector and in line with the slot allowed the electron beam to enter the chamber strike the fluorescent glass screen and the focal spot to be observed. This collector was suspended from the lid of the target chamber and insulated from the latter by means of three perspex rods. A graduated scale was fixed by a locking screw to the copper tube allowing the target to be positioned at any angle relative to the incident electron beam. Two suitably cut spacers resting on the boss of the lid and supporting the scale allowed the electron beam to impinge either on the fluorescent screen or the target. A short length of 2" diameter brass tubing was threaded and silver soldered to the base of the chamber. This tubing provided both the vacuum line connection to the target chamber as well as the support for two V blocks which were carried on a rotating arm attached to the brass tubing by a collar.

The detector was mounted on the V blocks and held in position by a brass clamp. The arm also carried an attachment which supported a $\frac{1}{2}$" sliding brass block in which was drilled a hole for the pin hole mounting, the brass block

being adjusted vertically by means of a thumb screw. A slit was provided in the sliding block which carried the brass insert to enable filters to be placed in the path of the X ray beam.

3·24

The sensitivity and linearity of the galvanometer used to measure the electron beam current entering the target chamber was determined by using a Crompton potentiometer of 40 ohms resistance. A standard 1 Megohm resistor was connected in series with the Galvanometer which had an internal resistance of 1300 ohms, and the potential varied in equal steps. A graph of galvanometer deflection against applied current is shown in Fig. 52.

FIG 52

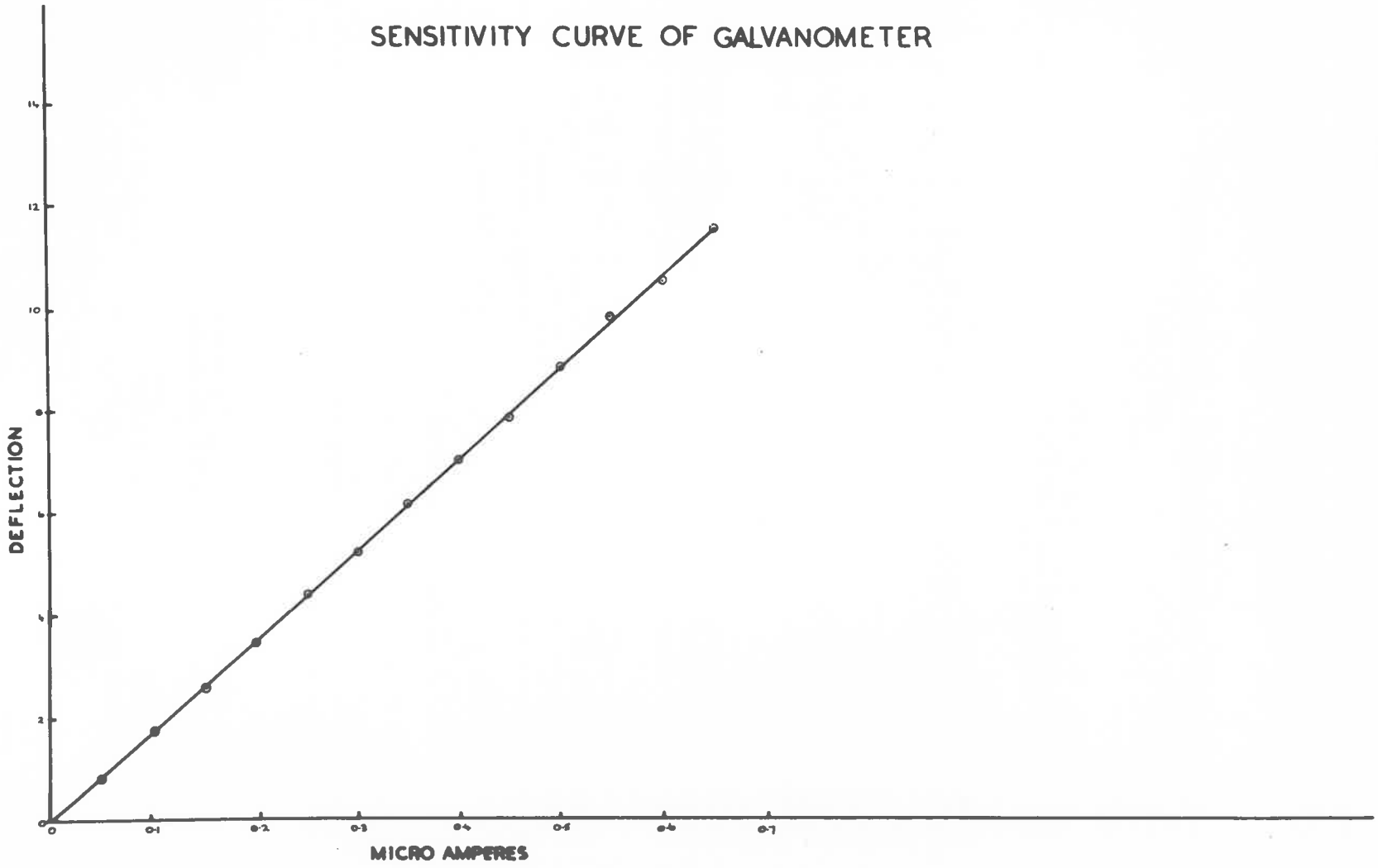
SENSITIVITY CURVE OF GALVANOMETER
DEFLECTION
MICRO AMPERES
0
0·1
0·2
0·3
0·4
0·5
0·6
0·7
2
10
12

3·25

Scintillation Counter used for the Measurement of Copper Kα Radiation.

The Scintillation Counter used comprised a NaI Tℓ crystal 1 mm. thick and a 6097 photomultiplier the latter being an 11 stage tube. The dynode supply consisted of a total resistance of 13 megohms of which two megohms were connected between the cathode (which was earthed) and the first dynode, the reason being that since the source of noise generated in the tube is due to the random fluctuations of the multiplication processes, it is preferable to keep the potential between cathode and first dynode high in order to maintain the gain from the first stage as high as possible.

Furthermore since the gain varies roughly as the eighth power of the overall voltage for an eleven stage tube, a highly stabilized power supply in necessary for consistent results.

Great care was taken that the photomultiplier tube was never exposed to light, since the dark current would then be high when a voltage was first applied to the tube, this current falling steadily to a constant value over a period of time which varies according to the amount of light to

which the photomultiplier has been exposed.

Since the NaI Tℓ crystal is extremely hygroscopic, it is hermetically sealed in an aluminium holder, the latter being itself completely opaque to visible light. One side of the crystal mount had a flat glass plate which was 'sealed' on to the photomultiplier tube face with a very thin layer of Silicon oil to minimise reflection losses. The photomultiplier shield consisted of a brass tube with two knurled sleeves. Two terminals on one of the knurled sleeves were connected to the H.T. supply of the Scaler and to the input of the preamplifier respectively by means of two coaxial cables, the cable connecting the photomultiplier to the preamplifier being made as short as possible to minimise distortion and attenuation.

To ensure that the aluminium holder did not move over the face of the photomultiplier tube, a thin circular brass plate having a rectangular slit 1 cm. by 4 mm. cut in its centre, was placed on the aluminium holder and a knurled sleeve with a 1" diameter hole in its centre was fitted on to the brass tube till it rested firmly on the brass circular plate.

PRELIMINARY TESTS CARRIED OUT ON THE EQUIPMENT.

4·1

Since the size of the focal spot could be varied by varying the current passing through the coil of the magnetic lens, it was immediately noticed that there was an upper limit to the size of the focal spot, estimated to be larger than 2 mm, beyond which the number of Copper Kα quanta recorded by the Scaler in a fixed time decreased as the beam current was kept constant. However, if for every accelerating voltage used in the measurements of intensities the magnetic lens currents were chosen so as to give a small and sharp focal point (the values of the magnetic lens current are those shown in Fig. 49) then the number of counts recorded increased as the electron beam current was increased. For an accelerating voltage range of 30 - 60 kilovolts, the angle of emission ϕ being arbitrarily chosen as 30°, the number of Copper Kα counts was found to be proportional to the incident beam current.

Fig. 54 is a plot of the number of Copper Kα counts recorded in 100 secs per unit beam current against the beam current.

FIG 54

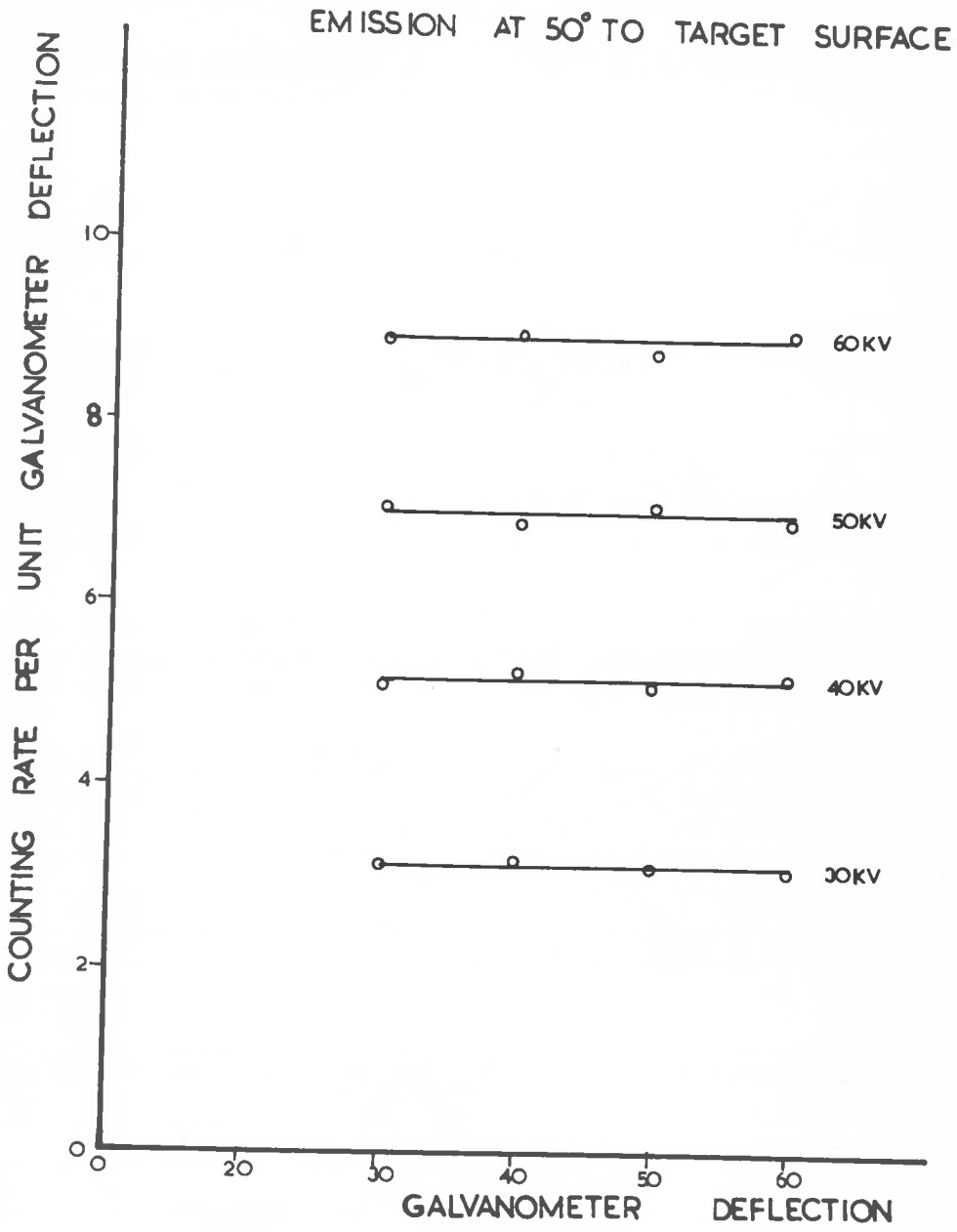
EMISSION AT 50° TO TARGET SURFACE
COUNTING RATE PER UNIT GALVANOMETER DEFLECTION
0
2
4
6
8
10
60KV
50KV
40KV
30KV
0
20
30
40
50
60
GALVANOMETER DEFLECTION

4·2

Measurement of Intensity of the Copper Kα Emission for Normal Incidence of the Electron Beam.

In every case that intensity measurements were made, a warm-up time of half an hour was allowed to prevent any drift troubles. A 'mains' switch on the scaler allowed the counting rate to be checked against the mains frequency. The differentiating and integrating time constants of the main amplifier were both set at 1·6 micro seconds and the gain set at 110 db. The base level and window width of the Pulse Height Discriminator were fixed at 13 volts and 20 volts respectively, while the voltage on the Scintillation Counter was raised to 1400 volts. These settings correspond to the optimum values obtained from the integral curve described in Section 2·12. With the auto-time on the scaler fixed at 100 secs and the auto count on the 'off' position, the background count was found to vary between 200 - 250 counts during the whole course of the measurements. It was found expedient to place a mirror facing both the galvanometer (which measured the beam current) and the lead glass window on the target chamber, so that when the filament heating current and the bias controlling the beam current were

adjusted by means of the two insulating rods, both the focal spot on the fluorescent screen and the galvanometer deflection could be observed by the experimentor at the control panel.

To ensure that the focal spot on the target, the pin hole and the aperture on the photomultiplier were correctly aligned, the focal spot was first adjusted by means of the magnetic lens so that it was at the centre of the fluorescent screen. The vertical height of the brass block carrying the pin hole was adjusted by means of a thumb screw until the scaler recorded the maximum number of counts. It was essential to ensure that the Scintillation Counter was actually receiving X radiation from an angle ϕ with respect to the target surface. Setting the pointer of the rotating arm carrying the Scintillation Counter on the graduated scale of the target chamber at the desired angle ϕ would certainly not measure the emission at the selected angle if the target were not perpendicular to the incident beam of electrons. The pointer was therefore first set on the zero mark of the graduated scale and the target rotated until the counting rate was just above that for dark current. The Scintillation Counter was then accurately parallel to the target surface and the former

could now be positioned at any angle and the intensity measurements recorded.

In Section 1 the formula for the emission N_ϕ was derived

$$N_\phi = k\int_0^{x_m}\int_{-\pi/2}^{\pi/2} \exp(-\theta^2/2\Delta^2)\exp(-\mu\rho x \operatorname{Cosec}\phi \cos\theta)\frac{\partial n}{\partial x}\,dx\,d\theta$$

Since N_ϕ is defined as the number of Kα quanta emitted at an angle ϕ to the target surface per unit solid angle per incident electron, it is essential that the electrons actually incident on the target be measured. This is achieved by connecting the collector and target through the two way switch S to the Galvanometer, Fig. 55. With S connected to A the reading of the Galvanometer is equal to the incident beam current. From the sensitivity curve of the Galvanometer, Fig. 52 it is seen that a deflection of 100 mms corresponds to a current of $0{\cdot}56 \times 10^{-6}$ ampere. The solid angle subtended by the pin hole at the centre of the target was calculated from the following data:

FIG 55

SCHEMATIC DIAGRAM OF TARGET AND COLLECTOR

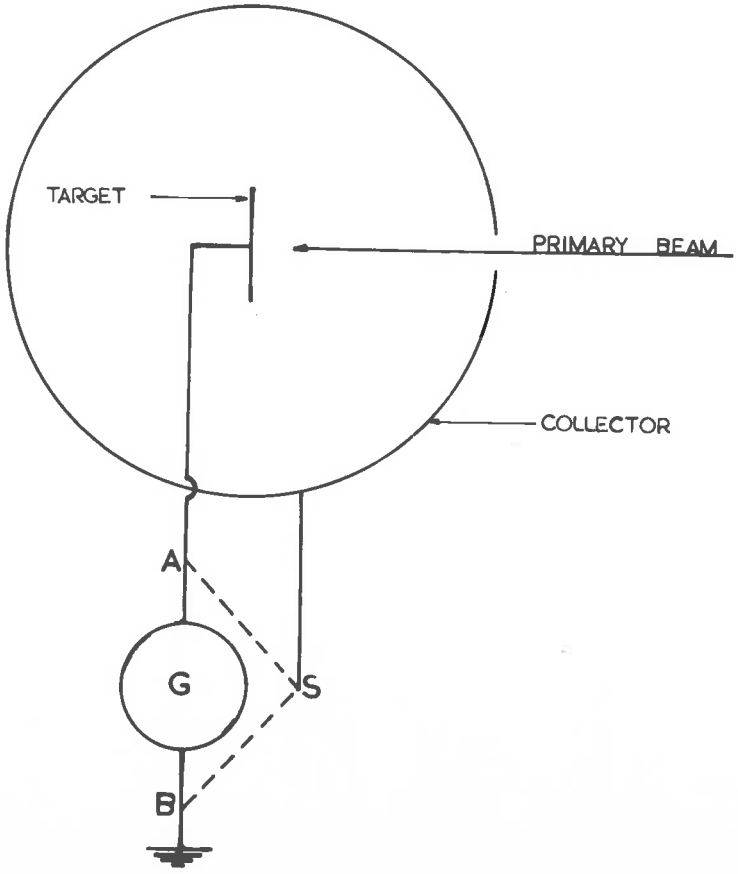

Distance of aluminium window of X ray tube to pin hole = 2·7 cm.

Distance of target to X ray window = 10·16 cm.

Diameter of pin hole = 0·070 cm.

∴ Solid angle ω subtended by pin hole at target is

$$\omega = \frac{\pi}{4} \cdot \frac{(0{\cdot}070)^2}{(12{\cdot}86)^2} = 0{\cdot}24 \times 10^{-4} \text{ steradians.}$$

Calling N_1 the number of counts recorded by the scaler in 100 secs when the Nickel filter is made to intercept the X ray beam, and N_2 the number of counts for the same time with the Iron filter, each of these values was corrected for the 'dead time' of the scaler which was 5×10^{-6} seconds. Let the difference between N_1 and N_2 after dead time correction be denoted by P. Since the radiation leaving the target of the X ray tube was modified by the factors listed below, additional corrections had to be made before the final value of N_ϕ could be determined.

(a) Absorption in the Aluminium window of the X ray tube,

(b) Absorption in the air path between X ray window and detector

(c) Absorption in the Nickel filter,

(d) Quantum Counting Efficiency of the detector.

The thickness of the Aluminium window of the

X ray tube = $2 \cdot 74 \times 10^{-3}$ cm.

thickness of Aluminium holder of the

NaI Tℓ crystal = $2 \cdot 54 \times 10^{-3}$ cm.

thickness of Nickel filter = $2 \cdot 28 \times 10^{-3}$ cm.

distance of detector to X ray window = 3·5 cms.

The mass absorption coefficients of Aluminium, Nickel and air for Copper Kα radiation were obtained from the literature and the following results calculated.

Transmission of X ray window = 69·7 per cent,

Transmission of Aluminium holder = 71·0 per cent,

Transmission of Nickel filter = 36·8 per cent,

Transmission of air path = 96·0 per cent.

The mass absorption coefficient for the NaI Tℓ crystal was calculated from the formula

$$\left(\frac{\mu}{\rho}\right)_{NaI} = \frac{1}{W_{NaI}} \sum_i W_i \left(\frac{\mu}{\rho}\right)_i$$

$$= \frac{1}{W_{NaI}} \left\{ W_{Na} \left(\frac{\mu}{\rho}\right)_{Na} + W_I \left(\frac{\mu}{\rho}\right)_I \right\}$$

Where W_{NaI}, W_{Na} and W_I are the atomic weights of NaI, Na and I respectively, and $\left(\frac{\mu}{\rho}\right)_{Na}$ and $\left(\frac{\mu}{\rho}\right)_I$ are the mass absorption coefficients of Na and I respectively for Copper Kα radiation. The mass absorption coefficient of NaI was calculated to be 270. Since the NaI Tℓ crystal used in the Scintillation Counter was 0·1 cm. thick, these figures show that over 99·5 per cent of the Copper Kα radiation incident on the crystal is absorbed.

If the corrections for (a), (b), (c) and (d) are denoted by R, then the final expression for Copper Kα emission is

$$N_\phi = \frac{4\pi \times P \times R \times 10^{-8}}{\text{Galvanometer deflection in mms} \times 0{\cdot}84}$$

The range of accelerating voltages used in these experiments varied from 14 - 17 kilovolts while the angles of emission ϕ were chosen as 1°, 3°, 5°, 10°, 20°, 30°, 40° and 50°. Results of these measurements are shown in the Appendix and a comparison of the experimental and theoretical results for Copper Kα emission is made in Section 6.

4.3

Measurement of the Intensity of Copper Kα Emission for Oblique Incidence.

Measurements were also made for the determination of Copper Kα emission when the normal to the target surface was inclined at an angle θ to the incident electron beam. These measurements were made for values of $\theta = 20^{\circ}$, 30°, 40° and 50°, and for accelerating voltages in the range of 20 - 50 kilovolts. Results of these measurements are shown tabulated in the Appendix. A comparison of the experimental and theoretical results for Copper Kα emission is made in Section 6.

4·4

Measurement of Copper Kα Emission using (a) Proportional Counter, (b) Geiger Counter.

As a check on the results obtained with a Scintillation Counter, it was decided to measure the Copper Kα emission by using a Proportional Counter and a Geiger Counter. In both cases the emission was obtained when the normal to the target was parallel to the incident electron beam.

4·41

Proportional Counter.

The Proportional Counter had two Beryllium side windows, and was filled with Xenon at 70 cm. Hg.

Thickness of Beryllium window = 0·5 mm.

Diameter of Counter = 19 mm.

For Copper Kα radiation:

Mass absorption coefficient of Beryllium = 1·35

Transmission = 88.4 per cent

Mass absorption coefficient of Xenon = 330

Transmission = 3·3 per cent

An E.C.K.O. power unit (Type N 570 B) was used in conjunction with the Proportional Counter, having a variation not greater than 0·1 per cent for 10 per cent change in mains input.

The emission of Copper Kα radiation was obtained for values of the angle of emission $\phi = 1^{\circ}, 3^{\circ}, 5^{\circ}, 10^{\circ}, 20^{\circ}, 30^{\circ}, 40^{\circ}$ and 50° and for values of the accelerating voltage equal to 20, 30 and 40 kilovolts.

4·42

Geiger Counter.

The Geiger Counter was of the end window type and was filled with Argon at 60 cm. Hg.

Length of Counter = 10 cms.

For Copper Kα radiation

Mass absorption coefficient of Argon = 112·9

Transmission = 20·6 per cent

The Mica-Beryllium window of the Geiger Counter weighed

2·5 milligrams/cm^2

Transmission = 97·3 per cent.

The emission of Copper Kα radiation was obtained for values of the angle of emission ϕ = 1°, 3°, 5°, 10°, 20°, 30°, 40° and 50° and for values of the accelerating voltage equal to 20, 30 and 40 kilovolts. Results for both the Proportional Counter and the Geiger Counter are tabulated in the Appendix, and graphs of Copper Kα emission as a function of Angle of emission ϕ are shown in Section 6.

4.5

Measurements of the Intensity of Copper Kα Radiation Using a Crystal Monochromator.

To check the results obtained for the emission of Copper Kα radiation by the method of balanced filters, it was decided to use a crystal monochromator in conjunction with a Scintillation Counter. The crystal chosen was LiF((200) plane) with a 2d spacing of 4.02 Å. This choice of crystal is governed by the fact that it has a very strong peak intensity, is very stable and has very weak higher orders of reflection.

Letting ρ be the integrated reflection coefficient for a particular wavelength

$$\text{then } \rho = \frac{E\omega}{I}$$

where E is the total energy reflected during a sweep of the crystal at a uniform angular velocity ω through the position of maximum reflection, and I is the intensity of the primary monochromatic beam.

To measure ρ, the integrated reflection coefficient for

Copper Kα radiation a double crystal monochromator was constructed. This is shown in Fig. 56. A brass tube soldered to an adjustable collar carried the collimator. The collimator could be adjusted vertically by means of a set screw and horizontally by means of a slotted guide and set screw.

The two crystal holders were both capable of rotating about a vertical axis the settings of the two crystals for any particular angle being achieved by means of fixed graduated scales on each of the two holders. A rotating arm attached to the first crystal mounting by means of a brass collar carried an attachment for the support of the 2nd crystal holder and a mounting for a pin hole. The latter was supported on a brass tube which was screwed on to a dove tail block, a micrometer screw allowing for fine adjustments in a horizontal direction. This brass tube carried a brass block drilled to receive the pin hole mounting, the block being able to slide in a slotted guide vertical adjustments being achieved by means of a thumb screw.

To the second crystal holder mounting was attached a rotating arm bored at one end to allow a brass tube carrying two V blocks welded on to a brass plate to be

FIG 56

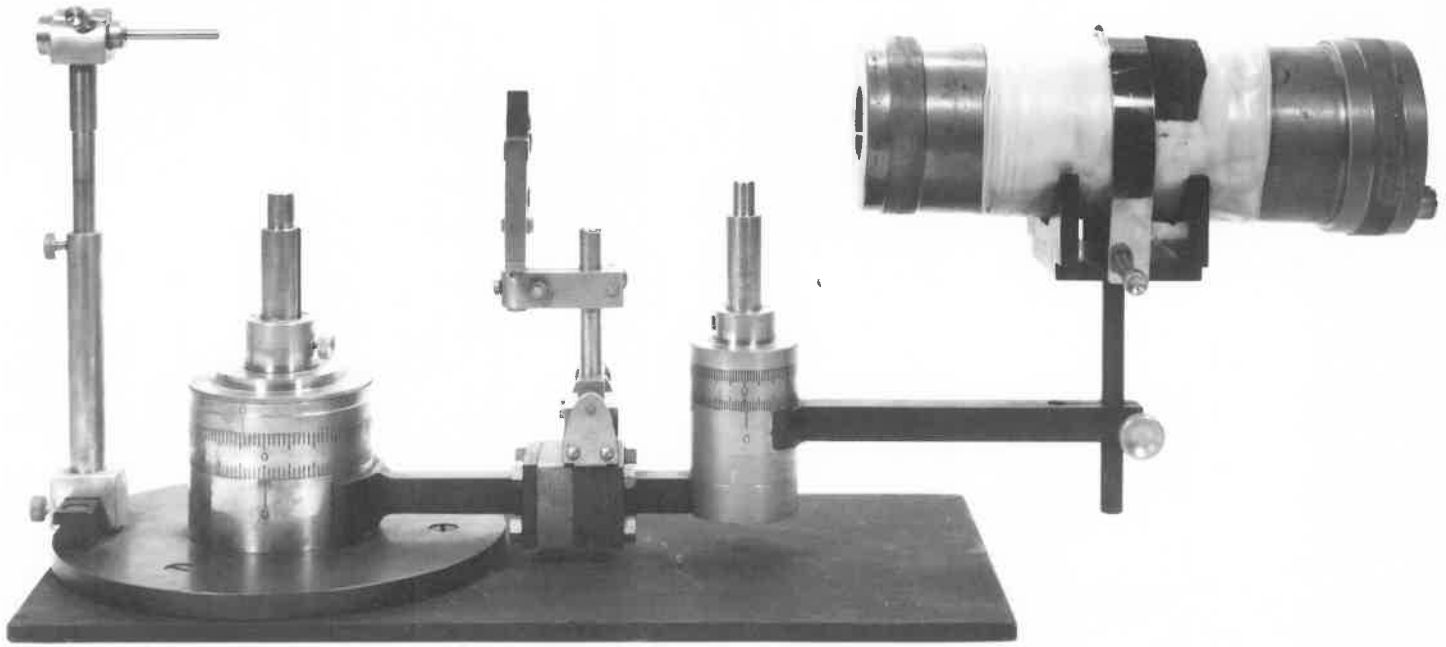

adjusted for vertical height by means of a clamping screw. The Scintillation Counter rested on the two V blocks and was rigidly held in position by means of an aluminium strip screwed to the brass plate.

A clock motor having a speed of 1 revolution per minute was fixed to the rotating arm of the second crystal holder. A worm fixed to the shaft of the motor engaged a gear clamped around the crystal holder such that the latter rotated at a speed of 1° per minute.

The X ray tube described in Section 3 had a beam current of a few microamperes and hence for the determination of ρ, the integrated reflection coefficient, the double crystal monochromator was used in conjunction with a Hilger Micro Focus Tube having a maximum beam current of 5 milliamperes.

Since it is essential that only the Copper Kα radiation incident on the 2nd crystal be recorded by the scaler, the inhomogeneous radiation diffracted from the first Li F crystal was eliminated by setting the base line and window width of the pulse height analyser so as to record only the Copper Kα radiation.

As a final check, a Nickel absorber was inserted in the path of the diffracted beam, and the reduction in intensity compared with the known absorption of the Nickel foil.

The counts recorded in 100 seconds by the scaler from the first Li F crystal = 210×10^3

The counts recorded from the second Li F crystal during one sweep about the maximum setting = 1700

Angular velocity ω of second crystal = $2{\cdot}9 \times 10^{-4}$ radians/sec

$\therefore$ The integrated reflection coefficient $\rho = \frac{E\omega}{I} = 2{\cdot}3 \times 10^{-4}$

The second crystal holder was then detached from the double crystal monochromator and attached to the rotating arm of the X ray tube. The crystal was rotated through the position of maximum reflection and the number of Copper $K\alpha$ quanta emitted per unit solid angle per electron calculated from the following data.

Distance of target to X ray window = 10·16 cm.

Distance of X ray window to pin hole = 6·30 cm.

Diameter of pin hole = 0·70 mm.

Solid angle subtended by pin hole at target = $\frac{\pi}{4}\left(\frac{0{\cdot}070}{16{\cdot}46}\right)^2$

= $0{\cdot}142 \times 10^{-4}$ steradians

Distance from X ray tube window to Scintillation Counter = 7·8 cm.

Transmission of Aluminium window of X ray tube = 69·7 per cent

Transmission of Aluminium holder of Na I Tℓ crystal = 71·0 per cent

Transmission of air path = 93·0 per cent

The emission was measured for accelerating voltages equal to 30, 40, 50 and 60 kilovolts, and for angles of emission ϕ = 1°, 3°, 5°, 10°, 20°, 30° and 40°, and results are tabulated in the Appendix. A comparison of the results obtained by using balanced filters and a crystal monochromator are shown in Section 6. Accelerating voltages below 30 kilovolts were not used since the maximum beam current available at that voltage was not sufficient to produce a suitable counting rate especially at the low angles of emission.

Before discussing the results of the absolute intensity of emission of Copper Kα radiation, the theory and results of secondary electron emission and rediffusion are considered in the following section.

5. SECONDARY ELECTRON EMISSION AND REDIFFUSION.

5·1

It has already been shown in Section 1, that for a thick target the effect of rediffusion is to diminish the intensity of X rays emitted, since the electrons that have suffered rediffusion are removed from the target before they have made their full quota of impacts. Before attempting a correction for rediffusion it is necessary to review certain facts pertaining to this problem.

Fig. 57 is a schematic diagram of the target and collector. The target is connected to earth through a galvanometer G. The collector is connected to either A or B via a two way switch S. To measure the primary current I_p incident on the target, the collector is connected to A. With the collector connected to B, the galvanometer reading is equal to $I_p - I_s$ where I_s is the secondary current due to the secondary electrons leaving the target surface. Thus both I_p and I_s can be measured. The ratio of I_s to I_p is defined as the yield Y.

Measurements were made to determine the yield Y from a Copper target. For a fixed primary voltage V_p, the

SCHEMATIC DIAGRAM OF TARGET AND COLLECTOR

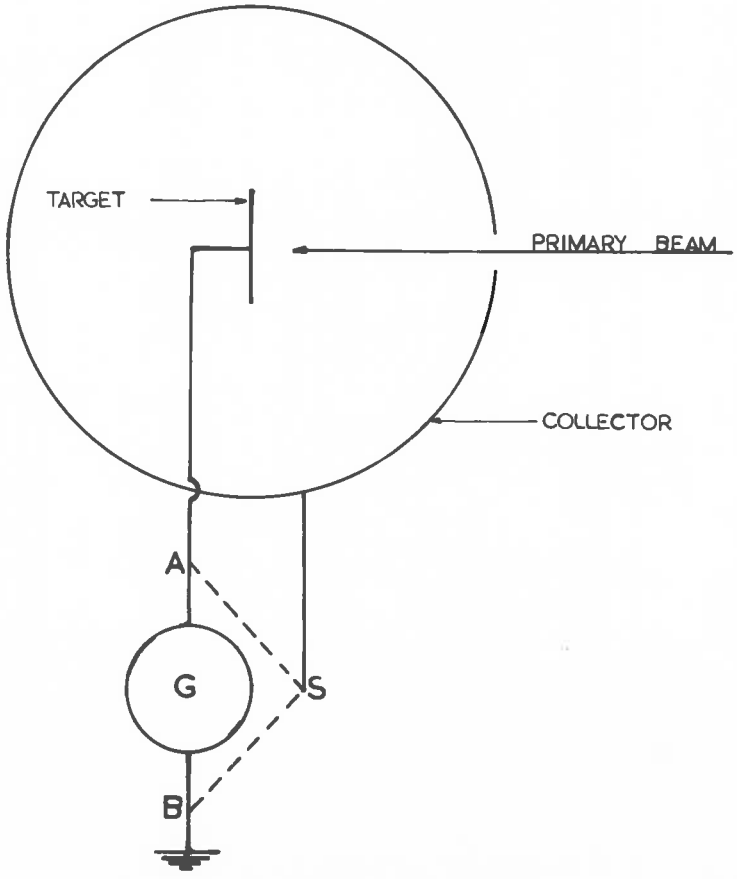

yield Y was found to be independent of the primary current. However the yield Y was found to diminish with increasing primary voltage V_p. This decrease in yield was obtained for values of V_p = 20, 30 and 40 kilovolts.

V_p	Y
20	0·262
30	0·260
40	0·258

That such a result is to be expected can be seen from the following qualitative considerations. If from the surface of the target one defines a maximum depth d_p of production of the secondaries, and a maximum depth d_s from which the secondaries can escape into the vacuum then a plot of yield Y against primary voltage V_p should give

$$\frac{\partial Y}{\partial V_p} > 0 \qquad \text{for } d_p < d_s$$

$$\text{and } \frac{\partial Y}{\partial V_p} < 0 \qquad \text{for } d_p > d_s$$

Most of the published data are for voltage ranges between 0 - 4000 volts. Recently Trump and van der Graph (1948) obtained yield curves for a voltage range from 50 - 300 kilovolts using targets of Tungsten, Steel, Aluminium and Graphite. All these curves show a decrease in the yield as the primary voltage is increased.

5·2

Energy Distribution of Secondary Electrons.

In attempting to arrive at an empirical formula which would satisfactorily represent the energy distribution of the rediffused secondary electrons, Webster (1933) made a survey of the existing results. Thus Wagner (1927) carried out measurements which enabled him to obtain a velocity spectrum of high speed secondary electrons emitted from Au, Ag and Al when bombarded with electrons of energies ranging from 16 - 40 kilovolts. The densities in these photographs beginning at the high velocity end show that the density is zero for energies equal to that of the primary beam. For energies equal to a fraction W of the primary electron beam, the density rises to a maximum for W = 0·94 for Gold and Silver and W = 0·85 for Aluminium. As the value of W decreases the density then declines. Furthermore the density is everywhere continuous although its first derivative may be discontinuous at W = 1. Independent confirmation was obtained from the work of Nicholas and Lorenz (1928) on Copper and Tungsten respectively in which the spectra of X rays produced by the rediffused electrons was studied. Here again there is no appreciable change in

the distribution of rediffused secondaries with primary voltage. Schonland (1929) found that the fraction of electrons that were rediffused from a Copper target with energies greater than 50 volts for primary beams with energies varying from 10 - 100 kilovolts, was 29 per cent of the total number of secondaries emitted and this result was independent of primary voltage.

From these considerations Webster deduced an empirical formula for the energy distribution of the rediffused electrons from a Copper target and his results are shown in Section 5·3.

5·3

Measurements of the Energy Distribution of Secondary Electrons for Normal Incidence.

The practical determination of the energy distribution of the secondary electrons has received very little attention. Thus Rudberg (1936) whose results are frequently quoted in the literature measured the electron velocity distribution from Gold using an accelerating voltage equal to 160 volts for the primary electrons. His method made use of a transverse magnetic analyser which measured the velocity distribution of electrons which were emitted in a specified direction with respect to the target surface.

A method which determines the energy distribution of all the emitted secondaries is by the use of a Retarding Electric Field. In principle this method consists of surrounding the target by a collector. A current meter connected to the latter will measure the electron current emitted by the target. If now an increasing negative voltage is applied to the collector, more and more electrons will be prevented from reaching the collector until when the voltage of the collector is equal to the accelerating voltage of the primary beam of electrons, no electrons will reach the

collector and the current meter will show a zero reading.

To measure the energy distribution of secondary electrons from a Copper target using an accelerating voltage of 20 kilovolts for the primary electron beam an important factor must be taken into account. When the primary beam of electrons strike the target, secondary electrons together with both white and characteristic X radiation are produced. This X radiation on striking the collector will produce photoemission. Hence a galvanometer connected to the collector would show at any instant a reading that is smaller by an amount due to the photoelectric current. It is therefore necessary to measure this photoelectric current.

Since the galvanometer in series with the collector had to be raised to a potential of 20 kilovolts, the galvanometer was placed on a perspex base which rested on two supporting insulating ebonite rods each 1 foot in length. Inaccuracy in reading of the galvanometer arose from the presence of excessive vibration from the backing pump transmitted to the galvanometer via the supporting ebonite rods. This vibration was eliminated by placing a layer of foam polystirene between the perspex base of the galvanometer and a similar base supported by the insulating rods.

Preliminary tests carried out on the equipment showed that with 20 kilovolts applied to the collector, there was no leakage current between collector and target chamber or between collector and the brass support for the fluorescent screen and target.

With an accelerating voltage of 20 kilovolts the electron beam was then focussed on the target and the voltage on the collector gradually raised to 20 kilovolts, the reading of the galvanometers connected to the target and collector being recorded.

To measure the photoelectric current, a metallic cylindrical framework covered by Aluminium foil was constructed. This consisted of two pairs of two concentric rings spaced and supported by thin metal rods. The entire framework was insulated from the collector by two rods of perspex screwed to the removable base of the collector, Fig. 58. Two circular holes cut at opposite ends of the curved portion of the Aluminium cylinder allowed the primary electron beam to impinge on the target. The thin cylindrical foil of Aluminium was placed between target and collector so as to completely surround the former. This foil was $0{\cdot}7 \times 10^{-3}$ inches thick sufficient to stop any electrons leaving the target from reaching the collector, but allowing the X radiation to fall on it.

FIG 58

To test for any leakage between the aluminium cylinder and the target holder or the aluminium cylinder and collector, galvanometers G_1 and G_2 were connected as shown in Fig. 59. With the voltage on the aluminium cylinder raised to 20 kilovolts no deflection of either galvanometer was observed.

With the X ray tube voltage at 20 kilovolts the beam current was then switched on and the increase in reading of galvanometer G_1 recorded as the voltage on the aluminium cylinder was raised to 20 kilovolts. Since the number of photoelectrons emitted is proportional to the intensity of the incident radiation, the absorption of the X radiation due to the aluminium cylinder was found by recording the intensity of the X radiation falling on the Scintillation Counter once with a piece of Aluminium of the same thickness interposed between the X ray tube window and the Counter and once without.

It was found that the aluminium cylinder absorbed 25 per cent of the incident X radiation.

For these experiments, it was found that the fraction of the secondary electrons leaving the target with an energy greater than 12 kilovolts is 23 per cent.

FIG 59

SCHEMATIC DIAGRAM OF ALUMINIUM CYLINDER AND COLLECTOR

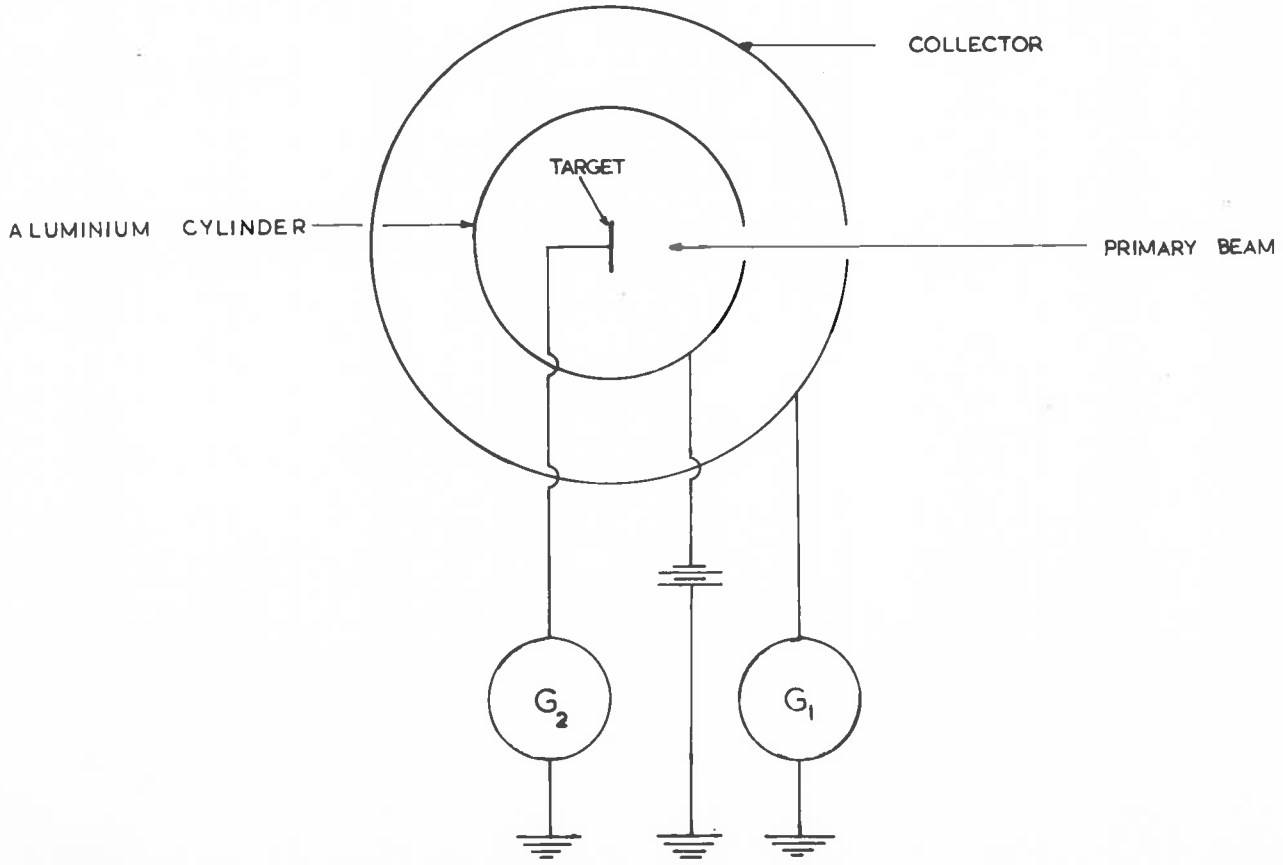

These measurements were also carried out for accelerating voltages of 10 and 25 kilovolts of the primary electron beam. It was found that the fraction of the number of secondary electrons leaving the target with an energy loss of 8·9 kilovolts was constant and equal to 0·23. Webster's values for the fraction W of the secondary electrons leaving a Copper target with an energy loss of V_k = 8·93 kilovolts (the K shell ionisation of Copper) when the primary electron beam is accelerated by a potential of V kilovolts is given in the following table.

$U = \frac{V}{V_k}$	W
1·0	0
1·5	0·100
2·0	0·138
2·5	0·153
3·0	0·160
3·5	0·167
4·0	0·175
5·0	0·180
6·0	0·187
7·0	0·195
8·0	0·200

The choice of 12 kilovolts can be appreciated from the following considerations. If V_k (8·93 kilovolts) is the ionization potential of Copper for Kα radiation and V is the primary accelerating voltage, then the effect of the rediffused electrons on the intensity of the Kα radiation can be determined by finding the area under the curve of the energy distribution of the secondary electrons as a function of the voltage between the limits $V = V_k$ and V. However, the area under the energy distribution curve is very small around the point $V = V_k$ so that even if the lower limit were taken as $V = V_k \pm R$ where R = 2000 volts, the fraction of the secondary electrons leaving the target would certainly not differ by more than 1 per cent from the value 0·23.

5.4

Yield at Oblique Incidence.

It has been shown in Section 1 that the absolute intensities of Copper Kα emission for the case when the normal to the target in inclined at an angle θ to the incident beam of electrons is given by

$$N_\phi = k\int_{-\pi/2}^{\pi/2}\int_0^{x_k} \exp(-\theta^2/2\Delta^2)\exp\left(-\mu\rho x \operatorname{Cosec}\phi \operatorname{Cos}(\theta+\alpha)\right)\frac{\partial n}{\partial x}\,dx\,d\theta$$

It must be emphasized that the factor k that appears in the above expression for the emission embodies the following corrections.

(a) Indirect production of the characteristic radiation by the photoelectric absorption of the continuous radiation,

(b) Fluorescence Yield,

(c) Electron rediffusion,

(d) Ratio of number of Kα quanta to the total number of K quanta produced.

For varying angle of incidence of the primary beam, (a), (b) and (d) would be expected to remain constant. However this

is certainly not the case for (c). Since a distinction between the slow and fast secondary electrons must be made, it is advantageous at this stage to study the total yield at oblique angles of incidence.

That more secondaries are produced for a given primary current I_p when the target is inclined to the incident electron beam can be seen from the following considerations. If one assumes that for normal incidence the average range of a primary electron is d_p, then in the case of oblique incidence, secondaries produced at the end of the range d_p will only be a distance $d_p \cos \theta$ from the target surface where θ is the angle of incidence, and will thus have less chance of being absorbed before reaching the surface. Hence keeping the primary voltage V_p constant the yield Y should increase the larger the angle of incidence. The yield was measured for a primary voltage V_p equal to 20, 30 and 40 kilovolts at angles of incidence 20°, 30°, and 40° and results are shown in the following table.

	YIELD		
ANGLE	20 KV	30 KV	40 KV
0°	0·262	0·260	0·258
20°	0·276	0·271	0·266
30°	0·295	0·290	0·284
40°	0·323	0·317	0·313

It should be further noticed that for weak diffusion, that is in the case of the primary electron beam taking a nearly linear path in the target, the range perpendicular to the surface of the target decreases with Cos θ. For strong diffusion however, the influence of the direction of incidence on the distribution of the primaries decreases and therefore a corresponding decrease of the dependence of the yield on the angle of incidence from the lighter to the heavier elements should be observed.

For primary voltages up to 3000 volts, Bruining (1936) was able to represent the dependence of the yield on the angle of incidence by the relation

$$\ln\left(\frac{\gamma_\theta}{\gamma_0}\right) = G(1 - \cos\theta)$$

where G is a constant and Y_θ and Y_0 are the yields at angles of incidence equal to θ° and 0° respectively for a fixed primary voltage V_p. This relation was verified experimentally by Bruining (1936) for Lithium, Barium and Nickel. Applying this relation to the results obtained for Copper, one notices that there is a 20 per cent variation in the value G. However it must be realized that in all measurements of yield quoted in the literature, a great deal of time and effort was expended in producing clean surfaces free from adsorbed gas layers since the effects of surface contamination on the target will alter the work function and hence alter the yield. The dependence of yield on work function has been demonstrated by Treloar (1937), de Boer and Bruining (1939). Furthermore even when relatively clean surfaces have been prepared, the yield will still be affected by the degree of roughness of the surface. Bruining showed that a rough surface shows practically no variation of yield with incident angle, a result that is to be expected since the actual angle of incidence in this case is very poorly defined.

In the measurements of yield carried out by the Author, the target surface was well polished every two hours of continuous running of the X ray tube, but no attempt was made

at obtaining a surface that was completely degassed and free from any surface contamination. Rather the target was prepared as when the intensity measurements were performed, since it is under these conditions that the yield was of interest.

5·5

Rediffusion at Oblique Incidence.

To determine whether the number of high energy electrons leaving the target increase with increasing angle of incidence, it is advantageous to write the secondary current I_S leaving the target in the form

$$I_S = I_T + \eta I_p + r I_p$$

where I_T is the current due to the 'true secondaries', i.e. those electrons that leave the target surface with energies not greater than 50 volts.

η is the fraction of the primary current I_p that is rediffused, r is the fraction of the primary current I_p that is reflected.

The sum of η and r has been measured for Copper by several Authors. Becker at 35 kilovolts, Schonland for a voltage range between 10 - 100 kilovolts and Stehberger between 2- 12 kilovolts. However it is important to notice that Schonland's measurements referred to normal incidence, Stehberger's referred to the electron beam making an oblique angle of incidence of 50° with the normal to the

target, while Becker's measurements were made with the primary beam already diffused before striking the target. More recently the sum of η and r for a number of metals have been measured by Palluel (1947) and by Holliday and Sternglass (1957). Their results show that $\eta + r$ for normal incidence of the primary beam approaches an upper limit between 0·05 and 0·5 with increasing primary voltage up to 20 kilovolts. Their apparatus consisted essentially of a target at one end of a long cylindrical collector. A suppressor grid was placed between the collector and target and was biased at -50 volts so as to prevent any secondaries produced at the collector from reaching the target. However since secondaries emitted from the grid wires themselves cannot be prevented from reaching the target, a small correction had to be applied in order to obtain a true value of $\eta + r$. For Copper they obtained a value of 0·29.

Now although the yield increases with increasing angle of incidence of the primary beam, the main point is whether both $\eta + r$ increase for voltages above that for Copper Kα ionization (8·93 kilovolts), since an increase in these factors would indicate that a greater proportion of electrons are removed from the target before they have

made their full quota of impacts.

Measurements were carried out to determine whether $\eta + r$ increased with increasing angle of incidence. The angles chosen were 20°, 30° and 40° for a fixed primary voltage of 20 kilovolts. At 20°, the ratio of the number of electrons leaving the target whose energy is larger than 12 kilovolts, to the total number of secondaries was found to be 25·8 per cent. At 30° this ratio was 28·2 per cent, while at 40° this ratio was 30 per cent.

6·1 EXPERIMENTAL RESULTS OF COPPER Kα EMISSION.

The results of the experiments for the determination of N_ϕ, defined as the number of Copper Kα quanta emitted per second per unit solid angle at an angle of emission ϕ to the target surface are shown in Fig. 60. The emission N_ϕ is plotted against accelerating voltage for the case of normal incidence, i.e. when the normal to the target is parallel to the incident electron beam. These results were obtained by using a Scintillation Counter as detector together with a pair of balanced filters.

In Figs. 61 - 66 these experimental results are compared with the theoretical values of emission N_ϕ calculated from the formula

$$N_\phi = k\int_0^{x_k}\int_{-\pi}^{\pi} \exp(-\theta^2/2\Delta^2)\exp(-\mu\rho x \operatorname{Cosec}\phi \cos\theta)\,\frac{\partial n}{\partial x}\,dx\,d\theta$$

The correction for electron rediffusion embodied in the factor k which occurs outside the double integral was the value obtained experimentally by the Author.

For an angle of emission $\phi = 1^\circ$, the value of the emission N_ϕ is a maximum for an accelerating voltage of 30 kilovolts. For higher accelerating voltage the experimental points are seen to fall off more rapidly than

FIG 60

C_uK_α EMISSION AS A FUNCTION OF VOLTAGE RECORDED WITH A SCINTILATION COUNTER.

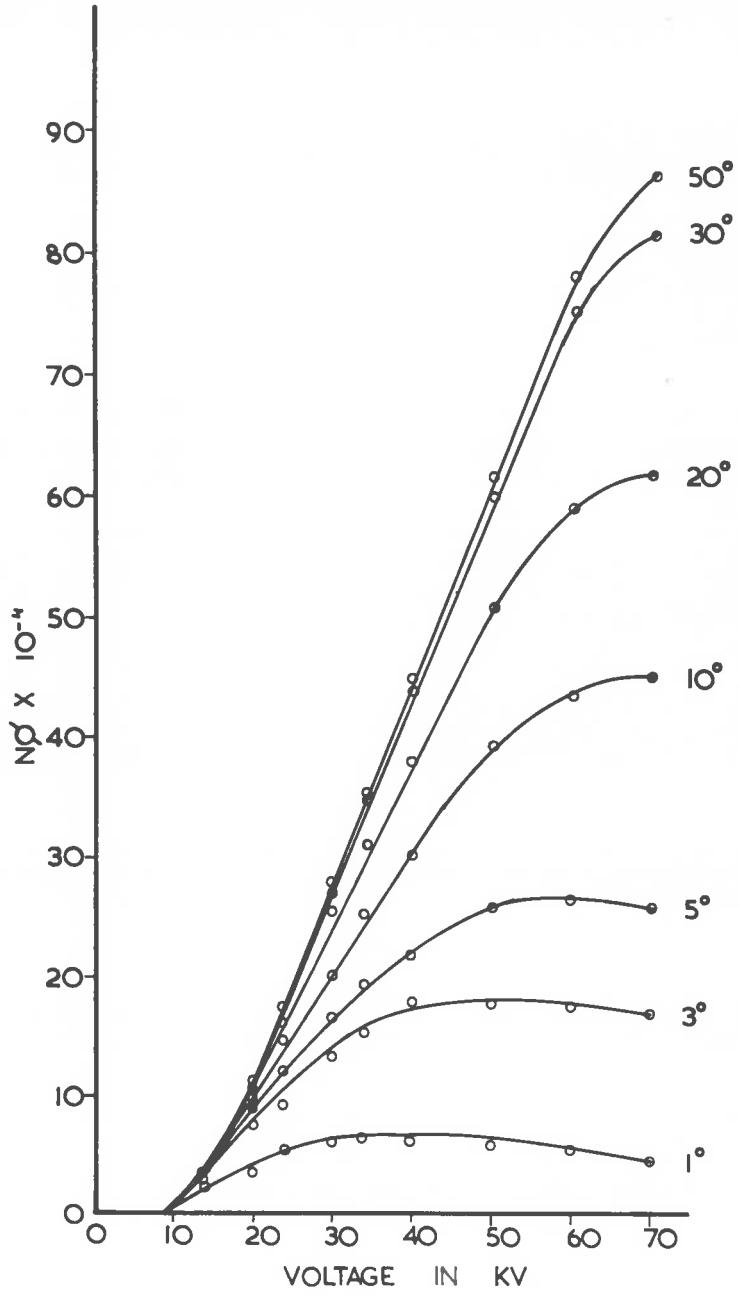

FIG 61

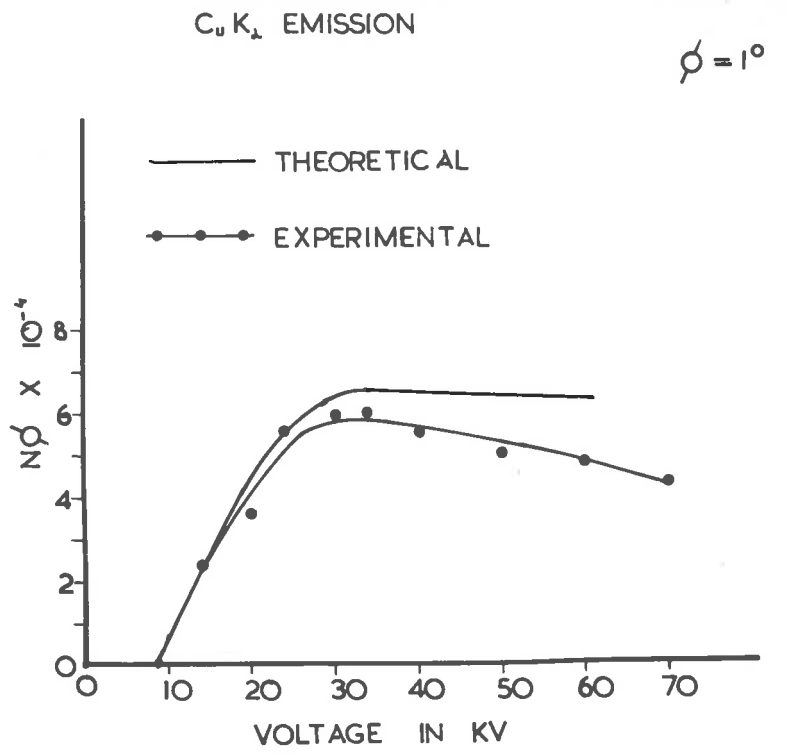
Cu Kα EMISSION
φ = 1°
THEORETICAL
EXPERIMENTAL
Nφ X 10⁻⁴
0
2
4
6
8
0
10
20
30
40
50
60
70
VOLTAGE IN KV

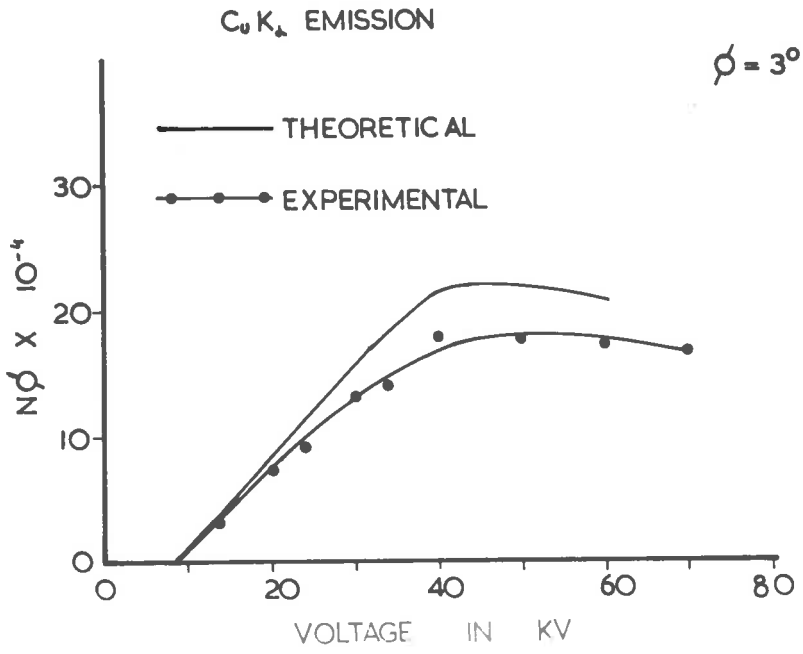
Cu Kα EMISSION
φ = 3°
THEORETICAL
EXPERIMENTAL
Nφ X 10⁻⁴
0
10
20
30
0
20
40
60
80
VOLTAGE IN KV

FIG 62

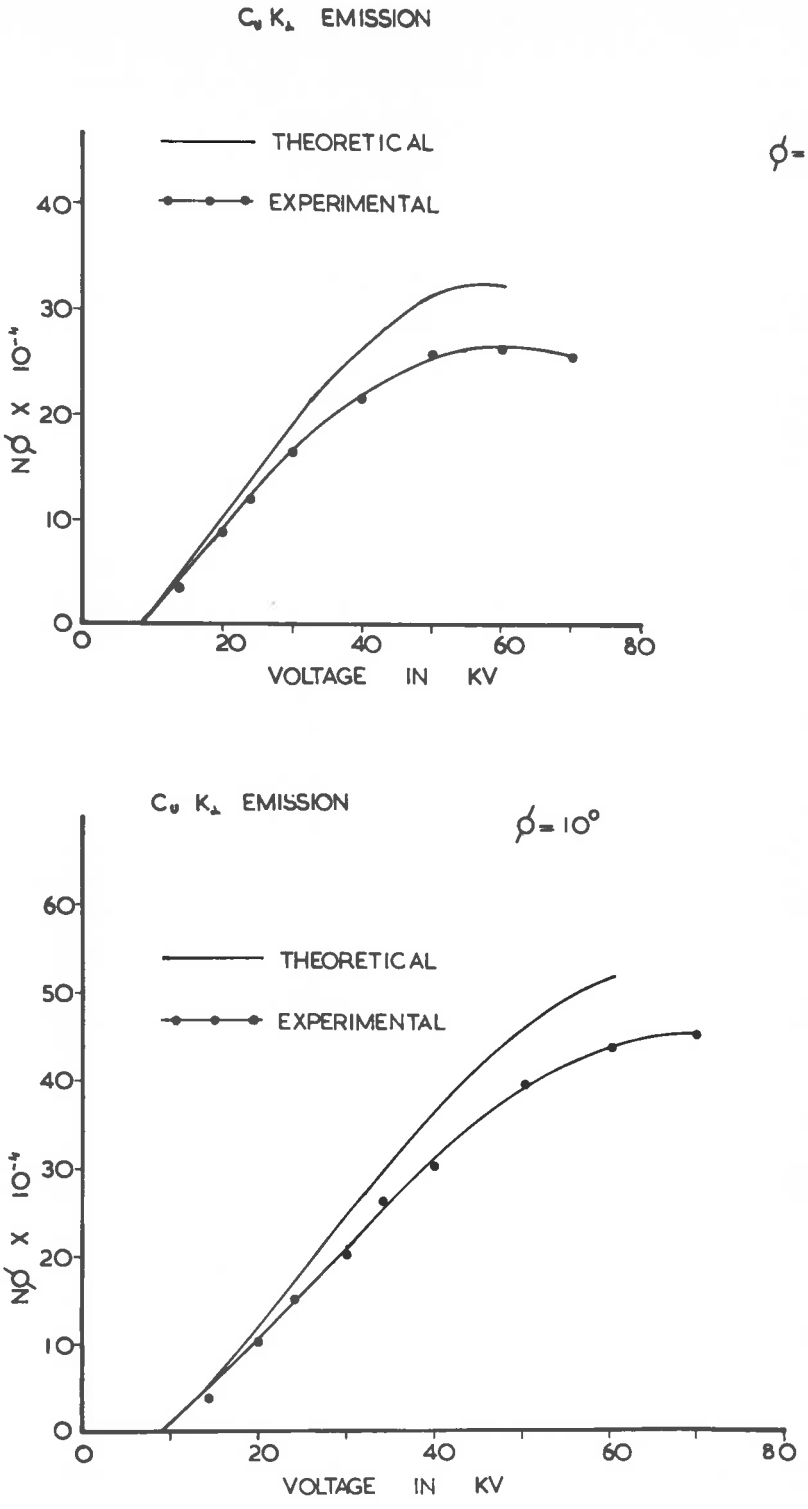
$C_u K_\perp$ EMISSION
THEORETICAL
EXPERIMENTAL
$\phi = 5°$
$N\phi \times 10^{-4}$
0
10
20
30
40
0
20
40
60
80
VOLTAGE IN KV
$C_u K_\perp$ EMISSION
$\phi = 10°$
THEORETICAL
EXPERIMENTAL
$N\phi \times 10^{-4}$
0
10
20
30
40
50
60
0
20
40
60
80
VOLTAGE IN KV

FIG 63

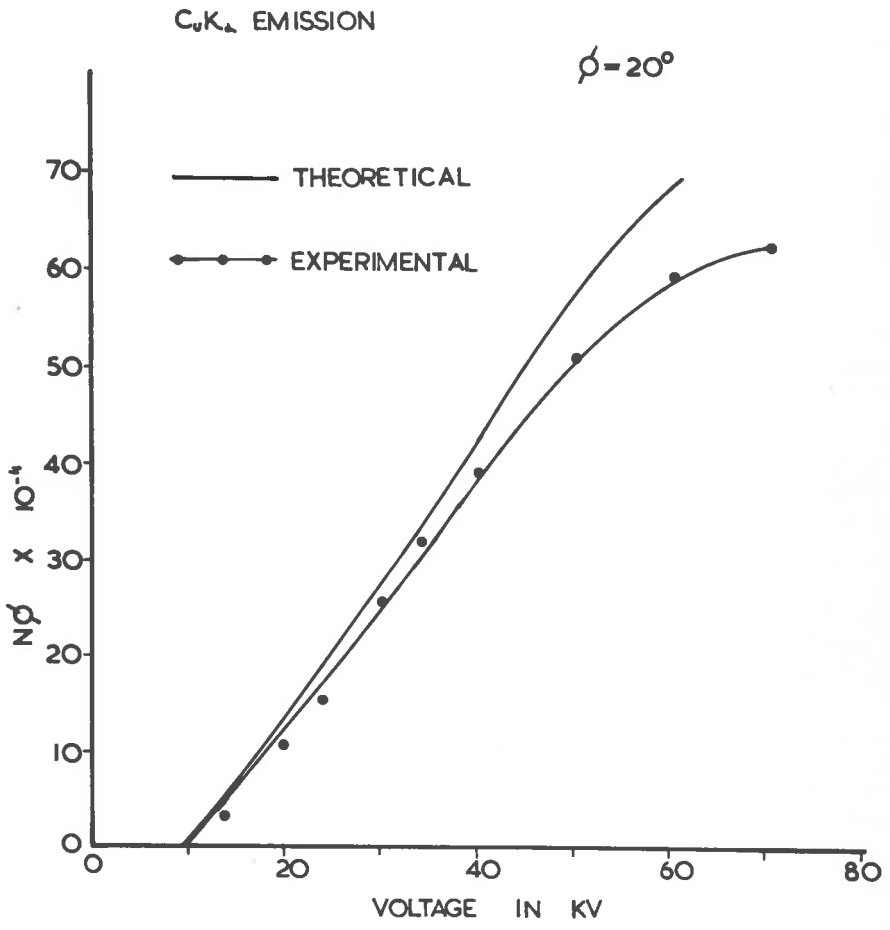
C_uK_α EMISSION
$\phi = 20°$
THEORETICAL
EXPERIMENTAL
$N\phi \times 10^{-4}$
0
10
20
30
40
50
60
70
0
20
40
60
80
VOLTAGE IN KV

FIG 64

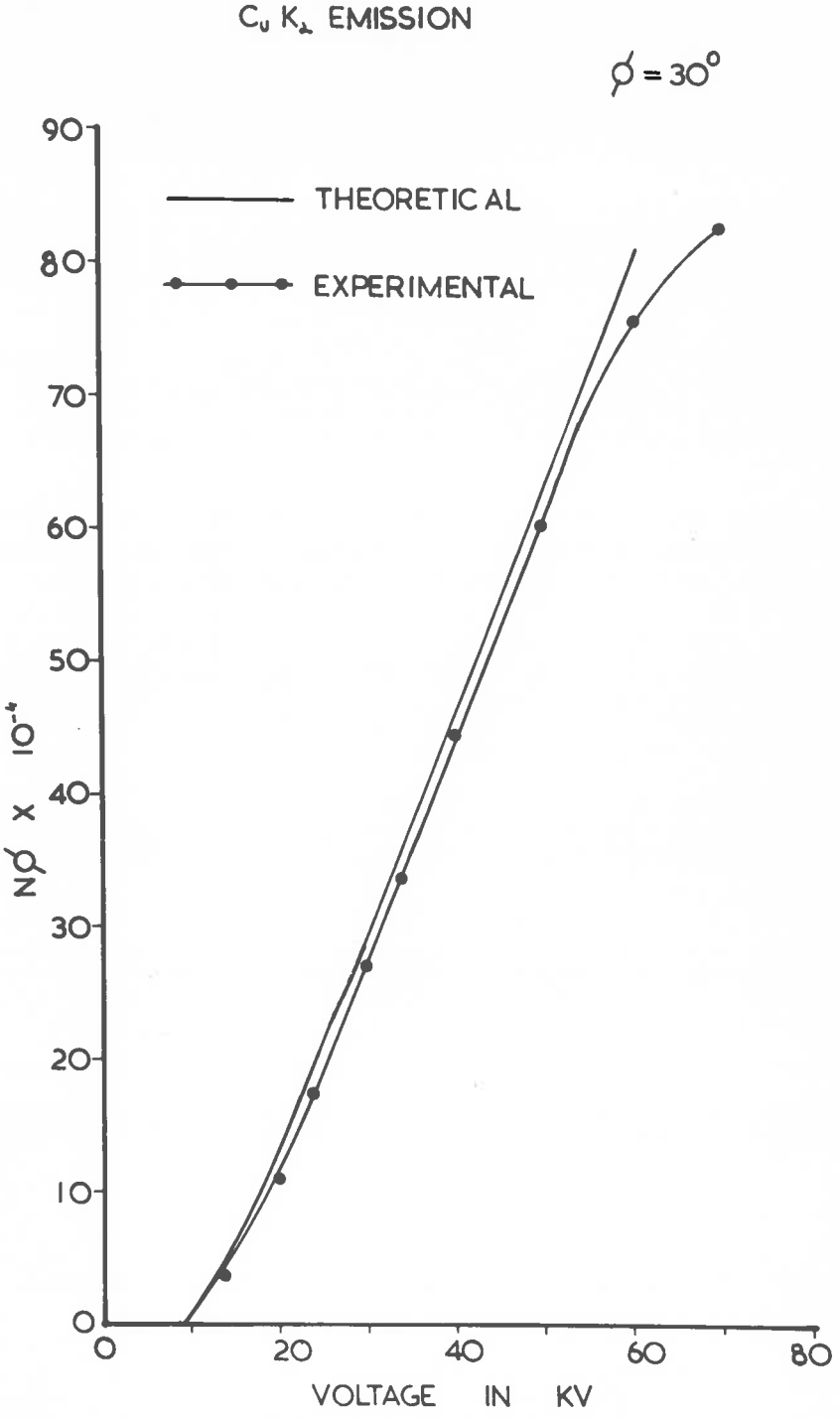
Cu Kα EMISSION
φ = 30°
THEORETICAL
EXPERIMENTAL
Nφ x 10⁻⁴
90
80
70
60
50
40
30
20
10
0
0
20
40
60
80
VOLTAGE IN KV

FIG 65

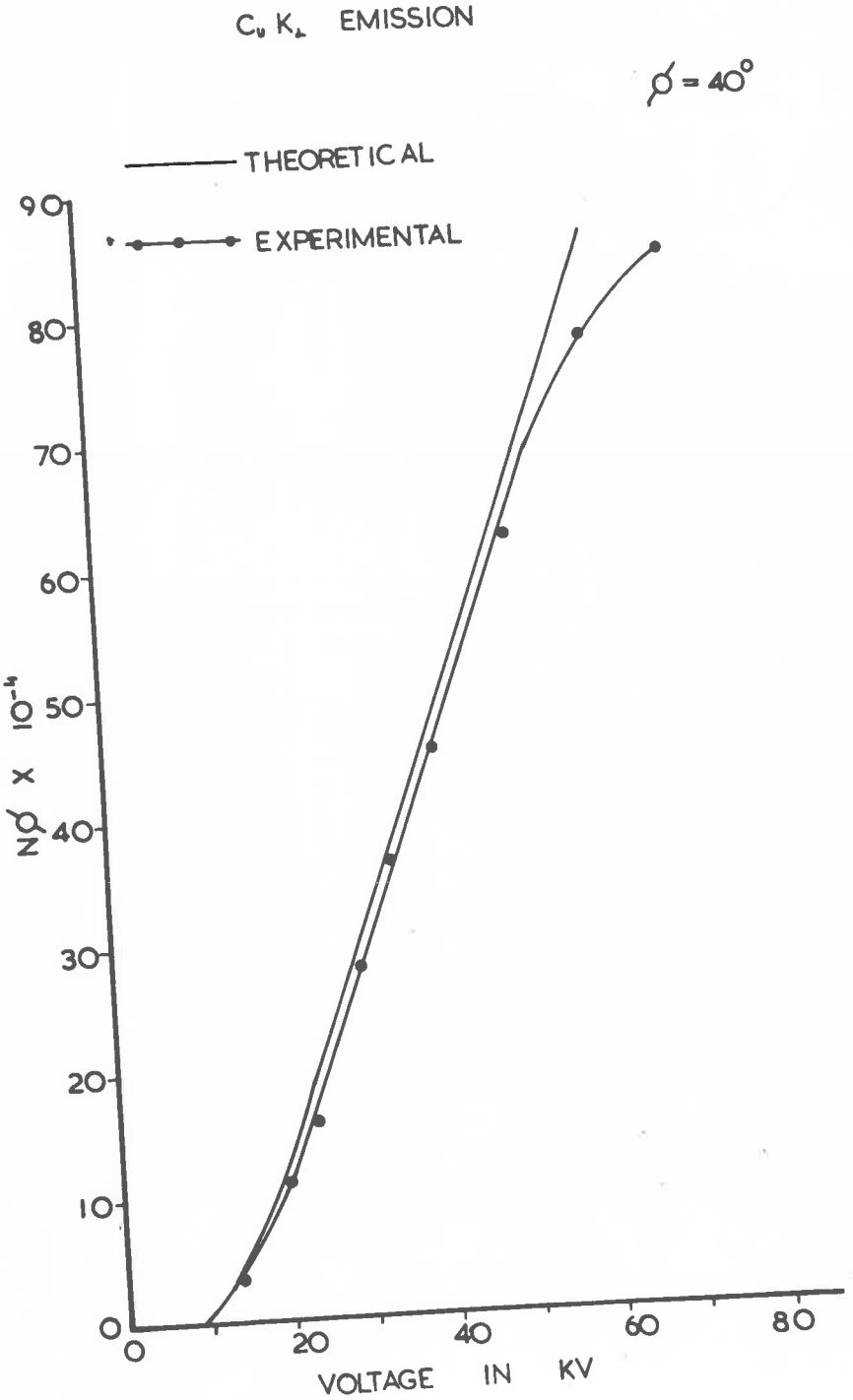
Cu Kα EMISSION
φ = 40°
THEORETICAL
EXPERIMENTAL
Nφ x 10⁻⁴
90
80
70
60
50
40
30
20
10
0
0
20
40
60
80
VOLTAGE IN KV

FIG 66

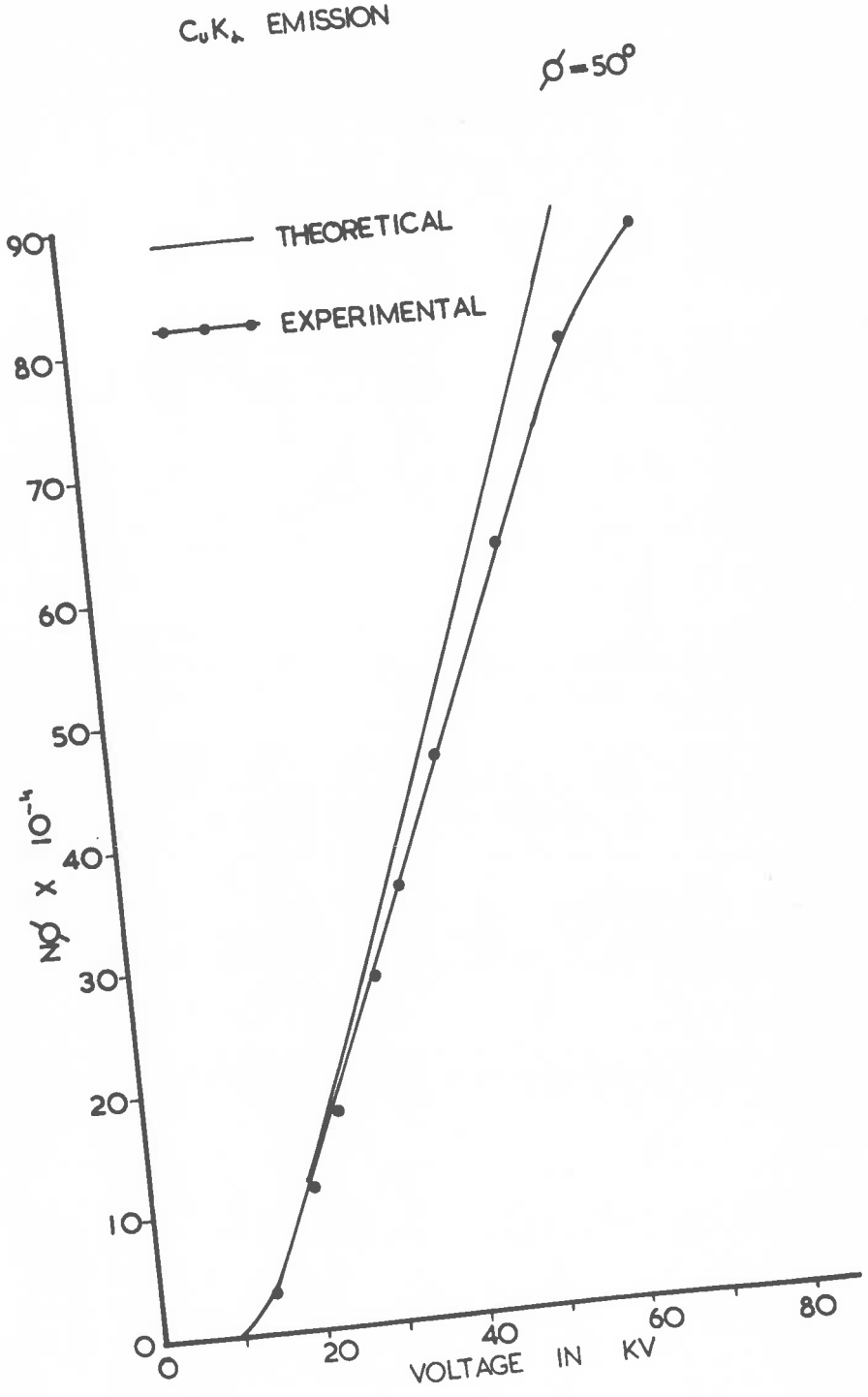
$C_u K_\alpha$ EMISSION
$\phi = 50^\circ$
THEORETICAL
EXPERIMENTAL
90
80
70
60
50
40
30
20
10
0
$\gamma N \times 10^{-4}$
0
20
40
60
80
VOLTAGE IN KV

is predicted by theory. At $\phi = 3^{\circ}$ the optimum voltage occurs at 50 kilovolts while at $\phi = 5^{\circ}$ the emission N_{ϕ} has reached its maximum at 60 kilovolts. For angles of emission $\phi \geq 10^{\circ}$ no maximum in emission N_{ϕ} has been reached for an accelerating voltage equal to 70 kilovolts. However it must be emphasized that for a sufficiently large accelerating voltage and for all angles of emission ϕ, the emission N_{ϕ} will decrease owing to the fact that as the voltage increases the depth of penetration of the electrons in the target increases more rapidly than the number of K ionizations produced. Since most X rays are produced at large distances below the target surface, then owing to the increased absorption the number of X ray quanta emerging from the target surface will be reduced.

Furthermore it can be seen from Fig. 60 that for any fixed accelerating voltage $N_{\phi}\ (1^{\circ}) < N_{\phi}\ (3^{\circ}) < N_{\phi}\ (5^{\circ}) < \ldots\ldots\ldots < N_{\phi}\ (50^{\circ})$. Figs. 67 - 68 show the emission N_{ϕ} plotted as a function of the angle of emission ϕ. These curves show that for accelerating voltages up to 24 kilovolts very little gain in emission N_{ϕ} is obtained for $\phi > 20^{\circ}$. Even for an accelerating voltage of 70 kilovolts the increase in emission for $\phi > 30^{\circ}$ is certainly not greater than 10 per cent of the value of the emission at $\phi = 30^{\circ}$.

EXPERIMENTAL RESULTS OF CuK_α EMISSION

AS A FUNCTION OF ANGLE

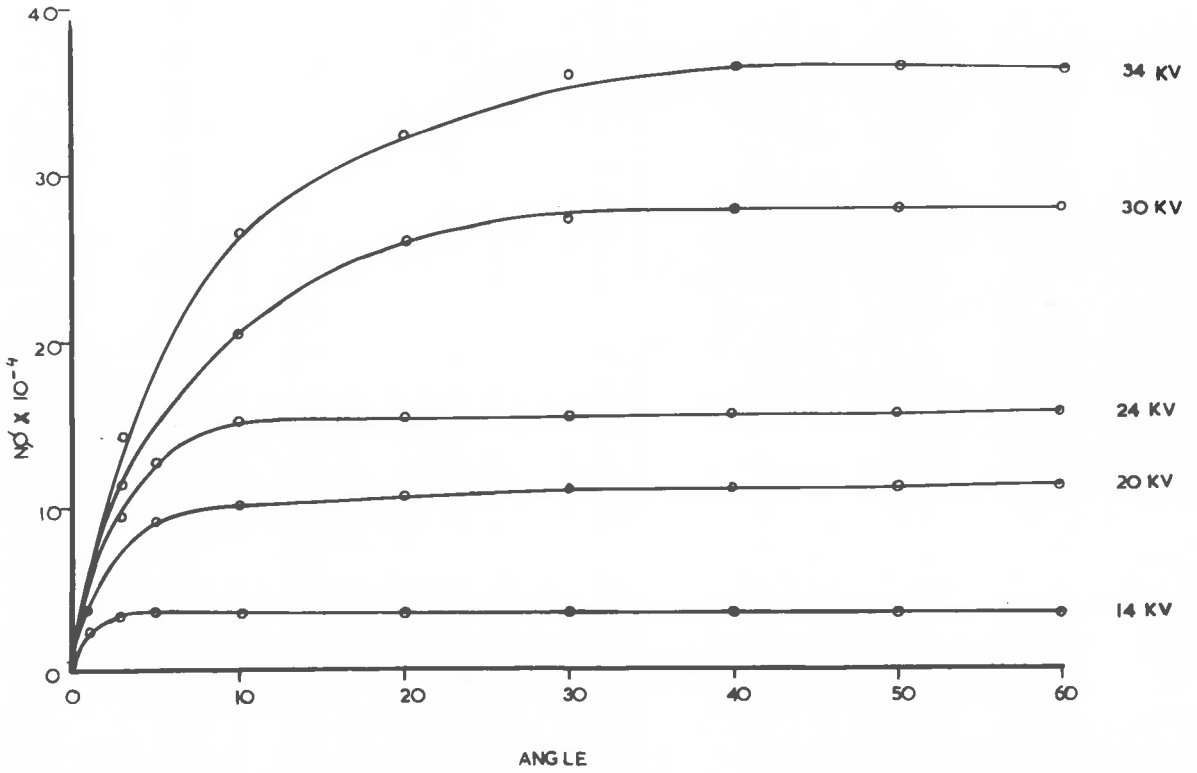

FIG 68

$C_u K_\alpha$ EMISSION AS A FUNCTION OF ANGLE.

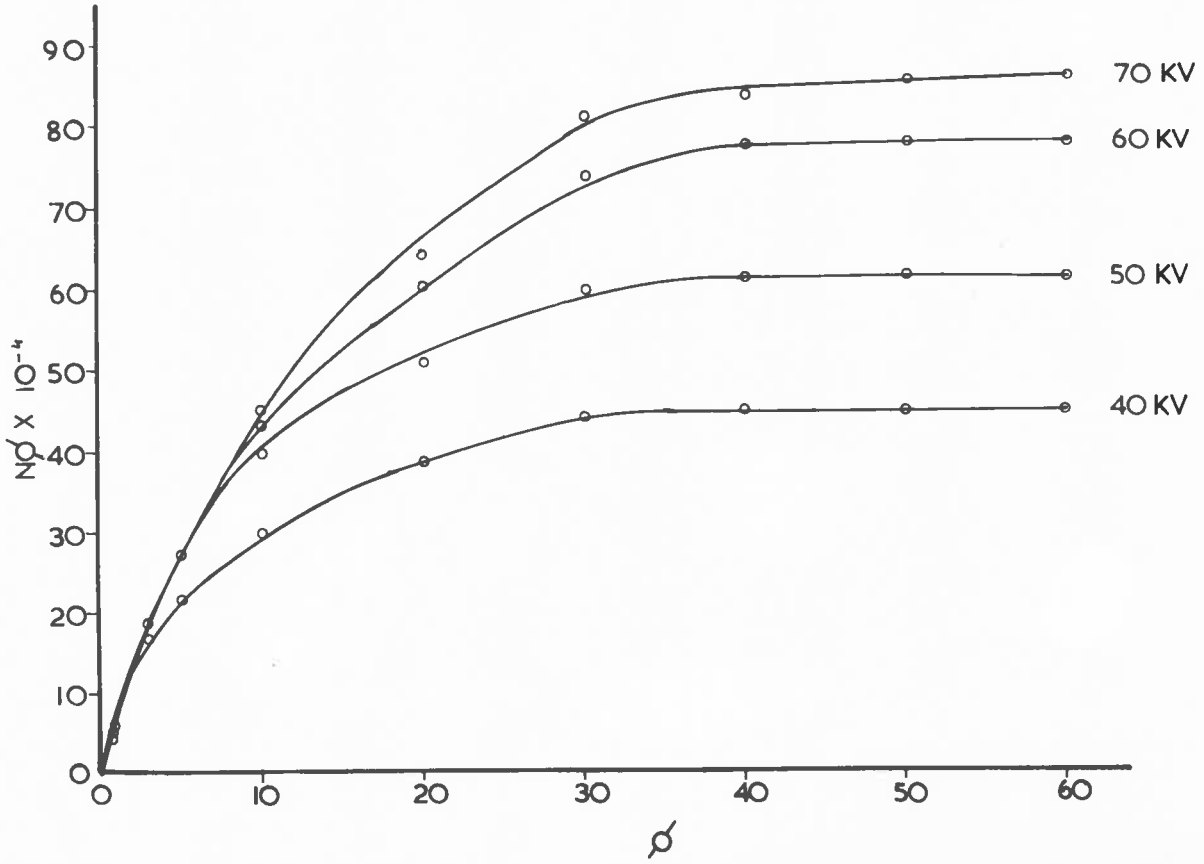

6·12

The results for the emission N_ϕ for Copper Kα radiation obtained by using a Proportional Counter and a Geiger Counter as detectors together with a pair of balanced filters are shown plotted in Fig. 69 where the emission N_ϕ is plotted as a function of the angle of emission ϕ. For comparison there is plotted the emission N_ϕ when a Scintillation Counter was used as a detector. It can be seen that the results obtained by using these three different detectors do not differ by more than 8 per cent.

6·13

Fig. 70 shows the emission N_ϕ as a function of angle of emission ϕ obtained by using a crystal monochromator (LiF) in conjunction with a Scintillation Counter. For comparison there is shown the emission N_ϕ obtained with a pair of balanced filters and a Scintillation Counter. The agreement is within 10 per cent.

FIG 69

$C_6 K_1$ EMISSION

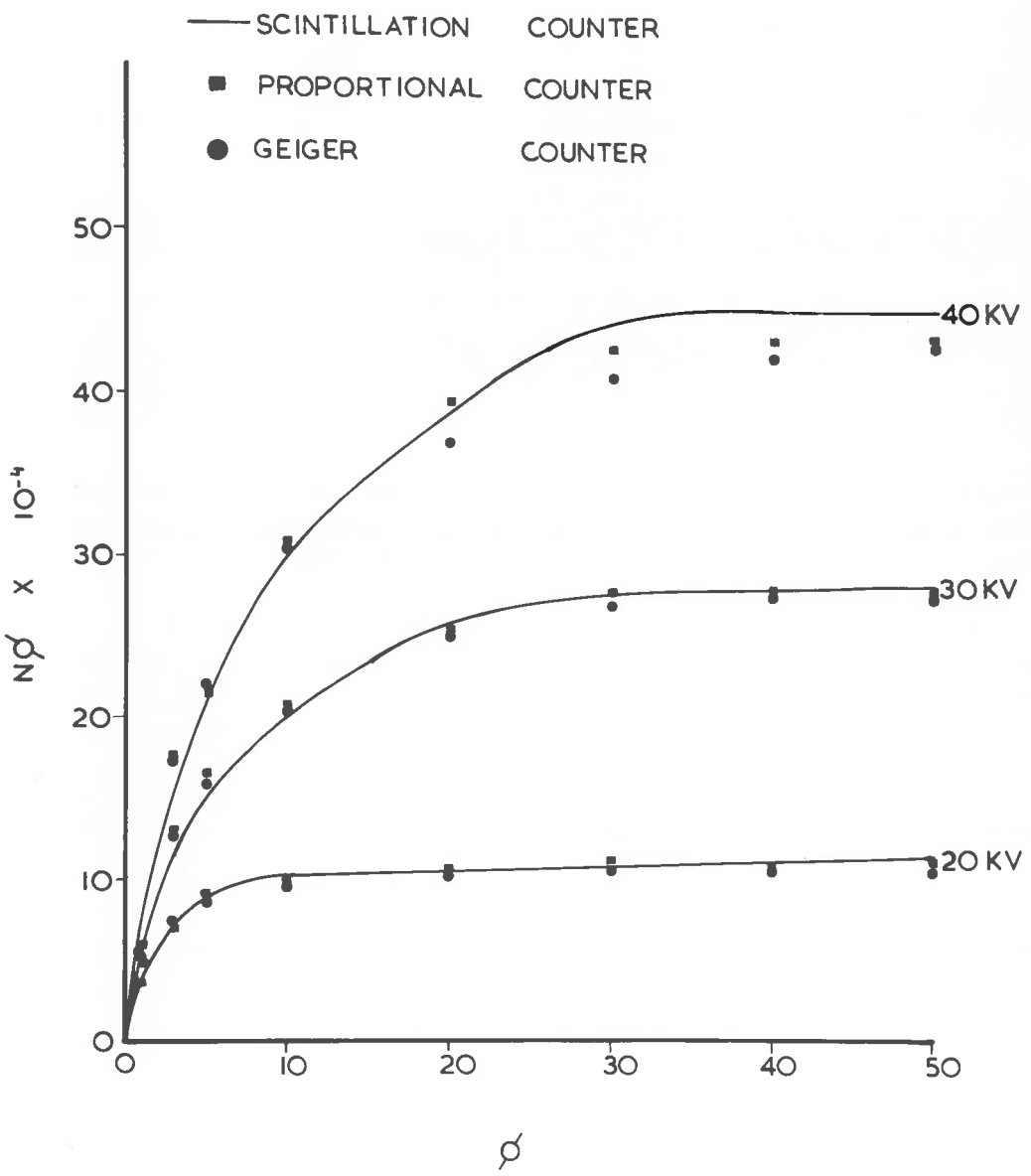

FIG 10

$C_u K_\alpha$ EMISSION AS A FUNCTION OF ANGLE

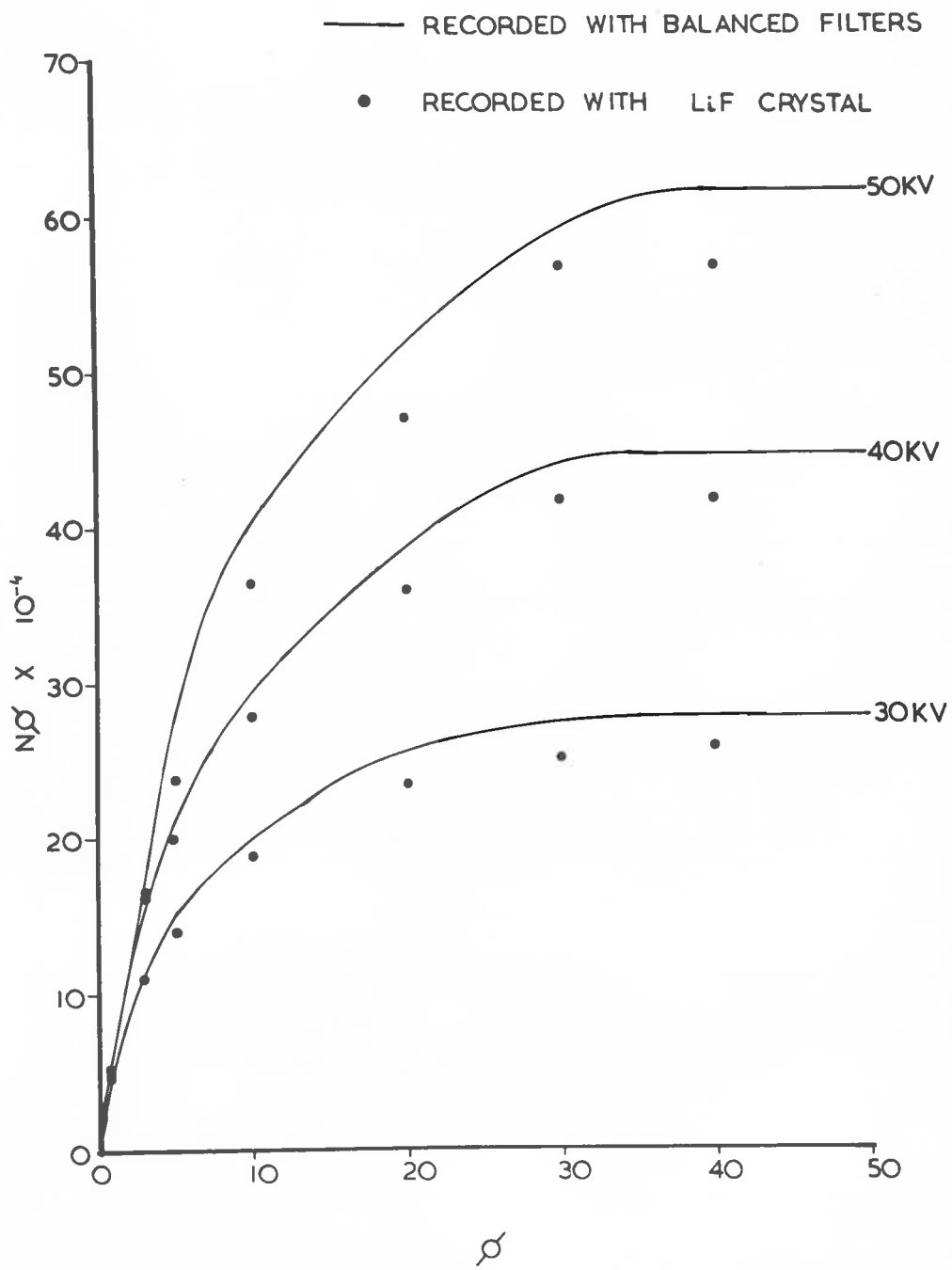

6•2

Copper Kα Emission for Oblique Incidence.

The results of Copper Kα emission plotted as a function of accelerating voltage when the normal to the target is inclined at an angle θ to the incident electron beam is shown in Figs. 71 - 74 for an arbitrary chosen angle θ = 30°. For comparison there is plotted the theoretical results of Copper Kα emission for an equal value of δ calculated from the formula derived in Section 1•43 i.e.

$$N_{\phi} = k\int_{0}^{x_{m}}\int_{-\infty}^{\infty} \exp(-\delta^{2}/2\Delta^{2})\exp\Big(-\mu\rho x \operatorname{Cosec}\phi \operatorname{Cos}(\theta+\alpha)\Big)\frac{\partial n}{\partial x}\,dx\,d\theta$$

The corrections for electron rediffusion for varying angle of incidence which are embodied in the factor k were the values obtained experimentally by the Author. For an angle of emission $\phi = 1^{\circ}$, the experimental values for emission are seen to fall off more rapidly than theory suggests especially as the accelerating voltage is increased above 30 kilovolts.

For larger angles of emission, i.e. for $\phi = 3^{\circ}$, 5° and 10° the experimental curves for emission show good agreement with the theoretical results for accelerating voltages up to

$C_u K_\perp$ EMISSION

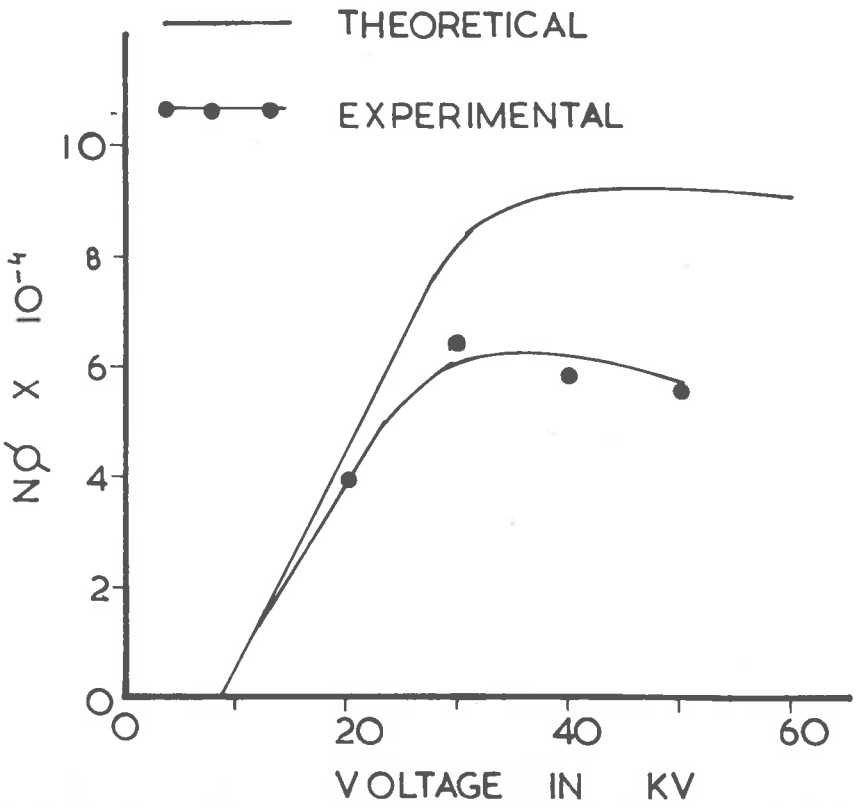

$\phi = 1°$

$\perp = 30°$

FIG 72

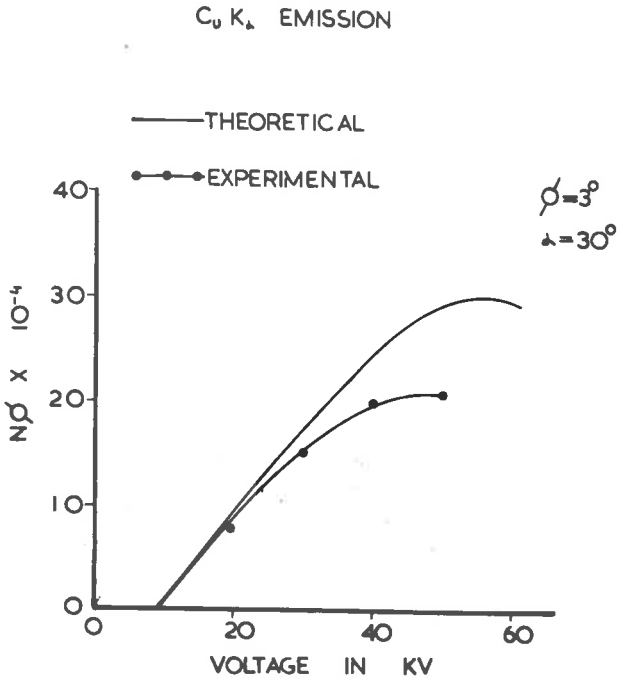
Cu Kλ EMISSION
THEORETICAL
EXPERIMENTAL
ϕ=3°
λ=30°
Nϕ x 10⁻⁴
40
30
20
10
0
0
20
40
60
VOLTAGE IN KV

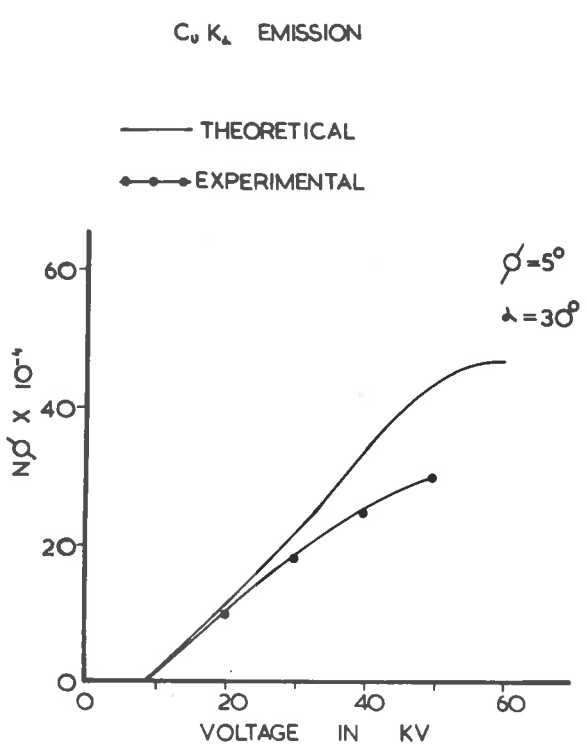
Cu Kλ EMISSION
THEORETICAL
EXPERIMENTAL
ϕ=5°
λ=30°
Nϕ x 10⁻⁴
60
40
20
0
0
20
40
60
VOLTAGE IN KV

FIG 13

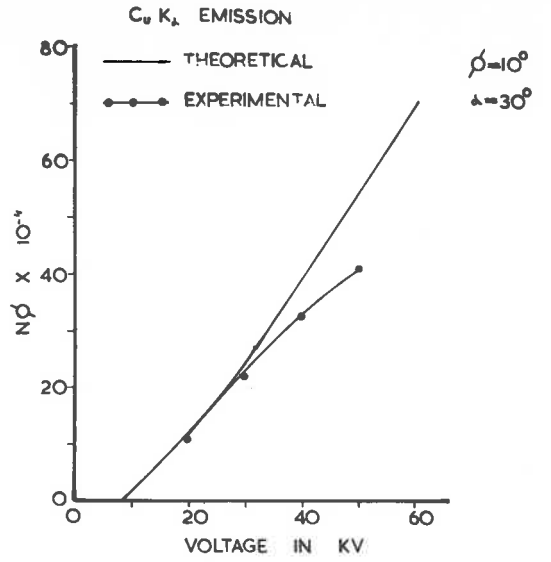
Cu Kα EMISSION
THEORETICAL
EXPERIMENTAL
ρ=10°
ϕ=30°
Nρ x 10⁻⁴
0
20
40
60
80
0
20
40
60
VOLTAGE IN KV

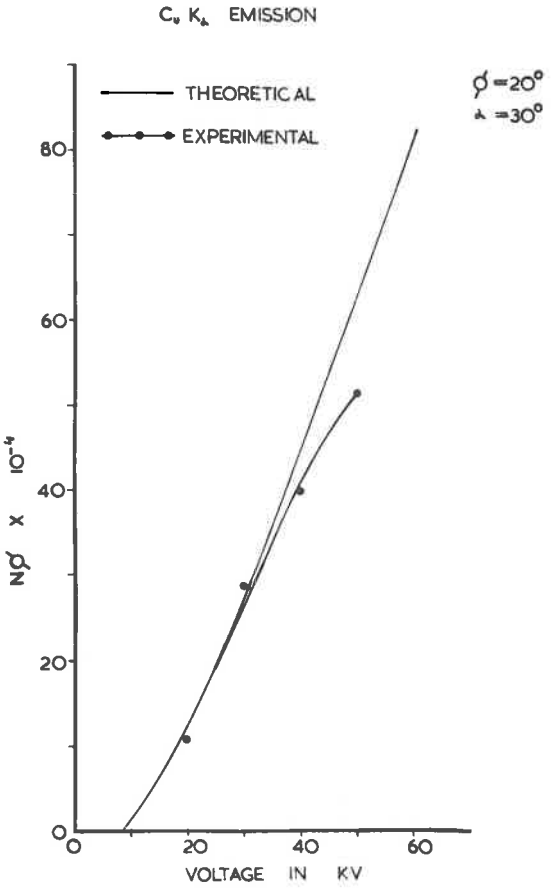
Cu Kα EMISSION
THEORETICAL
EXPERIMENTAL
ρ=20°
ϕ=30°
Nρ x 10⁻⁴
0
20
40
60
80
0
20
40
60
VOLTAGE IN KV

FIG 74

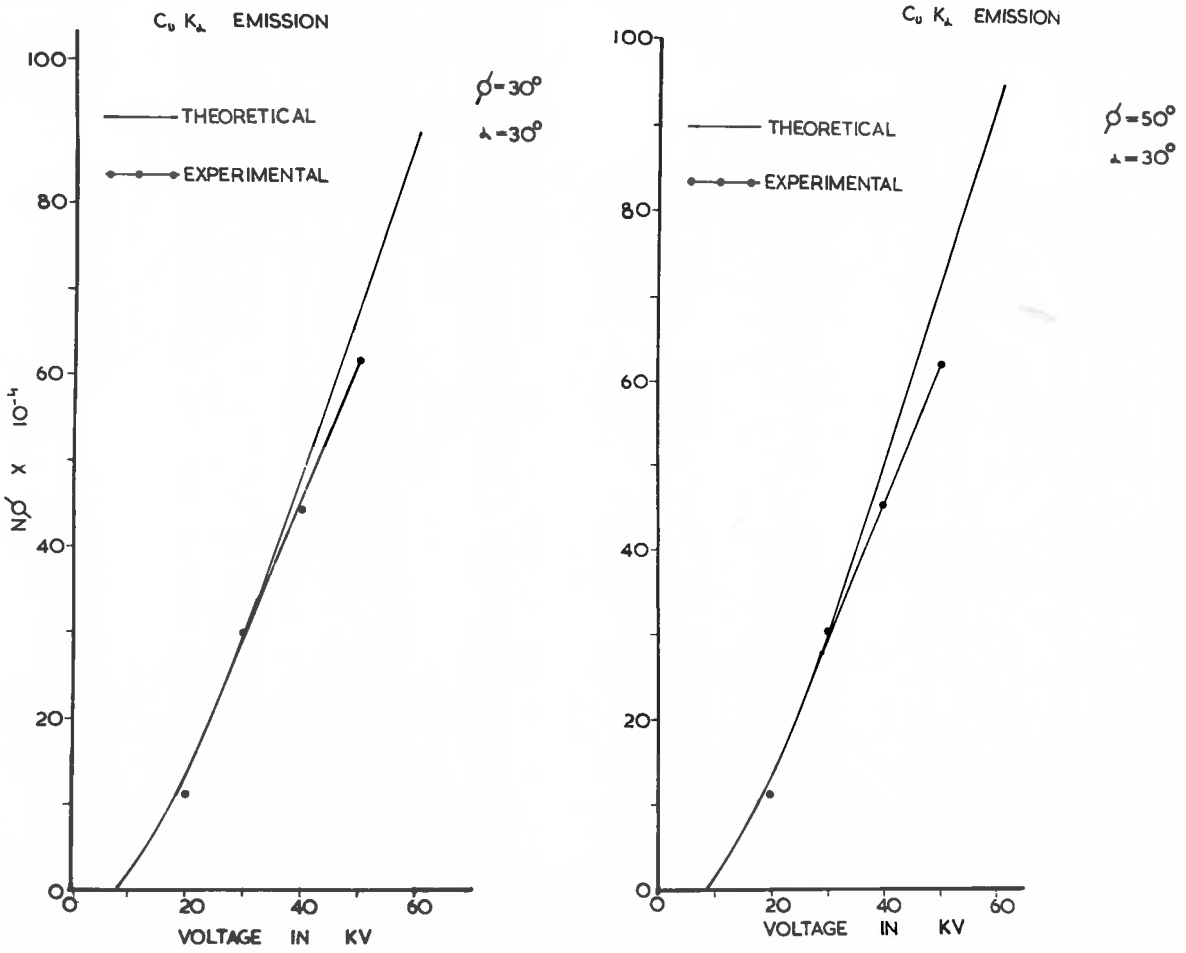
C_u K_α EMISSION
THEORETICAL
EXPERIMENTAL
ϕ=30°
ψ=30°
$N\phi \times 10^{-4}$
VOLTAGE IN KV
C_u K_α EMISSION
THEORETICAL
EXPERIMENTAL
ϕ=50°
ψ=30°
VOLTAGE IN KV

35 kilovolts, beyond which the decrease in slope of the experimental curves is faster than that of the theoretical curves. For values of $\phi \geq 20^{\circ}$ there is very good agreement between the experimental and theoretical results for the voltage range used in these experiments.

AG Kα EMISSION.

7·1
Theoretical.

For Ag Kα radiation the emission N_ϕ for normal incidence of the electron beam was calculated from the equation

$$N_\phi = k\int_0^{x_k} \exp(-\mu\rho x \operatorname{Cosec}\phi)\ \frac{\partial n}{\partial x}\,dx \qquad \ldots(1)$$

i.e. when diffusion in the target of the incident electron beam is neglected. These results are shown in Fig. 75 where the emission N_ϕ is plotted against accelerating voltage.

Calculations were also carried out to determine the emission of Ag Kα radiation for the case when the normal to the target was inclined at an angle θ to the incident electron beam using the expression for N_ϕ derived in Sec. 1·4, i.e.

$$N_\phi = k\int_0^{x_k} \exp(-\mu\rho x \operatorname{Cosec}\phi \operatorname{Cos}\theta)\ \frac{\partial n}{\partial x}\,dx \qquad \ldots(2)$$

FIG 15

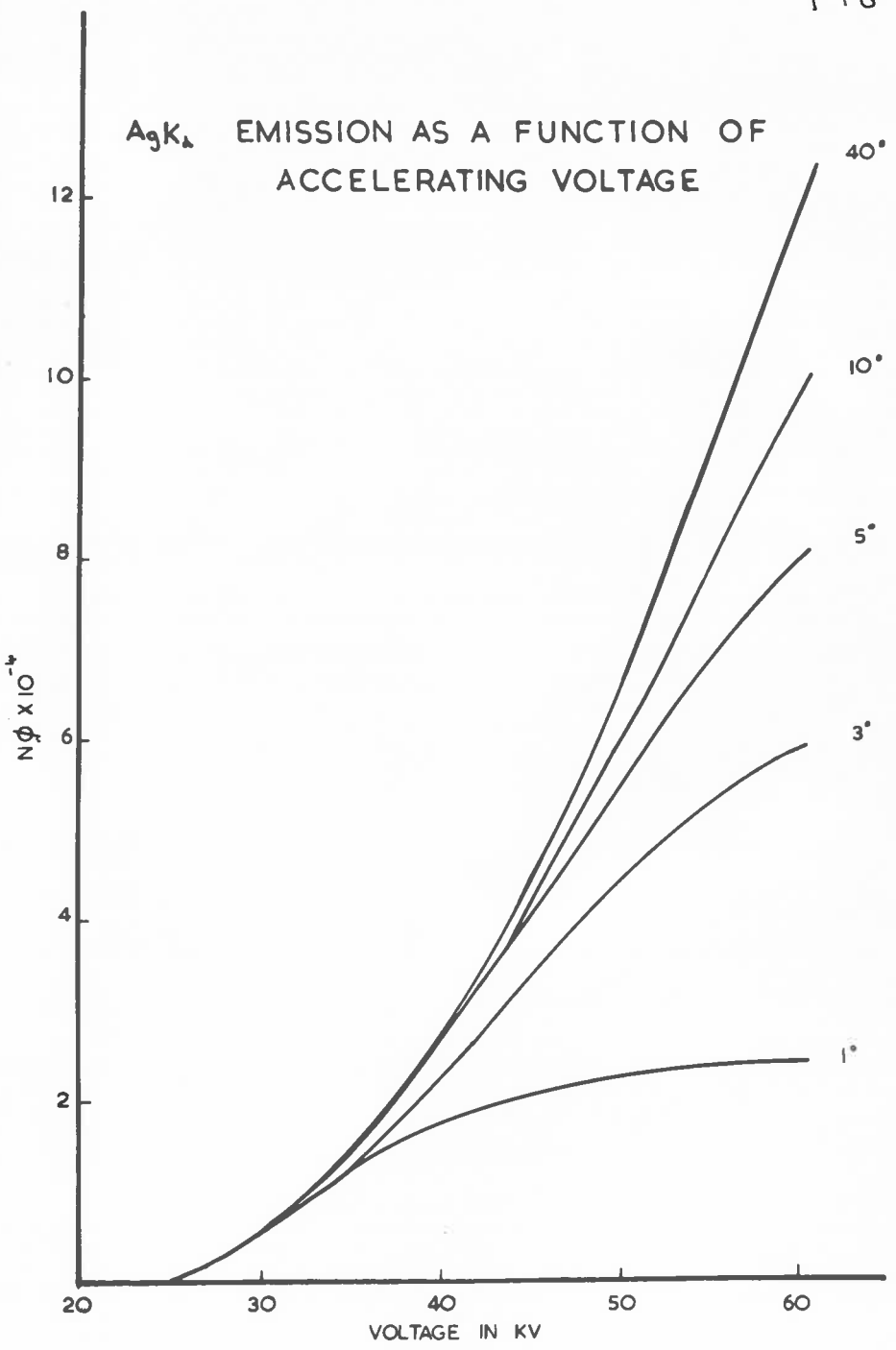
$Ag K_\alpha$ EMISSION AS A FUNCTION OF ACCELERATING VOLTAGE
40°
10°
5°
3°
1°
12
10
8
6
4
2
$N\phi \times 10^{-4}$
20
30
40
50
60
VOLTAGE IN KV

The above integral was evaluated for values of $\phi = 1^\circ$, 3°, 5°, 10°, 20°, 30°, 40° and 50°, and for correaponding values of $\theta = 20^\circ$, 30°, 40° and 50°. The range of accelerating voltages being from 25·5 - 60 kilovolts. Graphs of these calculations are shown in Figs. 76 - 81 where the emission N_ϕ is plotted as a function of the accelerating voltage for$\theta = 30^\circ$ and 50°, and compared with the values of N_ϕ for $\theta = 0^\circ$, i.e. when the normal to the target is parallel to the incident electron beam.

These curves show that for an angle of emission $\phi \leq 10^\circ$ the increase in N_ϕ becomes appreciable for accelerating voltages above 40 kilovolts. For $\phi > 10^\circ$ there is very little increase in emission at 60 kilovolts even when $\theta = 50^\circ$. This is to be expected since the absorption of the Ag Kα radiation in the target far outweighs the shorter path length when the target is inclined to the incident electron beam.

Figs. 82 - 84 show the theoretical results of Ag Kα emission plotted as a function of accelerating voltage for normal incidence of the electron beam when diffusion in the target is allowed for, i.e. when

$$N_\phi = k\int_0^{x_k}\int_{-\pi}^{\pi} \exp(-\theta^2/2\Delta^2)\exp(-\mu\rho x \operatorname{Cosec}\phi \cos\theta)\frac{\partial n}{\partial x}\,dx\,d\theta \qquad \ldots(3)$$

FIG 76

$Ag K_\alpha$ EMISSION AS A FUNCTION OF VOLTAGE

WITH TARGET INCLINED TO INCIDENT ELECTRON BEAM

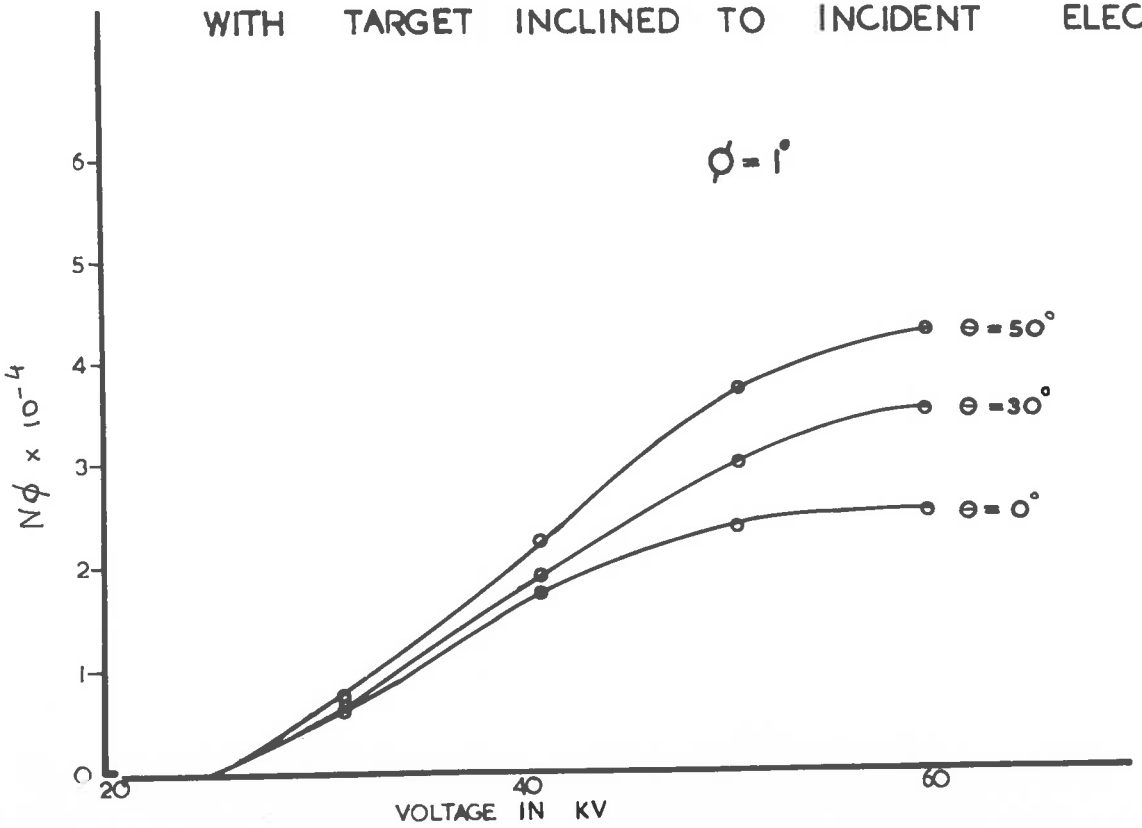

FIG 77

$Ag K_{\alpha}$ EMISSION AS A FUNCTION OF VOLTAGE

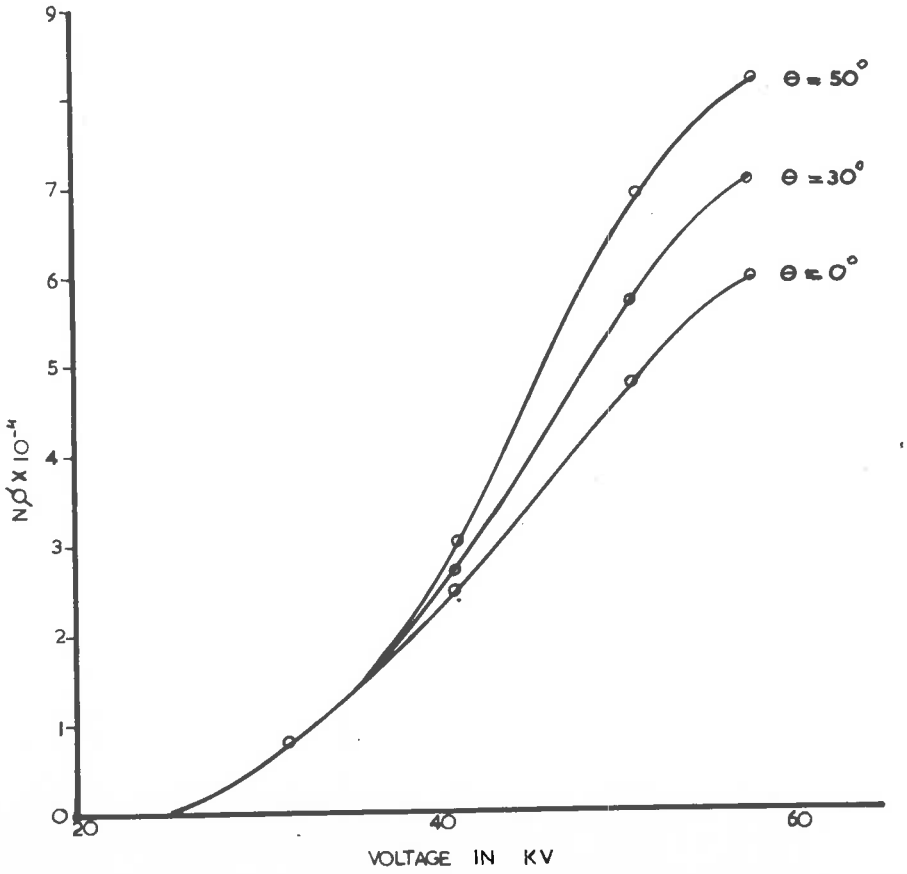

$\phi = 3°$

FIG 18

$Ag K$ EMISSION AS A FUNCTION OF VOLTAGE

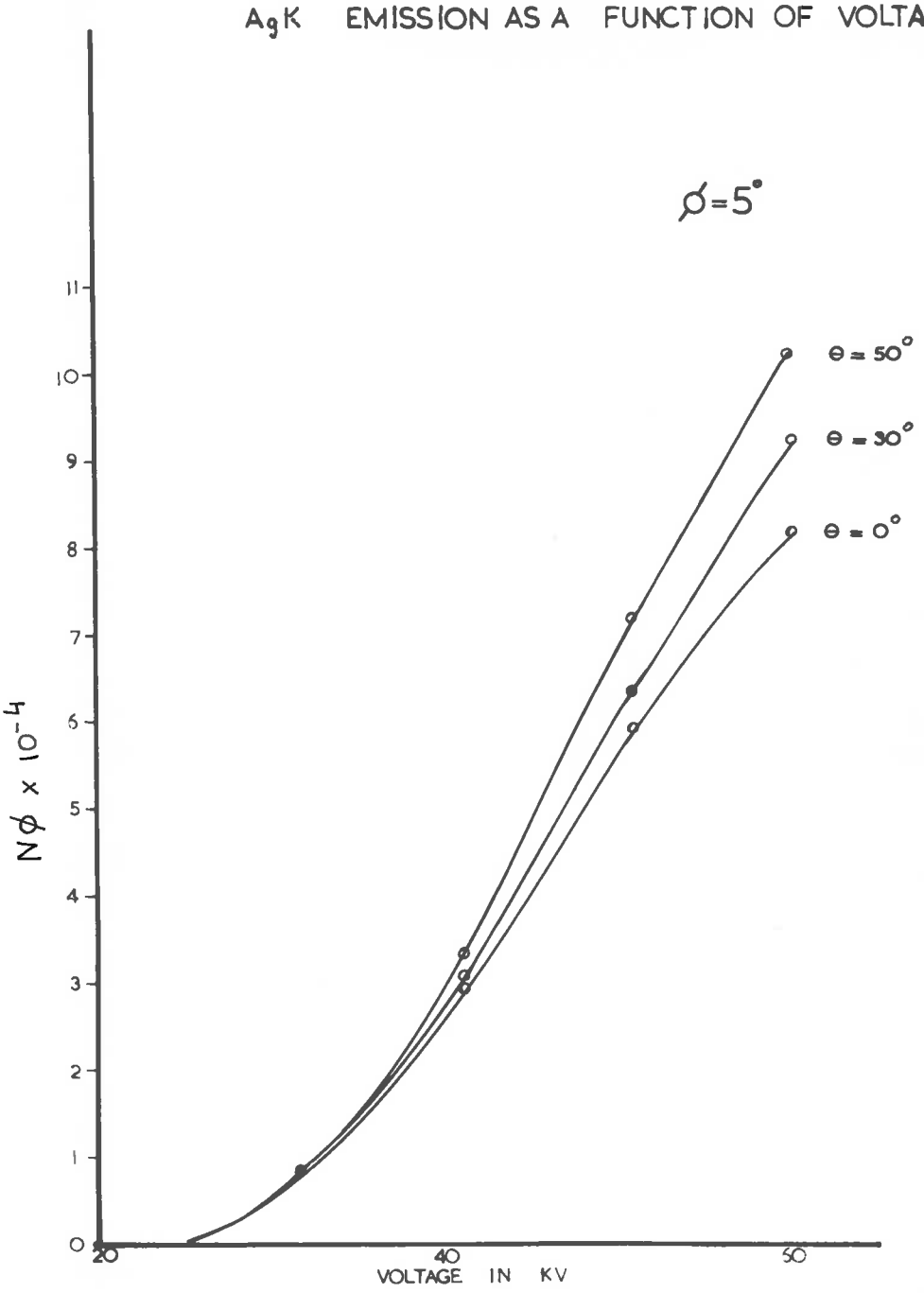

Fig 79

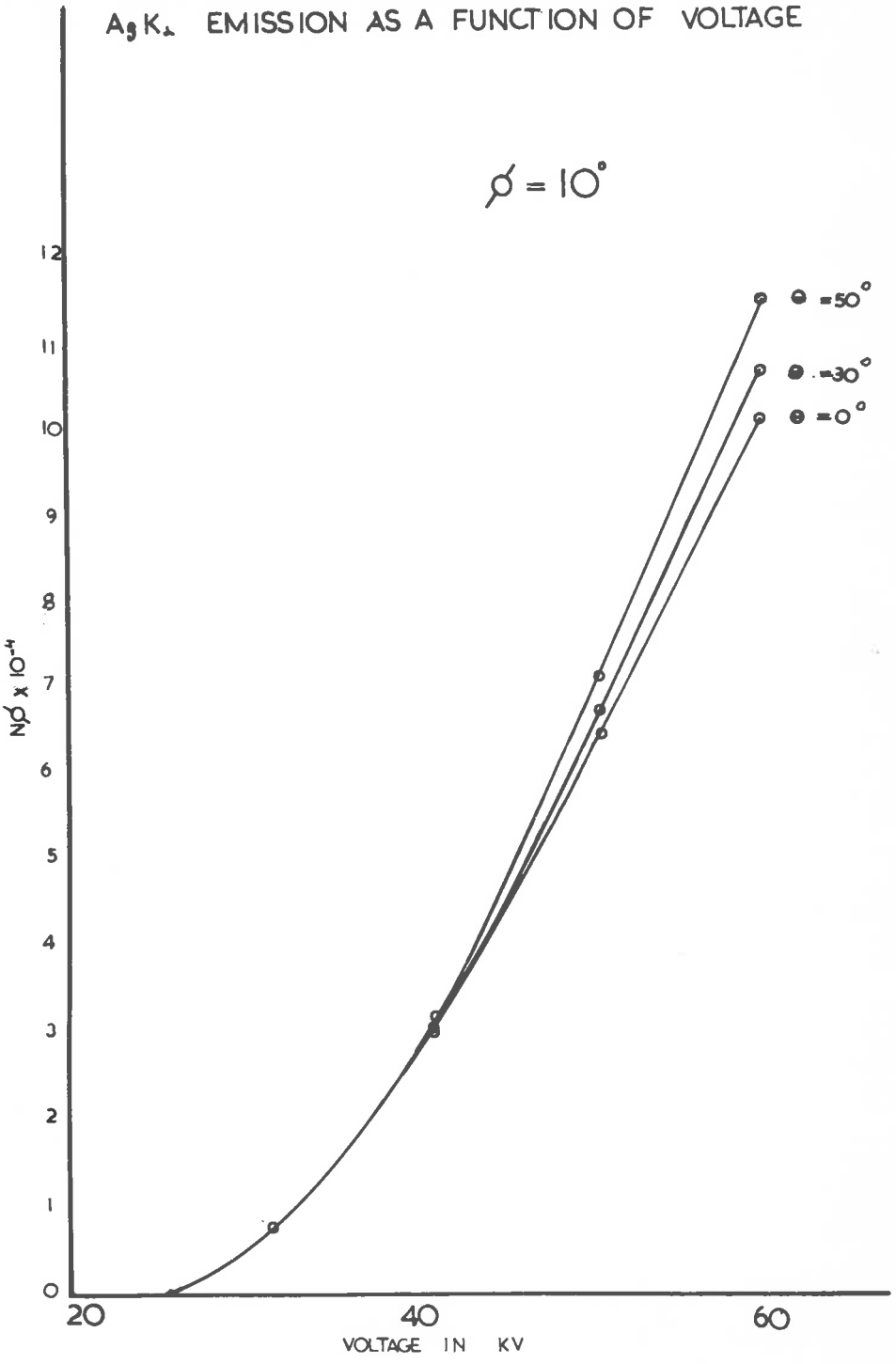
Ag Kα EMISSION AS A FUNCTION OF VOLTAGE
φ = 10°
θ =50°
θ =30°
θ =0°
Nφ x 10⁻⁴
0
1
2
3
4
5
6
7
8
9
10
11
12
20
40
60
VOLTAGE IN KV

FIG 80

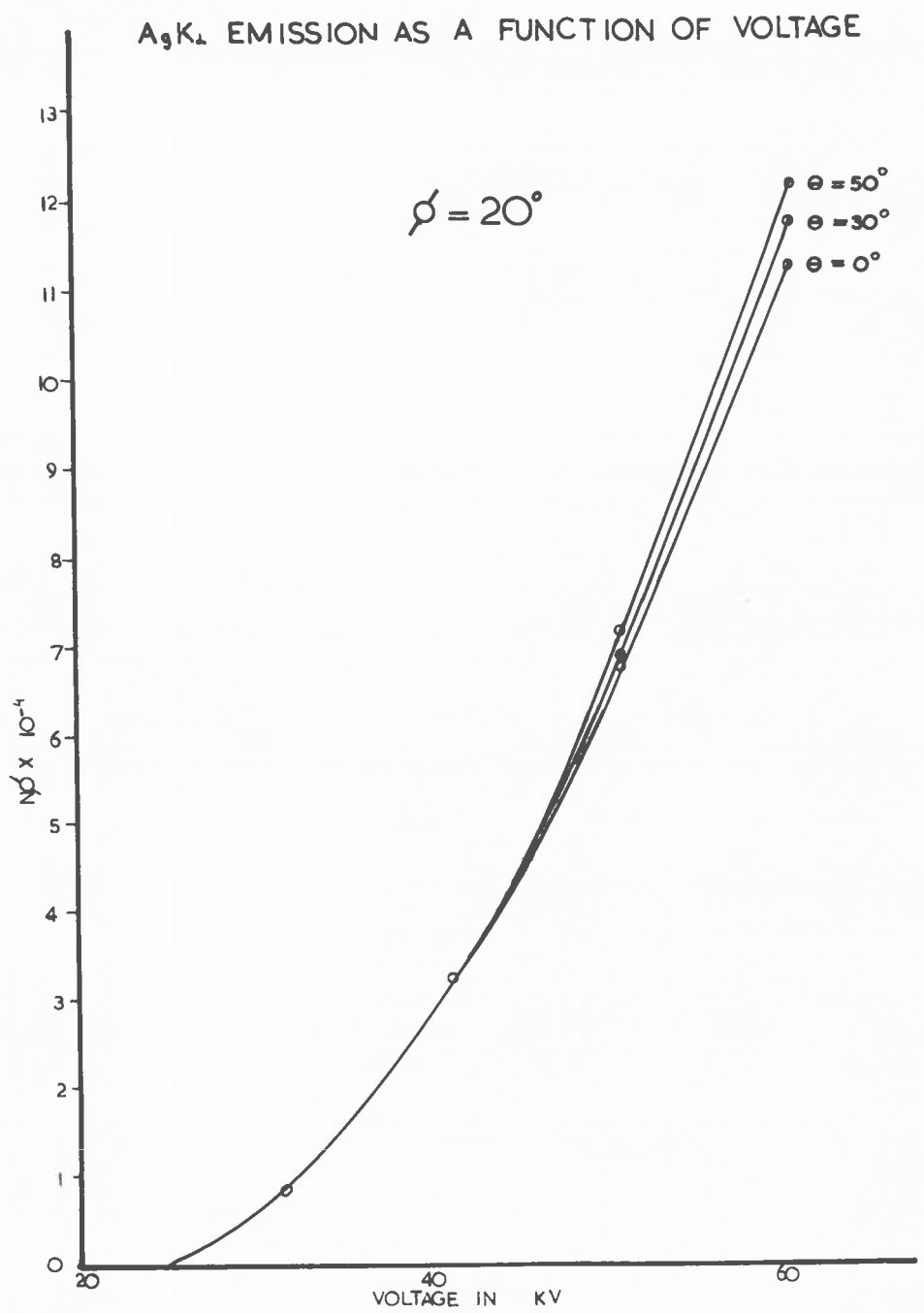
$A_g K_\alpha$ EMISSION AS A FUNCTION OF VOLTAGE
$\phi = 20°$
$\theta = 50°$
$\theta = 30°$
$\theta = 0°$
$N_\phi \times 10^{-4}$
0
1
2
3
4
5
6
7
8
9
10
11
12
13
20
40
60
VOLTAGE IN KV

FIG 81

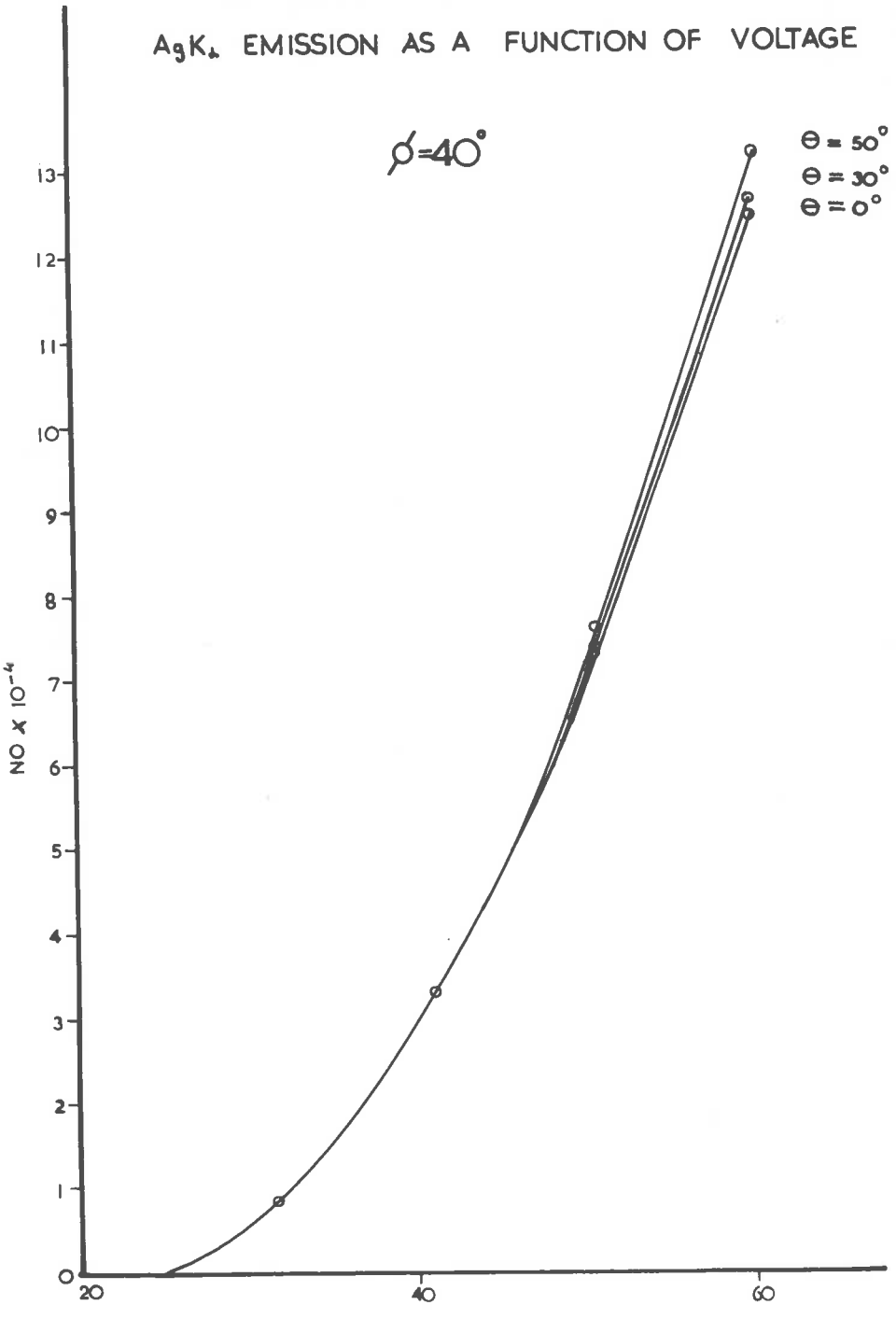
$Ag K_\alpha$ EMISSION AS A FUNCTION OF VOLTAGE
ϕ=40°
Θ = 50°
Θ = 30°
Θ = 0°
NO X 10^{-4}
0
1
2
3
4
5
6
7
8
9
10
11
12
13
20
40
60

FIG 82

$A_g K_\perp$ EMISSION AS A FUNCTION OF VOLTAGE

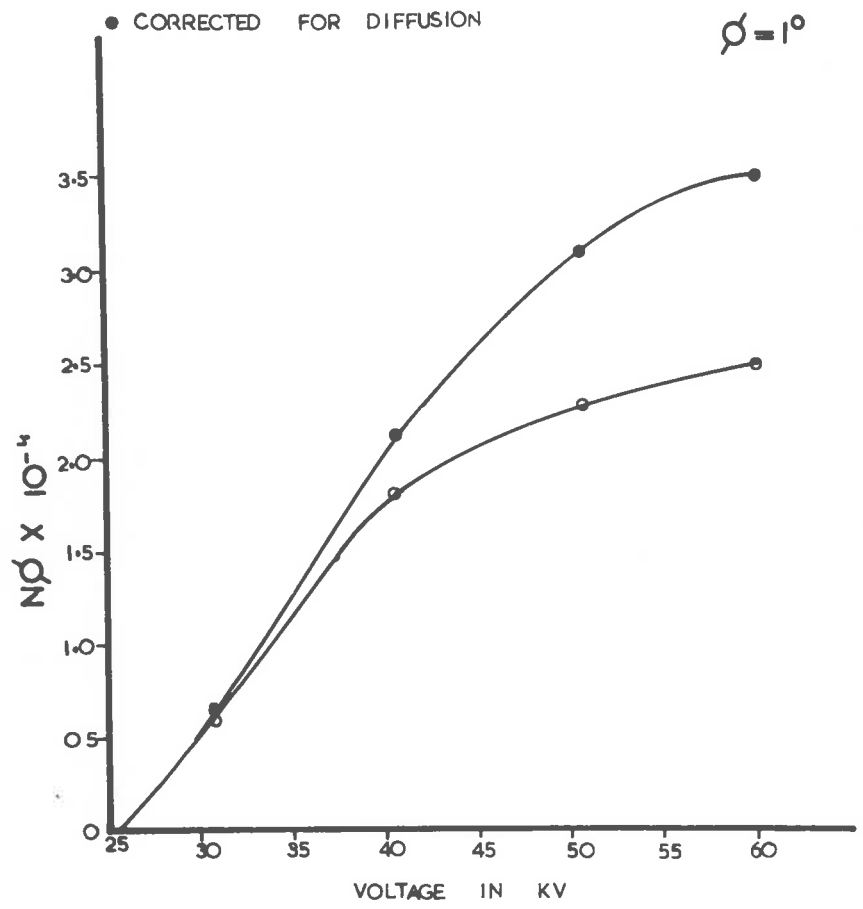

FIG 83

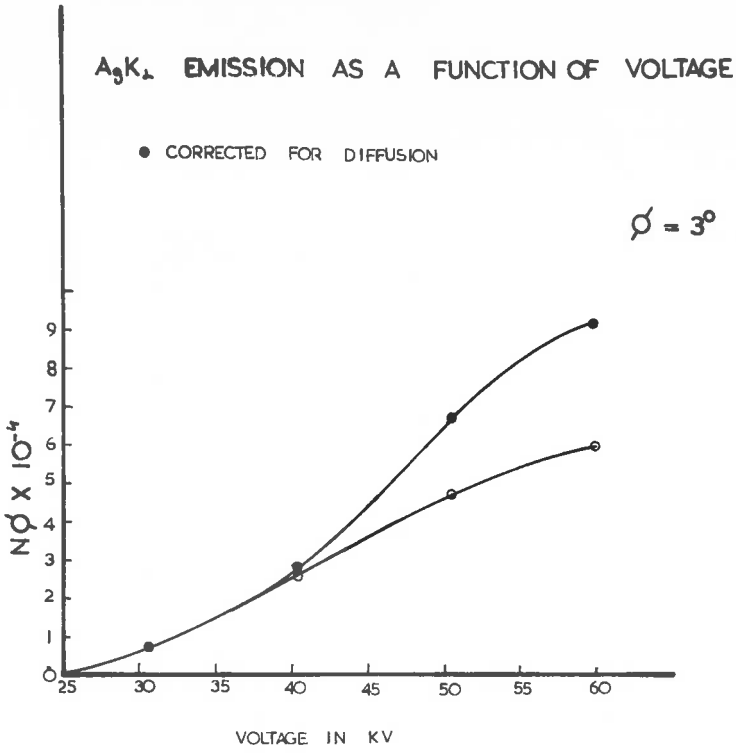
$A_g K_\perp$ EMISSION AS A FUNCTION OF VOLTAGE
● CORRECTED FOR DIFFUSION
$\phi = 3°$
$N\phi \times 10^{-4}$
0
1
2
3
4
5
6
7
8
9
25
30
35
40
45
50
55
60
VOLTAGE IN KV

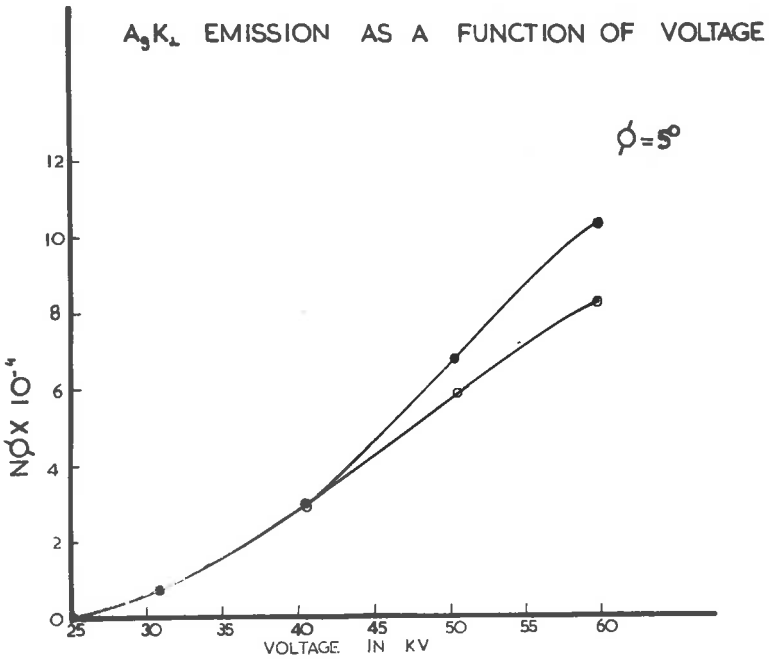
$A_g K_\perp$ EMISSION AS A FUNCTION OF VOLTAGE
$\phi = 5°$
$N\phi \times 10^{-4}$
0
2
4
6
8
10
12
25
30
35
40
45
50
55
60
VOLTAGE IN KV

Fig 84

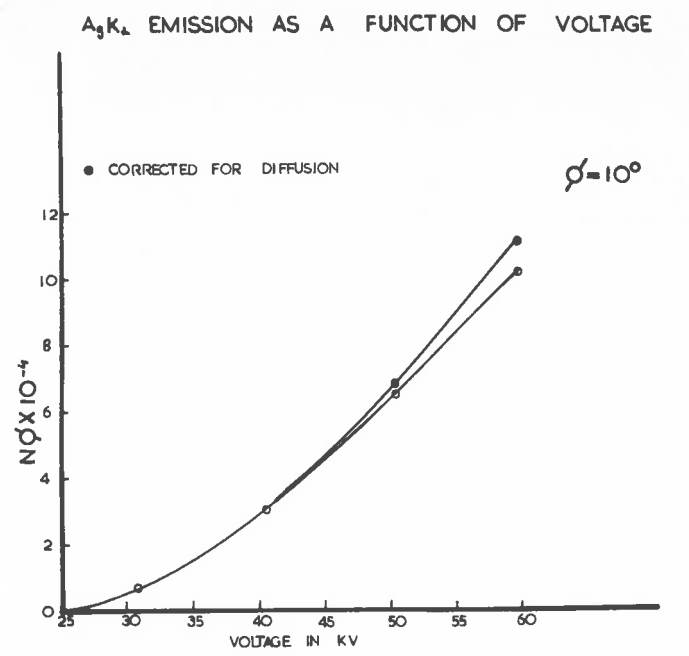
$A_g K_\perp$ EMISSION AS A FUNCTION OF VOLTAGE
● CORRECTED FOR DIFFUSION
$\phi = 10°$
$N\phi \times 10^{-4}$
0
2
4
6
8
10
12
25
30
35
40
45
50
55
60
VOLTAGE IN KV

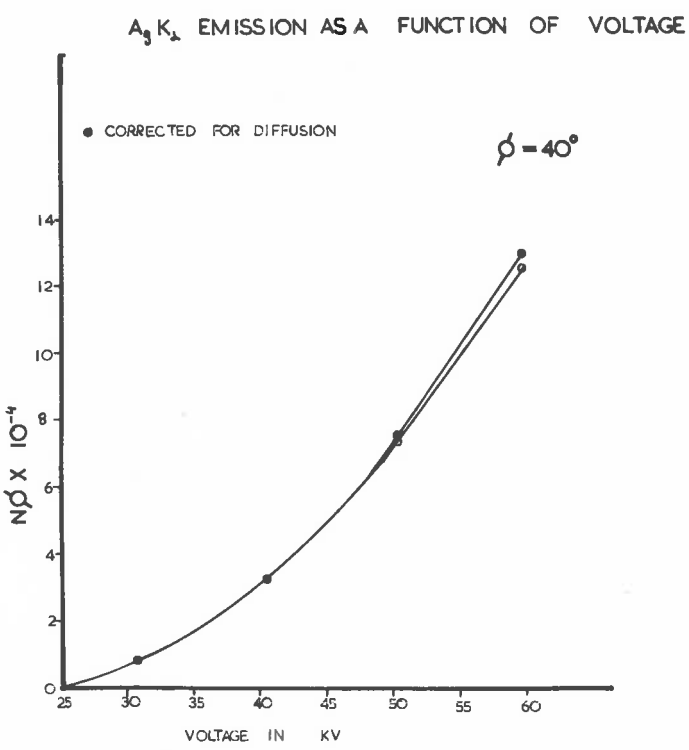
$A_g K_\perp$ EMISSION AS A FUNCTION OF VOLTAGE
● CORRECTED FOR DIFFUSION
$\phi = 40°$
$N\phi \times 10^{-4}$
0
2
4
6
8
10
12
14
25
30
35
40
45
50
55
60
VOLTAGE IN KV

For comparison there is plotted for each angle of emission ϕ the corresponding values of emission N_ϕ neglecting diffusion in the target. It can immediately be seen that for all angles of emission and for an accelerating voltage equal to 60 kilovolts the values of N_ϕ have not reached a maximum. Furthermore for any given accelerating voltage $N_\phi\ (1^\circ) < N_\phi\ (3^\circ) < N_\phi\ (5^\circ) < \ldots\ldots < N_\phi\ (40^\circ)$.

For values of $\phi > 10^\circ$ the values of the emission N_ϕ calculated from (3) show a small increase with respect to those calculated using (1), the increase becoming apparent for accelerating voltages greater than 50 kilovolts. For values of $\phi < 10^\circ$ the increase in emission is much more apparent starting from accelerating voltages of about 35 kilovolts. That this is to be expected can be seen from the fact that the smaller the angle of emission ϕ the longer is the path length in the target that the X radiation must travel before reaching the target surface and hence the larger the absorption. The effect of diffusion of the incident electron beam in the target is to shorten the path length and hence decrease the absorption of the X radiation.

7·2

Experimental Determination of Ag Kα Emission.

To determine the absolute intensity of emission of the characteristic Kα radiation from a Silver target, a pair of balanced filters Mo and Pd are needed. These however were not available to the Author and it was therefore decided to use a crystal monochromator (Li F) to separate the Ag Kα radiation from the rest of the heterogenous radiation emitted from the Silver target of the X ray tube.

Since it is necessary that the integrated reflection coefficient for Ag Kα radiation be determined, use was made of the double crystal monochromator described in Sec. 4·5 in conjunction with the Hilger Micro Focus Tube. The following results were obtained.

Number of Ag Kα quanta recorded by the scaler after diffraction from the first Li F crystal in 100 secs. = 160×10^3

Number of Ag Kα recorded by the scaler from the second Li F crystal when the latter was rotated about the position of maximum reflection. = 2100

Angular velocity of the second

Li F crystal ω = $2{\cdot}9 \times 10^{-4}$ radians per sec.

$\therefore$ the integrated reflection coefficient for

Ag Kα radiation ρ Ag = $3{\cdot}8 \times 10^{-4}$

From the literature the mass absorption coefficient of Aluminium for Ag Kα radiation was found to be 2·74.

For Ag Kα radiation,

Diameter of pin hole	= 0·70 cm.
Distance of X ray window to pin hole	= 6·30 cm.
Distance of target to X ray window	= 10·16 cm.
Transmission of Aluminium window of X ray tube	= 98 per cent
Transmission of Aluminium holder of Na I Tℓ crystal	= 98·2 per cent
Path length from X ray window to detector	= 7·80 cm.
Solid angle subtended by pin hole at target	= $0{\cdot}142 \times 10^{-4}$ steradians

From the above data the absolute intensity for Ag Kα radiation per unit solid angle per electron was determined experimentally for angles of emission ϕ = 1°, 3°, 5°, 10°, 20°, 30° and 40°, and for accelerating voltages equal to 36, 40, 46, 50, 56 and 60 kilovolts when the normal to the target was parallel to the incident electron beam. Emission for an accelerating voltage of 30 kilovolts could not be obtained satisfactorily owing to the fact that the number of Ag Kα recorded with the Scintillation Counter as detector was very low even with the maximum beam current available at that voltage.

7·21

Electron Rediffusion.

Measurements were carried out to determine the fraction of the secondary electrons leaving the target with an energy greater than $V = V_k$, where V is the accelerating voltage of the primary electron beam and V_k = 25·5 kilovolts is the K shell ionization potential for Silver. These measurements were carried out for values of V = 28, 34 and 40 kilovolts. It was found that this fraction was constant and equal to 0·33.

7.3

Results.

The results of the measurements of the absolute intensity of emission of Ag Kα radiation are shown plotted in Figs. 85 - 90 where the emission N_ϕ is plotted as a function of the accelerating voltage. The results of the measurements of the absolute intensity of emission of Ag Kα radiation are shown plotted in Figs. 85 - 90 where the emission N_ϕ is plotted as a function of the accelerating voltage. In Figs. 85 - 90 these experimental results are compared with the theoretical values of emission N_ϕ calculated from the formula

$$N_\phi = k\int_0^{\pi_k}\int_{-\theta}^{\theta} \exp(-\theta^2/2\Delta^2)\exp(-\mu\rho x \operatorname{Cosec}\phi \operatorname{Cos}\theta)\frac{\partial n}{\partial x}\,dx\,d\theta$$

The correction for electron rediffusion embodied in the factor k was the value obtained experimentally by the Author. It is readily seen that for all angles of emission ϕ the emission N_ϕ has not reached a maximum even for an accelerating voltage of 60 kilovolts.

The experimental curves for Ag Kα emission also show that even with accelerating voltages equal to 50 kilovolts the gain in emission at $\phi = 40^0$ is only 20 per cent above

FIG 85

EXPERIMENTAL RESULTS OF $Ag K_2$
EMISSION AS A FUNCTION OF VOLTAGE

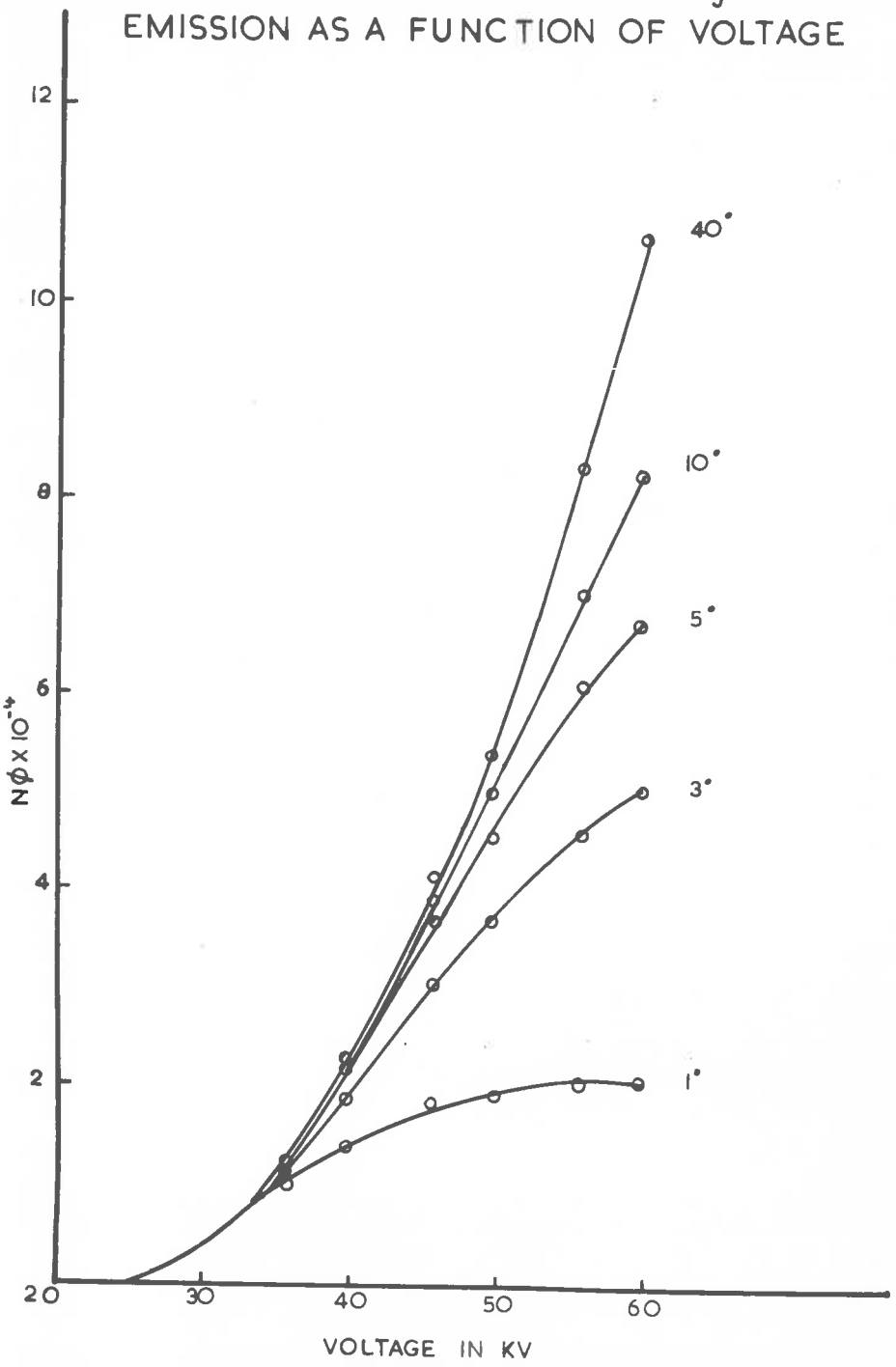

FIG 86

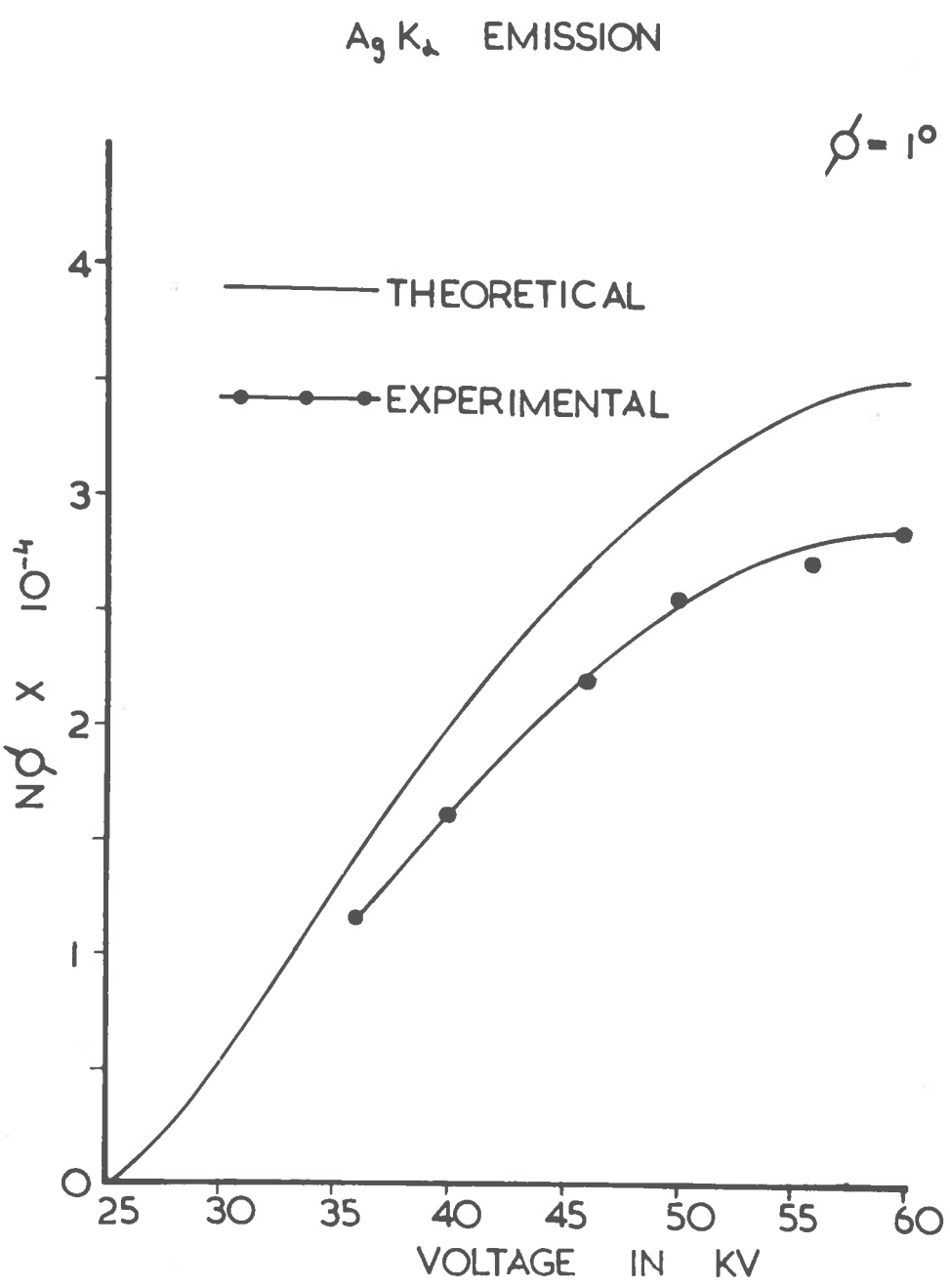
Ag Kα EMISSION
φ = 1°
THEORETICAL
EXPERIMENTAL
Nφ X 10⁻⁴
0
1
2
3
4
25
30
35
40
45
50
55
60
VOLTAGE IN KV

Fig 87

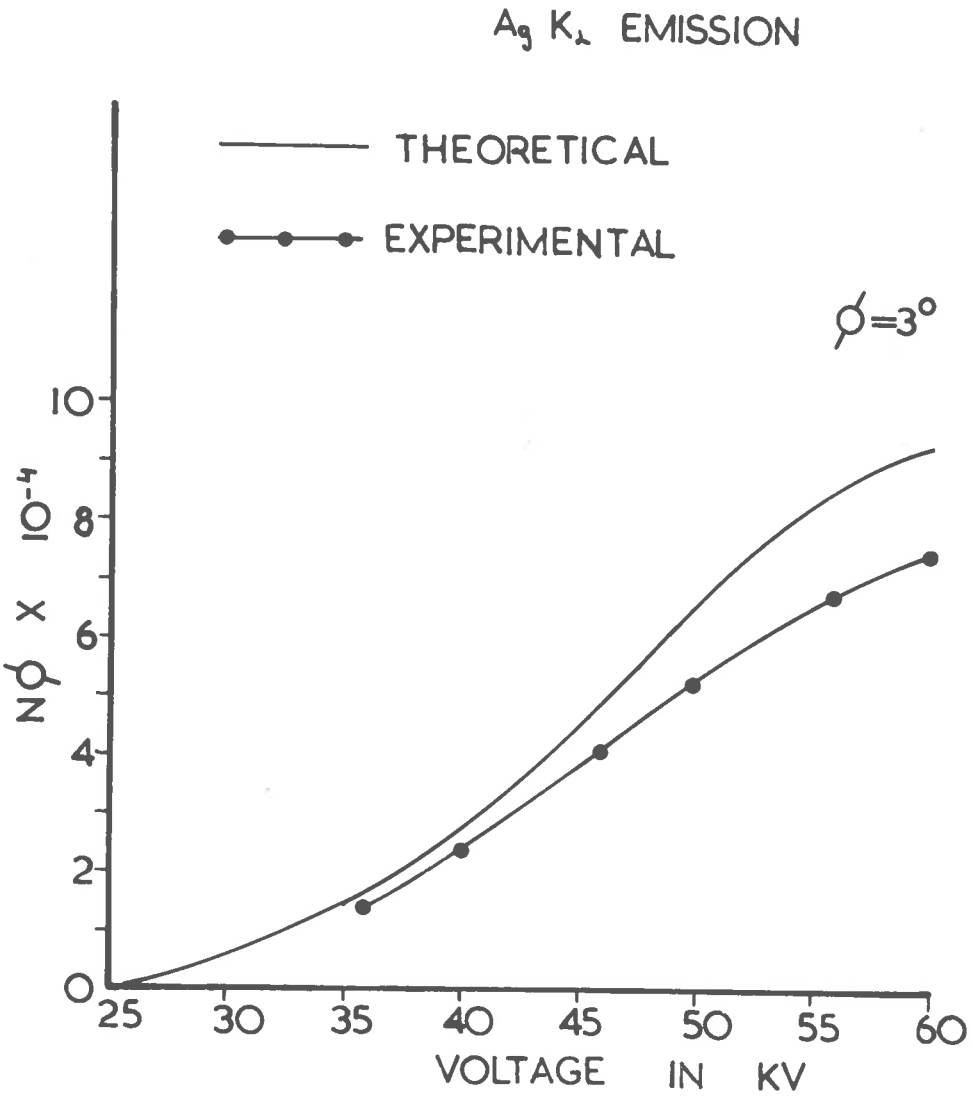
Ag Kα EMISSION
THEORETICAL
EXPERIMENTAL
φ=3°
Nφ X 10⁻⁴
0
2
4
6
8
10
25
30
35
40
45
50
55
60
VOLTAGE IN KV

FIG 88

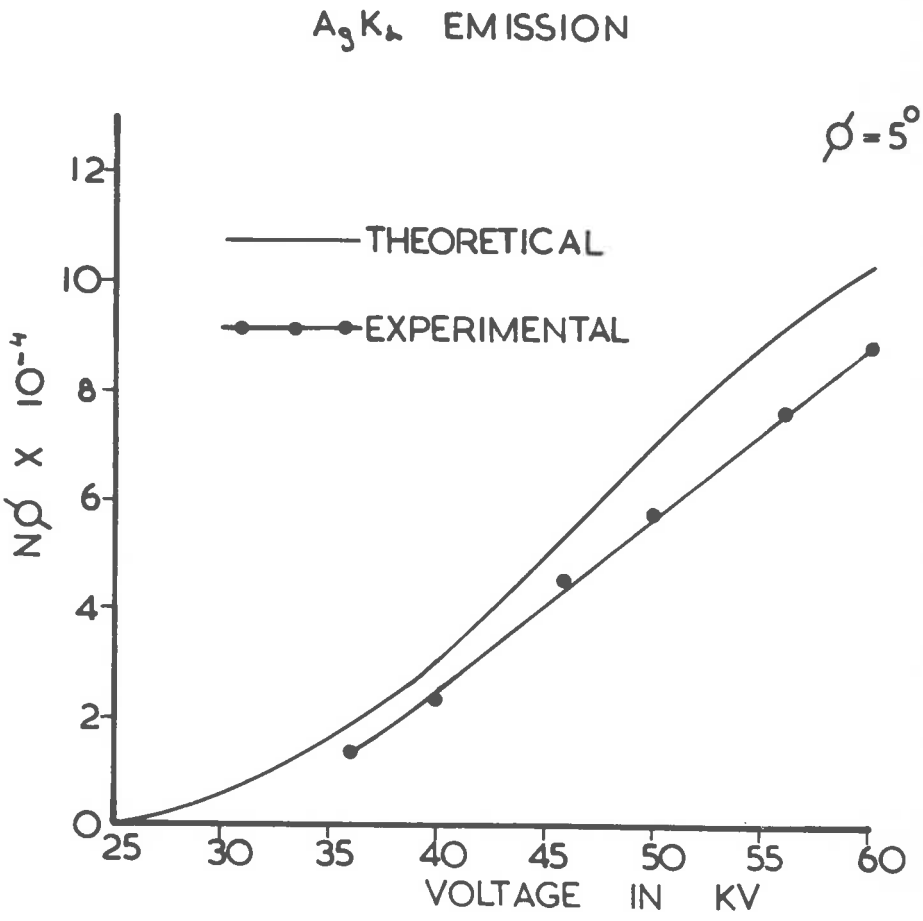
$A_g K_\alpha$ EMISSION
$\phi = 5°$
THEORETICAL
EXPERIMENTAL
$N\phi \times 10^{-4}$
0
2
4
6
8
10
12
25
30
35
40
45
50
55
60
VOLTAGE IN KV

FIG 89

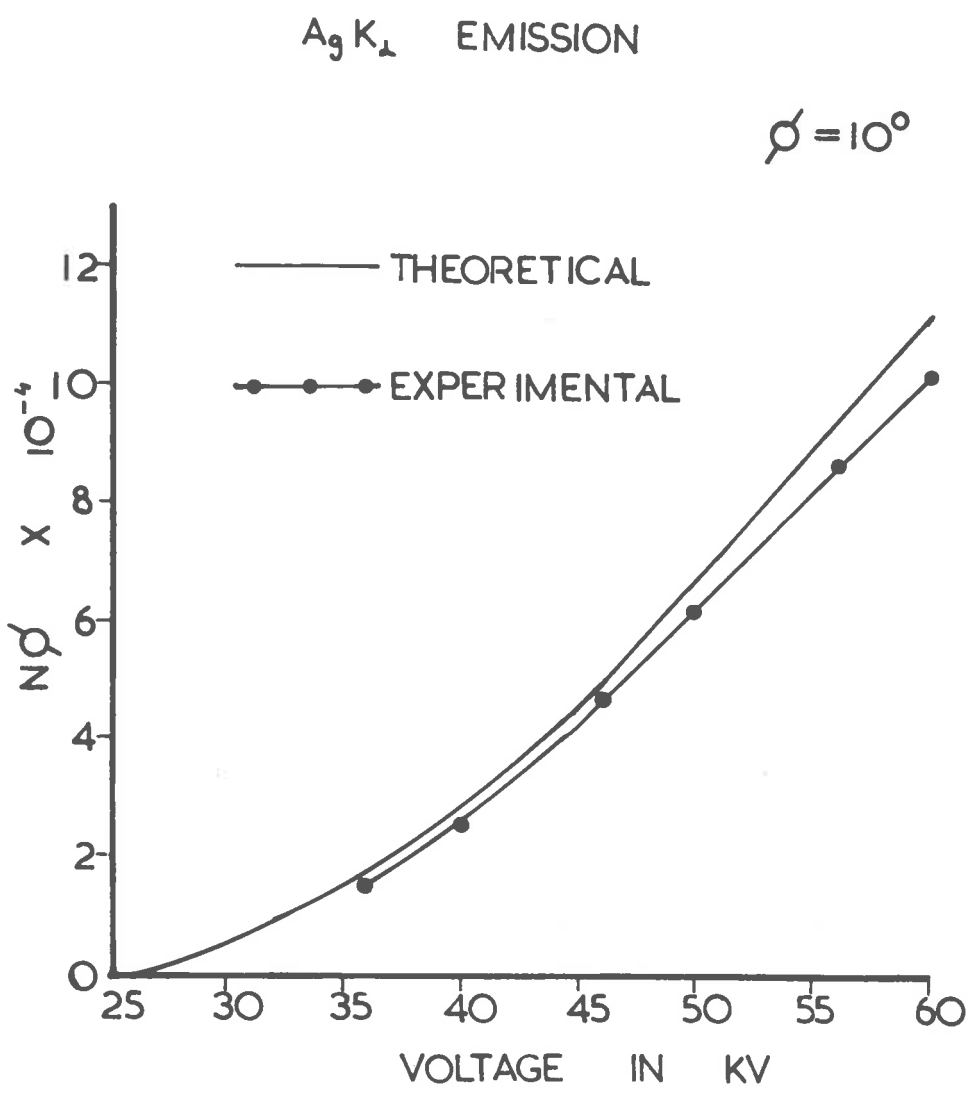
$A_g K_\perp$ EMISSION
$\phi = 10°$
THEORETICAL
EXPERIMENTAL
$N\phi \times 10^{-4}$
0
2
4
6
8
10
12
25
30
35
40
45
50
55
60
VOLTAGE IN KV

FIG 90

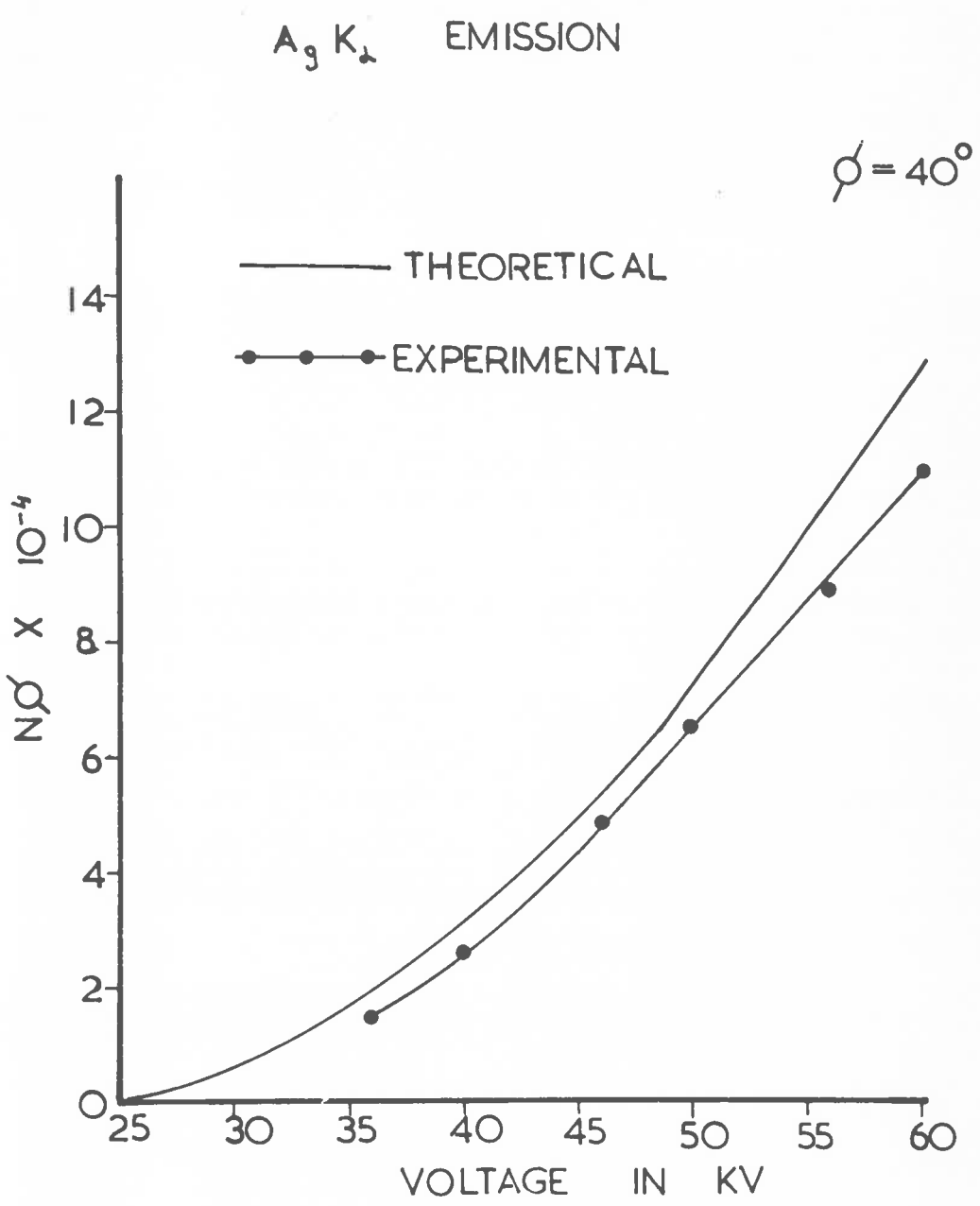
Ag Kα EMISSION
φ = 40°
THEORETICAL
EXPERIMENTAL
Nφ X 10⁻⁴
0
2
4
6
8
10
12
14
25
30
35
40
45
50
55
60
VOLTAGE IN KV

that for $\phi = 3^{\circ}$. For all angles of emission ϕ and for all values of the accelerating voltages used in these experiments, the experimental results for Ag Kα emission are lower by 15 per cent then the theoretical results.

8. RATIO OF CHARACTERISTIC TO WHITE RADIATION FROM A COPPER TARGET.

It might at first appear that the ratio of characteristic to white radiation from the target of an X ray tube could be determined by automatic recording of the spectrum with a pen recorder, in conjunction with an appropriate detector and crystal monochromator. By integration of the area under the curve the desired ratio can be obtained. It must be realized however that the original X radiation leaving the target is modified by the following factors:

1. Absorption in the window of the X ray tube,
2. Absorption in the air between the X ray window and detector,
3. Quantum Counting Efficiency of the detector,
4. Reflectivity of the crystal analyser and higher order reflections.

A record of the continuous X ray spectrum would entail the use of a standard crystal and detector such that as the crystal rotated through an angle θ, the detector would have had to rotate through an angle 2θ to intercept the diffracted beam. This equipment was unfortunately not

available, and recourse was therefore made to the literature in the hope of finding a suitable spectrum.

Ulrey (1918) obtained a series of spectra from a Tungsten target with accelerating voltages varying from 20 - 50 kilovolts. However the range of wavelengths covered is only up to 1 Å and no corrections are applied. Beauvillier's curves (1920) were not corrected for crystal reflectivity and his upper wavelength limit is only 0·8 Å.

Kulenkampff (1922) corrected for all but the orders of reflection from the crystal analyser and limited his wavelength region to $\lambda_0 < \lambda < 2\lambda_0$. However his curves only cover the range of wavelengths from 1 - 3 Å, and his highest accelerating voltage is only 12 kilovolts.

Kulenkampff fitted his curves to the empirical equation

$$I_\lambda = \frac{CZ}{\lambda^2}\left(\frac{1}{\lambda_0} - \frac{1}{\lambda}\right) + \frac{bZ^2}{\lambda^3}$$

where

I_λ is the intensity of the radiation at wavelength λ,

λ_0 is the Duane-Hunt short wavelength limit,

Z is the atomic number of the target material,

C and b are constants.

Kirkpatrick (1923) who applied all the corrections used a voltage range of 51 - 70 kilovolts, the upper limit of the wavelengths being 1 Å.

More recently Arndt and Riley (1952) using a new Copper target X ray tube operated at 30 kilovolts d.c. obtained an intensity distribution (Fig. 91) using a Calcite crystal with both a Proportional and a Geiger Counter. They corrected for wavelength variation of absorption in air, absorption in the counter window and counter gas. They also corrected for variation of the reflection coefficient with wavelength for Calcite. Unfortunately these authors do not specify any angle of emission. They found that the integrated intensities of the $K\alpha$, $K\beta$ and white radiations outside the window of the X ray tube are in the ratio of 100:13·3:18·5 which gives a $K\alpha$ to white ratio of 5·4:1.

Parrish and Kohler (1956) operated their Copper target X ray tube at 40 kilovolts.p (full wave rectification) using a Silicon (III) crystal monochromator with a Scintillation Counter. These authors applied no correction and estimated that the continuous spectrum had an integrated intensity of more than an order of magnitude greater than that of the $K\alpha$ line.

Fig 91

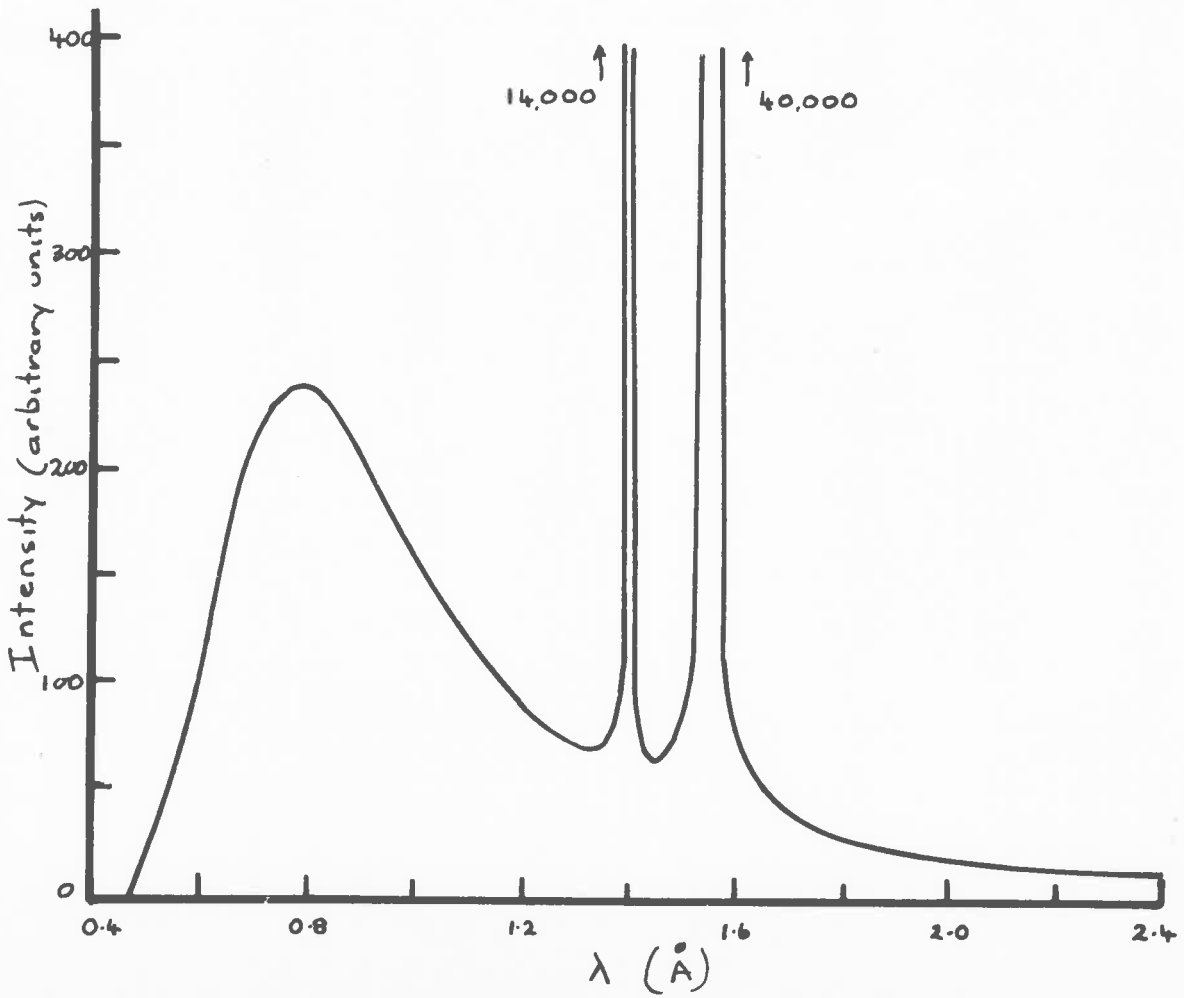
400
300
200
100
0
Intensity (arbitrary units)
14,000
40,000
0·4
0·8
1·2
1·6
2·0
2·4
λ (Å)

Bendit (1957) making use of Arndt and Riley's curve at 30 kilovolts d.c. and using Kulenkampff's curve as a general guide drew an assumed spectral curve for 35 kilovolts. Using a Geiger Counter, Bendit corrected for absorption in air with wavelength, and Geiger Counter Quantum Efficiency obtained from a report by Parrish and Taylor. His results for angles of emission of 1°, 3°, and 5°, show the ratio of Copper Kα to white radiation to equal 2·2 with a very small increase for increasing angle of emission.

Experimental.

The ratio of the characteristic Kα to white radiation from a Copper target was determined for angles of emission ϕ equal to 6°, 15° and 30° and for an accelerating voltage of 30 kilovolts with a beam current of $0{\cdot}56 \times 10^{-7}$ amperes. The total radiation leaving the window of the X ray tube was measured by means of a Scintillation Counter. The amount of Copper Kα radiation was also measured by placing balanced Nickel and Iron filters alternately in the path of the X ray beam. The following results were obtained with the 'Auto-time' of the Scaler set for 100 seconds:

For an angle of emission $\phi = 30^{\circ}$

Number of Quanta of Copper Kα radiation as determined by the difference in counts between the balanced Nickel and Iron filters = 29×10^{3}

Number of Quanta of total radiation actually counted = 127×10^{3}

Thickness of Nickel filter = $2{\cdot}28 \times 10^{-3}$ cm.

Thickness of Aluminium window of X ray tube = $2{\cdot}74 \times 10^{-3}$ cm.

Thickness of Aluminium holder of NaI Tℓ crystal = $2{\cdot}54 \times 10^{-3}$ cm.

Distance of detector to X ray window (air path) = 3·5 cms

A plot of the mass absorption coefficient against wavelength for Aluminium obtained from the literature is shown in Fig. 92 while Fig. 93 shows the mass absorption coefficient against wavelength for air taken from a report by Taylor and Parrish (1955)

The number of Copper Kα radiation leaving the target = 165×10^3

From the data on the relative intensities of the K series given by Meyer and Williams, we have that:

Number of Quanta of Copper Kβ radiation leaving the target = $22{\cdot}6 \times 10^3$

Owing to the absorption of the Aluminium window of the X ray tube, the Aluminium holder of the NaI Tℓ crystal and the air path, the number of Quanta of Copper Kβ and Copper Kα falling on the NaI Tℓ crystal can be calculated.

Number of Quanta of Copper Kβ radiation falling on the NaI Tℓ crystal = $13{\cdot}1 \times 10^3$

Number of Quanta of Copper Kα radiation falling on the NaI Tℓ crystal = $78{\cdot}2 \times 10^3$

Fig 92

MASS ABSORPTION COEFFICIENT FOR ALUMINIUM
AS A FUNCTION OF WAVELENGTH

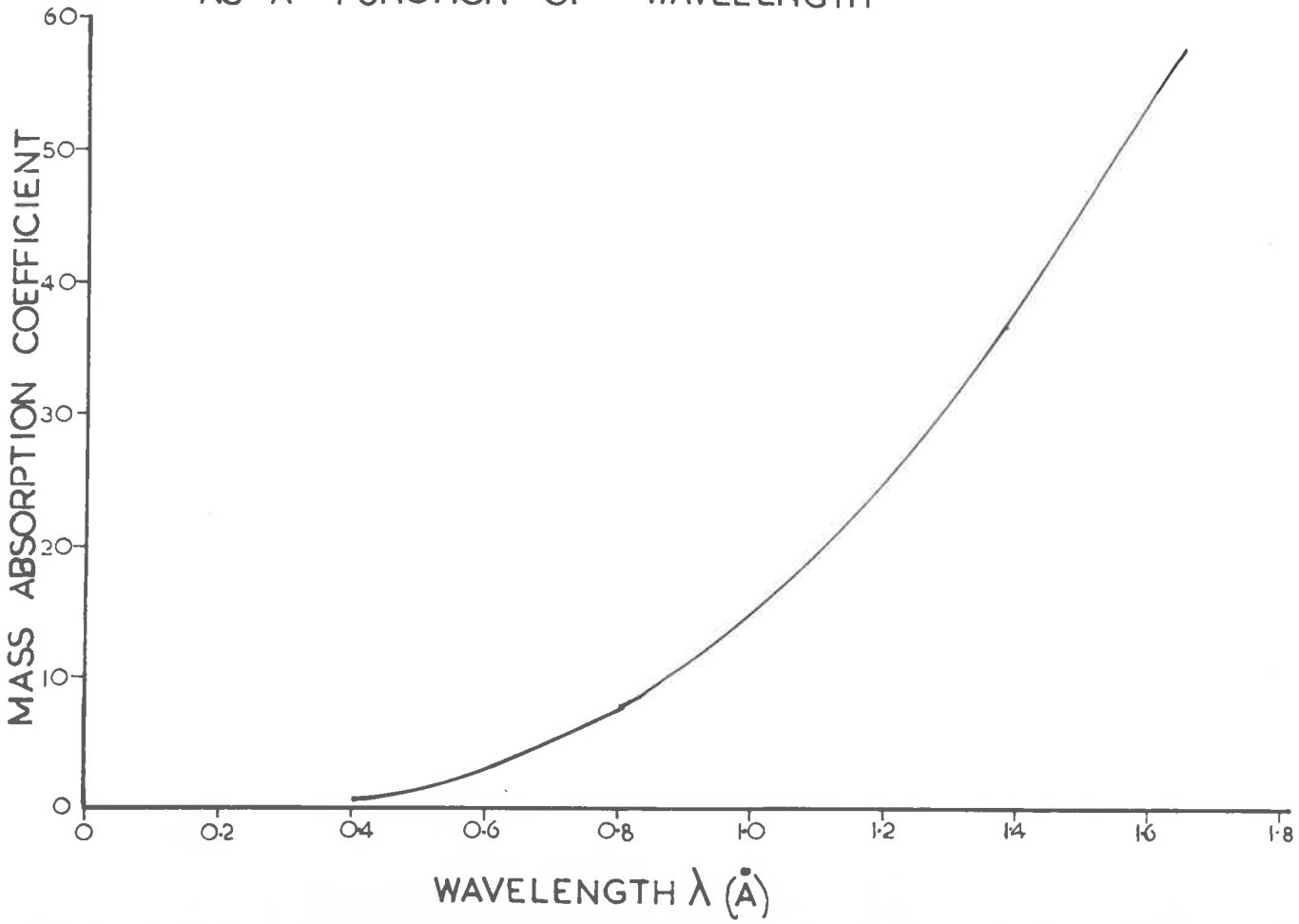

FIG 93

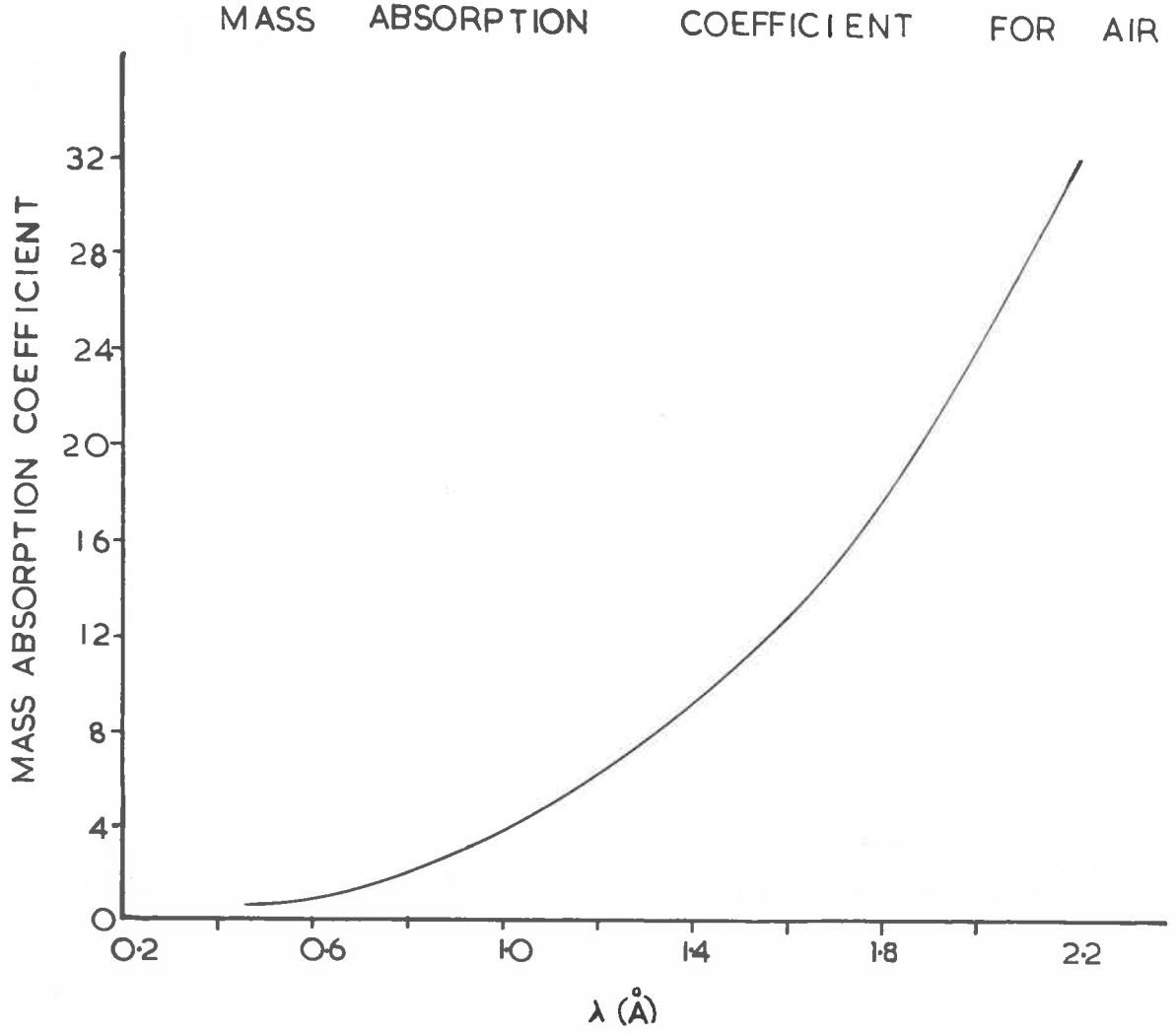
MASS ABSORPTION COEFFICIENT FOR AIR
MASS ABSORPTION COEFFICIENT
32
28
24
20
16
12
8
4
0
0·2
0·6
1·0
1·4
1·8
2·2
λ (Å)

∴ Number of Quanta of white radiation falling on the NaI Tℓ crystal is $(127{\cdot}0 - 13{\cdot}1 - 78{\cdot}2) \times 10^3$

$= 35{\cdot}7 \times 10^3$

Using Arndt and Riley's curve for the spectrum from a Copper target outside the window of the X ray tube and the values of the mass absorption coefficients for Aluminium and air from Figs. 92 and 93, the absorption of the white radiation in passing through the Aluminium window of the X ray tube, the Aluminium holder of the NaI Tℓ crystal and the air path from the X ray window to the detector was determined.

Number of Quanta of white radiation leaving the target $= 38{\cdot}1 \times 10^3$

It should be noticed that although this procedure is not strictly correct (the distribution of the spectrum obtained by Arndt and Riley refers to the spectrum outside the X ray tube window and is different from that at the target surface), the error cannot be so large as to alter the conclusions to be drawn from the calculations.

The integrated intensities of the Kα, Kβ and white radiations at the surface of the target are in the ratio of

100 : 13·6 : 23·1

This gives a Kα to white ratio of 4·35 : 1. For an angle of emission $\phi = 6^{\circ}$ this ratio was equal to 4·2 while for $\phi = 15^{\circ}$ it was equal to 4·27. Outside the window of the X ray tube and for an angle of emission $\phi = 30^{\circ}$ the Kα to white radiation is in the ratio of 3·2 : 1.

A comparison of these results with those of Bendit and Arndt and Riley is not possible without a knowledge of window absorption.

Bendit found from a single oscillation photograph that his X ray tube contained some iron contamination. This has the effect of increasing the white radiation (the iron lines lie outside the 'pass band' of the balanced Nickel-Iron filters) resulting in a smaller value of Kα to white radiation.

<u>The Efficiency of X ray Production.</u>

Experiments by Röntgen (1896) showed that when a target was bombarded with an electron beam the amount of X rays produced increased with the atomic number of the

target and with the accelerating voltage of the electron beam. From direct measurements of X ray and Cathode ray energies, Beatty (1913) found that for thick targets the efficiency η, defined as the ratio of the X ray energy of the white spectrum to the Cathode ray energy was proportional to the atomic number Z of the target material and to the accelerating voltage V of the incident cathode rays, i.e.

$$\eta = kZV \quad \text{where k is a constant}$$

From the measurements on efficiency that were subsequently made, Compton and Allison (1935) concluded that $k = 1{\cdot}1 \times 10^{-9}$ a value which these authors regarded as 'probably correct to within 20 per cent.' Calculations of Kirkpatrick and Wiedmann (1945) on the yields to be expected from thick targets indicate that the constant of proportionality is $1{\cdot}3 \times 10^{-9}$.

The measurements carried out on the ratio of Kα to white radiation show that the variations in this ratio are less than 3 per cent for angles of emission $\phi = 6^{\circ}$, 15° and 30°. The results obtained by Bendit indicate that this ratio shows very little variation for angles of emission $\phi = 3^{\circ}$ and 5°.

To determine the efficiency of production of the white radiation from a Copper target the ratio of the Kα to white radiation was taken as constant and equal to 4·25. (This number being the average of the values obtained at $\phi = 6^{\circ}$, 15° and 30°) for angles of emission ϕ varying from $0^{\circ} - 90^{\circ}$. Since the variation of intensity with angle of emission and accelerating voltage was determined for the characteristic radiation, the variation of intensity of the white radiation with angle of emission for an accelerating voltage of 30 kilovolts could be calculated. From Arndt and Riley's curve Fig. 91 the energy of the white radiation per unit solid angle $F(\phi)$ as a function of ϕ the angle of emission with respect to the target surface was calculated. Fig. 94 shows $F(\phi)$ plotted as a function of ϕ. The total energy E of the white radiation is then calculated from

$$E = 2\pi \int_{0}^{\pi/2} F(\phi) \sin (90 - \phi)\, d\phi$$

This integral must necessarily be solved numerically and Fig. 95 shows $F(\phi) \sin (90 - \phi)$ plotted as a function of ϕ. From this graph the energy E of the white radiation was calculated and found to be equal to 168 ergs. The energy of the incident electron beam for 100 secs with an accelerating voltage of 30,000 volts and a beam current of $0{\cdot}56 \times 10^{-7}$

Fig 94

ENERGY OF WHITE RADIATION $F\phi$ AS A FUNCTION OF THE ANGLE OF EMISSION

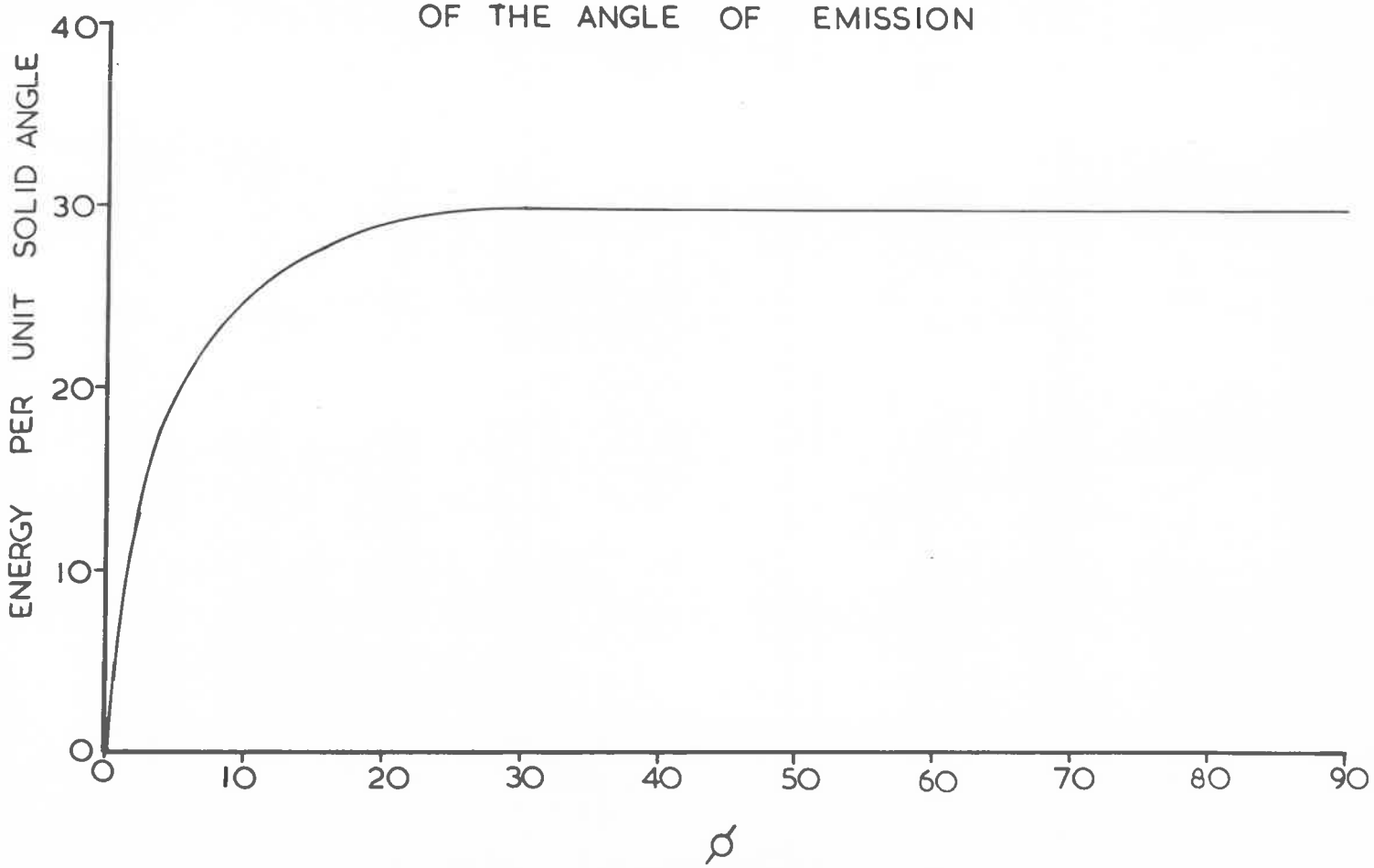

Fig 95

TOTAL ENERGY OF WHITE RADIATION

$$E = 2\pi \int_0^{\frac{\pi}{2}} F(\phi) \sin(90-\phi)\, d\phi$$

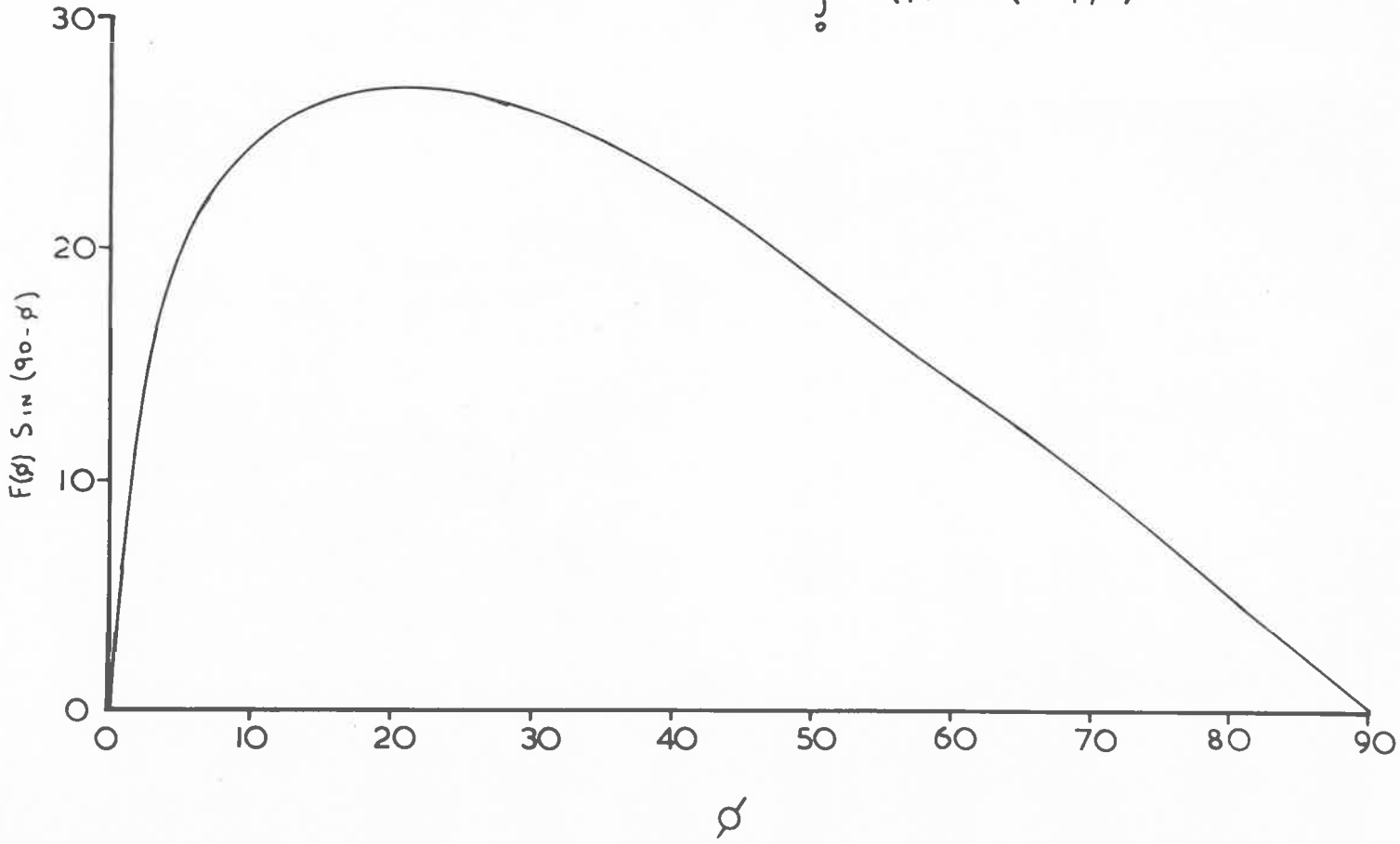

amps is $1{\cdot}68 \times 10^{6}$ ergs. Hence the efficiency $\eta = 1 \times 10^{-4}$. Comparing this result with the formula for efficiency $\eta = kZV$, we obtain

for $k = 1{\cdot}1 \times 10^{-9}$ (Compton and Allison) $\eta = 0{\cdot}87 \times 10^{-4}$

for $k = 1{\cdot}3 \times 10^{-9}$ (Kirkpatrick and Wiedmann) $\eta = 1{\cdot}1 \times 10^{-4}$

CONCLUSION

The derivation by Worthington and Tomlin of the absolute intensity of emission of the characteristic X radiation from thick targets has been modified to take into account electron scattering in the target. The fact that the total deflections produced by repeated scattering in a layer of matter have a distribution given by Gauss's error curve is still a correction of the first order since the contribution of the scattering by the atomic electrons (a second order correction) has been neglected. The importance of diffusion of the incident electron beam in the target in determining the intensity of X ray emission is particularly evident when the angle of emission with respect to the target surface $\phi \leq 5^{\circ}$. (See Sec. 1·45, Figs. 14 - 16).

The expression for N_ϕ the number of Kα Quanta emitted per unit solid angle per electron at an angle ϕ to the target surface when diffusion in the target is allowed for is given by

$$N_\phi = k\int_0^{x_k}\int_{-\pi/2}^{\pi/2} \exp(-\theta^2/2\Delta^2)\exp(-\mu\rho x \operatorname{Cosec}\phi \operatorname{Cos}\theta)\frac{\partial n}{\partial x}\,dx\,d\theta$$

The factor k embodies the following effects:

(a) Indirect production of characteristic radiation by the photo-electric absorption of the continuous radiation,

(b) fluorescence yield,

(c) electron rediffusion,

(d) ratio of the number of Kα quanta to the total number of K quanta.

Of these, (a), (b) and (d) have been determined experimentally by various authors (Sec. 1·2). Measurements on the fraction of the total number of secondaries emerging from a target with an energy larger than $V - V_k$, where V is the accelerating voltage of the primary electron beam and V_k is the K shell ionization potential of the target material, show that this fraction is 0·23 for Copper and 0·33 for Silver, these results being independent of the primary acceleration voltage. The results of Holliday and Sternglass seem to indicate that this fraction is 0·29 and 0·4 for Copper and Silver respectively for a voltage range up to 20,000 volts. However these results of Holliday and Sternglass were obtained for the fraction of the total secondaries emitted from the target surface with energies larger than 50 volts. It is therefore concluded that Webster's empirical derivation of the correction for rediffusion which shows a large increase in this factor with increasing accelerating voltage of the primary electron beam is incorrect. It must be realised however, that if R is the fraction of the total number of

secondaries emerging from the target with an energy loss of V_k volts, the correction for rediffusion enters into the factor k as 1 - R. The theoretical values for the emission N_ϕ were calculated from

$$N_\phi = k\int_0^{x_k}\int_{-\pi/2}^{\pi/2} \exp(-\theta^2/2\Delta^2)\exp(-\mu\rho x \operatorname{Cosec}\phi \operatorname{Cos}\theta)\frac{\partial n}{\partial x}\,dx\,d\theta$$

using R = 0·23 and 0·33 for Copper and Silver respectively and do not differ by more than 15 per cent from the values of emission when Webster's values for rediffusion are used, the differences becoming smaller the larger the accelerating voltage.

Measurements of the absolute intensity of emission of Copper Kα radiation using balanced filters and a crystal monochromator show good agreement both qualitatively and quantitatively with theory especially at the large angles of emission. At small angles of emission $\phi = 1^\circ$ and 3°, the experimental results for emission are certain to be affected by the degree of roughness of the target.

Experimental results with which these measurements may be compared are meagre. Braxton et al. (1945) measured the Kα radiation emerging at an angle of emission $\phi = 10^\circ$ from a thick target of Copper. They used an ionization chamber

as detector and isolated the Kα radiation by means of balanced filters (Cobalt and Nickel). After correcting for absorption and detection losses they found that: "The efficiency of production of Copper Kα radiation in massive targets produced by electron bombardment at 15·5 kilovolts is 0·01 per cent," which corresponds to $1·95 \times 10^{-4}$ quanta per electron. If this is taken to mean that the radiation was produced only by electron bombardment, and that it excludes the fluorescent contribution, then this value must be increased by a factor of 1·15 from Stoddard's data (1934). This would however, still make the experimental result only 60 per cent of the theoretical value for emission. (Unfortunately, Braxton's paper is very brief, and a critical discussion of his work is not possible).

Dyson (1960) measured the efficiency of Kα radiation in the forward direction from Copper targets 0·75, 1·63 and 3·0 μ thick, the highest accelerating voltage being 13 kilovolts. The Kα radiation was detected using a gas flow proportional counter in conjunction with a single channel pulse height analyser. The characteristic Kα and Kβ radiation appeared as a single peak superimposed on the continuous background. After correcting for the continuous radiation and for absorption and detection losses, the energy in the peak was calculated.

Knowing the fraction of the total K radiation which appears in the Kα line (Compton and Allison 1935) and relating the result to the incident beam current, Dyson calculated the efficiency for Kα production. He compared his measurements in the foreward direction with the calculations of Worthington and Tomlin (1956) at an angle of emission $\phi = 45^{\circ}$ where for an accelerating voltage of 13 kilovolts, the effective thickness of target involved was less than 0·5 μ and the absorption of characteristic Kα radiation was only about 2·5 per cent. He found that the values for the number of Kα quanta per electron calculated in this manner were higher than his experimental results (at accelerating voltages of 11·2, 12·2 and 13 kilovolts) by a factor of approximately 2. Even when the correction for fluorescent radiation was considered (for a massive target about half the total continuous radiation is absorbed giving rise to fluorescence, whereas for a target consisting of a thin foil considerably less than half the total continuous radiation is absorbed) his experimental results would be increased only by a factor of 1·15 (Stoddard 1934). With these corrections the experimental results of Dyson would certainly not be greater than 70 per cent of the theoretical values for emission.

The measurements on the characteristic radiation carried out by the Author using balanced filters in conjunction with

three different types of detectors and a crystal monochromator gave consistently good results with theory. It is concluded therefore that the experimental results of Braxton et al. and Dyson are too low compared with the present measurements. The experimental results of Ag Kα emission obtained with a crystal monochromator are in good agreement with the theoretical results. Measurements of intensities at accelerating voltages below 36 kilovolts can certainly be carried out without any modification to the X ray tube provided that a pair of balanced filters Mo and Pd are available. The experimental values of emission of the characteristic intensities for both Copper and Silver are less than the theoretical calculations. This may be attributed to the fact that for Copper, the experimental values of the total cross-section for K shell ionization for Nickel were used in calculating the emission on the assumption that these would be close to the figures for Copper, and for Copper and Silver the efficiency of the counters was calculated from absorption data.

It is of interest to note that a comparison between the theoretical and experimental results of characteristic Kα emission involves a knowledge of the following factors:

(a) Absorption in the air path between X ray window and detector,

(b) Absorption in the X ray tube window,

(c) Absorption in the balanced filters,

(d) Quantum counting efficiency of the detector,

(e) Ratio of the number of Kα quanta to the total number of K quanta produced,

(f) Indirect production of Kα quanta by photoexcitation of K shells by the continuous radiation,

(g) Fluorescence Yield,

(h) Electron Rediffusion,

(i) Total cross-section for K-shell ionisation.

In view of the above, the results obtained between theory and experiment for thick targets of Copper and Silver are good. It would be of great interest to extend this analysis to characteristic Kα radiation of long wavelength. Calculated curves of emission for Al Kα by Worthington and Tomlin (1956) are encouraging. These curves predict that the emission N_ϕ for Aluminium at 4 kilovolts should be approximately equal to that of Copper at 50 kilovolts. Because of the long wavelength of the Al Kα line (8 Å) this would entail having the detector system in the target chamber. The results of the measurements of the ratio of characteristic to white radiation from a Copper target indicate that the value of this ratio estimated by Arndt and Riley is too high. The calculations on the efficiency η of the white radiation

show good agreement with the relation $\eta = kZV$.

APPENDIX I.

The following tables show the results obtained for Copper Kα emission using a pair of balanced filters and a Scintillation Counter as detector. These results are for the case when the normal to the target was parallel to the incident electron beam. The second and third columns are the counts as recorded by the Scaler in 100 secs the Nickel and Iron filters interposed in the path of the X ray beam.

Accelerating voltage = 14 kilovolts ; Galvanometer deflection = 15 mm.

Angle of emission ϕ	Counts with Ni $\times 10^3$	Counts with Fe $\times 10^3$	Difference in counts $\times 10^3$	Counts corrected for absorption $\times 10^5$	$N_\phi \times 10^{-4}$
1	4·77	0·7	4·07	0·232	2·4
3	6·23	0·8	5·43	0·309	3·2
5	6·54	0·9	5·64	0·321	3·31
10	6·65	1·0	5·65	0·323	3·34
20	6·77	1·1	5·67	0·324	3·35
30	6·96	1·0	5·96	0·34	3·62
40	6·96	1·0	5·96	0·34	3·62
50	6·96	1·0	5·96	0·34	3·62

Accelerating voltage = 20 kilovolts : Galvanometer deflection = 30 mm.

Angle of emission ϕ	Counts with Ni $\times 10^3$	Counts with Fe $\times 10^3$	Difference in counts $\times 10^3$	Counts corrected for absorption $\times 10^5$	$N_\phi \times 10^{-4}$
1	14·4	2·0	12·2	0·695	3·6
3	28·6	3·4	25·2	1·43	7·4
5	34·9	3·6	31·3	1·78	9·2
10	38·4	4·2	34·2	1·95	10·1
20	40·1	4·3	35·8	2·04	10·6
30	42·0	4·4	37·6	2·14	11·0
40	42·4	4·5	37·9	2·16	11·2
50	43·7	5·3	38·4	2·20	11·4

Accelerating voltage = 24 kilovolts : Galvanometer deflection = 30 mm.

Angle of emission ϕ	Counts with Ni $\times 10^3$	Counts with Fe $\times 10^3$	Difference in counts $\times 10^3$	Counts corrected for absorption $\times 10^5$	$N_\phi \times 10^{-4}$
1	20·9	2·0	18·9	1·08	5·6
3	34·78	2·78	32·0	1·76	9·1
5	46·88	3·88	43·0	2·45	12·7
10	52·71	3·91	48·8	2·88	15·0
20	56·8	4·5	52·3	2·98	15·4
30	63·8	4·2	59·6	3·4	15·7
40	64·0	4·4	59·6	3·4	15·7
50	63·9	4·3	59·6	3·4	15·7

Accelerating voltage = 30 kilovolts ; Galvanometer deflection = 30 mm.

Angle of emission ϕ	Counts with Ni $\times 10^3$	Counts with Fe $\times 10^3$	Difference in counts $\times 10^3$	Counts corrected for absorption $\times 10^5$	$N_\phi \times 10^{-4}$
1	23·5	3·1	20·4	1·16	6·0
3	43·5	6·4	37·1	2·17	11·2
5	59·5	8·5	51·0	2·9	15·0
10	78·5	10·5	68·0	3·88	20·0
20	100·7	12·4	88·3	5·03	26·0
30	105·7	13·3	92·4	5·26	27·2
40	107·4	13·4	94·0	5·3	28·0
50	107·4	13·3	94·1	5·3	28·0

Accelerating voltage = 34 kilovolts ; Galvanometer deflection = 30 mm.

Angle of emission ϕ	Counts with Ni x 10^3	Counts with Fe x 10^3	Difference in counts x 10^3	Counts corrected for absorption x 10^5	N_ϕ x 10^{-4}
1	24·8	2·4	22·4	1·28	6·6
3	53·3	5·7	47·6	2·71	14·0
5	74·1	7·9	66·2	3·78	19·5
10	100·7	11·1	89·6	5·1	26·4
20	122·0	12·5	109·5	6·24	32·3
30	132·4	13·2	119·2	6·81	36·5
40	132·7	13·4	119·3	6·82	36·6
50	133·1	13·7	119·4	6·82	36·5

Accelerating voltage = 40 kilovolts : Galvanometer deflection = 30 mm.

Angle of emission ϕ	Counts with Ni x 10^3	Counts with Fe x 10^3	Difference in counts x 10^3	Counts corrected for absorption x 10^5	N_ϕ x 10^{-4}
1	36·3	17·7	18·6	1·06	5·47
3	90·3	29·3	61·0	3·48	18·0
5	107·8	35·3	72·5	4·2	21·7
10	142·1	40·1	102·0	5·8	30·0
20	184·3	52·8	131·5	7·5	38·8
30	213·0	61·0	152·0	8·65	44·5
40	217·8	64·3	153·5	8·75	45·1
50	220·3	66·8	153·5	8·75	45·1

Accelerating voltage = 50 kilovolts ; Galvanometer deflection = 30 mm.

Angle of emission ϕ	Counts with Ni $\times 10^3$	Counts with Fe $\times 10^3$	Difference in counts $\times 10^3$	Counts corrected for absorption $\times 10^3$	$N\phi \times 10^{-4}$
1	35·9	19·0	16·9	·965	5·0
3	99·3	38·9	60·4	3·44	17·7
5	136·5	48·0	88·5	5·05	26·0
10	200·3	60·3	140·0	7·7	39·8
20	249·5	76·5	173·0	9·85	51·1
30	284·4	78·9	205·5	11·7	60·4
40	283·0	76·5	207·0	11·8	61·9
50	285·6	74·6	211·0	12·0	62·0

Accelerating voltage = 60 kilovolts ; Galvanometer deflection = 30 mm.

Angle of emission ϕ	Counts with Ni $\times 10^3$	Counts with Fe $\times 10^3$	Difference in counts $\times 10^3$	Counts corrected for absorption $\times 10^5$	$K_\phi \times 10^{-4}$
1	33·7	17·4	16·3	·93	4·8
3	92·3	33·3	59·0	3·36	17·4
5	142·8	41·8	101·0	5·74	26·2
10	209·7	61·8	147·9	8·43	43·6
20	287·1	77·1	210·0	11·5	59·6
30	335·5	81·5	254·0	14·6	75·7
40	342·3	78·3	264·0	15·0	77·9
50	347·7	80·7	267·0	15·2	78·4

Accelerating voltage = 70 kilovolts : Galvanometer deflection = 30 mm.

Angle of emission ϕ	Counts with Ni x 10^3	Counts with Fe x 10^3	Difference in counts x 10^3	Counts corrected for absorption x 10^3	$N_\phi \times 10^{-4}$
1	39·8	24·8	15·0	·86	4·4
3	126·2	67·7	58·5	3·34	17·0
5	168·0	81·7	86·3	4·91	25·9
10	243·5	90·5	153·0	8·71	45·1
20	324·7	113·7	211·0	12·0	62·3
30	401·8	123·8	278·0	15·85	82·0
40	410·2	124·1	286·1	16·3	84·1
50	416.6	124·6	292·0	16·8	86·8

APPENDIX II.

Results of Copper Kα emission recorded with a Proportional Counter, when the normal to the target is parallel to the incident electron beam.

Accelerating voltage = 20 kilovolts : Galvanometer deflection = 30 mm.

Angle of emission ϕ	Counts with Ni x 10^3	Counts with Fe x 10^3	Difference in counts x 10^3	Counts corrected for absorption x 10^5	$\frac{N}{\phi}$ x 10^{-4}
1	13.9	3.2	10.7	.49	3.8
3	25.6	4.8	20.8	.95	7.4
5	29.6	4.3	25.3	1.16	9.9
10	33.3	5.8	27.5	1.26	9.8
20	37.9	7.8	30.1	1.38	10.7
30	40.2	9.3	30.9	1.415	11.0
40	39.8	8.9	30.9	1.415	11.0
50	39.8	8.9	30.9	1.415	11.0

Accelerating voltage = 30 kilovolts ; Galvanometer deflection = 30 mm.

Angle of emission ϕ	Counts with Ni x 10^3	Counts with Fe x 10^3	Difference in counts x 10^3	Counts corrected for absorption x 10^5	N_ϕ x 10^{-4}
1	34.2	8.4	25.8	1.18	6.1
3	68.2	11.6	56.6	2.59	13.4
5	84.6	13.6	71.0	3.25	16.8
10	105.3	15.6	89.7	4.06	21 0
20	126.5	16.5	110.0	5.03	26 0
30	132.6	16.6	116.0	5.32	27.5
40	134.6	16.6	118.0	5.42	28.0
50	135.7	16.7	119.0	5.42	28.1

Accelerating voltage = 40 kilovolts ; Galvanometer deflection = 30 mm.

Angle of emission ϕ	Counts with Ni x 10^3	Counts with Fe x 10^3	Difference in counts x 10^3	Counts corrected for absorption x 10^5	N_ϕ x 10^{-4}
1	36.4	14.9	21.5	.985	5.1
3	91.0	16.0	75.0	3.43	17.7
5	117.2	25.4	91.8	4.20	21.7
10	173.7	42.7	131.0	6.0	31.2
20	235.5	69.5	166.0	7.6	39.4
30	242.8	62.8	180.0	8.23	42.6
40	250.4	66.9	183.5	8.4	43.4
50	250.0	65.5	184.5	8.45	43.8

Results of Copper Kα emission recorded with a Geiger Counter when the normal to the target is parallel to the incident electron beam.

Accelerating voltage = 40 kilovolts ; Galvanometer deflection = 30 mm.

Angle of emission ϕ	Counts with Ni x 10^3	Counts with Fe x 10^3	Difference in counts x 10^3	Counts corrected for absorption x 10^5	N_ϕ x 10^{-4}	N_ϕ x 10^{-4} corrected for dead volume
1	20.9	4.8	16.1	.86	4.46	5.0
3	68.2	9.4	58.8	2.99	15.45	17.3
5	87.9	12.3	75.6	3.83	19.8	22.2
10	119.0	16.0	103.0	5.25	27.2	30.4
20	145.9	17.9	128.0	6.53	33.8	37.1
30	155.5	18.3	137.2	7.0	36.35	40.6
40	156.7	18.4	142.3	7.25	37.6	42.0
50	164.9	18.6	146.3	7.45	38.6	43.3

Accelerating voltage = 30 kilovolts ; Galvanometer deflection = 30 mm.

Angle of emission ϕ	Counts with Ni $\times 10^3$	Counts with Fe $\times 10^3$	Difference in counts $\times 10^3$	Counts corrected for absorption $\times 10^5$	$N_\phi \times 10^{-4}$	$N_\phi \times 10^{-4}$ corrected for dead volume
1	23.2	3.2	20.0	1.02	5.3	5.9
3	49.7	6.4	43.3	2.21	11.4	12.8
5	62.9	8.5	54.4	2.77	14.37	16.1
10	78.4	10.1	68.3	3.48	18.0	20.2
20	96.3	11.7	84.6	4.32	22.4	25.1
30	102.9	11.9	91.0	4.64	24.0	26.9
40	104.8	11.8	93.0	4.73	24.5	27.5
50	104.9	11.9	93.0	4.73	24.5	27.5

Accelerating voltage = 20 kilovolts ; Galvanometer deflection = 30 mm.

Angle of emission ϕ	Counts with Ni x 10^3	Counts with Fe x 10^3	Difference in counts x 10^3	Counts corrected for absorption x 10^5	N_ϕ x 10^{-4}	N_ϕ x 10^{-4} corrected for dead volume
1	15.0	2.7	12.3	.63	3.26	3.64
3	28.9	4.5	24.4	1.24	6.42	7.2
5	35.0	5.3	29.7	1.51	7.76	8.7
10	38.1	5.7	32.4	1.65	8.46	9.5
20	41.3	6.3	35.0	1.78	9.15	10.2
30	41.8	5.9	35.9	1.83	9.4	10.5
40	41.7	5.7	36.0	1.83	9.4	10.5
50	41.6	5.6	36.0	1.83	9.4	10.5

Results of Copper Kα emission using a crystal monochromator (Li F) in conjunction with a Scintillation Counter.

Copper Kα emission using Li F crystal

30 KV		GALV. 50	
Angle of emission ϕ	Counts	Corrected for absorption	$N_\phi \times 10^{-4}$
1	408	880	5·6
3	786	1700	10·8
5	1000	2180	13·9
10	1389	3000	19·1
20	1760	3800	24·2
30	1840	3980	25·3
40	1890	4090	26·0

Copper Kα emission using Li F crystal

40 KV		CALV. 50	
Angle of emission ϕ	Counts	Corrected for absorption	$N_\phi \times 10^{-4}$
1	363	785	5·0
3	1228	2657	16·9
5	1459	3142	20·0
10	2028	4400	28·1
20	2640	5700	36·3
30	3071	6630	42·2
40	3080	6650	42·3

Copper Kα emission using Li F crystal

50 KV		GALV. 50	
Angle of emission ϕ	Counts	Corrected for absorption	$N_\phi \times 10^{-4}$
1	342	738	4·7
3	1191	2580	16·4
5	1765	3820	24·3
10	2670	5775	36·7
20	3430	7420	47·2
30	4164	9000	57·3
40	4166	9000	57·3

Copper K_α emission using L4 F crystal

60 KV		GALV. 50	
Angle of emission ϕ	Counts	Corrected for absorption	$N_\phi \times 10^{-4}$
1	328	707	4·5
3	1178	2542	16·2
5	1800	3890	24·7
10	2947	6370	40·5
20	4006	8760	55·8
30	5260	1138	72·3
40	5350	1157	73·5

Results for Copper Kα emission recorded with a Scintillation Counter when the normal to the target is inclined at an angle θ to the incident electron beam.

$\theta = 20^{\circ}$

Accelerating voltage = 20 kilovolts ; Galvanometer deflection = 20 mm.

Angle of emission ϕ	Counts with Ni x 10^3	Counts with Fe x 10^3	Difference in counts x 10^3	Counts corrected for absorption x 10^5	$N_\phi \times 10^{-4}$
1	10.88	4.8	6.08	.346	3.7
3	25.5	8.9	16.6	.945	7.4
5	31.0	9.9	21.1	1.2	9.3
10	34.2	11.0	23.2	1.32	10.2
20	35.4	11.2	24.2	1.38	10.7
30	35.5	10.6	24.9	1.42	11.0
40	35.8	10.5	25.3	1.44	11.2
50	35.8	10.5	25.3	1.44	11.2
60	35.9	10.6	25.3	1.44	11.2

$\theta = 20^{\circ}$

Accelerating voltage = 30 kilovolts ; Galvanometer deflection = 30 mm.

Angle of emission ϕ	Counts with Ni $\times 10^3$	Counts with Fe $\times 10^3$	Difference in counts $\times 10^3$	Counts corrected for absorption $\times 10^5$	$N_\phi \times 10^{-4}$
1	32.6	11.2	21.4	1.22	6.3
3	71.0	24.3	46.7	2.66	13.6
5	83.7	26.7	57.0	3.25	16.3
10	104.0	31.7	72.3	4.13	21.1
20	124.1	32.1	92.0	5.54	28.3
30	131.9	31.9	100.0	5.72	29.4
40	133.1	33.0	100.1	5.75	29.6
50	132.8	32.7	100.1	5.75	29.6
60	132.7	32.6	100.1	5.75	29.6

$\theta = 20^{\circ}$

Accelerating voltage = 40 kilovolts : Galvanometer deflection = 30 mm.

Angle of emission ϕ	Counts with Ni $\times 10^{3}$	Counts with Fe $\times 10^{3}$	Difference in counts $\times 10^{3}$	Counts corrected for absorption $\times 10^{5}$	$N_{\phi} \times 10^{-4}$
1	31.6	10.0	21.6	1.23	6.4
3	86.4	21.1	65.3	3.72	19.2
5	105.8	25.2	80.6	4.6	23.8
10	140.5	32.5	108.0	6.17	32.0
20	169.7	37.2	132.5	7.55	39.0
30	189.2	38.2	151.0	8.61	44.7
40	190.3	37.3	153.0	8.7	45.1
50	190.4	36.4	154.0	8.75	45.2
60	190.1	36.1	154.0	8.75	45.2

$\theta = 20^{\circ}$

Accelerating voltage = 50 kilovolts ; Galvanometer deflection = 30 mm.

Angle of emission ϕ	Counts with Ni $\times 10^3$	Counts with Fe $\times 10^3$	Difference in counts $\times 10^3$	Counts corrected for absorption $\times 10^5$	$N_\phi \times 10^{-4}$
1	47.2	24.2	23.0	1.31	6.8
3	121.2	52.1	69.1	3.94	20.4
5	155.2	59.7	95.5	5.45	28.2
10	217.2	75.2	142.0	8.1	42.0
20	259.0	84.6	175.0	9.95	51.6
30	293.4	89.4	208.0	11.84	61.3
40	292.2	82.2	210.0	12.0	62.2
50	290.1	80.1	210.0	12.0	62.2
60	290.1	80.1	210.0	12.0	62.2

$\theta = 30^{\circ}$

Accelerating voltage = 20 kilovolts ; Galvanometer deflection = 30 mm.

Angle of emission ϕ	Counts with Mn $\times 10^3$	Counts with Fe $\times 10^3$	Difference in counts $\times 10^3$	Counts corrected for absorption $\times 10^5$	$N\phi \times 10^{-4}$
1	18.8	5.9	12.9	.735	3.8
3	35.5	9.7	25.8	1.47	7.6
5	44.2	11.2	33.0	1.88	9.7
10	43.0	12.2	35.8	2.04	10.5
20	49.3	12.7	36.6	2.08	10.8
30	50.9	12.3	38.6	2.2	11.4
40	50.8	12.2	38.6	2.2	11.4
50	50.4	11.8	38.6	2.2	11.4
60	50.1	11.5	38.6	2.2	11.4

$\theta = 30^{\circ}$

Accelerating voltage = 30 kilovolts : Galvanometer deflection = 30 mm.

Angle of emission ϕ	Counts with Ni $\times 10^3$	Counts with Fe $\times 10^3$	Difference in counts $\times 10^3$	Counts corrected for absorption $\times 10^5$	$N_\phi \times 10^{-4}$
1	31.3	9.1	22.2	1.26	6.5
3	69.0	16.7	52.3	2.98	15.4
5	82.1	20.4	61.7	3.52	18.2
10	91.1	24.4	76.7	4.37	22.7
20	126.3	27.7	98.6	5.62	29.1
30	132.3	28.0	104.3	5.9	30.8
40	132.2	26.9	105.3	6.0	31.0
50	131.2	25.1	106.1	6.04	31.0
60	131.3	25.2	106.1	6.04	31.0

$\theta = 30^{\circ}$

Accelerating voltage = 40 kilovolts ; Galvanometer deflection = 30 mm.

Angle of emission ϕ	Counts with Ni $\times 10^3$	Counts with Fe $\times 10^3$	Difference in counts $\times 10^3$	Counts corrected for absorption $\times 10^3$	$N_\phi \times 10^{-4}$
1	34.4	15.4	19.0	1.08	5.6
3	92.6	24.6	68.0	3.87	20.0
5	113.2	30.7	82.5	4.7	24.2
10	150.4	40.1	110.3	6.3	32.6
20	175.9	41.4	134.5	7.66	39.8
30	192.8	41.8	151.0	8.6	44.6
40	193.7	40.6	153.1	8.7	45.1
50	192.8	39.3	153.5	8.74	45.3
60	192.6	39.1	153.5	8.74	45.3

$\theta = 30^{\circ}$

Accelerating voltage = 50 Kilovolts ; Galvanometer deflection = 30 mm.

Angle of emission ϕ	Counts with Ni x 10^3	Counts with Fe x 10^3	Difference in counts x 10^3	Counts corrected for absorption x 10^5	$N_\phi \times 10^{-4}$
1	42.4	26.7	15.7	.895	5.1
3	121.7	51.4	70.3	4.0	20.8
5	160.7	61.7	99.0	5.65	29.2
10	223.4	78.4	145.0	8.25	42.7
20	264.9	89.6	175.3	10.0	51.8
30	297.0	88.5	209.0	11.9	61.9
40	295.4	85.2	210.2	12.0	62.0
50	296.1	84.0	212.1	12.1	62.2
60	296.4	84.3	212.1	12.1	62.2

$\theta = 40^{\circ}$

Accelerating voltage = 20 kilovolts ; Galvanometer deflection = 30 mm.

Angle of emission ϕ	Counts with Ni $\times 10^3$	Counts with Fe $\times 10^3$	Difference in counts $\times 10^3$	Counts corrected for absorption $\times 10^5$	$N_\phi \times 10^{-4}$
1	20.0	6.7	13.3	.76	3.92
3	37.2	10.7	26.5	1.51	7.8
5	44.6	12.6	32.0	1.86	9.6
10	49.5	12.8	36.7	2.09	10.8
20	52.3	13.2	39.1	2.23	11.9
30	52.4	13.1	39.3	2.24	11.56
40	51.7	12.4	39.3	2.24	11.56
50	51.3	12.0	39.3	2.24	11.56
60	50.9	11.6	39.3	2.24	11.56

$\theta = 40^{\circ}$

Accelerating voltage = 30 kilovolts : Galvanometer deflection = 30 mm.

Angle of emission ϕ	Counts with Ni $\times 10^3$	Counts with Fe $\times 10^3$	Difference in counts $\times 10^3$	Counts corrected for absorption $\times 10^5$	$N_\phi \times 10^{-4}$
1	33.5	11.7	21.8	1.24	6.4
3	75.2	21.2	54.0	3.08	15.9
5	90.7	25.4	65.3	3.72	19.2
10	109.5	30.1	79.4	4.52	23.4
20	133.1	30.1	103.0	5.87	30.4
30	139.4	31.2	108.2	6.16	31.9
40	141.7	30.4	111.3	6.34	32.8
50	141.6	29.6	112.0	6.38	33.0
60	141.7	29.7	112.0	6.38	33.0

$\theta = 40^{\circ}$

Accelerating voltage = 40 kilovolts ; Galvanometer deflection = 30 mm.

Angle of emission ϕ	Counts with Ni $\times 10^3$	Counts with Fe $\times 10^3$	Difference in counts $\times 10^3$	Counts corrected for absorption $\times 10^5$	$N_\phi \times 10^{-4}$
1	33.6	14.3	19.3	1.1	5.7
3	106.7	36.0	70.7	4.03	20.8
5	130.1	44.9	85.2	4.85	25.1
10	168.8	55.8	113.0	6.45	33.4
20	195.8	57.7	138.1	7.87	40.7
30	210.8	58.5	152.3	8.66	44.9
40	210.6	57.6	153.0	8.74	45.2
50	209.8	56.8	153.0	8.74	45.2
60	210.7	56.7	154.0	8.75	45.3

$\theta = 40^{\circ}$

Accelerating voltage = 50 kilovolts ; Galvanometer deflection = 30 mm.

Angle of emission ϕ	Counts with Ni $\times 10^3$	Counts with Fe $\times 10^3$	Difference in counts $\times 10^3$	Counts corrected for absorption $\times 10^5$	$N\phi \times 10^{-4}$
1	43.9	26.2	17.7	1.01	5.2
3	125.6	54.1	71.5	4.08	21.1
5	165.7	61.7	104.0	5.92	30.6
10	224.2	77.2	147.0	8.37	43.4
20	262.0	86.5	175.5	10.0	51.8
30	297.4	87.4	210.0	12.02	62.1
40	295.2	84.2	211.0	12.05	62.3
50	294.0	82.0	212.0	12.08	62.4
60	294.1	82.1	212.0	12.08	62.4

$\theta = 50^{\circ}$

Accelerating voltage = 20 kilovolts ; Galvanometer deflection = 30 mm.

Angle of emission ϕ	Counts with Ni x 10^3	Counts with Fe x 10^3	Difference in counts x 10^3	Counts corrected for absorption x 10^5	N_ϕ x 10^{-4}
1	21.1	7.1	14.0	0.8	4.14
3	38.4	11.2	27.2	1.55	8.0
5	45.3	12.9	32.4	1.84	9.5
10	50.0	13.1	36.9	2.1	10.85
20	52.4	13.3	39.1	2.22	11.5
30	52.0	12.8	39.2	2.23	11.53
40	51.6	12.4	39.2	2.23	11.53
50	51.0	11.8	39.2	2.23	11.53
60	50.7	11.5	39.2	2.23	11.53

$\theta = 50^{\circ}$

Accelerating voltage = 30 kilovolts ; Galvanometer deflection = 30 mm.

Angle of emission ϕ	Counts with Ni $\times 10^3$	Counts with Fe $\times 10^3$	Difference in counts $\times 10^3$	Counts corrected for aberration $\times 10^5$	$N_\phi \times 10^{-4}$
1	33.2	11.5	21.7	1.235	6.39
3	75.1	20.6	54.5	3.11	16.1
5	89.2	23.9	65.3	3.72	19.2
10	110.3	30.5	79.8	4.55	23.7
20	134.0	30.6	103.4	5.9	30.5
30	141.2	31.8	109.4	6.24	32.2
40	144.8	32.0	112.8	6.42	33.2
50	144.5	31.7	112.8	6.42	33.2
60	143.7	30.9	112.8	6.42	33.2

$\theta = 50^{\circ}$

Accelerating voltage = 40 kilovolts ; Galvanometer deflection = 30 mm.

Angle of emission ϕ	Counts with Ni $\times 10^3$	Counts with Fe $\times 10^3$	Difference in counts $\times 10^3$	Counts corrected for absorption $\times 10^5$	$N_\phi \times 10^{-4}$
1	34.5	15.2	19.3	1.1	5.7
3	103.9	33.1	70.8	4.04	20.9
5	127.9	41.8	86.1	4.9	25.3
10	168.1	54.7	113.4	6.46	33.4
20	195.6	57.8	137.8	7.85	40.6
30	211.2	59.3	151.9	8.65	44.7
40	211.0	58.5	152.5	8.7	45.0
50	209.7	57.1	152.6	8.71	45.1
60	209.7	56.9	152.8	8.72	45.1

$\theta = 50^{\circ}$

Accelerating voltage = 50 kilovolts ; Galvanometer deflection = 30 mm.

Angle of emission ϕ	Counts with Ni $\times 10^3$	Counts with Fe $\times 10^3$	Difference in counts $\times 10^3$	Counts corrected for absorption $\times 10^5$	$N_\phi \times 10^{-4}$
1	41.7	24.0	17.7	1.01	5.2
3	123.7	51.7	72.0	4.1	21.2
5	167.0	63.4	103.6	5.9	30.5
10	227.0	79.2	147.8	8.4	43.5
20	261.0	84.8	176.2	10.05	52.0
30	296.3	86.9	209.4	11.9	61.5
40	296.4	87.3	211.1	12.0	62.1
50	299.5	88.1	211.4	12.03	62.4
60	299.8	88.4	211.4	12.03	62.4

Results of Ag Kα emission using a crystal monochromator (Li F) in conjunction with a Scintillation Counter.

Ag Kα emission using Li F crystal

36 KV		GA.V. 60	
Angle of emission ϕ	Counts	Corrected for absorption	$H_\phi \times 10^{-4}$
1	336	355	1.14
3	363	382	1.23
5	389	410	1.32
10	423	443	1.43
20	430	448	1.44
30	430	448	1.44
40	430	448	1.44

Ag Kα emission using Li F crystal

40 KV		CALV. 60	
Angle of emission ϕ	Counts	Corrected for absorption	$N_\phi \times 10^{-4}$
1	473	496	1.6
3	680	715	2.3
5	735	776	2.5
10	770	806	2.6
20	770	806	2.6
30	770	806	2.6
40	770	806	2.6

Ag Kα emission using Li F crystal

46 KV		GALV. 50	
Angle of emission ϕ	Counts	Corrected for absorption	$N_\phi \times 10^{-4}$
1	570	600	2.2
3	978	1003	4.0
5	1130	1190	4.6
10	1143	1210	4.7
20	1165	1230	4.75
30	1180	1247	4.82
40	1190	1253	4.83

Ag Kα emission using Li F crystal

50 KV		GAIN. 50	
Angle of emission ϕ	Counts	Corrected for absorption	$N_\phi \times 10^{-4}$
1	631	663	2.56
3	1280	1347	5.2
5	1420	1500	5.8
10	1510	1590	6.1
20	1560	1640	6.3
30	1585	1670	6.4
40	1615	1700	6.5

Ag Kα emission using 14 F crystal

56 KV		GALV. 50	
Angle of emission ϕ	Counts	Corrected for absorption	$N_\phi \times 10^{-4}$
1	666	705	2.71
3	1625	1710	6.6
5	1820	1920	7.7
10	2070	2180	8.4
20	2140	2250	8.7
30	2160	2280	8.8
40	2190	2310	8.9

Ag Kα emission using Li F crystal

60 KV		GAIN . 50	
Angle of emission ϕ	Counts	Corrected for absorption	$N_\phi \times 10^{-4}$
1	689	724	2.8
3	1785	1880	7.3
5	2160	2280	8.8
10	2340	2460	9.5
20	2430	2560	9.9
30	2530	2660	10.3
40	2550	2690	10.4

SECONDARY ELECTRON EMISSION

The absorption of X radiation in the aluminium cylinder when the incident electron beam is accelerated with an energy of 20 kilovolts was calculated from the following data:

With the auto time of the scaler set for 100 seconds, and the window of the Pulse Height Discriminator open at its maximum,

Number of counts obtained with the aluminium absorber in the path of the X ray beam 117.2×10^3

Number of counts obtained without the aluminium absorber 156.5×10^3

Transmission of aluminium absorber = $\frac{117.2}{156.5} = 0.75$

Reading of Galvanometer for incident electron beam current = 14

Voltage applied to collector	Reading of Galvanometer connected to collector after correction for absorption
Volts	Reading
0	3.7
10	2.8
20	2.1
30	1.6
40	1.4
50	1.25
60	1.25
70	1.25
80	1.25
90	1.25
100	1.25
1,000	1.20
2,000	1.20
3,000	1.00
4,000	1.00
5,000	1.00
6,000	0.95
7,000	0.93
8,000	0.90
9,000	0.88
10,000	0.88
11,000	0.85
12,000	0.85
13,000	0.85
14,000	0.85
15,000	0.84
16,000	0.76
17,000	0.48
18,000	0
19,000	0
20,000	0

Voltmeter Multiplier Calibration

String Number	25 μA R x 10^4	50 μA R x 10^4	75 μA R x 10^4	100 μA R x 10^4
1	9,780	9220	9020	8780
2	9,750	9210	9090	8710
3	10,000	9510	9410	9020
4	9,800	9290	9180	8820
5	9,700	9200	9120	8720
6	10,600	9970	9820	9490
7	10,120	9490	9340	8980
8	9,810	9320	9080	8880
9	9,880	9310	9210	8830
10	9,950	9410	9260	8920

Each string consists of ten 10 megohms resistors in series.

GEIGER COUNTER SENSITIVITY CURVE

(Readings every 0.2 inches)

Distance from window	Intensity
0.2	10.67
0.4	11.6
0.6	12.3
0.8	13.4
1.0	14.2
1.2	14.3
1.4	14.3
1.6	14.3
1.8	14.3
2.0	14.3
2.2	14.6
2.4	14.5
2.6	14.5
2.8	14.5
3.0	14.5
3.2	13.2
3.4	12.7
3.6	12.0
3.8	11.8
4.0	10.7

Theoretical Results for Copper Kα Emission.

These results were calculated from the formula

$$N_\phi = k\int_0^{x_k}\int_{-\pi/2}^{\pi/2} \exp(-\theta^2/2\Delta^2)\exp\left(-\mu\rho x \operatorname{Cosec}\phi \cos(\theta+\alpha)\right)\frac{\partial n}{\partial x}\,dx\,d\theta$$

ϕ = Angle of emission with respect to the target surface,

α = Angle between target normal and incident electron beam,

V = Accelerating voltage of the incident electron beam in kilovolts.

$\phi = 1^\circ$: $\alpha = 20^\circ$

V	$N_\phi \times 10^{-4}$
60.5	9.4
51.2	9.4
40.5	9.3
31.8	8.0
19.3	4.0

$\phi = 3^\circ$: $\alpha = 20^\circ$

V	$N_\phi \times 10^{-4}$
60.5	28.8
51.2	28.9
40.5	23.2
31.8	15.1
19.3	7.5

$\phi = 5^{\circ}$: $\alpha = 20^{\circ}$

V	$N_{\phi} \times 10^{-4}$
60.5	43.4
51.2	40.4
40.5	27.7
31.8	19.7
19.3	9.6

$\phi = 10^{\circ}$: $\alpha = 20^{\circ}$

V	$N_{\phi} \times 10^{-4}$
60.5	66.8
51.2	50.6
40.5	36.5
31.8	22.1
19.3	10.3

$\phi = 20^{\circ}$: $\alpha = 20^{\circ}$

V	$N_{\phi} \times 10^{-4}$
60.5	83.8
51.2	64.8
40.5	45.2
31.8	29.2
19.3	11.9

$\phi = 30^\circ$: $\alpha = 20^\circ$

V	$N_\phi \times 10^{-4}$
60.5	87.5
51.2	68.2
40.5	48.0
31.8	32.4
19.3	12.2

$\phi = 40^\circ$: $\alpha = 20^\circ$

V	$N_\phi \times 10^{-4}$
60.5	90.5
51.2	71.2
40.5	49.3
31.8	32.9
19.3	12.3

$\phi = 50^\circ$: $\alpha = 20^\circ$

V	$N_\phi \times 10^{-4}$
60.5	91.0
51.2	72.1
40.5	50.2
31.8	33.4
19.3	12.3

$\phi = 1^\circ$: $\alpha = 40^\circ$

V	$N_\phi \times 10^{-4}$
60.5	9.5
51.2	9.5
40.5	9.3
31.8	8.1
19.3	4.2

$\phi = 3^\circ$: $\alpha = 40^\circ$

V	$N_\phi \times 10^{-4}$
60.5	31.4
51.2	31.3
40.5	25.4
31.8	17.8
19.3	7.9

$\phi = 5^\circ$: $\alpha = 40^\circ$

V	$N_\phi \times 10^{-4}$
60.5	50.4
51.2	41.6
40.5	28.5
31.8	22.1
19.3	9.9

$\phi = 10^{\circ}$: $\alpha = 40^{\circ}$

V	$N_{\phi} \times 10^{-4}$
60.5	75.6
51.2	58.4
40.5	41.7
31.8	25.6
19.3	10.9

$\phi = 20^{\circ}$: $\alpha = 40^{\circ}$

V	$N_{\phi} \times 10^{-4}$
60.5	87.0
51.2	68.6
40.5	47.8
31.8	32.1
19.3	12.0

$\phi = 30^{\circ}$: $\alpha = 40^{\circ}$

V	$N_{\phi} \times 10^{-4}$
60.5	90.0
51.2	70.5
40.5	49.0
31.8	33.4
19.3	12.2

$\phi = 40^{\circ}$: $\alpha = 40^{\circ}$

V	$N_{\phi} \times 10^{-4}$
60.5	94.3
52.2	73.4
40.5	50.5
31.8	33.6
19.3	12.2

$\phi = 50^{\circ}$: $\alpha = 40^{\circ}$

V	$N_{\phi} \times 10^{-4}$
60.5	94.5
51.2	74.8
40.5	51.1
31.8	33.8
19.3	12.2

$\phi = 1^\circ$: $\alpha = 50^\circ$

V	$N_\phi \times 10^{-4}$
60.5	9.6
51.2	9.6
40.5	9.5
31.8	8.3
19.3	4.3

$\phi = 3^\circ$: $\alpha = 50^\circ$

V	$N_\phi \times 10^{-4}$
60.5	32.0
51.2	32.0
40.5	26.7
31.8	18.4
19.3	8.2

$\phi = 5^\circ$: $\alpha = 50^\circ$

V	$N_\phi \times 10^{-4}$
60.5	53.1
51.2	42.6
40.5	29.3
31.8	22.8
19.3	10.2

$\phi = 10^{\circ}$: $\alpha = 50^{\circ}$

V	$N_{\phi} \times 10^{-4}$
60.5	77.0
51.2	65.1
40.5	45.6
31.8	30.0
19.3	11.2

$\phi = 20^{\circ}$: $\alpha = 50^{\circ}$

V	$N_{\phi} \times 10^{-4}$
60.5	93.0
51.2	71.4
40.5	48.0
31.8	32.0
19.3	12.1

$\phi = 30^{\circ}$: $\alpha = 50^{\circ}$

V	$N_{\phi} \times 10^{-4}$
60.5	94.5
51.2	73.5
40.5	50.0
31.8	33.6
19.3	12.3

$\phi = 40^\circ$: $\alpha = 50^\circ$

V	$N_\phi \times 10^{-4}$
60.5	95.5
51.2	75.5
40.5	52.2
31.8	34.0
19.3	12.3

$\phi = 50^\circ$: $\alpha = 50^\circ$

V	$N_\phi \times 10^{-4}$
60.5	97.5
51.2	77.0
40.5	53.0
31.8	34.6
19.3	12.4

REFERENCES

Arndt, W.W. (1949): J. Sci. Inst., 26, 45.

Arndt, W.W. (1953): J. App. Phys., 1, 169.

Arndt, W.W. and Riley (1952): Phys. Soc. of London, 65, 74.

Auger, P. (1925): Jour. de Phys., 6, 205.

Balderston, M. (1926): Phys. Rev., 27, 696.

Beatty, R.T. (1913): Proc. Soc. of London, 89, 314.

Becker, A. (1905): Ann. d. Physik, 17, 381.

Bendit, E.G. (1957): British J. of Appl. Phys., 9, 312.

Bethe, H. (1940): Ann. Phys., 5, 325.

Boethe, W. (1927): Handbuch der Physik, 24, 18.

Braxton, W.L. (1945): Phys. Rev., 68, 106.

Burhop, E.H. (1940): Proc. Camb. Phil. Soc., 36, 43.

Bruining, H. (1936): Physica, 3, 1046.

Bruining, H. and de Boer (1939): Physica, 6, 941.

Compton, A.H. (1929): Phil. Mag., 8, 961.

Compton, A.H. and Allison, S.K. (1935): X rays in Theory and Practice.

Curran, S.C. and Craggs, J.D. (1949): Theory and Application of Counting Tubes.

Dyson, N.A. (1959): British J. of Appl. Phys., 10, 505.

Holliday, J.E. and Sternglass, E.J. (1957): J. Appl. Phys. 28, 1189.

Kirkpatrick, P. and Baez, A.V. (1947): Phys. Rev., 71, 521.

Lorenz, E. (1928): Proc. Nat. Acad. of Sci., 14, 582.

Mott, N.F. and Massey, H.E. (1949): Theory of Atomic Collisions.

Nicholas, W.W. (1927): Phys. Rev., 29, 619.

Palluel, P. (1947): Compter. Rendus., 224, 1492.

Parrish and Kohler (1955): J. App. Phys., 27, 1215.

Pockman, L.T. (1947): Phys. Rev., 71, 330.

Rudberg, E. (1936): Phys. Rev., 50, 138.

Schonland, B.F.J. (1925): Proc. Roy. Soc., 108, 187.

Stehberger, K.H. (1928): Ann. d. Physik, 86, 825.

Stoddard, K.B. (1934): Phys. Rev., 36, 920.

Treloar, L.R. (1937): Proc. Phys. Soc., 49, 392.

Wagner, P.B. (1927): Physl. Rev., 35, 98.

Webster, D.L. (1933): Phys. Rev., 43, 839.

Webster, D.L. (1933): Phys. Rev., 44, 258.

Wilson, R. (1941): Phys. Rev., 60, 749.

Worthington, S.G. and Tomlin, S.G. (1956): Proc. Phys. Soc., 69, 401.

Zajac, B. and Ross, M. (1949): Nature, Lond., 164, 311.